Tunable conductivity level in nanosized phthalcon/polymer composites

Please check the document version of this publication:

**TUNABLE CONDUCTIVITY LEVEL IN NANOSIZED
PHTHALCON/POLYMER COMPOSITES**

PROEFSCHRIFT

ter verkrijging van de graad van doctor aan de
Technische Universiteit Eindhoven, op gezag van de
Rector Magnificus, prof.dr.ir. C.J. van Duijn, voor een
commissie aangewezen door het College voor
Promoties in het openbaar te verdedigen
op woensdag 12 november 2008 om 16.00 uur

door

Ming Yuan

geboren te Tianjin, China

Dit proefschrift is goedgekeurd door de promotor:

prof.dr. G. de With

Copromotor:
dr. J.C.M. Brokken-Zijp

TABLE OF CONTENTS

Chapter 4

Filler Size Effects on the Conductivity of Cross-linked Phthalcon/Epoxy
Nanocomposites **53**

Chapter 5

Influence of Curing Agent and Processing Conditions on the Conductivity of Cross-
linked Phthalcon/Epoxy Nanocomposites **77**

Chapter 6

Conductivity of Cross-linked Low Surface Energy Phthalcon/Epoxy Nanocomposites **111**

Chapter 7

Influence of Dispersing Solvent and Post-cure on the Conductivity of Cross-linked Phthalcon/Epoxy Nanocomposites..**133**

1

INTRODUCTION[⊛]

1.1. Polymer Nanocomposite Materials

Polymer composites, in general, are made by incorporating filler particles into a polymer matrix. These materials are of major interest, especially when a combination of properties which cannot be obtained in a single material is required.[1] With the development of polymer industry, numerous fillers, such as minerals, clays, glasses, graphite, etc. have been introduced as additives to improve (some of) the properties of neat polymers. Till the 1970s, mixing of the components was mainly performed on a micrometer scale; it was only three decades ago that technological advances allowed decreasing the size of various filler materials down to a nanometer scale. The term "nanocomposite" was, therefore, introduced.[2] Since then, nanocomposite materials have become a rapidly expanding area of research, which encompass an infinite variety of systems with potentially novel material properties.

Nanocomposite materials have become increasingly important due to their extraordinary properties, which arise from the synergism between the properties of the parent components and their unique interfacial characteristics.[1] These properties appear to be quite different from those of the conventional micrometer-sized composites. This mainly results from the nanometer-sized component which dramatically increases the available interacting surface area. Polymer nanocomposites are of significant interest, for instance, as materials for mechanically reinforced components and coatings for packaging, automotive and airspace industries,[3,4] as corrosion-inhibiting layers on metal surfaces,[1] and as flame retardant materials.[5] Furthermore, due to their electrical and optical performance, nanocomposite materials have potential applications in electronics and optoelectronics, such as optical switches, transparent electrodes, display devices, etc.[6-8]

Although polymer nanocomposites have been investigated actively for the last several decades, until now only a limited understanding of the physicochemical phenomena,

---

[⊛] Due to the extensive research in the area of (semi)conductive filler/polymer composites, only the most relevant references are quoted in this thesis.

which are responsible for the ultimate properties of these materials, have been obtained. The properties of a nanocomposite material are not simply the average properties of its components. On the contrary, these materials are complex and their properties depend on both the volume fractions of the components and their (individual) properties, such as size, shape, distribution, interfacial interactions, etc. Therefore, the study of nanocomposite materials requires a multidisciplinary approach,[1] which involves novel physical and chemical techniques for their synthesis and analysis.

1.2. Conductive Polymer Nanocomposites

1.2.1. Introduction

In recent years, blending an insulating polymer with conducting fillers has attracted considerable interest because of the potential applications of these composites in many areas where a certain level of conductivity is required.[9-16] The conducting fillers used range from metallic powders, inorganic (semi)conductive particles to carbonaceous fillers including carbon black, graphite and carbon fibers.[9,17,18] Doped conducting polymers, such as polyaniline or polypyrrole, sometimes are also used as fillers in polymers.[9,19-21] When particles with sizes well below 1 μm are added as conductive fillers into a polymer matrix, the resulting material, with a certain (semi)conductive level, is called a conductive polymer nanocomposite. This thesis focuses on such polymer nanocomposites that can conduct electrical currents due to the presence of (semi)conductive nanofiller particles.

1.2.2. Conductivity of Polymer Nanocomposites

Most polymers are insulators with conductivity well below 10^{-13} S/cm.[22] With the addition of conductive nanoparticles, the polymer changes from an insulator to a (semi)conductor if the conductive fillers form a continuous particle network through the polymer matrix.[9,23,24] Volume and surface conductivity are often used as measures for the electrical conductivity σ. In general, volume conductivity is an intrinsic material property which is defined as the conductance per volume, and it is usually expressed in the unit of S/cm. On the other hand, surface conductivity is defined as the conductance measured over a certain area at the surface, and it is expressed in the unit of S/☐. However, surface conductivity is not an intrinsic material property. The measured value is strongly dependent on the thickness and the surface area of the measuring material. Moreover, the surface conductivity is often enhanced by the

presence of antistatic agents which are molecules that increase the polarity/ionic concentration at the surface. These ions/polar groups at the surface attract moisture from air and consequently influence the charge transport. Hence, the surface conductivity is not permanent and strongly depends on the moisture in the air. Note that the semi-conductive nanoparticles discussed in this thesis do not contain antistatic agents and we only concentrate on the volume conductivity of the coating composites containing these semi-conductive particles.

Generally, the relation between the DC volume conductivity σ_v of a polymer composite and the amount of conductive filler φ is not linear. Normally the σ_v increases sharply above a critical filler concentration, known as the percolation threshold φ_c.[9,14-16] At φ well above φ_c, the increase in σ_v becomes smaller and reaches a level where σ_v hardly changes with increasing filler amount anymore. This level is called the maximum volume conductivity σ_{max} (Figure 1.1). The σ_v of a polymer nanocomposite is often orders of magnitude lower than the σ_v of the filler particle.[9-11,14-16] This makes these polymer nanocomposites only suitable for antistatic or semi-conductive materials ($\sigma_v = 10^{-11}$-10^{-2} S/cm). Nevertheless, sometimes this type of materials is still referred to as "conductive" materials. Applications of such materials are, for example, permanent antistatic floors in hospitals, safety garment and the upper layer of the paper transport rolls in printers and copying machines.
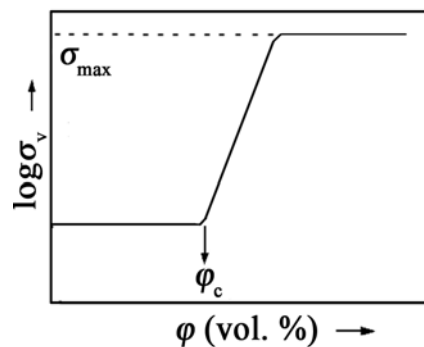
Figure 1.1. Relation between the volume conductivity σ_v and the filler volume percentage φ.

1.2.3. Challenges in (Semi)conductive Polymer Nanocomposites

Several theories were developed to understand the conductivity behaviour of (semi)conductive composites, especially the marked transition at φ_c,[11,13,23,25-28] of which statistical percolation models form an important part.[23,25] The values of φ_c for disordered or regular systems can be determined in these models by numerical

simulation using the Monte Carlo method.[17,23] For regular packing arrangements in three dimensions, the values of φ_c range from 12.5 to 40 vol. %, depending on the type of lattice selected for simulation.[23,28] For randomly distributed non-overlapping hard spheres which touch each other at the percolation threshold, φ_c is calculated to be 16 vol. %.[23,28] However, such a large amount of fillers deteriorates the mechanical properties and leads to poor processability of the polymer matrix. Furthermore, the cost of the final material is often beyond the acceptable range due to the large fraction of the expensive conducting species.[11] Another disadvantage of polymer composites is that normally the σ_{max} is orders of magnitude lower than the intrinsic conductivity of the filler itself.[9-11,14-16] A σ_{max} value closer to the conductivity of the filler would broaden the application possibilities of these composites considerably.

Intensive studies have been carried out during the last decades and, indeed, many researchers managed to achieve a φ_c much lower than 16 vol. %, even when spherical particles were used.[9-13,18,19,23,29-32] In some cases, the φ_c value was even as low as 0.1 vol. %.[11,18,31,32] However, the reasons used to explain the occurrence of such a low φ_c were often quite different and sometimes contradictory. Now, it is generally accepted that the properties of the fillers, such as size, aspect ratio and surface groups, the aggregate/agglomerate structure of the filler particles in the matrix before processing, the properties of the matrix including viscosity and crystallinity, and the interfacial energy between matrix and filler determine φ_c.[9-11,13,17,19,29,30,33-35] Moreover, a great deal of research has been done to model these conductive filler/polymer systems. At present, however, no model exists to explain all the differences reported in experimental studies or to account for the extensive influences of different processing methods on φ_c and σ_{max}.[11,23,25] Especially, limited knowledge is available on the percolation behavior in thermoset polymer composites.[11,12,29,30,33,34] However, the potential applications, for instance transparent layers, often require such materials.

1.3. Objectives of this Thesis

As mentioned above, both a low φ_c and a high σ_{max} are desired for many applications. In this thesis, we are interested in obtaining semi-conductive polymer nanocomposites with a low φ_c; we try to investigate whether it is possible to increase the σ_{max} of the polymer nanocomposites which have a φ_c much lower than the theoretically predicted 16 vol. %. If the answer is positive, we are eager to find out which factors are responsible for the low φ_c, which factors determine the high σ_{max}, and to what extent

these factors influence the conductivity behaviour of the polymer nanocomposites. With the better understanding of these factors, we hope that we could achieve materials with tunable conductivity levels for different applications.

Generally, nanocomposite becomes conductive due to the presence of a continuous conductive particle network through the insulating polymer matrix. The morphology of the particle network is very important with respect to the conductivity of the nanocomposites, because it influences the charge transport within the material. Therefore, we choose different cross-linking agents, different dispersing media, different cross-linking temperatures, different curing conditions such as thermal cure vs. UV cure and conductive nanoparticles with different particle sizes to visualize the particle network structure before/during/after cure and to understand the mechanism of charge transport.

1.4. Materials used in this Thesis

1.4.1. Semi-conductive Nanoparticle Phthalcon 11

One of the nanometer-sized semi-conductive particles studied in this thesis is aquocyanophthalocyaninato Co(III) (Phthalcon 11) (Scheme 1.1). Phthalcon 11 is a neutral molecule with a -CN group and a -H_2O group co-ordinately bonded to the Co(III) centred in a phthalocyanine ring.[11,29,35,36] We will show in this thesis that Phthalcon 11 is highly crystalline and can be synthesized to submicrometer-sized particles with high purity and yield.[11,29,35,36] Phthalcon 11 powders have excellent stability in air and in moisture. In addition, they are stable in contact with a broad range of solvents. They decompose in air at temperature above 300 °C.[34,36]
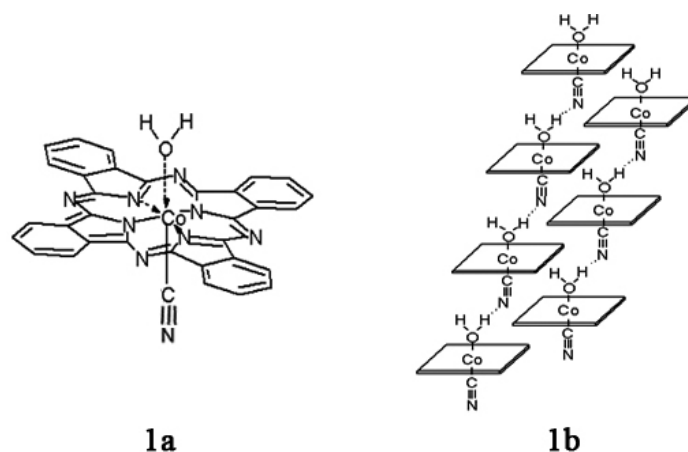
Scheme 1.1. Molecular (1a) and crystal (1b) structure of Phthalcon 11.

By varying the reaction conditions, aminocyanophthalocyaninato Co(III) (Phthalcon 12) and a single crystal mixture of Phthalcon 11 and Phthalcon 12 (Phthalcon 11/12) can also be synthesized (see Chapter 4).[35]

1.4.2. Phthalcon/Polymer Nanocomposite Coatings

It has been shown that Phthalcon 11 particles can be used as semi-conductive filler in a broad range of polymer matrices, such as cross-linked epoxy, polypropylene, polyethylene, cellulose and nylon, resulting in permanent antistatic polymer nanocomposites with a φ_c well below 16 vol. %.[29,33,34] More recent research on Phthalcon/polymer composites has concentrated on cross-linked epoxy thin coatings.[33,34] In this thesis we focus on thermally cured epoxy and UV cured acrylate coatings, mainly using Phthalcon 11/12 as conductive filler.

Thermally Cured Phthalcon/Epoxy Nanocomposite Coatings
The cross-linked epoxy coatings were prepared from a dispersion of Phthalcon particles in a dispersing medium; generally, to this dispersion prepolymer Epikote 828 and primary amine cross-linker were added (NH/epoxy molar ratio was 1:1). This mixture was then cast on a polycarbonate substrate using a doctor blade applicator. Finally, it was cross-linked at elevated temperature in vacuum and later post-cured in vacuum. Under these conditions smooth coatings were always obtained as long as the Phthalcon particle concentration in the starting formulation was below 13 vol. %.

UV Cured Phthalcon/Acrylate Nanocomposite Coatings
The Phthalcon/acrylate coatings were prepared starting from a dispersion of Phthalcon particles in an acrylate monomer; to this dispersion photoinitiator was added. This mixture was then cast on a polycarbonate substrate with a 10 μm coating thickness using a doctor blade applicator and cured by exposure to UV light under N_2 atmosphere for 2 min. Under these conditions smooth coatings were always obtained as long as the Phthalcon particle concentration in the starting formulation was below 7 vol. %.

1.5. Scope of this Thesis

The focus of this thesis is Phthalcon/thermoset thin layer coatings. The core chapters are dedicated to the factors determining the structure-electrical conductivity relations of these materials.

This thesis is structured as follows:

Chapter 2 gives brief background information on the conduction of charge transport, the mechanism of particle network formation and the characteristics of the particle network structure.

In *Chapter 3*, the synthesis of Phthalcon 11 particles is described. Results from extensive analyses are presented to prove the proposed molecular structure. A short summary of the crystal structure and the main properties of Phthalcon 11 are given as well.

Chapter 4 presents an in-depth study on the influence of Phthalcon particle size on the conductivity of cross-linked epoxy coatings. The synthesis of semi-conductive Phthalcon particles with various nanometer sizes is described in detail; two of them are new semi-conductive Phthalocyanine fillers (Phthalcon 12 and Phthalcon 11/12). The molecular and crystal structures, together with the sizes of these Phthalcon particles are characterized. The conductivity of the cross-linked epoxy matrices containing these Phthalcon particles is discussed concretely. Special attention is given to the influence of particle size and chemical composition on the characteristics of the particle network structures, on the way these networks are formed, and on the σ_v, σ_{max} and φ_c of the polymer composites.

Chapter 5 deals with a study concerning the influence of cross-linker and processing conditions on the conductivity of cross-linked Phthalcon 11/12/epoxy materials. Different cross-linking agents and curing temperatures are chosen. The log $\sigma_v - \varphi$ relation, the viscosity changes during cross-linking, the Phthalcon particle network structures in cross-linked coatings, how these particle networks are formed and to what extent they are influenced by the chosen cross-linker and processing conditions are discussed extensively. The impact of our findings on structure-electrical conductivity relations in other thermoset polymer matrices is also addressed.

Chapter 6 focuses on a more practical subject: how to realize conductivity and low surface energy in a single cross-linked Phthalcon 11/12/epoxy coating. The low surface energy is achieved by using a partially fluorinated amine cross-linker. The σ_v, the conductive particle network structures and distributions in these epoxy coatings are carefully examined. Variations in φ_c, σ_v, fractal particle network structure and Phthalcon-containing layer thickness are studied with respect to the amount of

fluorinated species present in the system.

As an extension to semi-conductive cross-linked Phthalcon/epoxy coatings, the influence of other factors on σ_v and Phthalcon particle network structures are demonstrated in *Chapter 7*. In this chapter the effects of post-cure, dispersing solvent and catalyst are studied.

In *Chapter 8* Phthalcon 11/12 particles are used as semi-conductive additive in UV cured acrylate coatings. The relation between the conductivity of these acrylate coatings and the amount of Phthalcon particles added is discussed. We particularly focus on the morphology of Phthalcon particle networks before and after cure, the fractal characteristics of the particle network structures and the mechanism of network formation. The results obtained from Phthalcon/acrylate coatings are also compared with those obtained from cross-linked epoxy coatings. Furthermore, the possibilities of using Phthalcon particles in other thermoset polymer matrices with different dispersing and processing conditions are discussed.

The final section, *Chapter 9*, highlights the most important conclusions described in this thesis. Suggestions for further work in the area of (semi)conductive filler/polymer nanocomposites are also given.

References

1. Judeinstein, P.; Sanchez, C. *J. Mater. Chem.* **1996,** 6, (4), 511-525.

2. Theng, B. K. G. *Clays. Clay. Miner.* **1970,** 18, (6), 357.

3. Editorial. *Plast. Addit. Compound.* **2002,** 4, (1), 30-33.

4. Chen, J. I.; Chareonsak, R.; Puengpipat, V.; Marturunkakul, S. *J. Appl. Polym. Sci.* **1999,** 74, (6), 1341-1346.

5. Beyer, G. *Plast. Addit. Compound.* **2002,** 4, (10), 22-28.

6. Godovsky, D. Y. *Adv. Polym. Sci.* **2000,** 153, 163-205.

7. van Bommel, M. J.; Groen, W. A.; van Hal, H. A. M.; Keur, W. C.; Bernards, T. N. M. *J. Mater. Sci.* **1999,** 34, (19), 4803-4809.

8. Kickelbick, G. *Prog. Polym. Sci.* **2003,** 28, (1), 83-114.

9. Skotheim, T. A.; Ed., *Handbook of Conducting Polymers, 2nd ed., Revised and Expanded*. Marcel Dekker: New York, 1997.

10. Karasek, L.; Sumita, M. *J. Mater. Sci.* **1996,** 31, (2), 281-289.

11. Brokken-Zijp, J. C. M.; Soloukhin, V. A.; Posthumus, W.; de With, G. *In Proceeding of 2003 Athens Conference on Coatings Science and Technology, Vouliagmeni, Greece.*

12. Kleinjan, W. E.; Brokken-Zijp, J. C. M.; van de Belt, R.; Chen, Z.; de With, G. *J. Mater. Res.* **2008,** 23, (3), 869-880.

13. Soloukhin, V. A.; Brokken-Zijp, J. C. M.; de With, G. *J. Polym. Sci. B* **2007,** 45, (16), 2147-2160.

14. Nalwa, H. S., *Handbook of Advanced Electronic and Photonic Materials and Devices*. Academic Press: London, 2000.

15. Chandrasekhar, P., *Conducting Polymers, Fundamentals and Applications: A Practical Approach*. Kluwer Academic: Dordrecht, 1999.

16. Gul, V. E., *Structure and Properties of Conducting Polymer Composites*. VSP: Utrecht, 1996.

17. Roldughin, V. I.; Vysotskii, V. V. *Prog. Org. Coat.* **2000,** 39, (2-4), 81-100.

18. Sumita, M.; Sakata, K.; Asai, S.; Miyasaka, K.; Nakagawa, H. *Poly. Bull.* **1991,** 25, (2), 265-271.

19. Banerjee, P.; Mandal, B. M. *Macromolecules* **1995,** 28, (11), 3940-3943.

20. Reghu, M.; Yoon, C. O.; Yang, C. Y.; Moses, D.; Heeger, A. J.; Cao, Y. *Macromolecules* **1993,** 26, (26), 7245-7249.

21. Fraysse, J.; Planes, J.; Dufresne, A.; Guermache, A. *Macromolecules* **2001,** 34, (23), 8143-8148.

22. Brandrup, J.; Immergut, E. H.; Grulke, E. A.; eds., *Polymer Handbook, 4th Edition*. John Wiley & Sons, 2003.

23. Huijbregts, L. J. *Charge Transport and Morphology in Nanofillers and Polymer Nanocomposites*. Ph.D. Thesis, Eindhoven University of Technology, Eindhoven, 2008.

24. Michels, M. A. J.; Brokken-Zijp, J. C. M.; Groenewoud, W. M.; Knoester, A. *Physica A* **1989,** 157, (1), 529-534.

25. Lux, F. *J. Mater. Sci.* **1993,** 28, (2), 285-301.

26. Slupkowski, T. *Phys. Stat. Sol.* **1984,** 83, (1), 329-333.

27. Yoshida, K. *J. Phys. Soc. Jpn.* **1990,** 59, 4087-4095.

28. Stauffer, D.; Aharony, A., *Introduction to Percolation Theory, 2nd ed.* Taylor & Francis: London, 1992.

29. Brokken-Zijp, J. C. M.; van Mechelen, J. B.; Emeis, C. A.; Datema, K. P.; Kramer, A. H.; de Bruijn, D. P.; Meruma, A. J. *US Patent 05319009* **1993**.

30. Brokken-Zijp, J. C. M.; van Mechelen, J. B.; Emeis, C. A.; Datema, K. P.; Kramer, A. H.; de Bruijn, D. P.; Meruma, A. J. *WO 9324562 A1, Eur. Patent 642547* **1992**.

31. Levon, K.; Margolina, A.; Patashinsky, A. Z. *Macromolecules* **1993,** 26, (15), 4061-4063.

32. Adriaanse, L. J.; Faneyte, I. P.; Martens, H. C. F.; Reedijk, J. A.; Brom, H. B.; Michels, M. A. J.; Brokken-Zijp, J. C. M. *Synth. Met.* **1997,** 84, (1-3), 871-872.

33. Chen, Z.; Brokken-Zijp, J. C. M.; Huinink, H. P.; Loos, J.; de With, G.; Michels, M. A. J. *Macromolecules* **2006,** 39, (18), 6115-6124.

34. Chen, Z.; Brokken-Zijp, J. C. M.; Michels, M. A. J. *J. Polym. Sci. B* **2006,** 44, (1), 33-47.

35. Yuan, M.; Brokken-Zijp, J. C. M.; Huijbregts, L. J.; de With, G. *J. Polym. Sci. B* **2008,** 46, 1079-1093.

36. Brokken-Zijp, J. C. M.; Yuan, M.; et.al. *"Synthesis and Structure of Novel Aquocyanophthalocyaninato Co(III) Semi-conductor and Its Applications in Conductive Polymer Composites"*. In Preparation.

2

THEORETICAL BACKGROUND

2.1. Introduction

This chapter gives background information that is most frequently applied in this thesis. This information will be discussed in more detail in different chapters, and they are essential to understand the obtained results and proposed explanations. However, it is beyond the scope of this thesis to discuss how this background information is deduced. Therefore, only the most important theories are summarized. Published results on cross-linked Phthalcon 11/epoxy coatings are briefly reviewed as well.

2.2. Statistical Percolation Models

Conductive polymer composites have attracted extensive scientific activity because of the possibility to combine electrical conductivity of the additives with good mechanical properties and fabrication versatility of the polymer matrices. However, the main question concerning these mixtures is how to explain the dramatic increase in conductivity, i.e., the insulating-conductive transition at percolation threshold φ_c (Figure 1.1). To understand this electrical percolation phenomenon, many so-called percolation models have been published.[1] Among them statistical percolation models have occupied the majority of the literature, although the classical percolation theory was not concerned with the electrical conductivity in binary mixtures.[2-13] The breakthrough of the statistical percolation models in the area of conductive binary mixtures was made in the early 1970s, especially stimulated by the work of Kirkpatrick and Zallen.[2,3]

Classical Statistical Percolation Model-The Model of Kirkpatrick and Zallen
To obtain an estimate of φ_c, according to the considerations of Kirkpatrick and Zallen, one usually starts with finite regular arrays of points and bonds (between the points). Then, the points or bonds are randomly added to the system. The next step is to determine whether the existing points or bonds are in contact with each other. It is

easy to realize that in this model the percolation point, which depends on the considered dimensionality, is reached when the occupied sites (bonds or points) first spans the relevant boundaries of the underlying array.

Equation (2.1) correlates the conductivity σ of real mixtures with the volume fraction φ of the conductive filler for $\varphi > \varphi_c$

$$\sigma = \sigma_0(\varphi - \varphi_c)^t \tag{2.1}$$

where σ_0 is the conductivity of the filler particle and t is the critical exponent which determines how fast σ increases above φ_c.

This model predicts that for randomly distributed non-overlapping hard spheres φ_c is 16 vol. %. This model also predicts a universal conductivity exponent t that depends only on the dimensionality D ($t = 2$ for 3-dimensional lattices) when all bonds have the same conductance. However, when there is a (large) spread in conductance of the bonds, t differs from 2. The non-universal behaviour with $t \neq 2$ has been studied in detail both experimentally[14-16] and theoretically.[17-21] In these studies a t value between 2 and the order of 10 has been reported.

2.3. Approaches to Achieve Semi-conductive Polymer Composites with a Low φ_c

A crucial aspect in the preparation of semi-conductive polymer composites is the filler concentration φ. The value for φ must be as low as possible but still allow the composite to fulfil its conductivity requirements, which means that the conductive particles must form a continuous particle network through the polymer matrix. Therefore, many efforts have been devoted to achieve semi-conductive polymer composites with a low φ_c.

2.3.1. Selectively Localized Conductive Fillers in Multiphase Polymer Blend

An effective way to reduce φ_c is to favour a local inhomogeneity in the material, such as using a two-phase polymer blend as polymer matrix. If one of the two polymer phases is continuous and the conductive particles are localized in the continuous phase or the two phases are co-continuous and the filler particles localize preferably in the minor phase or at the interface, φ_c can be reduced well below 16 vol. %.[22-26]

2.3.2. Using Conductive Fillers with a High Aspect Ratio

A random distribution of filler particles with a high aspect ratio through a polymer matrix can also lead to a continuous conductive network at a much lower φ_c.[27-29] A well-known example of such a filler material is given by carbon nanotubes/fibers.[28-32]

2.3.3. Form Fractal Particle Network

A low φ_c can also be created using fillers with a low aspect ratio by forming a fractal particle network through the polymer matrix.[33-36] The characteristic of a fractal structure is that it displays self-similarity on different length scales. Approximate fractals are easily found in nature. Examples include snowflakes and broccoli. These objects display a self-similar structure over an extended, but finite scale range. The mandelbrot set, a set of points in a plane (Figure 2.1), is a famous example of a fractal structure. Figure 2.1 shows that after 2000 times magnification the remaining structure still resembles the original one.
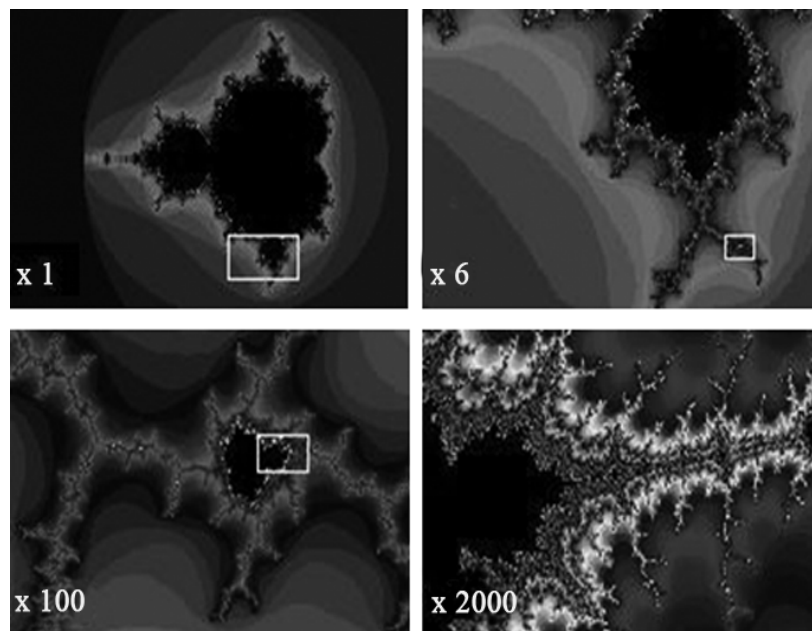
Figure 2.1. The Mandelbrot set is a famous example of a fractal structure. Even after 2000 times magnification the remaining structure still resembles the original one.

One of the earliest reports on the fractal structure in polymer composites is for a carbon black particle network.[35,36] Figure 2.2 shows a carbon black (CB) particle network structure in BF3-400 cross-linked Epoxy composites.[35] Fractal structure analyses show that the particle networks in Figure 2.2a (optical microscopic image on

a 10 μm thick sample), Figure 2.2b (optical microscopic image on a 0.1 μm thick sample) and Figure 2.2c (TEM image on a 0.1 μm thick sample) have the same fractal dimension. The hollow-sphere-like CB particle has a diameter of about 50 nm. However, because of the self-similarity, the formed fractal particle network has a large correlation length ξ (the average size of the building block from which the network is formed). Hence, the fractal particle network is visible under the OM. The same fractal dimension obtained for the various images in Figure 2.2 suggests that it is possible to use OM to analysis fractal particle networks as long as the correlation length is sufficiently large.
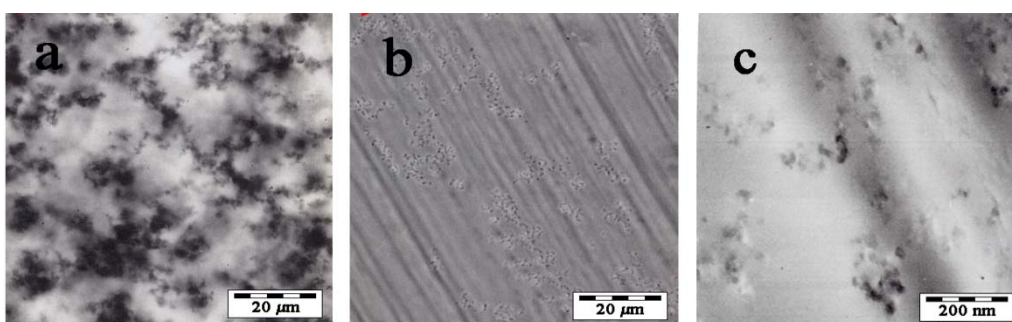
Figure 2.2. A fractal carbon black particle network formed in a BF3-400 cross-linked epoxy coating.[35] (a) optical microscopic image on a 10 μm thick sample; (b) optical microscopic image on a 0.1 μm thick sample; (c) TEM image on a 0.1 μm thick sample. Fractal structure analyses using tiling method show that these carbon black particle networks have the same fractal dimension ($d_f = 1.64$).
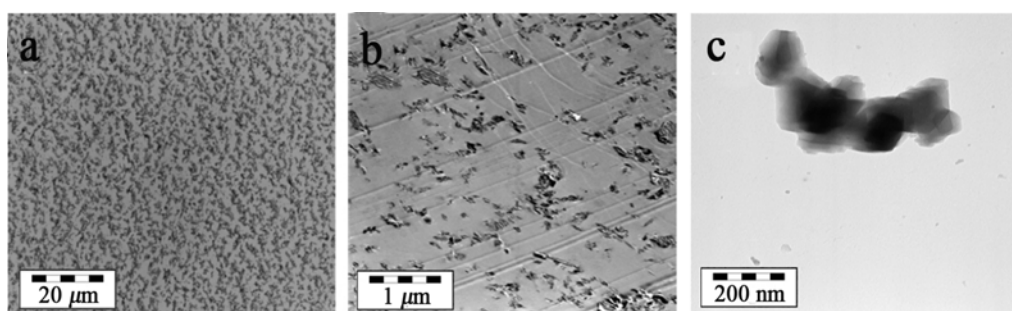
Figure 2.3. A fractal Phthalcon particle network formed in a Jeffamine D230 cross-linked epoxy coating. (a) OM image; (b) TEM image; (c) TEM image of primary Phthalcon particle aggregates. Fractal structure analyses using tiling method show that the Phthalcon particle networks in Figure 2.3a & 2.3b have the same fractal dimension ($d_f = 1.77$).[37]

Due to self-similarity, a fractal particle network is ramified. This means that particles do not have to fill up the entire space to form a continuous particle network. Hence, a percolating network arises at a φ_c much lower than 16 vol. %. These fractal particle networks are generally formed by Brownian movement of the initially well-dispersed particles before/during processing when the initial effective Hamaker constant A_H^{eff} of the system is large (see later discussion).[37-43]

It has been shown that Phthalcon particle networks are always present in Phthalcon/polymer composites.[37,38,40,43] Like for carbon black, a Phthalcon particle network is also fractal.[37,38,40,43] Figure 2.3 shows a fractal Phthalcon particle network formed through a Jeffamine D230 cross-linked epoxy coating.[37] Fractal structure analyses reveal that the Phthalcon particle networks in Figure 2.3a (optical microscopic image) and Figure 2.3b (TEM image) have the same fractal dimension.[37] In this thesis, we focus on Phthalcon/polymer nanocomposites with a low φ_c due to the presence of a fractal particle network.

2.3.4. Other Approaches

Besides above mentioned methods, conductive polymer composites with a low φ_c can also be achieved by, for instance, using intrinsic conductive polymer particles,[44-47] in-situ synthesis of conducting polymers in a thermoplastic or elastomer matrix,[48,49] or using particles with a small conductive layer.[50]

2.4. Mechanism of Fractal Particle Network Formation

2.4.1. Diffusion Limited Cluster Aggregation

As has been discussed before, the presence of a fractal particle network can dramatically reduce the φ_c of conductive polymer nanocomposites containing spherical particles. In principle, there are many ways to construct fractal networks. Among them an important mechanism is Diffusion Limited Cluster Aggregation (DLCA).[51] In DLCA, particles move by diffusive motion. Once meeting, they irreversibly stick to each other, forming a particle aggregate. Because particles immediately stick once they touch, the collisions mainly take place at their exteriors. Therefore, the resulting aggregates have a ramified structure with a low density. Simulations[52-54] and experiments[55] reveal that in a 3-dimensional system aggregates formed by this mechanism have a fractal dimension d_f of 1.75.

2.4.2. Reaction Limited Cluster Aggregation

A mechanism opposed to DLCA is Reaction Limited Cluster Aggregation (RLCA).[51] Unlike DLCA, in RLCA particles collide many times before they finally stick together. In another word, in RLCA the diffusion time, which is the interval between two collisions, does not form the bottleneck in the formation of the aggregates; the "reaction time", at which a (new) aggregate is eventually formed, is the decisive factor. As a consequence, particles statistically penetrate each other before they get stuck, leading to denser aggregates with a higher value of d_f. In 3-dimensional system, the d_f of aggregates formed by RLCA is 2.10.[54]

2.4.3. Relaxation of Particle Network

Aggregates formed by an aggregation process, either by DLCA or RLCA, may be subject to relaxation.[56] The effect of relaxation, among others, depends on the particle concentration φ, pH, temperature and chemical composition of the system.[56] Theoretical simulation on specific gel aggregates shows that during relaxation the side chains on the backbone can fold or rearrange, resulting in denser aggregates with a reduced d_f value (Figure 2.4).[56] Note the above described change in aggregate structure is called "ageing" in reference [56]. However, we think it is more appropriate to address this effect as "relaxation", because the aggregates/networks change from a non-equilibrium condition to an equilibrium state, or at least close to an equilibrium state.
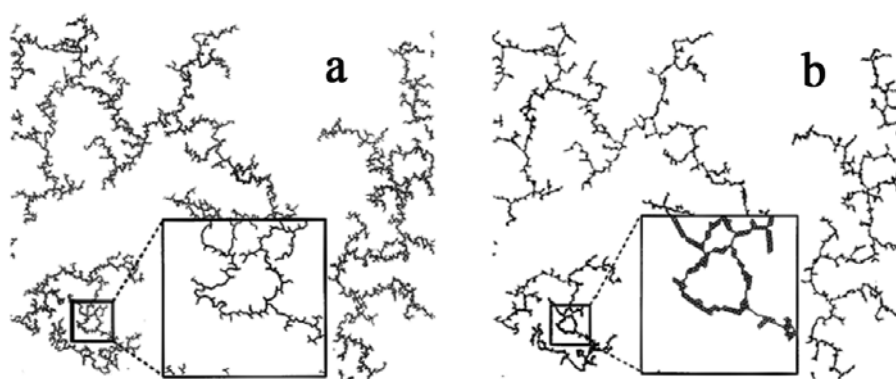
Figure 2.4. Theoretical simulation on specific gel aggregates. (a) non-relaxed aggregates (d_f = 1.42, 2D system); (b) aggregates after relaxation (d_f = 1.32, 2D system). A denser aggregate is obtained as a result of relaxation.[56]

2.5. Phthalcon Particle Network Structure and Mechanism of Network Formation in Cross-linked Epoxy Coatings

2.5.1. Phthalcon Particle Distribution in the Starting Dispersion

The chosen dispersing medium and dispersing method have large influences on the nanoparticle distribution.[38,40,41,57,58] The nanoparticle dispersion is generally made in a dispersing medium under high shear conditions, and then (part of) the coating components are added into the dispersion under low shear conditions. Finally the coating formulation is cured to obtain the composite material.

It has been shown that for Phthalcon 11 particles, even under low shear mixing conditions, the addition of coating components to the starting dispersion may influence considerably the particle distribution.[38] This has been explained by the differences in particle-medium interactions.[38] Phthalcon 11 primary particles are highly crystalline nanometer-sized flat plates. The surface groups at the bottom and the top of the plate are -OH/H_2O and -CN, whereas the surface groups at the sidewalls are phenyl rings.[38] The presence of -OH/H_2O and phenyl groups in the dispersing medium may interact strongly with the surface groups of Phthalcon 11 particles and may, therefore, influence the particle distribution.

Phthalcon 11 particles can be relatively easily dispersed in a number of polar solvents, such as *m*-cresol, ethylene glycol and *n*-methylpyrolidone, because of the specific interactions between Phthalcon and (some of) the active groups in the solvent. Hence, in the past *m*-cresol was often used as dispersing solvent. When a combination of magnetic and ultrasonic mixing is applied, a dispersion containing well-dispersed Phthalcon 11 particles/aggregates is obtained.[37,38] The fractal Phthalcon particle network can also be formed from a Phthalcon/Jeffamine D230 starting dispersion.[38] Although interactive groups in Jeffamine D230 are less present, Phthalcon particle agglomerates could still be broken down and fractal aggregates are observed.[38]

Besides these interactions, the particle-particle interactions should also be taken into account to explain the differences observed in different dispersions. The Gibbs energy of attraction per unit area between two flat surfaces separated by a distance *H* can be described as:[59]

$$\Delta G^{att} = - A_H / (12\pi H^2) \qquad (2.2)$$

where A_H is the Hamaker constant. Surfaces interacting through an intervening fluid medium will experience a reduced mutual attraction due to the presence of the third component.[60] In this case, the Hamaker constant in Equation (2.2) should be replaced by an effective Hamaker constant $A_H{}^{eff}$, which is approximated by:[61]

$$A_H^{eff} = \left[A_{Hp}^{1/2} - A_{Hm}^{1/2}\right]^2 \tag{2.3}$$

where A_{Hp} and A_{Hm} are the Hamaker constants of particle and medium in vacuum, respectively. When the Hamaker constants of particle and dispersing medium are equal in values, the $A_H{}^{eff}$ tends towards zero, and the energy of attraction between particles tends to reduce to zero. This favours the random distribution of well-separated particles in the medium. Likewise, the presence of a large $A_H{}^{eff}$ results in a higher energy of attraction between particles and particles tend to aggregate/agglomerate in order to lower the interfacial energy between particle and medium.

The difference in surface energies between particle and matrix influences the aggregate structure in a similar way as the Hamaker constant.[58] The reason is that except for highly polar hydrogen bonding liquid, such as water, the Hamaker constant A_H and the surface energy γ can be related through a simple formula:[62]

$$A_H \approx a\gamma \tag{2.4}$$

In this equation, $a \approx 2.1 \times 10^{-21}$ m^2, γ is in J/m^2 and A_H is in J. Equation (2.4) can be transformed into:

$$A_H^{eff} \approx a\left[\gamma_p^{1/2} - \gamma_m^{1/2}\right]^2 \approx 2.1 \times 10^{-21} \left[\gamma_p^{1/2} - \gamma_m^{1/2}\right]^2 \tag{2.5}$$

where γ_p and γ_m are the surface energies of particle and medium surrounding the particle, respectively.

Therefore, neglecting hydrogen bonding, it is possible to use experimentally determined surface energies to estimate the particle-particle and particle-medium interactions. When the surface energies of particle and medium are similar, the $A_H{}^{eff}$ tends towards zero; this facilitates the easy dispersion of particles and initially well-dispersed particles/aggregates may remain stable in the dispersing medium. When the difference between the surface energies of particle and medium is large, particles are much more difficult to disperse, and even after separation particles tend

to aggregate/agglomerate over time to reduce the interfacial energy. Note the words particle aggregation and agglomeration may have different definitions in the literature. In this thesis aggregation means direct mutual attraction between particles via van der Waals forces or chemical bonding; while agglomeration means coarse accumulation of large blocks of aggregates.

It is important to realize that, in general, nanometer-sized particles are much more difficult to disperse as compared to micrometer-sized particles under standard high shear conditions. Often the use of ultrasonic mixing offers better possibilities to disperse these particles. However, the mixing efficiency is very sensitive to small changes, such as actual energy input, the amount of solvent present and the size and shape of the dispersing vessel used.

When Phthalcon particles are dispersed in *m*-cresol, the very strong specific particle-medium interactions make it possible to break down the large agglomerates into (almost completely) separated submicrometer-sized particles/aggregates, and the relatively small A_H^{eff} ensures that the initially well-dispersed Phthalcon particles/aggregates remain stabilized in the dispersing solvent. The Phthalcon particle distribution in the dispersion, at least on an optical microscopic scale, does not change with the addition of Epikote 828 prepolymer and Jeffamine D230 cross-linker.[38]

2.5.2. Curing of Thermoset Matrix

Usually epoxy resins are cured by the use of multi-functional amines which undergo polyaddition reaction with the terminal epoxide groups in the manner indicated in Scheme 2.1.[63] Due to the use of multi-functional amines and epoxy resins, as the reaction proceeds further, branching reactions lead ultimately to the formation of complex network structures. Free-radical polymerization, on the other hand, is the most widely practised method and is used exclusively for the preparation of polymers. In common, the reaction can be divided into three distinct stages: initiation, propagation and termination as indicated in Scheme 2.2.[64]

For a specific Phthalcon/epoxy starting formulation, using Epikote 828 as epoxy prepolymer and Jeffamine D230 as primary amine, during cross-linking the two epoxy groups of Epikote 828 react with the two primary amine groups of Jeffamine D230, and ultimately form a three dimensional polymer network. Meanwhile, the solvent, if present, also starts to evaporate during cross-linking. As a consequence,

both the particle-particle and particle-matrix interactions change, and the particles tend to aggregate as long as the Brownian motion is sufficiently large and the viscosity of the system is sufficiently low. It has been shown that after cure fractal Phthalcon particle networks formed either from Phthalcon/*m*-cresol dispersions or Phthalcon/Jeffamine D230 dispersions are present through the matrix.[38] The results presented earlier suggest that these Phthalcon particle networks are formed during cure by DLCA.[37,65]
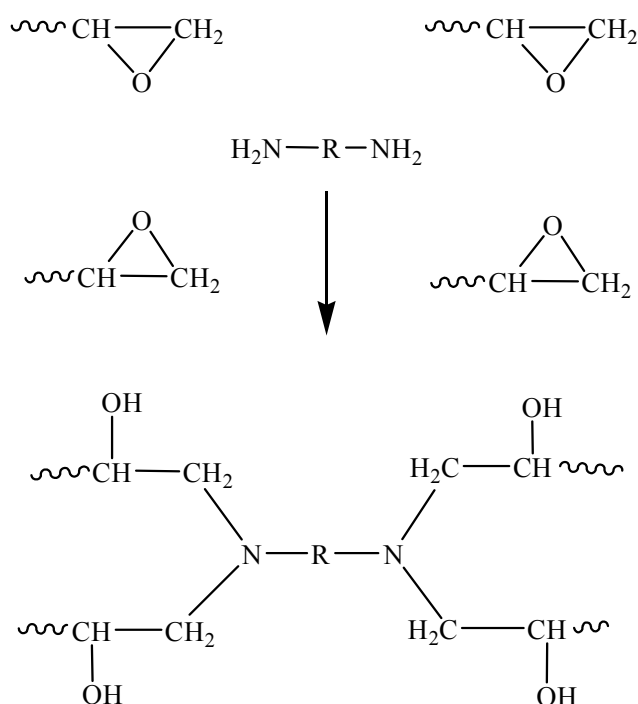
Scheme 2.1. Reactions between epoxy and cross-linker amine.
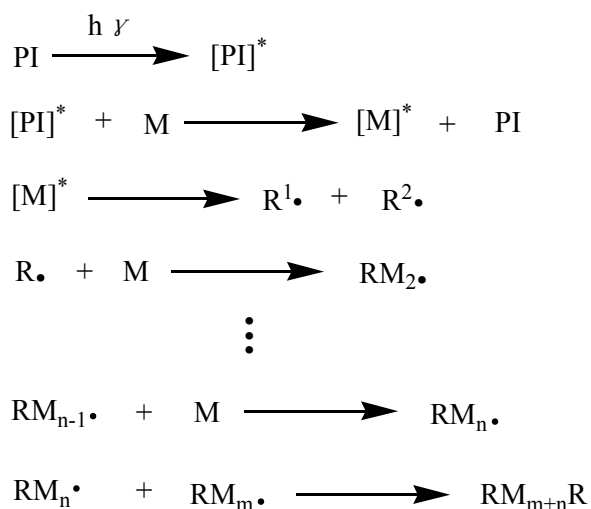
Scheme 2.2. Free-radical polymerization.

2.6. Proposed Model

To understand the relation between the structure of the Phthalcon particle network and the conductivity σ_v of the composite at different filler concentrations, a 12 vol. % cross-linked Phthalcon 11/epoxy coating cured with Jeffamine D230 was studied in detail.[37,38,51,66,67] Conductive AFM measurements combined with DC and AC conductivity measurements over a broad range of temperatures and frequencies on this coating, together with conductivity measurements on Phthalcon 11 powder suggest that in this coating Phthalcon particles really touch each other and there is no polymer matrix between the touching particles in the conducting network. These results also suggest that the most likely conduction mechanism in the particle network is variable-range hopping by cotunnelling.[51,66,67] Based on these conclusions, meanwhile taking into account the specific characteristics of fractal Phthalcon particle network, a upper-limit model was proposed on the log σ_v - φ relation for (semi)conductive filler/polymer nanocomposites.[51,66] This model not only explains the low φ_c value, but also explains the much lower σ_{max} obtained in polymer composites as compared to the intrinsic conductivity of the filler itself, even when no insulating matrix is present between particles in the network. Furthermore, this model quantitatively predicts the σ_{max} as a function of filler concentration φ for such materials.

The proposed model has following assumptions:
- ❖ The conductive particles are spherical and equal in size (with a radius R_p) and intrinsic conductivity σ_p;
- ❖ The particle aggregates are formed by DLCA and are equal in size and structure;
- ❖ The particle aggregates are placed randomly through the matrix and are impermeable;
- ❖ The conductive particle network structure is optimum in the sense that the neighbouring particles inside an aggregate always touch, and the aggregates are rotated in such a way that the particles in adjacent aggregates touch each other as well; Touching means no insulating matrix material present between particles in the network;
- ❖ In the nanocomposite the mobility of charge carriers inside the filler particles and between the contacting particles is equal to that in the compressed powder;
- ❖ The contribution of tunnelling between particles that do not touch each other is negligible; the influence of loops, dangling chains and isolating particle aggregates are negligible as well; and

❖ The matrix is a perfect insulator with a conductivity of 0.

A schematic picture of the particle network according to this model is shown in Figure 2.5.[51,66] The aggregates are (more or less spherical) building blocks from which percolation theory holds, therefore, they have a φ_c of 16 vol. %. As these building blocks are not completely filled with particles, the φ_c of the particles in the polymer matrix is low.
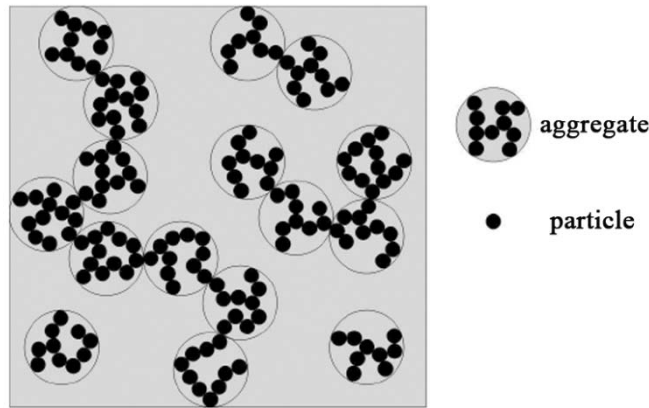
Figure 2.5. A schematic drawing of a random percolating network formed by fractal particle aggregates.[51,66]

The resulting model has the form:

$$\frac{\sigma_{max}}{\sigma_p} = 0.23 \left(\frac{\varphi_{p,c}}{0.16}\right)^{1+d_w-d_f/(3-d_f)} \tag{2.6}$$

where σ_{max} is the maximum volume conductivity of the polymer nanocomposite, σ_p is the volume conductivity of the compressed conductive particle powder, $\varphi_{p,c}$ is the percolation threshold of the particle, d_w is the so-called "random-walk dimension" and d_f is the fractal dimension of the particle aggregates.[51,66]

In general $d_w \geq 2$ holds, which gives the exponent in Equation (2.6) a value larger than 1. Hence, the relation between σ_{max} and $\varphi_{p,c}$ is supralinear. The influence of $\varphi_{p,c}$ on σ_v of the polymer composite (normalized by σ_p) as a function of volume fraction of particles φ_p and volume fraction of particle aggregates φ_a is shown in Figure 2.6. In Figure 2.6a the σ_v starts from $\varphi_{a,c} = 0.16$ and the model holds till $\varphi_a = 0.64$ which corresponds to the randomly close packing of spherical particle aggregates. Figure

2.6b is obtained from Figure 2.6a. It shows that, the lower $\varphi_{p,c}$, the lower $\sigma_{max,}$ and the lower φ_p at which the material reaches its σ_{max}.

In cross-linked Phthalcon/epoxy coatings, the σ_p of compressed Phthalcon powder is 4 x 10^{-4} S/cm and the φ_c is 0.55 vol. %. The proposed model predicts that a σ_{max} of 10^{-7} S/cm is reached at a filler concentration of 2.4 vol. %. However, the experimental results show that this σ_{max} is only reached at a much higher Phthalcon concentration (10 vol. %). This contradiction will be discussed in Chapter 5.
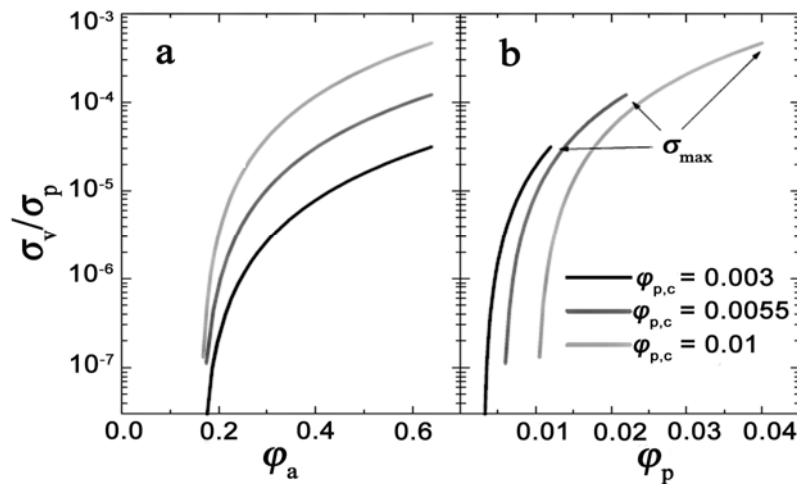
Figure 2.6. Normalized σ_v as a function of φ_a (a) and φ_p (b) for several values of $\varphi_{p,c}$. For the calculations, $1 + d_w - d_f = 2.25$ was used, which is in good agreement with aggregates formed by DLCA. In addition, d_f value of 1.75 was used.[37,51]

References

1. Lux, F. *J. Mater. Sci.* **1993,** 28, (2), 285-301.

2. Zallen, R., *The Physics of Amorphous Solids*. Wiley: New York, 1983.

3. Kirkpatrick, S. *Rev. Mod. Phys.* **1973,** 45, (4), 574-588.

4. Scarsbrick, R. M. *J. Phys. D* **1973,** 6, 2098-2110.

5. Bueche, F. *J. Appl. Phys.* **1972,** 43, (11), 4837-4838.

6. Janzen, J. *J. Appl. Phys.* **1975,** 46, (2), 966-969.

7. Pike, G. E.; Seager, C. H. *Phys. Rev. B* **1974,** 10, (4), 1421-1434.

8. Seager, C. H.; Pike, G. E. *Phys. Rev. B* **1974,** 10, (4), 1435-1446.

9. Quan, X. *J. Polym. Sci. B* **1987,** 25, (7), 1551-1560.

10. Etemad, S.; Quan, X.; Sanders, N. A. *Appl. Phys. Lett.* **1986,** 48, (9), 607-609.

11. Yamaki, J. I.; Maeda, O.; Katayama, Y. *Rev. Elec. Commun. Lab.* **1978,** 26, (3-4), 616-628.

12. Aharoni, S. M. *J. Appl. Phys.* **1972,** 43, (5), 2463-2465.

13. Gurland, J. *Trans. Met. Soc. AIME* **1966,** 236, (5), 642.

14. Lee, S. I.; Song, Y.; Noh, T. W.; Chen, X. D.; Gaines, J. R. *Phys. Rev. B* **1986,** 34, (10), 6719-6724.

15. Fabreguette, F.; Maglione, M.; Clerc, J. P.; Bourgeois, S.; Sacilotti, M. *J. Phys.: Condens. Matter* **2002,** 14, (34), 7911-7917.

16. Lu, W.; Lin, H. F.; Chen, G. H. *J. Polym. Sci. B* **2006,** 44, (13), 1846-1852.

17. Kogut, P. M.; Straley, J. P. *J. Phys. C* **1979,** 12, (11), 2151-2159.

18. Grimaldi, C.; Balberg, I. *Phys. Rev. Lett.* **2006,** 96, (6), 066602-4.

19. Balberg, I. *Phys. Rev. B* **1998,** 57, (21), 13351-13354.

20. Grimaldi, C.; Maeder, T.; Ryser, P.; Strassler, S. *Phys. Rev. B* **2003,** 68, (2), 024207-7.

21. Johner, N.; Ryser, P.; Grimaldi, C.; Balberg, I. *Phys. Rev. B* **2007,** 75, (10), 104204-9.

22. Sumita, M.; Sakata, K.; Hayakawa, Y.; Asai, S.; Miyasaka, K.; Tanemura, M. *Colloid Polym. Sci.* **1992,** 270, (2), 134-139.

23. Sumita, M.; Abe, H.; Kayaki, H.; Miyasaka, K. *J. Macromol. Sci., Phys.* **1986,** B25, (1-2), 171-184.

24. Tchoudakov, R.; Breuer, O.; Narkis, M.; Siegmann, A. *Polym. Eng. Sci.* **1996,** 36, (10), 1336-1346.

25. Tchoudakov, R.; Breuer, O.; Narkis, M.; Siegmann, A. *Polymer Networks & Blends* **1996,** 6, (1), 1-8.

26. Gubbels, F.; Blacher, S.; Vanlathem, E.; Jerome, R.; Deltour, R.; Brouers, F.;

Teyssie, P. *Macromolecules* **1995,** 28, (5), 1559-1566.

27. Zhang, Q. H.; Jin, H. F.; Wang, X. H.; Jing, X. B. *Synth. Met.* **2001,** 123, (3), 481-485.

28. Thongruang, W.; Balik, C. M.; Spontak, R. J. *J. Polym. Sci. B* **2002,** 40, (10), 1013-1025.

29. Lee, S. B.; Katayama, T.; Kajii, H.; Araki, H.; Yoshino, K. *Synth. Met.* **2001,** 121, (1-3), 1591-1592.

30. Chen, Q.; Xi, Y.; Bin, Y.; Matsuo, M. *J. Polym. Sci. B* **2008,** 46, (4), 359-369.

31. Feller, J. F.; Linossier, I.; Grohens, Y. *Mater. Lett.* **2002,** 57, (1), 64-71.

32. Zhang, W.; Dehghani-Sanij, A. A.; Blackburn, R. S. *J. Mater. Sci.* **2007,** 42, (10), 3408-3418.

33. Roldughin, V. I.; Vysotskii, V. V. *Prog. Org. Coat.* **2000,** 39, (2-4), 81-100.

34. Adriaanse, L. J.; Reedijk, J. A.; Teunissen, P. A. A.; Brom, H. B.; Michels, M. A. J.; Brokken-Zijp, J. C. M. *Phys. Rev. Lett.* **1997,** 78, (9), 1755-1758.

35. Michels, M. A. J.; Brokken-Zijp, J. C. M.; Groenewoud, W. M.; Knoester, A. *Physica A* **1989,** 157, (1), 529-534.

36. van der Putten, D.; Moonen, J. T.; Brom, H. B.; Brokken-Zijp, J. C. M.; Michels, M. A. J. *Phys. Rev. Lett.* **1992,** 69, (3), 494-497.

37. Chen, Z.; Brokken-Zijp, J. C. M.; Huinink, H. P.; Loos, J.; de With, G.; Michels, M. A. J. *Macromolecules* **2006,** 39, (18), 6115-6124.

38. Chen, Z.; Brokken-Zijp, J. C. M.; Michels, M. A. J. *J. Polym. Sci. B* **2006,** 44, (1), 33-47.

39. Kleinjan, W. E.; Brokken-Zijp, J. C. M.; van de Belt, R.; Chen, Z.; de With, G. *J. Mater. Res.* **2008,** 23, (3), 869-880.

40. Brokken-Zijp, J. C. M.; Soloukhin, V. A.; Posthumus, W.; de With, G. *In Proceeding of 2003 Athens Conference on Coatings Science and Technology, Vouliagmeni, Greece.*

41. Soloukhin, V. A.; Brokken-Zijp, J. C. M.; de With, G. *J. Polym. Sci. B* **2007,** 45, (16), 2147-2160.

42. Brokken-Zijp, J. C. M.; Noordam, A.; Groenewoud, W. M.; Klaren, C. H. J. *Eur. Patent 0370586* **1989**.

43. Brokken-Zijp, J. C. M.; van Mechelen, J. B.; Emeis, C. A.; Datema, K. P.; Kramer, A. H.; de Bruijn, D. P.; Meruma, A. J. *US Patent 05319009* **1993**.

44. Cao, Y.; Smith, P.; Heeger, A. J. *Synth. Met.* **1993,** 57, (1), 3514-3519.

45. Cao, Y.; Smith, P.; Heeger, A. J. *Synth. Met.* **1992,** 48, (1), 91-97.

46. Yoon, C. O.; Reghu, M.; Moses, D.; Cao, Y.; Heeger, A. J. *Synth. Met.* **1995,** 69,

(1-3), 255-258.

47. Yang, J. P.; Rannou, P.; Planes, J.; Pron, A.; Nechtschein, M. *Synth. Met.* **1998,** 93, (3), 169-173.

48. Chakraborty, M.; Mukherjee, D. C.; Mandal, B. M. *Synth. Met.* **1999,** 98, (3), 193-200.

49. Randriamahazaka, H.; Vidal, F.; Dassonville, P.; Chevrot, C.; Teyssie, D. *Synth. Met.* **2002,** 128, (2), 197-204.

50. Ouyang, M.; Chan, C. M. *Polymer* **1998,** 39, (10), 1857-1862.

51. Huijbregts, L. J. *Charge Transport and Morphology in Nanofillers and Polymer Nanocomposites*. Ph.D. Thesis, Eindhoven University of Technology, Eindhoven, 2008.

52. Jullien, R.; Kolb, M.; Botet, R. *J. Phys. Lett.* **1984,** 45, (5), L211-L216.

53. Meakin, P. *Phys. Lett. A* **1985,** 107, (6), 269-272.

54. Lachhab, M.; Gonzalez, A. E.; BlaistenBarojas, E. *Phys. Rev. E* **1996,** 54, (5), 5456-5462.

55. Weitz, D. A.; Huang, J. S.; Lin, M. Y.; Sung, J. *Phys. Rev. Lett.* **1984,** 53, (17), 1657-1660.

56. van Garderen, H. F.; Dokter, W. H.; Beelen, T. P. M.; van Santen, R. A.; Pantos, E.; Michels, M. A. J.; Hilbers, P. A. J. *J. Chem. Phys.* **1995,** 102, 480-496.

57. Karasek, L.; Sumita, M. *J. Mater. Sci.* **1996,** 31, (2), 281-289.

58. Sumita, M.; Sakata, K.; Asai, S.; Miyasaka, K.; Nakagawa, H. *Poly. Bull.* **1991,** 25, (2), 265-271.

59. Viswanathan, R.; Heaney, M. B. *Phys. Rev. Lett.* **1995,** 75, (24), 4433-4436.

60. Hamaker, H. C. *Physica* **1937,** 4, 1058.

61. Myers, D., *Surfaces, Interfaces, and Colloids; 2nd ed.* Wiley-VCH: New York, 1999.

62. Israelachvili, J. N., *Intermolecular and Surface Forces, Second Edition: With Applications to Colloidal and Biological Systems (Colloid Science)* Academic: London, 1992.

63. Henry Lee, K. N., *Handbook of Epoxy Resins*. Mcgraw-Hill: Texas, 1981.

64. Mehnert, R.; Pincus, A.; Janorsky, I.; Stowe, R.; Berejka, A., *UV & EB Curing Technology & Equipment*. Wiley & Sons: London, 1998; Vol. I.

65. Yuan, M.; Brokken-Zijp, J. C. M.; Huijbregts, L. J.; de With, G. *J. Polym. Sci. B* **2008,** 46, 1079-1093.

66. Huijbregts, L. J.; Brom, H. B.; Brokken-Zijp, J. C. M.; Kemerink, M.; Chen, Z.; de Goeje, M. P.; Yuan, M.; Michels, M. A. J. *J. Phys. Chem. B* **2006,** 110, (46),

23115-23122.

67. Huijbregts, L. J.; Brom, H. B.; Brokken-Zijp, J. C. M.; Yuan, M.; Michels, M. A. J. *Phys. Stat. Sol.* **2006,** 3, 259-262.

3

SYNTHESIS, STRUCTURE AND PROPERTIES OF AQUOCYANOPHTHALOCYANINATO CO(III) PHTHALCON 11[⊛]

SYNOPSIS

The synthesis, molecular and crystal structure of Phthalcon 11 are described in this chapter. Detailed studies on the structure of Phthalcon 11 and its precursor compounds show that Phthalcon 11 is a neutral molecule with H_2O and CN ligands axially bonded to the Co(III) of the phthalocyanine ring. In the crystal one of the hydrogen atoms from the H_2O ligand forms a hydrogen bond with the N atom of the CN group from the neighboring Phthalcon 11 molecule in the stack, resulting in an intermolecular polymeric structure with the van der Waals distance of about 3.35 Å between these phthalocyanine rings.

Phthalcon 11 is stable and almost monocrystalline platelet-shaped particle. The material is semi-conductive with a band gap of about 1.2 eV. The groups at the surface of the particle are likely to be -OH/H_2O, -CN and phenyl.

⊛ The content of this chapter will be submitted as an article: Brokken-Zijp, J. C. M.; Yuan, M.; et al. *"Synthesis and Structure of Novel Aquocyanophthalocyaninato Co(III) Semi-conductor and Its Applications in Conductive Polymer Composites"*.

3.1. Introduction

Conductive polymer composites are, in general, made by incorporation of conductive fillers into an insulating polymer matrix. It is widely accepted that the conductivity of these polymer composites is based on the presence of a continuous network of (touching) filler particles throughout the matrix.[1-4] The main problem involved in practice is that generally a large amount of conducting filler is required in order to achieve an increase in the volume conductivity. This large amount of filler deteriorates the mechanical properties and leads to poor processability of the matrix. Furthermore, the cost of the final material is often beyond the acceptable range due to the heavy fraction of the expensive conducting species.[5]

It has been shown that for specific (semi)conductive nanofillers the percolation threshold φ_c, at which a continuous particle network is formed throughout the polymer matrix, can be below 1 vol. %.[1,5-13] A specific class of phthalocyanine particles, such as aquocyanophthalocyaninato Fe(III) (Phthalcon 21) and aquocyanophthalocyaninato Co(III) (Phthalcon 11), is among these nanofillers. These fillers are prepared as nanometer-sized semi-conductive particles and used as additives in a broad range of polymer matrices.[13-15] The resulting polymer composite materials have a low value for φ_c.[13-15] In the past, a great deal of research was carried out at Shell Research and Technology Centre in Amsterdam (SRTCA) to unravel the structure and properties of Phthalcon 11 and its precursor compounds. The results obtained at SRTCA were confirmed by our own experiments.

In this chapter we describe the synthesis, structure and main properties of Phthalcon 11. The focus of this chapter is its molecular structure, the crystal structure of Phthalcon 11 has been discussed before.[16] The synthesis and structure characterization of different precursor compounds used to prepare Phthalcon 11 are complex. Due to the limited relevance to this thesis, here only the most important precursors are summarized and the complete results will be published elsewhere.[17]

3.2. Experimental

3.2.1. Materials
β-phthalocyanine Co(II) (β-PcCo) (97 %) (Scheme 3.1) was purchased from Fluka. Before use it was carefully dried at $80\,^{\circ}$C for 48 h under vacuum (~ 0.01 mbar) and

ground into fine powder in a mortar. Sodium cyanide NaCN, Na^{13}CN, NaC^{15}N, ^{2}H$_2$O and ethanol (absolute GR for analysis) were all purchased from Merck. Ethanol was dried with molecular sieves before use. The other chemicals were used as received.
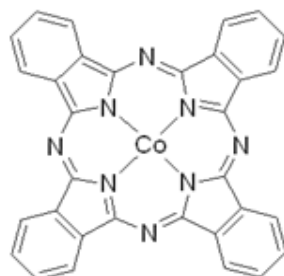
Scheme 3.1. Chemical structure of *β*-PcCo.

3.2.2. Characterization

UV-Vis Spectroscopy The UV-Vis spectra were recorded on ethylene glycol (dried with molecular sieves) dispersions using a Perkin-Elmer UV/Vis/NIR Lambda9 Spectrometer. For precursor the dispersion concentration was about 0.1-0.5 mg/100 mL; for Phthalcon 11 the concentration was about 4 mg/100 mL.

Infrared (IR) Spectroscopy The IR spectra were measured on nujol dispersions or by applying a small amount of powder/pentane slurry on a CsI, polyethylene or CaF$_2$ disk. These spectra were recorded using Digilab, Mattson Fourier Transform Instruments or Perkin Elmer 983G Instrument.

Field Desorption Mass Spectrometry (FD-MS) was performed on a JEOL HX110 spectrometer.

Pyrolysis Combustion Mass Spectroscopy Elemental Analysis (PCME) was obtained using an in-house apparatus at SRTCA (Scheme 3.2). During the measurement a sample (± 1.0 mg) is slowly heated in a helium atmosphere. The gasses involved are continuously combusted, and the combustion products (CO$_2$, H$_2$O, SO$_2$, N$_2$, NO, etc.) are measured by a computer controlled quadrupole mass spectrometer. The results obtained from PCME include a quantitative elemental composition (C, H, N, S, Cl, F, etc) of material and an evaporation/pyrolysis and combustion profile of all these elements versus temperature.
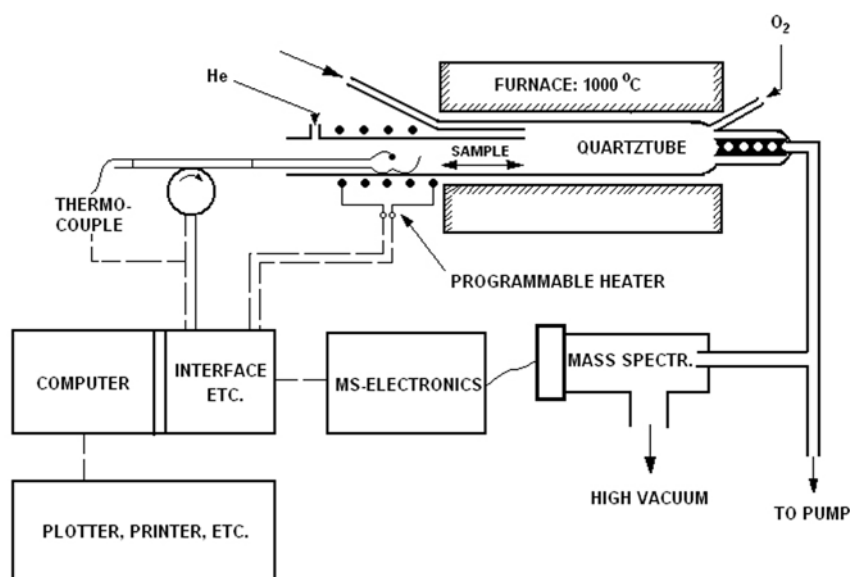
Scheme 3.2. Schematic drawing of a PCME set-up.

Transmission Electron Microscope (TEM), Selected Area Electron Diffraction (SAED) and Light Element Energy Dispersive X-ray (EDX) The characterization of different powders was performed using TEM, SAED and EDX analyses. Before use the sample was dried at 80 °C under 0.2 bar pressure for at least 24 h. For TEM measurements the sample/*n*-butanol dispersion was dropped on an ultrathin carbon film supported by a microscopic grid. The size of Phthalcon particles synthesized at TU/e was characterized with a Jeol2010 TEM. For this purpose, a 10^{-3} mol/L Phthalcon/ethylene glycol dispersion was prepared; this dispersion was later drop cast on a ultrathin carbon film supported by a copper grid. The TEM was operated at 200 kV. The local crystallography of the sample was investigated with SAED. Elemental analysis was carried out using an Oxford Instruments EDX detector, which allows the detection of light elements down to B.

X-ray Diffraction (XRD) and Neutron Diffraction Neutron diffraction was measured at the Energy Research Centre (Petten, the Netherlands). Both XRD and neutron diffraction measurements were performed on ^{2}H-labeled and non-labeled Phthalcon 11. XRD measurements were also performed on non-labeled, ^{13}CN- and C^{15}N-labeled precursors and Phthalcon 11.

Field Dependent High Speed ^{13}C Cross Polarization Magic Angle Spinning NMR (MAS-NMR) was performed on non-labeled and ^{13}CN-labeled precursors and

Phthalcon 11 at different frequencies (50, 75 and 125 MHz) over a spectral width of 1325 ppm. The spectra were recorded at room temperature on a Bruker MSL200, MSL300 or AM500 (sample ± 200 mg) with a repetition rate of 6-10 s and a 4-5 μs (90 °) pulse.

Solid State ^{2}H-NMR Solid State ^{2}H-NMR spectra were recorded with a quadrupolar echo pulse sequence on a Bruker MSL300 using approximately 500 mg ^{2}H$_2$O-enriched Phthalcon 11 powder. In addition, temperature-dependent series extended from - 60 to 90 °C was recorded. All spectra were measured with a repetition rate of 1-2 s and 4-5 μs (90 °) pulse. The recorded spectra were later analyzed qualitatively, in terms of an ordering and asymmetry parameter, and quantitatively, in terms of relative contributions by means of Depakeing.

Dynamic Light Scattering (DLS) DLS measurements were performed with a Malvern Instruments Zetasizer Nano ZS. All DLS measurements were recorded at 20 °C on 10^{-3} mol/L Phthalcon/ethylene glycol dispersions. This technique was also used to characterize the size of Phthalcon particles synthesized at TU/e.

3.2.3. Synthesis of Precursor Compounds
[PcCo(CN)(X$_1$)]$^-$Na$^+$ (Precursor I)
15.0 g β-PcCo and 25.0 g NaCN were suspended in 1.5 L ethanol. This suspension was then refluxed at 72 °C for 72 h while air was introduced into the reaction mixture (Scheme 3.2). After cooling the reaction mixture to room temperature, the blue solid was filtered off, washed with demi-water and dried in air at room temperature. FT-IR (nujol): ν_{CN} = 2123 cm^{-1} (w); FD-MS: 571 (PcCo$^+$), 594 (PcCo$^+$ + Na), 285 (PcCo^{2+}); PCME: Pc/CN = 1/1. In PCME peaks which could be attributed to ethoxy and adsorbed water were observed as well. Precursor I is not stable in air or N$_2$ or vacuum at room temperature.

[PcCo(CN)(OH)]$^-$Na$^+$ (Precursor II)
Precursor I [PcCo(CN)(X$_1$)]$^-$Na$^+$ can be used directly to prepare Phthalcon 11 or further purified to obtain [PcCo(CN)(OH)]$^-$Na$^+$ (Precursor II). To do so, the obtained precursor I from the first reaction step was extracted with dry acetone in a Soxhlet extractor. After extraction part of the acetone was distilled and the precipitation of the blue product was enhanced by the addition of diethyl ether. It was then filtered off, washed with diethyl ether and dried at 80 °C (~ 27 mbar) for three days. The overall yield was 93 % (based

on the amount of precursor obtained with respect to the amount of β-PcCo added to the reaction mixture). FT-IR (nujol): $\nu_{CN} = 2137$ cm^{-1} (w); UV/Vis (ethylene glycol): $\lambda_{max} = 669$ nm, $\varepsilon = 1.33 \times 10^5$ L/mol.cm; ^{1}H-NMR (deuterated acetone): $\delta_{(ppm)}$ 8.36 (q), $\delta_{(ppm)}$ 9.28 (q); ^{13}C-NMR (deuterated acetone): $\delta_{(ppm)}$ 122.49 (s), $\delta_{(ppm)}$ 130.01 (s), $\delta_{(ppm)}$ 140.24 (s), $\delta_{(ppm)}$ 146.94 (s); FD-MS: 571 (PcCo$^+$), 594 (PcCo$^+$ + Na), 285 (PcCo^{2+}); PCME: Pc/CN/OH = 1/1/1 (corrected for the adsorbed water, however, there was still a small amount of adsorbed water present ≈ 0.8 wt. %). Contrary to precursor I, at room temperature precursor II is stable in air and N$_2$ under a low pressure for at least several weeks.
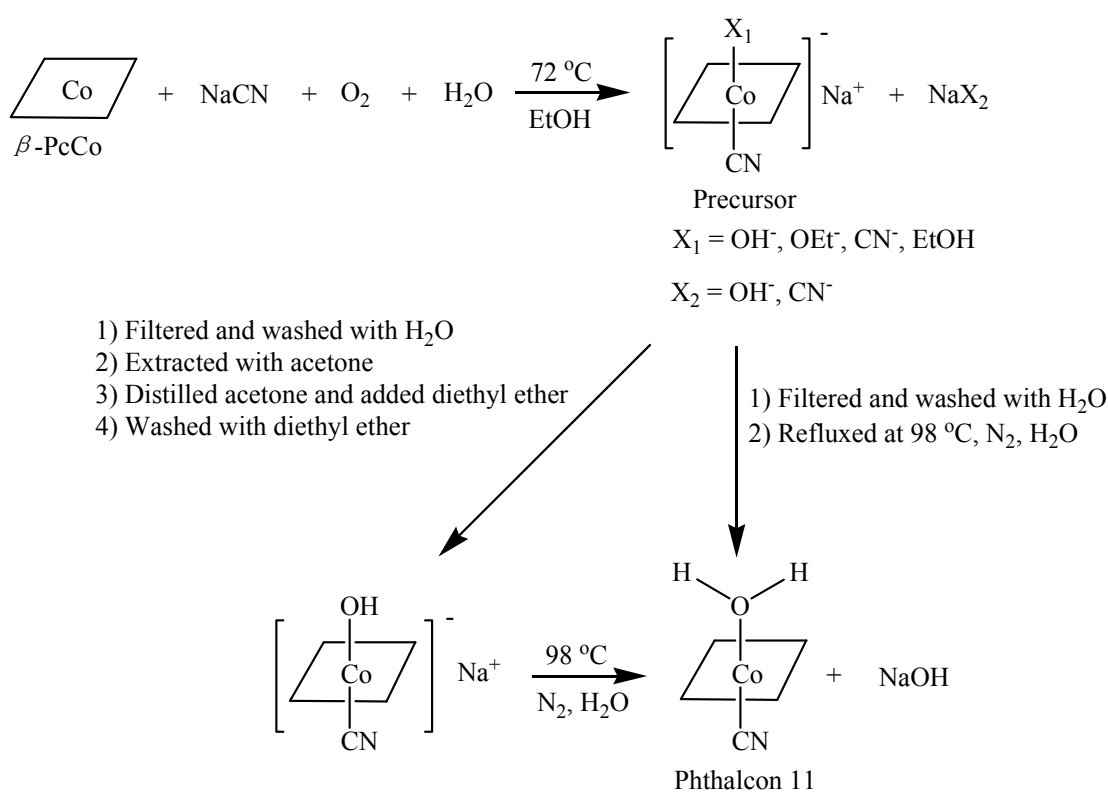
Scheme 3.3. Synthesis of Phthalcon 11.

Labeled Precursor Compounds

[PcCo(^{13}CN)(OH)]$^-$Na$^+$, [PcCo(C^{15}N)(OH)]$^-$Na$^+$ and [PcCo(CN)(O^{2}H)]$^-$Na$^+$ were prepared with Na^{13}CN, NaC^{15}N or ^{2}H$_2$O using a very similar method as described for the non-labeled precursor. For ^{13}CN- and C^{15}N-labeled precursors the amount of Na^{13}CN and NaC^{15}N used was lower and the precursors were always purified using the acetone extraction route. The experimental details are given in Table 3.1. PCME spectra show that the enrichment of ^{13}CN and C^{15}N ligands appears to be > 95 %.

Furthermore, identical XRD spectra were obtained for the labeled and non-labeled compounds. The IR analytical results are listed in Table 3.2. Detailed PCME and solid state NMR data will be published elsewhere.[17]

Table 3.1. Experimental details of synthesis of precursors.

Label	β-PcCo (g)	Sodium cyanide (g)	Ethanol (ml)	Yield (%)[#]
^{13}CN	2.86	0.50	250	43[*]
$C^{15}N$	2.54	0.40	160	65[*]
^2H_2O	10.0	5.00	120	89[&]
Non-labeled	2.90	0.50	250	43[*]
Non-labeled	2.24	0.40	160	66[*]
Non-labeled	11.0	3.90	110	88[@]

[#] Actual amount isolated after purification and drying; reaction time was 72 h.

[*] Purified by extracting with dry acetone, filtered and washed with diethyl ether, and then dried in vacuum.

[&] Filtered and washed with ^2H_2O; experiments were performed under a careful exclusion of H_2O in EtO^2H.

[@] Filtered and washed with H_2O, and then dried in vacuum.

Table 3.2. CN stretching vibration (υ_{CN}) of labeled precursor and Phthalcon 11.

Compound	υ_{CN} (experimental) (cm^{-1})	υ_{CN} (calculated)[*] (cm^{-1})
$PcCo(^{13}CN)(OH)^-Na^+$	2089	2093
$PcCo(C^{15}N)(OH)^-Na^+$	2102	2104
$PcCo(CN)(O^2H)^-Na^+$	2139	
$PcCo(CN)(H_2O)$	2154	
$PcCo(^{13}CN)(H_2O)$	2108	2109
$PcCo(C^{15}N)(H_2O)$	2125	2123
$PcCo(CN)(^2H_2O)$	2156	

[*] υ_{CN} was calculated by simple mass correction.

3.2.4. Synthesis of Semi-conductive Phthalcon 11

The synthesis of Phthalcon 11 was studied extensively. Here only the synthetic routes which are strongly linked to the synthesis of pure non-labeled and labeled Phthalcon 11 compounds are described.

Non-labeled Phthalcon 11

[PcCo(CN)(H$_2$O)] was prepared as follows: 1.0 g dried precursor I or II was dispersed in 100 mL demi-water and refluxed at 98 ^{o}C under N$_2$ for 72 h. The blue crystalline solid was filtered off, washed and dried at 80 °C under vacuum for 72 h. The yield was 95 %. No precursor was detected in the product (XRD and IR). For Phthalcon 11 synthesized from the extracted precursor compounds, the content of β-PcCo was less than 0.1 wt. % (XRD). FT-IR (nujol): ν_{CN} = 2154 cm^{-1} (w); UV/Vis (ethylene glycol): λ_{max} = 820-860 nm (broad band), ε = 2.35 x 10^4 L/mol.cm. The Phthalcon 11 crystals are platelet-shaped with dimensions of about 50 x 50 x 15 nm^3 as measured from TEM. The SAED, XRD and PCME spectra were also obtained and will be discussed later.

Pure Phthalcon 11 powder was synthesized using the following procedure: 10.0 g precursor II was washed with 200 mL demi-water/ethanol (95/5), and then it was dried for 24 h in air. In a 250 mL round bottom flask this dried precursor was added together with 110 mL demi-water. While stirring under a N$_2$ blanket the reaction temperature was increased to 98 °C and the reaction was continued for 72 h. After cooling to room temperature the slurry was filtered off, washed with demi-water and dried at 80 °C (~27 mbar) for 72 h. The overall yield was 95 %. FT-IR (nujol): ν_{CN} = 2154 cm^{-1} (w); UV/Vis (ethylene glycol): λ_{max} = 877 nm (broad band), ε = 2.35 x 10^4 L/mol.cm; solid state ^{13}C-NMR: $\delta_{(ppm)}$ 122.4 (s), $\delta_{(ppm)}$ 128.3 (s), $\delta_{(ppm)}$ 137.1 (s), $\delta_{(ppm)}$ 146.3 (s). Elemental analysis (theoretical values are between brackets): C = 64.2 % (64.4 %), H = 3.0 % (3.1 %), N = 20.5 % (20.5 %), Co = 9.5 % (9.6 %); the EDX spectrum shows a Co/O ratio of 1/1 and the amount of Na present is very small (Figure 3.1c). Phthalcon 11 particle is stable in air and in contact with a broad range of solvents. It decomposes in air before melting at temperature above 300 ^{o}C.[17]

Labeled Phthalcon 11

PcCo(^{13}CN)(H$_2$O), PcCo(C^{15}N)(H$_2$O) and PcCo(CN)(^{2}H$_2$O) were prepared from the corresponding labeled precursors following a similar synthetic route as described for the non-labeled Phthalcon 11. The detailed reaction conditions are listed in Table 3.3. The experiments with ^{2}H$_2$O were performed under a careful exclusion of H$_2$O, and the

reaction time was longer to compensate the slow conversion of the precursor. All final products were characterized with IR, PCME and XRD. The deuterated product was also analyzed with neutron diffraction and ^{2}H-NMR; the ^{13}CN-enriched Phthalcon 11 was characterized with solid state ^{13}C-NMR as well. For the labeled and non-labeled Phthalcon 11, very similar XRD spectra were obtained. PCME analyses show that the enrichment of ^{13}CN, C^{15}N and ^{2}H$_2$O is above 95 %.

Table 3.3. Experimental details of synthesis of Phthalcon 11 compounds.

Label	Precursors (g)	Water (ml)	Reaction time (h)	Yield (%)
^{13}CN	0.7	70	72	89[#]
C^{15}N	1.2	125	72	97[#]
^{2}H$_2$O	6.1	120	120	92[*]
Non-labeled	1.0	100	72	95

[#]Experiments were performed under the careful exclusion of H$_2$O; a longer reaction time was chosen to obtain a higher conversion from precursor to Phthalcon 11.

[*]Actual amount obtained after washed with water and dried.

3.3. Results and Discussion

3.3.1. Synthesis of Labeled and Non-labeled Precursor Compounds

Non-labeled Precursors

Apart from the two precursor compounds mentioned before, six other different precursors were identified using XRD, NMR, IR, PCME, TEM, EDX and SAED analyses, among them only precursor II is stable. All these precursor compounds contain Co(III). The Co(II) present in β-PcCo is oxidized by air during the first reaction step. Due to the complexity of the results and the lack of relevance to this thesis, only the overall conclusions are summarized here.

The precursor compounds are different with respect to the chemical composition, crystal structure and crystallinity. Often the chemical composition of one of the axial ligands is varied (-OH, -OC$_2$H$_5$, acetone dimer, HOC$_2$H$_5$, acetone or -CN), depending on the purification steps used, the chosen reaction conditions and the solubility of the products. Apparently this axial ligand is very loosely bonded. Under the optimum conditions the conversion of β-PcCo to precursor is above 99 %. The main impurity in

precursor is β-PcCo. However, it can be separated from the precursor by extraction with acetone. All precursor compounds could be easily converted to Phthalcon 11 by following the steps shown in Scheme 3.3. The influence of chosen precursors on the reaction rate and the purity of Phthalcon 11 appears to be minimal.[17]

Labeled Precursors

Isotopically enriched precursors were also prepared by selectively building the ^{13}CN, C^{15}N and ^{2}H$_2$O fragments following the reaction steps and conditions shown in Scheme 3.3 and Table 3.1. The reaction conditions chosen for the preparation of ^{13}CN- and C^{15}N-enriched precursor compounds deviated from those used for the non-labeled compounds (Table 3.1). The reason was the expensiveness of Na^{13}CN and NaC^{15}N reagents. The amount of these compounds used in the first step was much lower than generally applied, resulting in a much lower conversion of β-PcCo. Therefore, these labeled precursors were purified using the acetone extraction step before they were converted to corresponding labeled Phthalcon 11.

3.3.2. Synthesis of Non-labeled and Labeled Phthalcon 11

The conversion of different precursors to Phthalcon 11 is high as long as the reaction is performed under N$_2$. The rate of reaction and the purity of the final product are, apart from the amount of β-PcCo present, independent of the starting precursor compounds. This may indicate that a (partially) soluble five-coordinated precursor is formed as an intermediate. When the reaction is performed in ^{2}H$_2$O the conversion rate slows down which suggests that the rate-determine step is the five-coordinated precursor complex reacting with water. Within the uncertainty of measurements the use of labeled Na^{13}CN and NaC^{15}N does not influence the rate of conversion. This is in agreement with the proposed mechanism.

All labeled Phthalcon 11 compounds have a high purity. The main impurity in labeled Phthalcon 11 is β-PcCo (about 4 wt. %; β-PcCo is also present in the corresponding precursors). However, when very similar reaction and purification steps are used, the amount of β-PcCo present in the non-labeled Phthalcon 11 is much lower (< 0.1 wt. %). This difference cannot be explained yet.
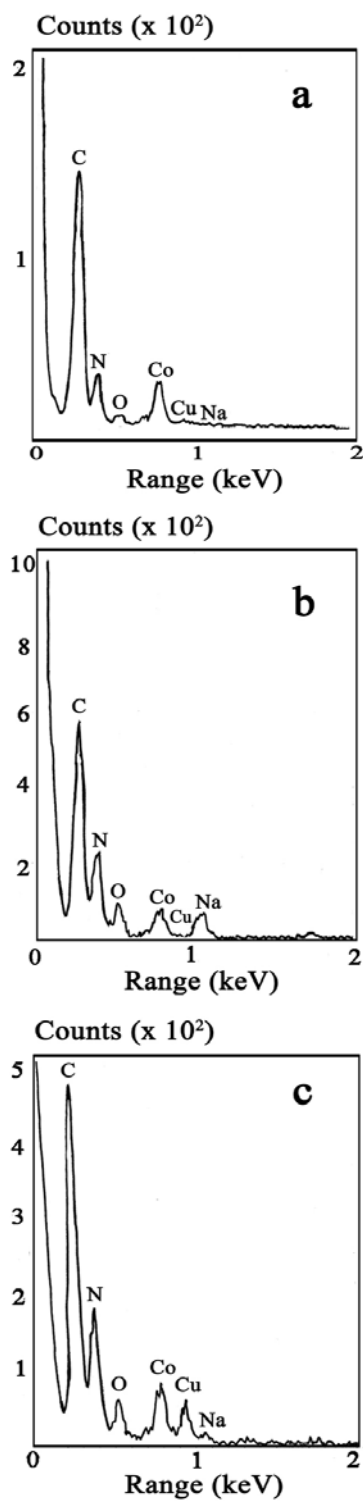
Figure 3.1. EDX spectra of (a) *ß*-PcCo; (b) precursor I and (c) Phthalcon 11.
In Figure 3.1c, Cu signal is from the Cu grid.

3.3.3. Molecular Structure of Phthalcon 11

The elemental analysis of pure Phthalcon 11 corresponds to the composition $C_{33}N_9H_{18}OCo$. PCME was also performed because of the dominance of the PcCo ring ($C_{32}N_8H_{16}Co$) in the elemental analysis. PCME analysis is a programmed heating procedure in a helium atmosphere. During the measurement, the fragments formed react with O_2, and the products are followed by on-line monitoring the combustion gases (CO_2, H_2O, NO, N_2, etc.) by means of a quadrupole mass spectrometer. Using reference samples, products detected at a certain temperature are quantified. Due to the programmed heating procedure, fragmental decomposition of the sample can be studied in detail. Figure 3.2 shows the PCME patterns of a non-labeled Phthalcon 11. This figure shows that indeed in Phthalcon 11 well-separated products were observed. At 100-110 ^{o}C the first H_2O peak (mass 18) occurs and the second one occurs at about 250-350 ^{o}C. For both peaks no O_2 uptake was required, which strongly suggests that the water fragment is already present in Phthalcon 11. The peak at 100-110 ^{o}C is likely caused by water adsorbed during the second reaction step (Scheme 3.3). The other water signal suggests that it is part of the structure in Phthalcon 11. This suggestion is also confirmed by measuring the ^2H_2O-labeled Phthalcon 11 in which both signals disappeared from the PCME spectrum. The next two peaks at 350-450 ^{o}C are N_2 and CO_2 in almost equal amounts next to a small amount of NO. These peaks at mass 28, 44 and 30 can be attributed to a CN fragment (the O_2 uptake was needed for the formation of CO_2 and NO). The N_2 peak at mass 28 disappeared when $C^{15}N$-labeled Phthalcon 11 was used. At the same time a strong increase in mass 30 ($^{15}N_2$) was observed. When ^{13}CN-labeled Phthalcon 11 was used the CO_2 peak at mass 44 disappeared. The rest of the peak patterns are specific for non-labeled Phthalcon 11. However, peaks above 450 ^{o}C can only be used semi-quantitatively because at 670 ^{o}C some residue solid material was detected. Elemental analysis of this solid material shows that it mainly contains C and Co. It is known that phthalocyanine compounds only partly decompose at 670 ^{o}C under the combustion conditions used here. Because the FT-IR spectra also show that the PcCo ring is present (Figure 3.3) and the EDX spectrum confirms the ratio between Co/O is 1/1 (Figure 3.1), the structure of Phthalcon 11 is likely to be built-up with the following fragments: H_2O, CN and PcCo, and the ratio between them is 1/1/1.
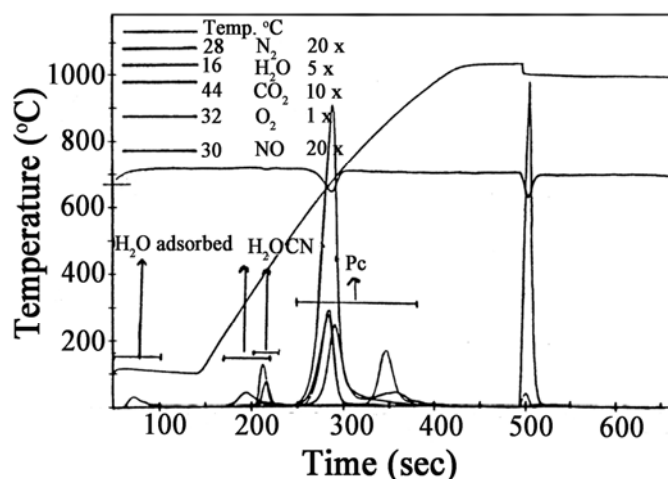
Figure 3.2. PCME Patterns of Phthalcon 11.
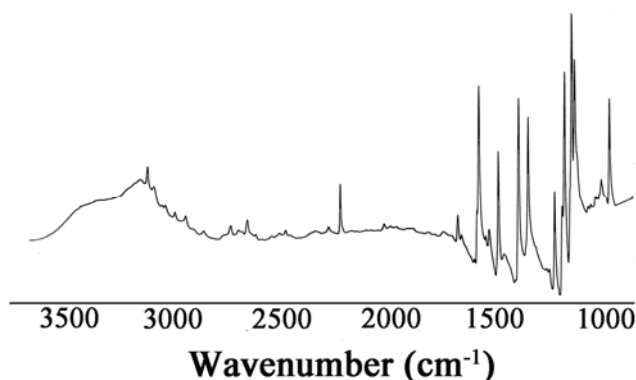
Figure 3.3. FT-IR spectrum of non-labeled Phthalcon 11.

The PCME spectra of several precursors confirm this conclusion as well. For precursor I the PCME shows that apart from the adsorbed water/ethanol signal at 100-110 $^\circ$C two signals appeared at 220-320 $^\circ$C (H/C $\approx$ 2.2) which can be attributed to an ethoxy/ethanol fragment. Two other signals at 340-510 $^\circ$C (C/N $\approx$ 1) can be assigned to a CN fragment. These last two signals at mass 28 and 44 disappeared in the PCME spectra when C^{15}N- and ^{13}CN-labeled precursor compounds were used. The EDX spectrum of this precursor compound confirms this assignment and shows that the ratio between Co/O = 1/1 (Figure 3.1).

Based on these results the following possible structures are proposed for Phthalcon 11:

1) A linear polymer μ-cyanophthalocyaninato Co(III), (PcCoCN)$_n$, containing crystal water (Scheme 3.4a).

2) Nonpolymeric PcCo(OH$_2$)(CN) containing water coordinated with the Co and the CN coordinated with the C to the Co (Scheme 3.4b).

3) As 2) but the CN coordinated with the N to the Co (structure not shown).

4) Nonpolymeric ionic [PcCo(OH$_2$)]$^+$CN$^-$ (Scheme 3.4c).

5) Ionic [PcCo]$^+$CN$^-$ containing crystal water (Scheme 3.4d).

6) Nonpolymeric PcCo(CN), the CN coordinated with the C to the Co, containing crystal water (Scheme 3.4e).

7) As 6) but the CN coordinated with the N to the Co (structure not shown).
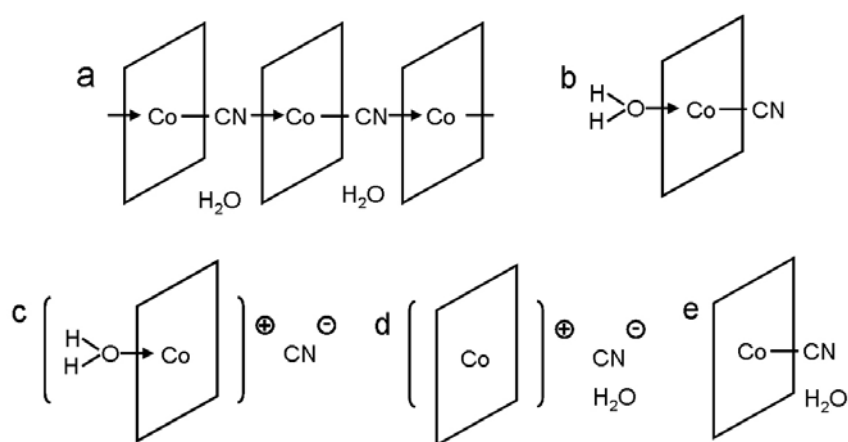
Scheme 3.4. Possible structures of Phthalcon 11.
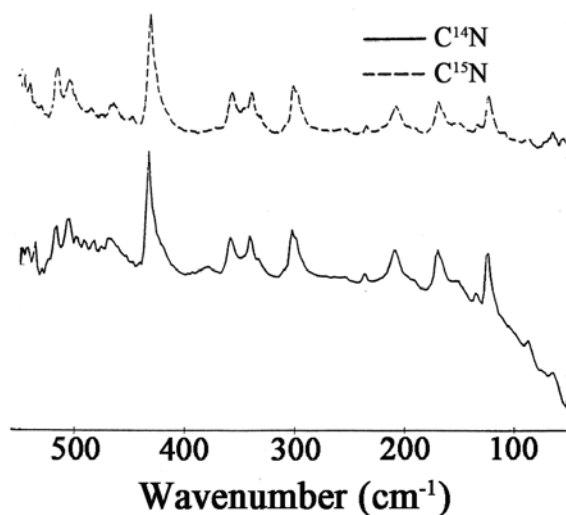
Figure 3.4. Far-IR spectra of non-labeled and C^{15}N-enriched Phthalcon 11.

An important difference between these structures is the presence/absence of a band between the Co and the N of the CN group. The position of this band is expected in the far-IR range.[18] When we compare the far-IR spectra of C[15]N-enriched Phthalcon 11 with the non-labeled Phthalcon 11 no significant difference was found (Figure 3.4), showing that the Co is possibly not coordinated with the N of the CN. Moreover, for precursor II no clear shifts were observed as well, indicating that the C of the CN is coordinated with the Co.

The band between the Co and the C of the CN is also expected in the far-IR range.[18] The far-IR spectra of non-labeled and [13]CN-enriched Phthalcon 11 are shown in Figure 3.5. A band lying at 466 cm^{-1} in the spectrum of Phthalcon 11 shifts to 457 cm^{-1} after the enrichment. A similar shift was observed when the spectrum of [13]CN-enriched precursor II was compared with the non-enriched one (from 485 to 475 cm^{-1}). It is concluded from these results that the C atom, not the N atom, of the CN group is coordinating the Co (for further proof, see later discussion). This rules out the polymeric structure shown in Scheme 3.4a, the structures shown in Scheme 3.4c and 3.4d and the non-polymeric structure in which the CN is coordinated with the N to the Co. It follows that either Scheme 3.4b or 3.4e represents the structure of Phthalcon 11.
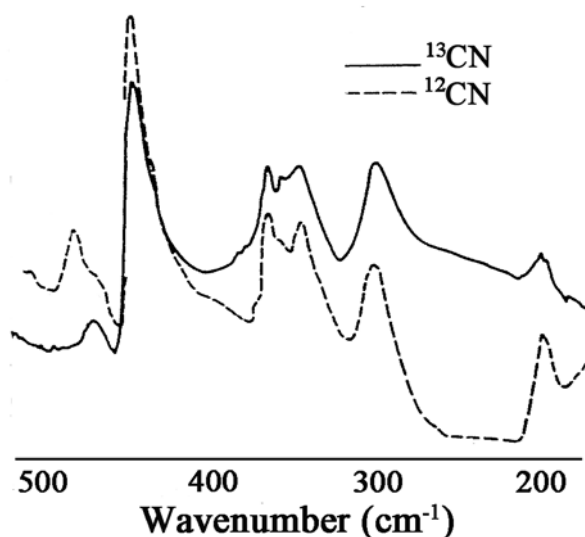
Figure. 3.5. Far-IR spectra of non-labeled and [13]CN-enriched Phthalcon 11.
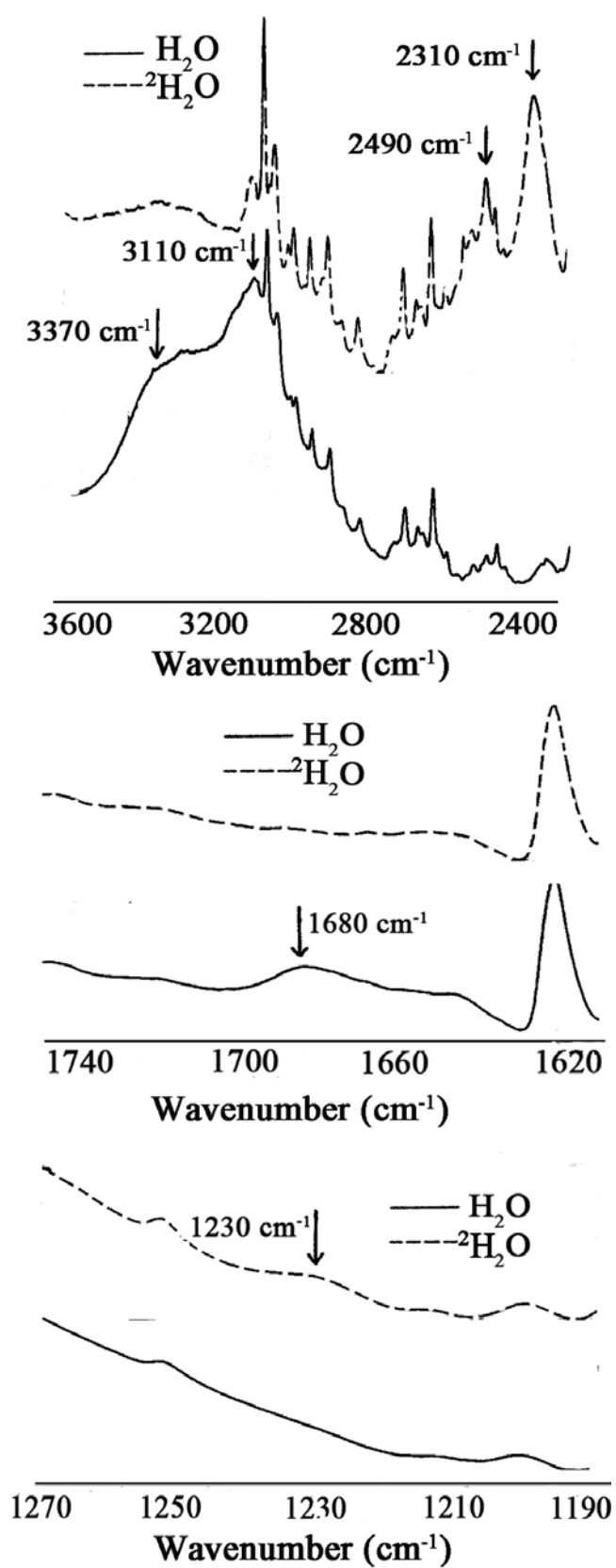
Figure 3.6. IR spectra of non-labeled and ^2H_2O-enriched Phthalcon 11.

In general, the CN stretching vibration is expected to be around 2200 cm^{-1}, a region in which only a very few bands are observed.[19] Hence, the bond at 2154 cm^{-1} in Figure 3.3 is the CN stretching vibration. Moreover, as observed in the spectra of Phthalcon 11, the C≡N stretching vibration at 2153 cm^{-1} shifts to 2108 cm^{-1} after ^{13}CN enrichment and to 2125 cm^{-1} after C^{15}N enrichment (Table 3.2). These shifts are almost, quantitatively, in agreement with the expected theoretically isotopic effects (2109 and 2123 cm^{-1}, respectively). A very similar shift of the CN stretching vibration was observed after labeling precursor II with ^{13}CN and C^{15}N. Hence, it is very likely that the CN group is a ligand that is coordinately connected with the Co.

The water in Phthalcon 11 can be present as lattice water (bonded by weak hydrogen bonds or weak ionic bonds, Scheme 3.4e) or it can be coordinatively bonded by its oxygen to the Co (Scheme 3.4b). In general, lattice water shows a moderate downward shift of the two O-H stretching vibrations and a moderate upward shift of the H-O-H bending vibration as compared to the vapor phase values (Table 3.4).[18] Coordinatively bonded water is expected to be much more strongly perturbed.[18] The FT-IR spectrum of Phthalcon 11 shows an H-O-H bending band at 1680 cm^{-1} and two O-H stretching bands at 3370 and 3110 cm^{-1} (Figure 3.3). To confirm the position of water, the IR spectrum of ^{2}H$_2$O-enriched Phthalcon 11 was also measured (Figure 3.6). It contains new broad bands at 2490 and 2310 cm^{-1}, whereas the bonds at 3370 and 3110 cm^{-1} (almost) disappeared. The shift observed after labeling with ^{2}H$_2$O is about 1.35, which is much larger than what can be expected for lattice water (Table 3.4 & Figure 3.6) and is in agreement with the isotopic shift for coordinated water molecules. This strongly suggests that the water is coordinatively bonded to the Co, in accordance with the structure shown in Scheme 3.4b.

Table 3.4. Frequencies of H$_2$O and ^{2}H$_2$O.

	O-H stretch (cm^{-1})		H-O-H bending
H$_2$O vapor	3755	3650	1595
H$_2$O (lattice)	3550-3200		1600-1630
PcCo(CN)(H$_2$O)	3370	3110	1680
^{2}H$_2$O vapor	2790	2670	1180
PcCo(CN)(^{2}H$_2$O)	2490	2310	1230

Through a very similar synthetic route, it was claimed by Hanack et al. that using precursor compound containing two CN ligands as an intermediate, a polymeric structure (Scheme 3.4a) was obtained.[20] The structure of their conductive compound was analyzed using limited analyses: powder XRD, IR and single crystal XRD. Unfortunately, the single crystal XRD does not match powder XRD. This makes their structure assignment doubtful.

3.3.4. Crystal Structure and Surface Groups of Phthalcon 11

The crystal structure of Phthalcon 11 has been studied in detail at SRTCA. By measuring the dependence of the broadness of the main peaks in the XRD spectrum on the particle size, it suggests that Phthalcon 11 particles are single crystals.[17] However, the obtained single Phthalcon 11 crystal particle size is too small to directly characterize its structure using single crystal XRD technique. Analytic results on powder XRD, density data and crystallographic modeling indicate that Phthalcon 11 has a monoclinic P_{21} unit cell with $a = 7.308 \pm 0.001$ Å, $b = 24.89 \pm 0.01$ Å and $c = 7.149 \pm 0.001$ Å; while $\alpha = \gamma = 90\,^\circ$.[16] The unit cell contains two PcCo fragments. However, the water molecule could not be located and the presence/absence of a band between the Co and the C of the CN fragment was uncertain. To better allocate these fragments, high resolution XRD and neutron diffraction on ^2H_2O-labeled and non-labeled Phthalcon 11 were performed. These spectra were analyzed using Rietveld refinement procedure and Cerius software by assuming that the molecular structure is b, c, or e in Scheme 3.3. Apart from the actual position of the ^2H of the water molecule, the actual positions of the C, N, Co and O atoms were also obtained.[16] The results show a quantitative agreement with the structure shown in Scheme 3.3b, which is in line with the one based on the IR analyses using labeled and non-labeled compounds.

The position of the water molecule was also studied using ^2H-NMR on ^2H_2O-labeled Phthalcon 11.[17] From these data it appears that the ^2H atoms are not equally surrounded. One of the ^2H atoms is hydrogen bonded with the CN group of a neighboring Phthalcon 11 molecule, forming an intermolecular polymeric structure (Scheme 3.4).

The overall crystal structure is schematically shown in Scheme 3.5, 3.6 & 3.7. An important aspect of this crystal structure is that the π orbitals of the phthalocyanine

rings in two neighboring stacks interact, with the van der Waals distance (3.35 Å) between them.[17]
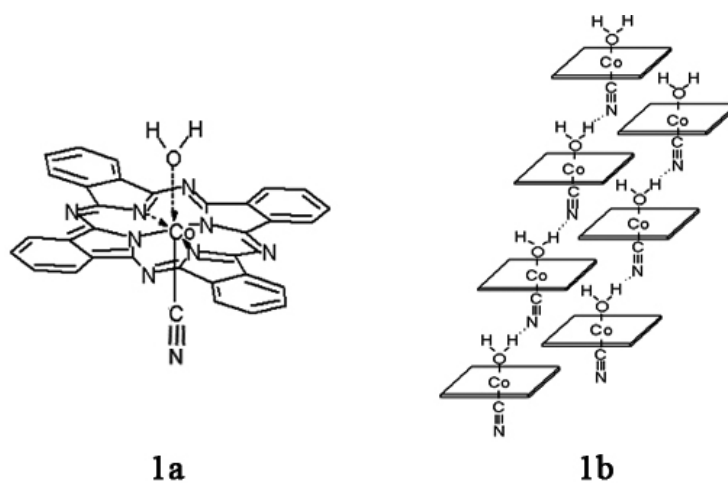
Scheme 3.5. Molecular (1a) and crystal (1b) structure of Phthalcon 11.
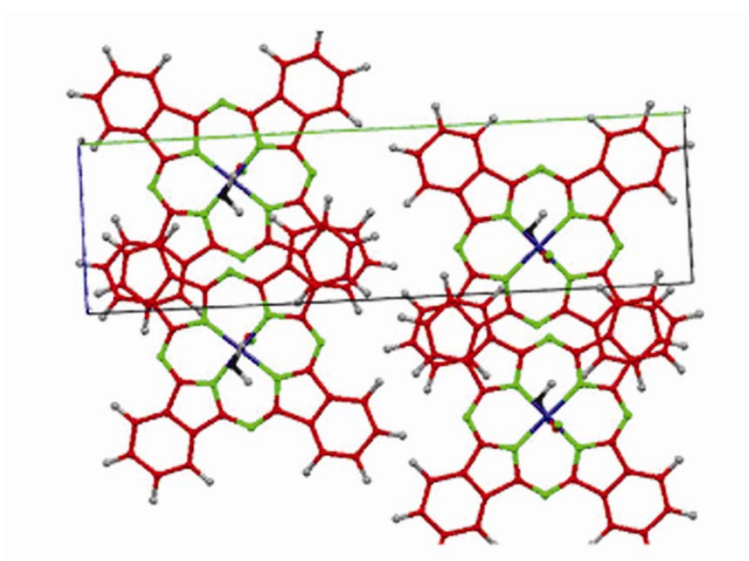
Scheme 3.6. Top view of Phthalcon 11.

The unit cell is repeated in the $\vec{c}$-direction. In the $\vec{a}$-direction, all unit cells exactly fall on each other (i.e. $\vec{a}$ is perpendicular to the paper). $\vec{b}$ is the green line and $\vec{c}$ is the blue line. The rest of the unit cell is shown with black lines. All carbon atoms (and half of the corresponding bonds) are depicted in red, the nitrogen atoms are in green, the oxygen atom is in black, the cobalt atom is in blue and the hydrogen atoms are in grey.[16]
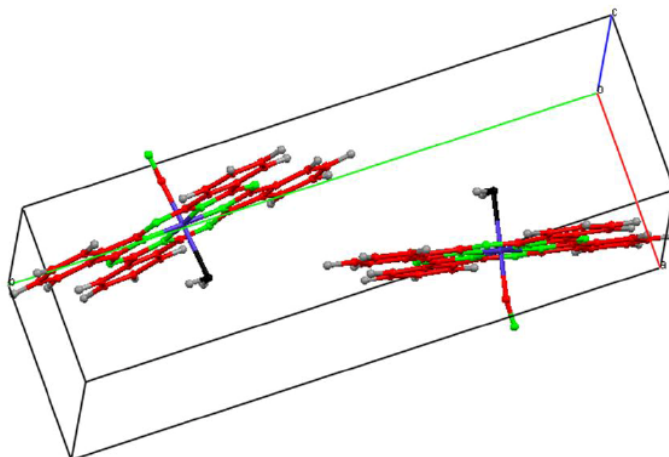
Scheme 3.7. One unit cell of Phthalcon 11.

It contains two molecules which rotate to each other. $\vec{a}$ is the red edge, $\vec{b}$ is the green edge

and $\vec{c}$ is the blue edge. The rest of the unit cell is shown with black lines. All carbon atoms

(and half of the corresponding bodings) are depicted in red, the nitrogen atoms are in green,

the oxygen atom is in black, the cobalt atom is in blue and the hydrogen atoms are in gray.[16]

Position of the hydrogen bonds is not corrected on the information obtained from ^{2}H$_2$O-NMR.

^{2}H-NMR also indicates the presence of an -OH/H$_2$O group at the surface of the particle.[17] Apart from a ^{13}CN signal in the bulk of the particle, another ^{13}CN signal was observed in the solid state ^{13}C-NMR spectrum,[17] indicating that the CN groups are present at the surface of the particle. The orientation of the unit cell in the actual platelet-shaped Phthalcon 11 particle was identified using TEM and ED.[16] Combining all these data, it is likely that -OH/H$_2$O, -CN as well as phenyl groups are present at the surface of the particle.

3.3.5. Primary Particle Size of Phthalcon 11

The size of Phthalcon 11 primary particle prepared at STRCA was somewhat smaller than that prepared at TU/e, which was synthesized using a somewhat different route as described in Chapter 4. The size of Phthalcon 11 prepared at TU/e was analyzed with TEM and DLS. In Figure 3.7 DLS as well as TEM data is presented. The TEM image shows mainly two dimensions of a Phthalcon 11 particle. These dimensions are almost equal with an average of 150 nm. Further TEM analysis reveals that for Phthalcon 11 the third dimension is around 30 nm.[17] Only one peak at 150 nm was found in the DLS spectrum. This value corresponds to the largest value obtained from

TEM. It has been shown that for non-spherical platelet particles, the largest dimension plays the dominant role in DLS.[21] Accordingly, since our Phthalcon particles are also platelet-shaped, the value obtained from DLS corresponds to the size of the largest dimension.
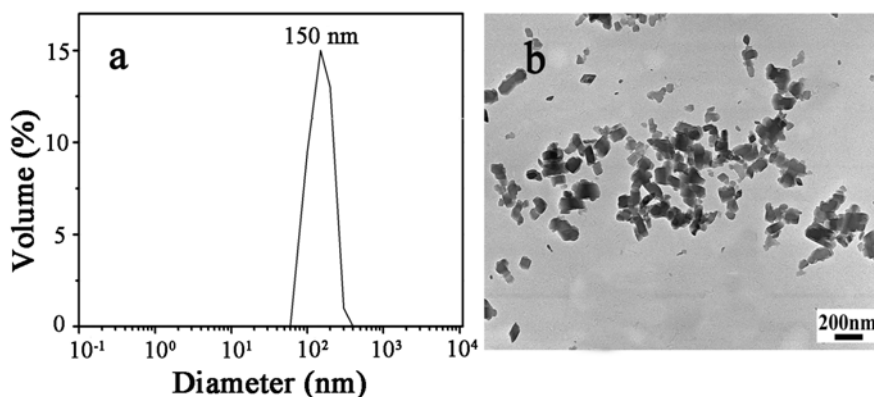
Figure 3.7. (a) Phthalcon 11 Particle size distribution obtained from DLS; (b) TEM image. Phthalcon 11 has a primary particle size of 150 x 150 x 30 nm³.

3.3.6. Conductivity of Phthalcon 11 Particles

At room temperature the intrinsic conductivity σ_v of Phthalcon 11 particles prepared at TU/e is about 2×10^{-2} S/cm, while the σ_v value of the compressed Phthalcon 11 powder is about 4×10^{-4} S/cm.[16,22] The temperature dependence of DC and AC conductivity measurements on compressed Phthalcon powder synthesized at TU/e shows that the conduction mechanism in the powder is probably variable-range hopping by cotunnelling.[16,22]

Using the crystal structure of Phthalcon 11 as a starting point, Density-Functional Theory (DFT) calculations were performed to determine the origin of the conductivity.[16] These calculations together with the experimentally determined values obtained from absorption spectroscopy at a temperature of 1.2 K on Phthalcon/epoxy composites[16,22] show that Phthalcon 11 particle is a bulk semi-conductor with a band gap of about 1.2 eV.[17]

3.4. Conclusions

The synthesis of non-labeled and ^{13}CN-, C^{15}N- and ^{2}H$_2$O-labeled Phthalcon 11 has been described in this chapter. PCME and elemental analyses show that Phthalcon 11

molecule has the composition of $C_{33}N_9H_{18}OCo$. The IR spectra of non-labeled and isotopically enriched Phthalcon 11 and its precursors show that Phthalcon 11 is a neutral molecule. This molecule contains water and CN ligands. The C atom of the CN group is coordinately bonded with the Co(III); and the water is coordinatively bonded with the O atom to the Co(III). The molecular structure has been confirmed by solid state NMR and crystallographic modeling as well. ^{2}H-NMR shows that one of the hydrogen atoms of the water ligand forms a hydrogen bond with the N atom of the CN group of the neighboring molecule in the stack, resulting in an intermolecular polymeric structure. Detailed studies on the crystal structure show that Phthalcon 11 has a monoclinic P_{21} unit cell. The unit cell contains two molecules which rotate to each other. The π orbitals of the phthalocyanine rings in the two neighboring stacks interact, with the van der Waals distance (3.35 Å) between them. The surface groups of the Phthalcon particles are probably -OH/H_2O, -CN and phenyl rings. Furthermore, earlier studies show that Phthalcon 11 particle is a bulk semi-conductor with a band gap of about 1.2 eV. The conduction mechanism in the compressed Phthalcon 11 powder is likely to be variable-range hopping by cotunnelling.

References

1. Skotheim, T. A.; Ed., *Handbook of Conducting Polymers, 2nd ed., Revised and Expanded*. Marcel Dekker: New York, 1997.

2. Nalwa, H. S., *Handbook of Advanced Electronic and Photonic Materials and Devices*. Academic Press: London, 2000.

3. Chandrasekhar, P., *Conducting Polymers, Fundamentals and Applications: A Practical Approach*. Kluwer Academic: Dordrecht, 1999.

4. Gul, V. E., *Structure and Properties of Conducting Polymer Composites*. VSP: Utrecht, 1996.

5. Brokken-Zijp, J. C. M.; Soloukhin, V. A.; Posthumus, W.; de With, G. *In Proceeding of 2003 Athens Conference on Coatings Science and Technology, Vouliagmeni, Greece.*

6. Karasek, L.; Sumita, M. *J. Mater. Sci.* **1996,** 31, (2), 281-289.

7. van der Putten, D.; Moonen, J. T.; Brom, H. B.; Brokken-Zijp, J. C. M.; Michels, M. A. J. *Phys. Rev. Lett.* **1992,** 69, (3), 494-497.

8. Adriaanse, L. J.; Reedijk, J. A.; Teunissen, P. A. A.; Brom, H. B.; Michels, M. A. J.; Brokken-Zijp, J. C. M. *Phys. Rev. Lett.* **1997,** 78, (9), 1755-1758.

9. Soloukhin, V. A.; Brokken-Zijp, J. C. M.; de With, G. *J. Polym. Sci. B* **2007,** 45, (16), 2147-2160.

10. Sumita, M.; Sakata, K.; Asai, S.; Miyasaka, K.; Nakagawa, H. *Poly. Bull.* **1991,** 25, (2), 265-271.

11. Sumita, M.; Abe, H.; Kayaki, H.; Miyasaka, K. *J. Macromol. Sci., Phys.* **1986,** B25, (1-2), 171-184.

12. Levon, K.; Margolina, A.; Patashinsky, A. Z. *Macromolecules* **1993,** 26, (15), 4061-4063.

13. Brokken-Zijp, J. C. M.; van Mechelen, J. B.; Emeis, C. A.; Datema, K. P.; Kramer, A. H.; de Bruijn, D. P.; Meruma, A. J. *US Patent 05319009* **1993**.

14. Chen, Z.; Brokken-Zijp, J. C. M.; Huinink, H. P.; Loos, J.; de With, G.; Michels, M. A. J. *Macromolecules* **2006,** 39, (18), 6115-6124.

15. Chen, Z.; Brokken-Zijp, J. C. M.; Michels, M. A. J. *J. Polym. Sci. B* **2006,** 44, (1), 33-47.

16. Huijbregts, L. J. *Charge Transport and Morphology in Nanofillers and Polymer Nanocomposites*. Ph.D. Thesis, Eindhoven University of Technology, Eindhoven, 2008.

17. Brokken-Zijp, J. C. M.; Yuan, M.; et.al. *"Synthesis and Structure of Novel Aquocyanophthalocyaninato Co(III) Semi-conductor and Its Applications in*

Conductive Polymer Composites". In Preparation.

18. Nakamoto, K., *Infrared and Raman Spectra of Inorganic and Coordination Compounds*. Wiley: New York, 1978.

19. Lin-Vien, D.; Colthup, N. B.; Fateley, W. G.; Grasselli, J. G., *The Handbook of Infrared and Raman Characteristic Frequencies of Organic Molecules*. Academic Press: New York, 1991.

20. Metz, J.; Hanack, M. *J. Am. Chem. Soc.* **1983,** 105, (4), 828-830.

21. Voorn, D. J. *Polymer/Platelet Nanocomposite Particles*. Ph.D. Thesis, Eindhoven University of Technology, Eindhoven, 2006.

22. Huijbregts, L. J.; Brom, H. B.; Brokken-Zijp, J. C. M.; Kemerink, M.; Chen, Z.; de Goeje, M. P.; Yuan, M.; Michels, M. A. J. *J. Phys. Chem. B* **2006,** 110, (46), 23115-23122.

4

FILLER SIZE EFFECTS ON THE CONDUCTIVITY OF CROSS-LINKED PHTHALCON/EPOXY NANOCOMPOSITES⊛

SYNOPSIS

Three Co(III) phthalocyanine (Phthalcon) powders with different particle sizes and chemical compositions, but almost equal XRD spectra and powder conductivity were synthesized and used as conductive fillers in cross-linked epoxy matrices. Two of these Phthalcons are new compounds. All three composites have a percolation threshold of 0.9 vol. % and a maximum volume conductivity of 10^{-7} S/cm. The relation between the conductivity of the composites and the type and amount of filler used was determined. The influence of particle size and chemical composition on this relation appears to be minimal. Detailed analysis shows that these particle networks have very similar fractal structures and that they are likely to be formed by diffusion limited cluster aggregation during processing. Evidence is presented that these particle networks are formed at the early stage of cross-linking and that at 12 vol. % the charge transfer between particles in the networks is neither limited by Phthalcon particle size, nor by the presence of polymer matrix between particles. The maximum volume conductivity of these composites is likely to be limited by the amount of filler used, the crystal structure defects on the particle surface, and the fractality and the imperfection of the particle network.

4.1. Introduction

Conductive polymer composites are, in general, made by incorporation of (semi)conductive fillers into an insulating polymer matrix.[1-4] Generally, at room temperature the DC volume conductivity σ_v of the polymer composites increases sharply above a critical conducting filler concentration, known as the percolation threshold φ_c. At larger filler concentrations ($\varphi > \varphi_c$), the increase in σ_v becomes smaller and reaches a level where the σ_v hardly changes with increasing filler amount. This level is called the maximum volume conductivity σ_{max} (Figure 1.1). The main problem is that often a large amount of conducting filler is required in order to obtain reasonable conductivity levels. Statistical percolation models predict a φ_c of 16 vol. % for randomly distributed non-overlapping hard spheres.[5-7] Such a large amount of filler deteriorates the mechanical properties and leads to poor processability of the matrix. Furthermore, the cost of the final material is often beyond the acceptable range due to the large fraction of the expensive conducting species.[8] Another disadvantage of polymer composites is that normally the σ_{max} is orders of magnitude lower than the intrinsic conductivity of the filler itself.[8] A σ_{max} value closes to the conductivity of the filler would broaden the application possibilities of these composites considerably.

It is widely accepted that the conductivity of a polymer composite is based on the presence of a continuous network of (semi)conductive filler particles throughout the matrix.[1-4] The particle network is, generally, formed during processing. During the network formation the size of the particles may play an important role, because it influences the rate of diffusion.[9-11] In addition, it has been reported that in compressed powder the size of the (semi)conductive particles tremendously affect the charge transfer between particles.[12,13] Hence, it is expected that a difference in nanoparticle size may influence φ_c and σ_{max} of the polymer composites.

For specific (semi)conductive nanofillers the φ_c can be lower than 1 vol. %.[1,14-20] Aquocyanophthalocyaninato Co(III) (Phthalcon 11) (Scheme 4.1) is one of these nanofillers. It can be used as nanometer-sized semi-conductive additive in a broad range of polymer matrices, resulting in composites with low values of φ_c.[8-10,21-24] Phthalcon 11 is a promising semi-conductive nanofiller because of its high thermal stability and attractive health, safety and environmental properties.[9,10] Amazingly, we found that Phthalcon particles with different compositions can be synthesized in different sizes, but they still have very similar XRD patterns and powder conductivity.

Furthermore, Phthalcon/epoxy composites can be made in a broad range of filler concentrations.[9,10] In depth information on the conductivity of intrinsic, powder and particle/polymer composites is available for one of the Phthalcon compounds.[9,10,21-26] Therefore, we decided to use cross-linked epoxy matrices containing Phthalcon fillers as a model system for our study on particle size effects.
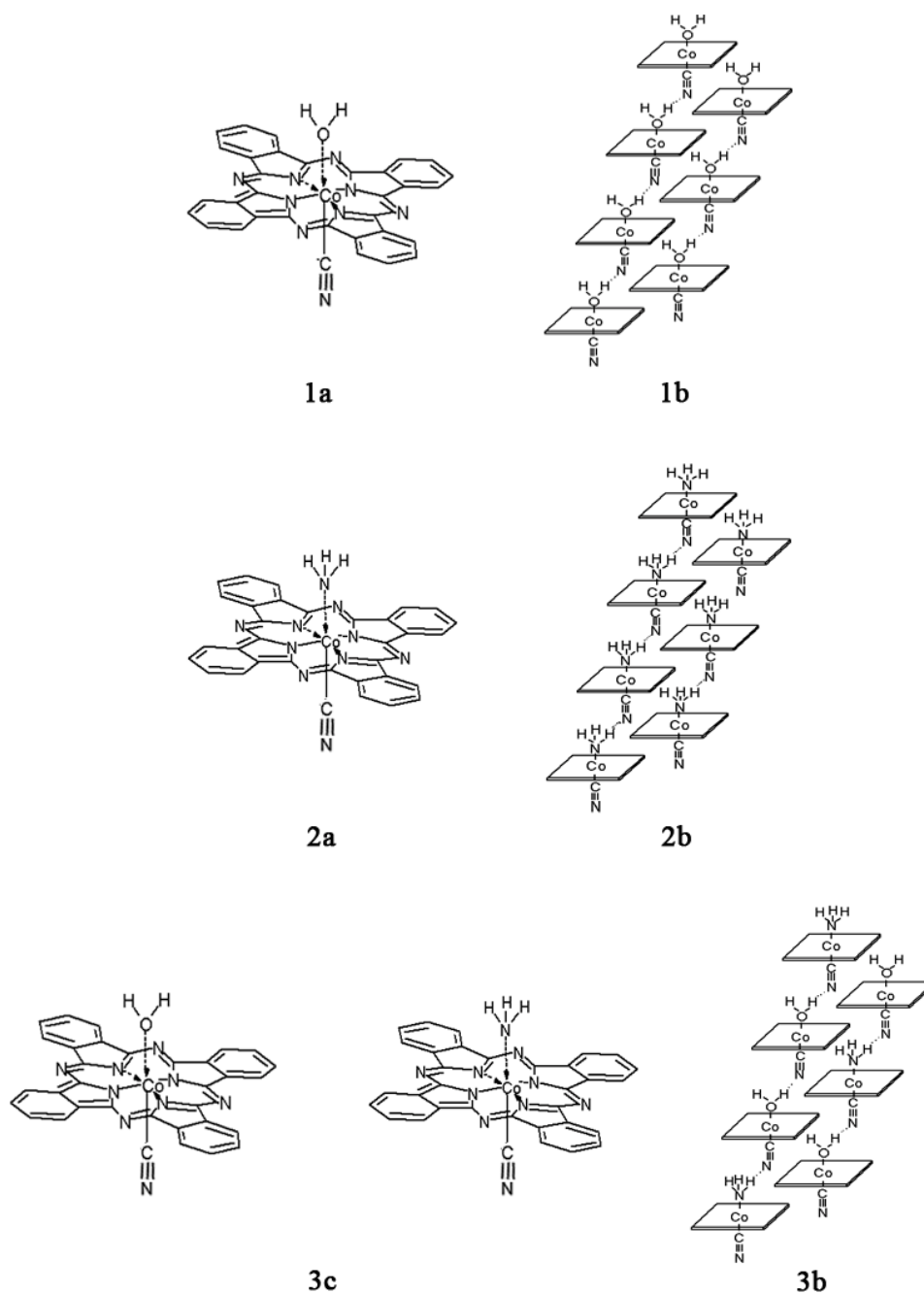
Scheme 4.1. Molecular and crystal structures of Phthalcon 11 (1a, 1b), Phthalcon 12 (2a, 2b) and Phthalcon 11/12 (3a, 3b). Phthalcon 11/12 contains both NH_3 and H_2O, its molecular structure is a mixture of 1a and 2a, but Phthalcon 11/12 is still crystalline (3b).

In this chapter we describe the synthesis of semi-conductive Phthalcon particles with various nanometer sizes. Two of them are new semi-conductive phthalocyanine fillers. The conductivity of cross-linked epoxy matrices containing these Phthalcon particles is also discussed. Special attention is given to the influence of particle size and chemical composition on the characteristics of the particle networks, on the way these networks are formed, and on σ_v, σ_{max} and φ_c of the polymer composites.

4.2. Experimental

4.2.1. Materials

β-phthalocyanine Co(II) (β-PcCo) (97 %) was purchased from Merck. It was carefully dried at 80 °C for 48 h under vacuum (~ 0.01 mbar) and ground into fine powder in a mortar before use. Acetone (99.5 %), sodium cyanide (NaCN, ≥ 97.0 %) and ammonium hydroxide water solution (28.0-30.0 % as NH_3) were purchased from Aldrich. *m*-cresol (spectrophotometric grade) and ethanol (absolute GR for analysis) were purchased from Merck. Epoxy prepolymer (Epikote 828) was purchased from Resolution Nederland BV. The amine cross-linker Jeffamine D230 was purchased from Huntsman BV, Belgium. The structures of coating components are shown in Scheme 4.2. All these chemicals were used as received.

Epikote 828 (m ≈ 0.1)

Jeffamine D230 (n ≈ 2.6)
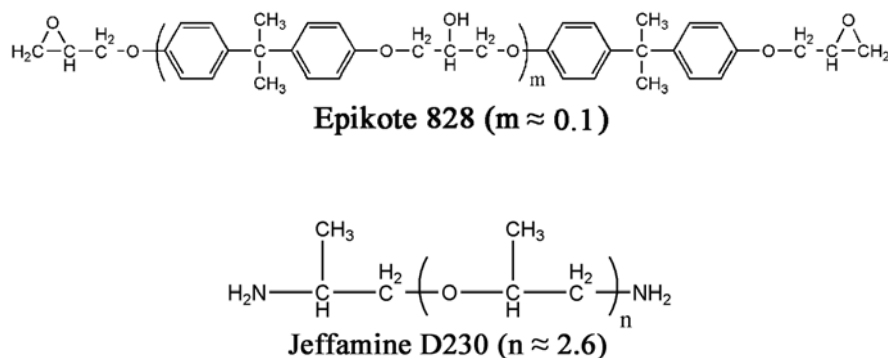
Scheme 4.2. Chemical structures of epoxy coating components.

4.2.2. Synthesis of Phthalcon Particles

Phthalcon 11 (Scheme 4.1) is a patented semi-conductive phthalocyanine compound.[21,23] It can be synthesized in high purity (> 99%) and yield (> 97 %) using a two-step reaction (Scheme 4.3).[9,10,21,23] In the first step, 15.1 g starting material β-PcCo was dispersed in 200 mL ethanol under magnetic stirring; a saturated NaCN/demi-water solution (7.8 g/11 mL) was added to this dispersion. Air, which

was used for the oxidation of the Co(II) ion, was introduced; the temperature of the reaction mixture was increased to 72 °C and the slurry was gently refluxed for 72 h. During reaction a solid ionic precursor compound was formed, which was filtered off, washed with water/ethanol and then extracted with acetone. The precursor powder was obtained by distillation of the acetone solution. In the second step Phthalcon 11 was prepared by refluxing this precursor powder (7.9 g) in water (75 mL) under a nitrogen stream (Scheme 4.3B). The reaction temperature was 98 °C and the reaction time was 72 h.
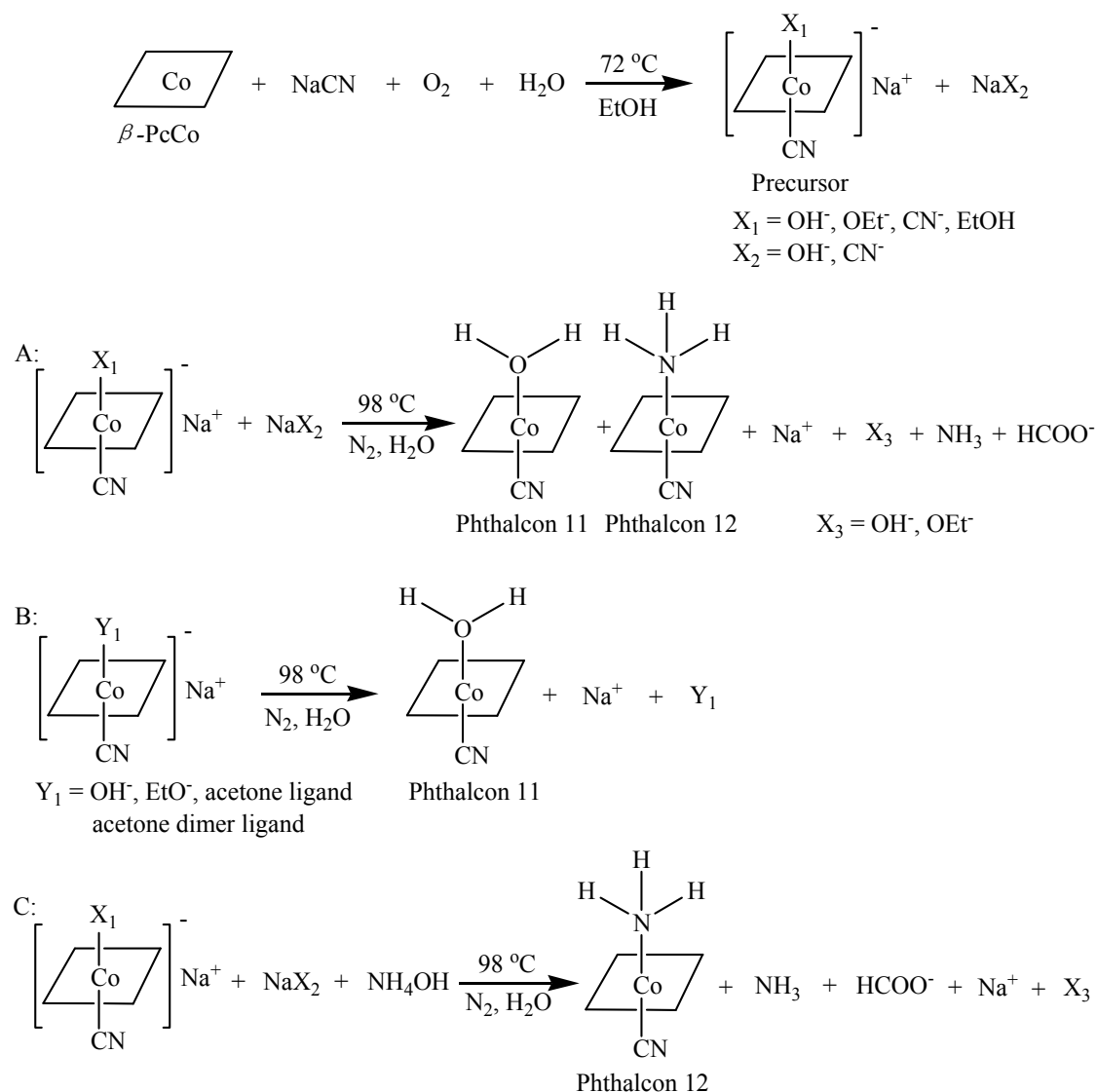
Scheme 4.3. Two-step synthesis of Phthalcon 11, Phthalcon 12 and Phthalcon 11/12.

When a non-washed precursor (12.0 g) was used in step 2 in the presence of a sufficient amount of NH_4OH (2.0 g) following the same reaction conditions as described above, aminocyanophthalocyaninato Co(III) (Phthalcon 12) was formed instead of Phthalcon 11 (Scheme 4.3C). When a non-washed precursor was used in step 2 with/without the addition of a small amount of NH_4OH, Phthalcon 11/12 was formed (Scheme 4.3A). During reaction both NH_3 and formiate were detected in step A and C. At the end of the reaction the blue Phthalcon powder was filtered, washed with water and dried under vacuum (~0.01 mbar) at 80 ^{o}C for at least 2 days before use. The density of these Phthalcon compounds is 1.65 g/cm^3.[22]

The same precursor batch was used as starting material in step A and C. This batch was also used in the acetone extraction step to prepare the starting compound needed for step B. The pH of the reaction medium was always between 10 and 11 in both reaction steps.

4.2.3. Coating Preparation

All Phthalcon compounds were added as fillers in epoxy matrices using the same preparation method as described before elsewhere.[9,10] The Phthalcon powder was first dispersed in *m*-cresol under magnetic (1 h) and ultrasonic (1 h) stirring. To this dispersion Jeffamine D230 and Epikote 828 were added by keeping the NH/epoxy molar ratio at 1/1. This mixture was magnetically stirred for 5 min, ultrasonically degassed for 5 min, and then cast on a polycarbonate substrate using a doctor blade applicator with an opening of 120 μm. Next it was cured at 100 ^{o}C under vacuum (~ 0.01 mbar) for 4 h and later post-cured at 120 ^{o}C under vacuum (~ 0.01 mbar) for 8 h.

The concentrations of Phthalcon in the cross-linked materials ranged from 0 to 12 vol. % based on the total volume of the final cross-linked composites. Coatings with Phthalcon concentrations higher than 15 vol. % could not be made. The thicknesses of the coating materials studied were between 10 and 70 μm, as determined by a digital screw micrometer. Coatings with thicknesses between 50 and 70 μm were used for the conductivity measurements. For the optical microscopic analyses the coatings used had a thickness of about 10 μm.

4.2.4. Characterization

Fourier Transform Infrared (FT-IR) FT-IR spectra were measured in transmission by means of Biorad UMA500 IR microscope coupled to a FTS6000 IR spectrometer.

All spectra were recorded between 4000 and 650 cm^{-1} with a resolution of 2 cm^{-1} co-adding 200 scans.

Powder X-ray Diffraction (XRD) XRD spectra were measured using a Rigaku diffractometer. The XRD spectra were recorded in the range of 5 $^{\circ}$ < 2θ < 40 $^{\circ}$ using Cu-K$_{\alpha 1}$ radiation with a scanning speed of 0.01 $^{\circ}$ min^{-1}.

Phthalcon 11 particles are too small to determine the molecular and crystal structure by single crystal XRD. Therefore, a broad range of techniques were used in combination with crystallographic modeling. The techniques used were XPS, XRD, neutron diffraction, FT-IR, UV-Vis, liquid and solid state NMR and Pyrolysis Combustion Mass Spectrometry Elemental analysis (PCME). To improve these analyses, specially labeled Phthalcon 11 compounds were also prepared (Chapter 3).[22,23] In depth information on the crystal structure of Phthalcon 11 was obtained by using powder XRD, neutron diffraction and ^{2}H-NMR. The modeling was carried out with a 3D graphic program named PLUVA, which makes it possible to obtain information on the space group and molecular packing. The complete patterns Rietveld analysis was performed with FOX (Free Objects for Xtallography) and GSAS (General Structure Analysis System) programs to unravel the crystal structure in more detail. This last part of modeling was done by assuming that the fragments detected from PCME were present as connected ligands or separated molecules/ions in the crystal lattice.[22,23]

The molecular and crystal structures of Phthalcon 12 and Phthalcon 11/12 were determined in a similar way as that of Phthalcon 11.

Optical Microscopy (OM) The morphology of Phthalcon particle networks in the coatings after cross-linking was studied with OM. The OM analyses were carried out with a Reichert-Jung Polyvar-Met microscope using the transmission bright-field technique.

Transmission Electron Microscope (TEM) A Jeol2010 TEM was used to determine the Phthalcon particle sizes. For this purpose, 10^{-3} mol/L Phthalcon/ethylene glycol dispersions were prepared; the dispersions were later drop cast on a carbon film supported by copper grid. The TEM was operated at 200 kV.

Dynamic Light Scattering (DLS) DLS measurements were performed with a Malvern Instruments Zetasizer Nano ZS. All DLS measurements were recorded at 20 $^{\circ}$C on 10^{-3} mol/L Phthalcon/ethylene glycol dispersions. This technique was also used to characterize the sizes of Phthalcon particles.

DC Volume Conductivity σ_v The σ_v of the compressed powder was determined at room temperature using a standard two-electrode measuring method. The powder was pressed in a homemade powder holder by tightening screw; the powder holder had an inner diameter of 12 mm. The thickness of the powder layer was a few millimeters.[24,25,27]

The σ_v of the coatings was measured at room temperature using a standard four-point method with a Keithley 237 high voltage source measuring unit and a Keithley 6517A high voltage electrometer. The measurements were carried out according to standard ASTM D991 and instructions of Keithley "low conductivity level measurements". Silver paste (silver conductive adhesive 416, electron microscopy sciences, USA) was used to ensure good contact between sample surface and measuring electrodes.

From the measured voltage V, current I and coating thickness d, the value of σ_v was calculated using the following equation:

$$\sigma_v = \frac{IL}{bdV} \tag{4.1}$$

where L is the distance between neighboring silver paint traces and b is the trace length. Before each measurement, four silver paint traces were applied on the coating surface with a trace length b of 1 cm and distance L of 1 cm. Coatings used in the conductivity measurements had a thickness d between 50 and 70 μm, as determined using a digital screw micrometer caliper. The presented σ_v for each Phthalcon concentration is an average value of at least three different coatings measured at three different positions.

4.3. Results and Discussion

4.3.1. Synthesis and Characterization of Phthalcon Compounds

The main difference in the synthesis of Phthalcon compounds is the absence/presence of NH_3 in the second reaction step. In this step NH_3 can be formed from NH_4OH as well as from CN^-. The CN^- was present as a ligand in precursor and/or as a separated

impurity (route A and C, Scheme 4.3). Moreover, it is not stable in highly basic reaction medium (pH ≈ 11) and can convert to NH_3 and $HCOO^-$.

From PCME and XPS the empirical formula of Phthalcon 11 appears to be $PcCo(III)(CN)(H_2O)$ (Pc = $C_{32}H_{16}N_8$); the presence of Co(III) phthalocyanine ring, CN and H_2O was confirmed by FT-IR, solid state ^{13}C-NMR and ^2H-NMR. These measurements were also performed on specially labeled Phthalcon 11, namely $PcCo(III)(^{13}CN)(H_2O)$, $PcCo(III)(C^{15}N)(H_2O)$ and $PcCo(III)(CN)(^2H_2O)$. Results from these measurements strongly suggest that the CN and the H_2O are present as coordinated ligands. Using PLUVA program, powder XRD data and a method developed at Shell, the space group P_{21} and the molecular packing were obtained. Based on powder XRD and neutron diffraction data, whole patterns Rietveld analysis shows that indeed the H_2O and the CN are present as ligands; NMR and FT-IR spectra also indicate this. The presence of an intermolecular hydrogen bonding between the H of the H_2O and the N of the CN, as shown in Scheme 4.1(1b), was confirmed by ^2H-NMR. The unit cell data are summarized in Table 4.1. Detailed information on above described synthesis, molecular and crystal structure analyses on Phthalcon 11 will be published elsewhere.[23] The overall crystal structure of Phthalcon 11 is schematically presented in Scheme 4.1(1b). An important aspect of this crystal structure is that the π orbitals of the phthalocyanine rings in two neighboring stacks interact, with the van der Waals distance (3.35 Å) between them (Scheme 3.6).[23]

Table 4.1. Unit cell parameters of Phthalcon compounds.

Unit Cell Parameter	Phthalcon 11	Phthalcon 12	Phthalcon 11/12[#]
α	90 º	90 º	90 º
γ	90 º	90 º	90 º
β	102.6 ± 0.2 º	104.6 ± 0.1 º	104.3 ± 0.1 º
a	7.308 ± 0.001 Å	7.393 ± 0.005 Å	7.355 ± 0.006 Å
b	24.89 ± 0.01 Å	24.62 ± 0.02 Å	24.71 ± 0.02 Å
c	7.149 ± 0.001 Å	7.328 ± 0.0005 Å	7.240 ± 0.007 Å

[#] Phthalcon 11/12, the ratio between NH_3/H_2O is 3/10.
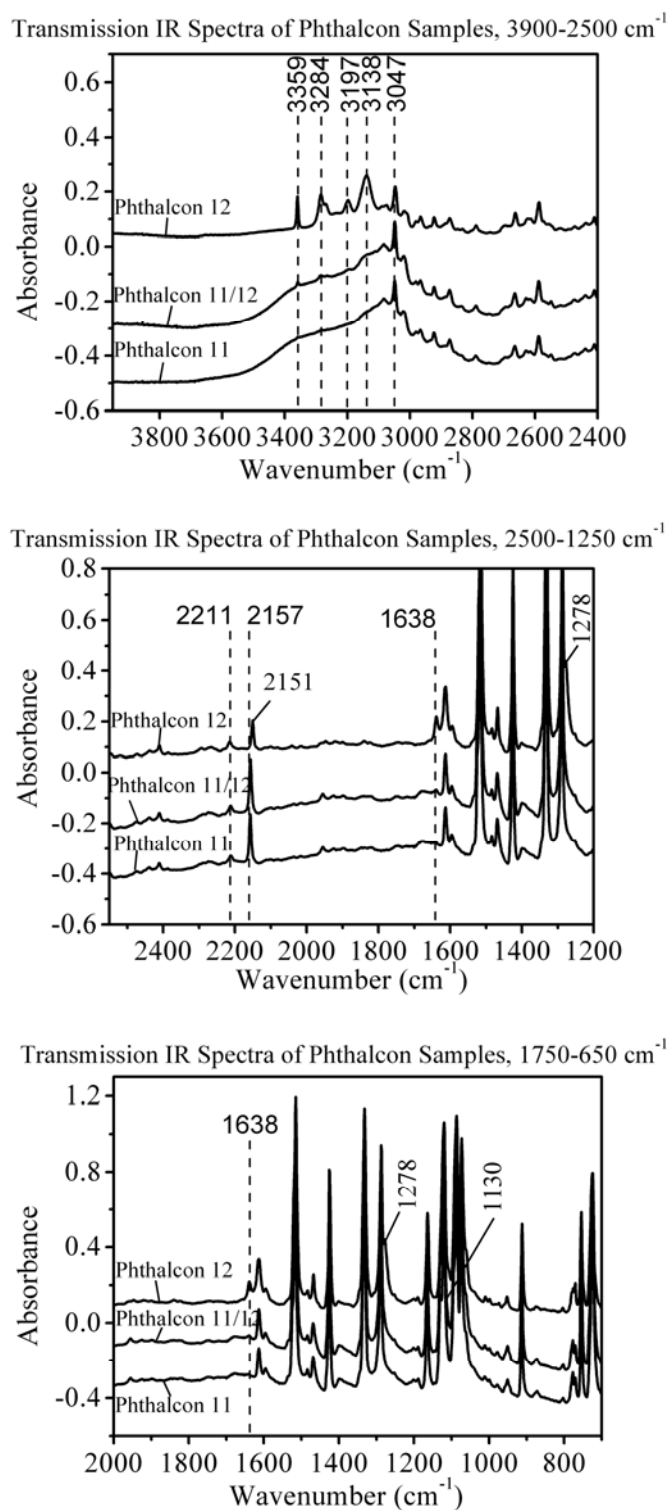
Figure 4.1. FT-IR spectra of Phthalcon compounds.

In Phthalcon 11/12 the ratio between NH_3/H_2O is 1/10.

With PCME it was determined that Phthalcon 12 has an empirical formula of $PcCo(III)(CN)(NH_3)$ and the empirical formula of Phthalcon 11/12 is $PcCo(III)(CN)(NH_3)_x(H_2O)_y$ with a NH_3/H_2O ratio about 1/10 or 3/10 for two samples studied. The latter one was synthesized by adding a small amount of NH_4OH in the second reaction step.

The absence of the H_2O ligand in Phthalcon 12 is also suggested by the lack of a shoulder at 3350 cm^{-1} in FT-IR spectrum (Figure 4.1). This shoulder was clearly observed in the spectrum of Phthalcon 11. As has been shown by FT-IR using a deuterium labeled water fragment, this band can be attributed to the O-H stretching vibration.[23]

When we compare the FT-IR spectrum of Phthalcon 12 with that of Phthalcon 11 in more detail, we observed the appearance of several new bands in the region of 3360-3100 cm^{-1} and single bands at 1638, 1278 and around 770 cm^{-1}. Furthermore, one band disappeared from Phthalcon 12 spectrum (1130 cm^{-1}); a shift from 2157 to 2150 cm^{-1} was also observed (Figure 4.1, Table 4.2).

Table 4.2 Characteristic IR vibrations of Phthalcon compounds.

v (cm^{-1})	Phthalcon 11	Phthalcon 12	Phthalcon 11/12	
OH Stretching	3350	-	3350[*]	3350[#]
	-	3360	3358	3360
NH$_3$ Stretching	-	3284	3284	3281
	-	3193	3191	3201
	-	3138	3140	3132
CN Stretching	2157	2150	2156	2153
NH$_3$ Scissor	-	1638	1639	1638
NH$_3$ Wagging	-	1278	1278	1279
Co – H$_2$O	1130	-	1130	1129
NH$_3$ Stretching	-	770	770	770

[*] Phthalcon 11/12, the ratio between NH_3/H_2O is 1/10.
[#] Phthalcon 11/12, the ratio between NH_3/H_2O is 3/10.

The band at 1130 cm^{-1} that disappeared in the spectrum of Phthalcon 12 is probably a Co-H$_2$O vibration.[28] The band at 2150 cm^{-1}, which occurs at a somewhat lower position than in the spectrum of Phthalcon 11, is likely a CN stretching vibration.[29] The shift of the CN vibration also indicates the replacement of the H$_2$O ligand by another ligand in Phthalcon 12. Hence, the molecular structure of Phthalcon 12 is likely to be the one shown in Scheme 4.1(2a).

In Phthalcon 11/12 the same new bands, which are attributed to the NH$_3$ vibrations, were observed (Table 4.2 & Figure 4.1), although at much lower intensities since the amount of NH$_3$ is smaller (0.1 or 0.3). The broad shoulder at 3350 cm^{-1} and the presence of a shoulder at 1130 cm^{-1} suggest that this compound still contains coordinated water; this is in agreement with the PCME analysis and therefore we conclude that the NH$_3$ as well as the H$_2$O is present as coordinated ligand. In both Phthalcon 11/12 samples, only one CN vibration was found at the position between those of Phthalcon 11 and Phthalcon 12. Therefore, the molecular structure of Phthalcon 11/12 is likely to be the one shown in Scheme 4.1(3a).

The XRD patterns of these Phthalcon compounds appear to be very similar (Figure 4.2), which points to a very similar crystal structure. Using whole pattern Rietveld refinement analysis and powder XRD data described previously, we found that the unit cell dimensions of Phthalcon 12 and Phthalcon 11/12 are very similar to that of Phthalcon 11 (Table 4.1). The NH$_3$ and/or H$_2$O are always presented as (a) coordinated ligand(s) and the distances between atoms are also similar (Scheme 4.4).[23]
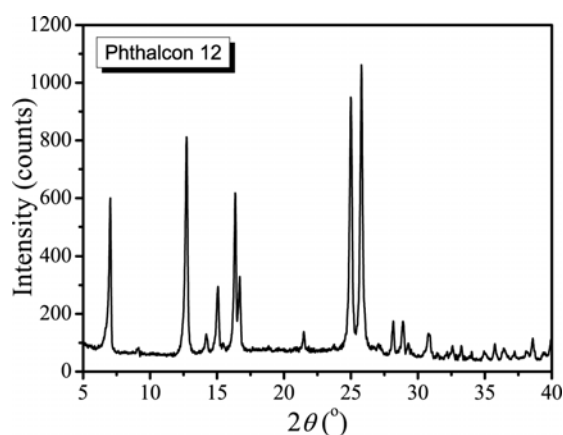
Figure 4.2. XRD patterns of Phthalcon 12.
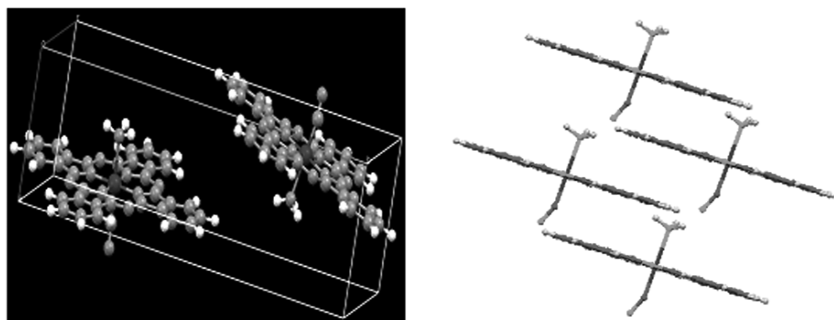
Scheme 4.4. One unit cell of Phthalcon 12 (left). It contains two molecules which are rotated to each other. (right) the phthalocyanine rings of two neighboring stacks interact; the distance between them is the van der Waals distance (3.35 Å).

In Phthalcon 11 crystal, the hydrogen bonding between the H of the H_2O and the N of the CN from the neighboring molecule in the stack is present. Hence, in Phthalcon 11 crystal an intermolecular polymeric structure exists (Scheme 3.6).[23] The modeling of Phthalcon 12 and Phthalcon 11/12, together with the FT-IR spectra also suggest the presence of a hydrogen bonding between the H atom of the NH_3 group and the N atom of the CN group. Therefore, similar intermolecular polymeric structures are proposed (Scheme 4.1, 2b, 3b).

Using the crystal structure of Phthalcon 11 as a starting point, Density-Functional Theory (DFT) calculations were performed to determine the origin of the powder conductivity. These calculations show that Phthalcon crystals are bulk semi-conductors with band gap of about 1.2 ev.[23]

The σ_v values of different Phthalcon powders are almost similar (about 4×10^{-4} S/cm), in agreement with the proposed similarity in crystal structures.

4.3.2. Particle Sizes

Besides variations in chemical composition, the main difference between these three types of Phthalcon particles is their sizes. The sizes were analyzed with TEM and DLS. In Figure 4.3 DLS as well as TEM data of Phthalcon 11/12 is presented. The TEM image shows mainly two dimensions of the particle. These sizes are almost equal with an average of 250 nm. Further TEM analysis reveals that for Phthalcon 11/12 the third dimension is 50 nm. Only one peak in DLS spectrum was found, which positions at 250 nm (Figure 4.3a). This value corresponds to the largest value observed with TEM. It has been shown that for non-spherical platelet particles the

largest dimension plays the dominant role in DLS.[30] Since our Phthalcon particles are also platelet-shaped, the value obtained from DLS is the size of the largest dimension as well. The particle sizes of the other two Phthalcon compounds were determined in the same way. Values of 150 x 150 x 30 nm^3 (Phthalcon 11) and 500 x 500 x 100 nm^3 (Phthalcon 12) were obtained.
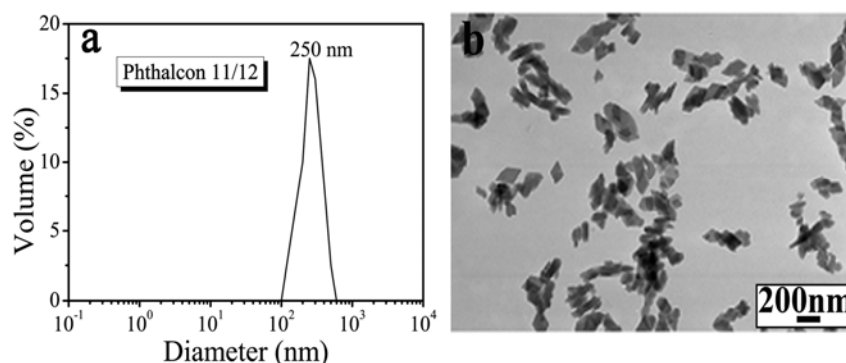
Figure 4.3. DLS measurement (a) and a TEM image (b) of Phthalcon 11/12. The compound has a primary particle size of 250 x 250 x 50 nm^3 and the ratio between NH$_3$/H$_2$O is 1/10.

4.3.3. Crystal Structure of Phthalcon 11/12

Phthalcon 11/12 can be, in principle, a physical mixture of two phases: Phthalcon 11 and Phthalcon 12, or a mixed single crystalline phase. In the later case each crystallite contains NH$_3$ as well as H$_2$O. We think that for Phthalcon 11/12 a mixed single crystalline structure is likely because:

1) Only one CN stretching vibration was observed, of which the position is between those of Phthalcon 11 and Phthalcon 12. If Phthalcon 11/12 was a physical mixture, two peaks would have been present at 2150 and 2157 cm^{-1}; moreover, this position also depends on the amount of NH$_3$ present (Table 4.1);

2) There is a gradual increase in lattice parameters (β, *a* and *c*) and a gradual decrease in *b* when the amount of NH$_3$ increases (Table 4.1);

3) Phthalcon compounds have almost the same unit cell. The interactions between ligands are small, therefore the crystal structure is dominated by the interactions between phthalocyanine rings, rendering a mixed single crystal likely;

4) Modeling shows that there is sufficient space to exchange a H$_2$O molecule with a NH$_3$ molecule within one unit cell without changing the positions of the other atoms;

5) DLS and TEM data only show one particle size, which is between those of Phthalcon 11 and Phthalcon 12. These data do not suggest a dual particle size distribution on Phthalcon 11/12.

All Phthalcon compounds were synthesized using the same reaction time and very similar starting compositions (Scheme 4.3 and experimental section). The formation of a larger crystallite size may be attributed to a lower amount of primary nuclei formed at the initial reaction stage when NH_3 is present in the reaction medium. Therefore, small variations in reaction composition can lead to Phthalcon particles with different particle sizes and chemical compositions, but still have very similar powder conductivity and XRD patterns.

4.3.4. Primary Particle Size and Chemical Composition Effects on the Powder Conductivity

The σ_v of the compressed (semi)conductive powder depends on the intrinsic conductivity of the particle and the efficiency of charge transport between particles (by hopping or tunneling).[31-36] Coulomb charging may also influence the powder conductivity when the size of the particle is below 100 nm.[12,13] However, at room temperature for particles larger than 100 nm Coulomb charging is expected to be negligible.[13] This has been confirmed by combining frequency dependence conductivity measurements together with infrared transmission and reflection measurements on compressed Phthalcon 11 powder.[13,25,26] These data show that at room temperature in compressed Phthalcon 11 powder the most likely mechanism for charge transport is variable range hopping by cotunneling.[13,25,26] The measurements also show that at room temperature the number of charge carriers involved in hopping process between particles is similar to the number of carriers that determines the conductivity inside a Phthalcon 11 crystal.[25,26] This means that at room temperature Phthalcon 11 crystals are large enough not to lower the overall charge transport by limiting the interparticle conduction caused by Coulomb charging effects. Therefore, at room temperature for Phthalcon 11 the particle size is not an important factor in determining the conductivity of the compressed powder.

Because the crystal structures of these Phthalcon compounds are very similar, and also because Phthalcon 12 and Phthalcon 11/12 are much larger in size, we may expect that for all Phthalcon compounds studied here the σ_v of the compressed powder will not be affected by the differences in particle size. Indeed, we found very similar

σ_v values for these compounds. Still, this value (4 x 10^{-4} S/cm) is two orders of magnitude lower than the intrinsic conductivity of Phthalcon (2 x 10^{-2} S/cm).[13,25,26] This difference may be due to the surface barriers caused by, for instance, a difference in coordination of the metal ions at the surface, a difference in ligand structure at the surface vs. those in the bulk of the particle, and/or by lack of contact due to imperfect packing of the platelet particles.

4.3.5. Primary Particle Size and Chemical Composition Effects on the Conductivity of Cross-linked Phthalcon/Epoxy Coatings

For each Phthalcon compound a number of cross-linked Phthalcon/epoxy coatings were prepared. The relation between the σ_v of the coatings as a function of Phthalcon volume concentration φ is shown in Figure 4.4a. These curves appear to be very similar. The value of σ_{max} is always around 10^{-7} S/cm. By extrapolating these curves to $\sigma_v = 10^{-16}$ S/cm (the conductivity of pure epoxy matrix[8]), the φ_c was determined, which is very similar and on average equals to 0.9 vol. %. Hence, within the uncertainty of measurements the log σ_v - φ relation is independent of the size and chemical composition of the Phthalcon particles.
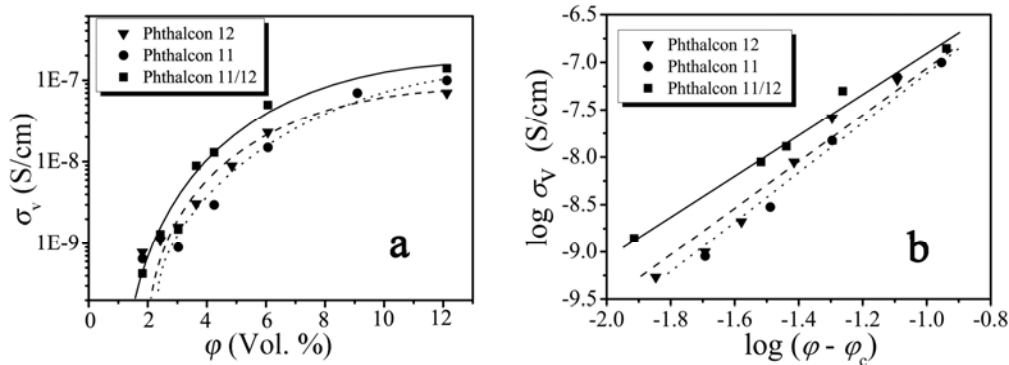
Figure 4.4. (a). log σ_v - φ relation of cross-linked Phthalcon/epoxy composites. (b) log σ_v - log (φ - φ_c) relation. In Phthalcon 11/12, the ratio between NH_3/H_2O is 1/10.

To further evaluate the Phthalcon particle network structure, data in Figure 4.4a was plotted as a function of log(φ - φ_c) based on equation:

$$\sigma_v = c(\varphi - \varphi_c)^t \qquad (4.2)$$

where c is a constant and t is the critical exponent. We found that t = 2.1 - 2.2 for all epoxy coatings studied here. These t values are in good agreement with the theoretical value t = 2.0 predicted for 3D random percolating system[37,38] and suggest a very

similar type of particle network formation, independent of particle size and chemical composition.

Although the primary Phthalcon particle sizes are too small to be seen under the OM, the particle networks could be easily observed when Phthalcon concentration is above φ_c because of the fractality of the network structures (Figure 4.5). In order to study the structures of these networks in detail, the fractal dimension of the particle network was determined using the method of tiling (Figure 4.6).[9,10,39,40] The method was applied as follows: a coating containing 2 vol. % Phthalcon was analyzed. First we converted the OM image into a binary version (Figure 4.6b), and then the binary image was broken into tiles of a given size. The number of tiles N containing Phthalcon network was counted and plotted on a logarithmic scale versus the size a of these tiles (Figure 4.6c). The relation between the number of tiles N and the tile size a was fitted by

$$N(a) \infty\, a^{-df} \tag{4.3}$$

In this expression the exponent d_f represents the fractal dimension of the aggregates.[41] Two linear regions which intersect around 20 μm were always observed (Figure 4.6c). The value of this intersection is called correlation length ξ, which is the average size of the particle aggregates from which the particle network is formed. The results from fractal structure analyses are summarized in Table 4.3. The values given are average values of at least three calculations with different sets of tile sizes. The slope of lines below 20 μm corresponds to a d_f of 1.68 - 1.70. When the tile size is larger than 25 μm, a d_f value of 1.94 - 1.97, which is close to Euclidean dimension D = 2, was obtained. This suggests that at dimensions above 25 μm the particle network is no longer fractal or may have a fractal dimension larger than 2. We observed that all images studied appear to be insensitive to the precise way of getting the threshold.

The d_f values of 1.68 - 1.70 observed here are close to the d_f value of 1.75 reported before for cross-linked Phthalcon 11/epoxy coatings, although the size of Phthalcon 11 used was somewhat different.[9,10] Within the uncertainty of measurements our d_f values are also close to the theoretical value for Diffusion Limited Cluster Aggregation (DLCA).[42-46] This suggests that the fractal particle networks observed in our coatings are formed by this mechanism.

Therefore, not only the σ_v of the compressed Phthalcon powders, but also the log σ_v - φ relation of the Phthalcon/epoxy coatings seems to be independent of Phthalcon chemical composition and particle size.
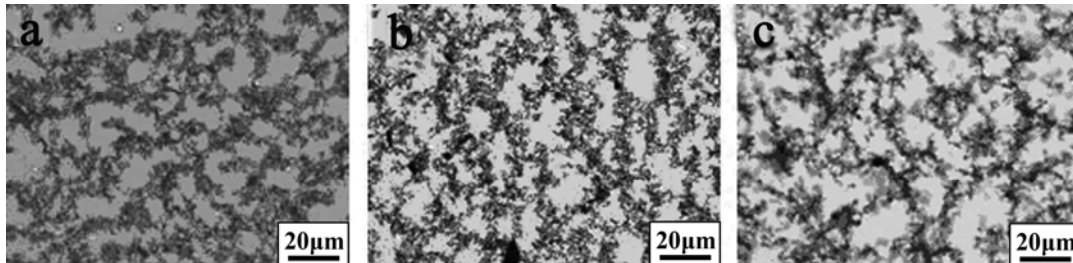
Figure 4.5. Coatings made from Phthalcon 11 (a), Phthalcon 11/12 (b) and Phthalcon 12 (c). A constant Phthalcon concentration of 2 vol. % was used. In Phthalcon 11/12, the ratio between NH_3/H_2O is 1/10.
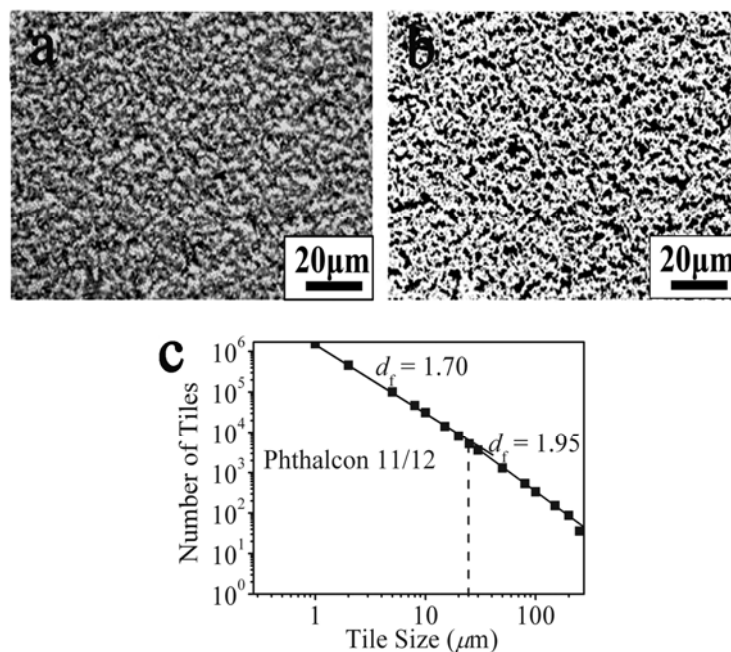
Figure 4.6. (a) OM image of Phthalcon 11/12 (2 vol. %) particle network in a cross-linked epoxy coating; (b) binary image converted from Figure 4.6(a); (c) results from fractal structure analysis. Phthalcon 11/12 has a NH_3/H_2O ratio of 1/10.

Table 4.3. Fractal dimensions and correlation lengths of Phthalcon particle networks.

Phthalcon	Particle Size (nm^3)	ξ (μm)	d_f (for $a < \xi$)	d_f (for $a < \xi$)
Phthalcon 11	150 x 150 x 30	25	1.68	1.94
Phthalcon 12	500 x 500 x 100	25	1.69	1.94
Phthalcon 11/12	250 x 250 x 50	20	1.70	1.95

The volume of an individual primary Phthalcon particle is far below 1 μm^3, so Brownian movement of the particles is possible as long as the viscosity of the system is sufficiently low and the size of the particle aggregates is sufficiently small. Earlier results show that Phthalcon 11 particles are very well-dispersed before cross-linking.[9,10] The lack of particle size effects on the log σ_v - φ relation and fractal network structure indicate that the particle network formation occurs at the early stage of cross-linking, far before the gel point of the epoxy matrix.

In general, the σ_v of a polymer composite containing semi-conductive particles may be influenced by the intrinsic conductivity of the particle itself, the σ_v of the compressed powder, the amount of insulating matrix between the conductive particles in the networks and the type of the network formed.[8,12,13,47-50] As has been shown that the intrinsic conductivity of Phthalcon crystal, the σ_v of the compressed powder, the σ_v of the Phthalcon/epoxy composites and the type of the particle network are all very similar for the three types of Phthalcon studied here. As a result, we expect that the amount of matrix between particles is also similar. From conductive AFM measurements we found for a specific cross-linked Phthalcon 11/epoxy coating that no epoxy matrix is present in the particle network.[24] This coating contained 12 vol. % Phthalcon 11 and has a σ_v of 3 x 10^{-8} S/cm.[24] Taking into account the uncertainty of measurements this value is comparable with the σ_max values of 1 x 10^{-7} S/cm shown in Figure 4.4. This suggests that for our coatings, at least when the Phthalcon concentration is sufficiently high, no epoxy matrix is present between Phthalcon particles in the conductive path and that these particles really touch each other. When no matrix material is present between Phthalcon particles in the network, individual cross-linked Phthalcon 11/epoxy coating should have a similar conduction mechanism and a similar temperature, frequency and field dependence as the compressed Phthalcon powder. This was indeed observed recently for the specific Phthalcon 11/epoxy coating mentioned above.[24,27]

Evidence has been presented that an insulating layer between particles does not exist for (some of) our Phthalcon/epoxy coatings. Also for these coatings the sizes of Phthalcon filler particles are too large to explain the low σ_{max} values by Coulomb charging effects with respect to the σ_v of the compressed powders. Hence, the difference between the σ_{max} of the composite and the σ_v of the compressed powder probably has to be attributed to, for instance, the volume concentration of Phthalcon used in the coatings, the fractality of the network structure and the imperfect particle network structure containing loops and dangling chains.[24,27]

In practice, the σ_{max} of the polymer composites containing (semi)conductive nanoparticles is always several orders of magnitude lower than the intrinsic conductivity of the filler itself. This has been explained, generally, by the presence of insulating polymer layers between filler particles in the network. Such insulating layers lower the electrical conductivity of the network by limiting the charge transfer efficiency. This has been described by tunneling through and/or hopping over these layers. Nevertheless, the low σ_{max} values reported in the past for polymer nanocomposites containing spherical nanofillers with sizes below 100 nm could not be explained only by the presence of insulating layers between particles, even when the networks are homogeneously distributed. We expect that in these composites the lowering in σ_{max} caused by Coulomb charging effects has to be taken into account. Our results also suggest that other factors, such as additional surface barriers between particles caused by inhomogeneous surface composition and the fractality and imperfection of the particle network structure, also need to be considered.

Recently, Zhang *et al.* showed that for thermoplastic nanocomposites containing carbon black or carbon fibers, the formation of a conductive particle network strongly depends on processing time and temperature used.[11] They showed that the viscosity change during processing plays an important role in the rate of particle network formation and they called this phenomena dynamic percolation. The time used for processing our materials is relatively long. Hence, the increase in viscosity during processing is more gradually because no particle size effects on the network formation was observed; and dynamic percolation is expected to be negligible in our materials. Whether dynamic percolation also plays a role in other thermoset polymer nanocomposites is unclear.

4.4. Conclusions

Intrinsically conductive Phthalcon nanoparticles can increase the conductivity of cross-linked epoxy composites by forming a continuous particle network throughout the insulating matrix. Phthalcon particles with three different nanometer sizes, but almost equal XRD patterns and powder conductivity levels have been successfully synthesized. Two of them have completely new chemical compositions. The influence of Phthalcon particle size and chemical composition on the relation between the conductivity of the composites and the amount of Phthalcon present appears to be minimal. For these three types of Phthalcon particles a percolation threshold of 0.9 vol. % and a maximum volume conductivity of 10^{-7} S/cm were found. Very similar fractal Phthalcon particle network structures were always observed in the coatings and these network structures are likely to be formed by diffusion limited cluster aggregation. Coulomb charging appears not to significantly lower the σ_{max} of these cross-linked Phthalcon/epoxy coatings, either. Evidence is present that the relatively low σ_{max} of Phthalcon/epoxy composites studied here cannot be explained by the presence of epoxy matrix between Phthalcon particles in the networks. Instead, the main reasons could be local crystal structure defects on the particle surface, and the fractality and imperfection of the particle network structures.

References

1. Skotheim, T. A.; Ed., *Handbook of Conducting Polymers, 2nd ed., Revised and Expanded*. Marcel Dekker: New York, 1997.

2. Nalwa, H. S., *Handbook of Advanced Electronic and Photonic Materials and Devices*. Academic Press: London, 2000.

3. Chandrasekhar, P., *Conducting Polymers, Fundamentals and Applications: A Practical Approach*. Kluwer Academic: Dordrecht, 1999.

4. Gul, V. E., *Structure and Properties of Conducting Polymer Composites*. VSP: Utrecht, 1996.

5. Zallen, R., *The Physics of Amorphous Solids*. Wiley: New York, 1983.

6. Kirkpatrick, S. *Rev. Mod. Phys.* **1973,** 45, (4), 574-588.

7. Sahini, M., *Applications of Percolation Theory*. Taylor & Francis: London, 1994.

8. Brokken-Zijp, J. C. M.; Soloukhin, V. A.; Posthumus, W.; de With, G. *In Proceeding of 2003 Athens Conference on Coatings Science and Technology, Vouliagmeni, Greece.*

9. Chen, Z.; Brokken-Zijp, J. C. M.; Huinink, H. P.; Loos, J.; de With, G.; Michels, M. A. J. *Macromolecules* **2006,** 39, (18), 6115-6124.

10. Chen, Z.; Brokken-Zijp, J. C. M.; Michels, M. A. J. *J. Polym. Sci. B* **2006,** 44, (1), 33-47.

11. Zhang, C.; Wang, P.; Ma, C. A.; Wu, G. Z.; Sumita, M. *Polymer* **2006,** 47, (1), 466-473.

12. Zhang, J. S.; Shklovskii, B. I. *Phys. Rev. B* **2004,** 70, (11), 115317-13.

13. Huijbregts, L. J.; Brom, H. B.; Brokken-Zijp, J. C. M.; Kleinjan, W. E.; Michels, M. A. *Phys. Rev. B* **2008**, (77), 075322.

14. Karasek, L.; Sumita, M. *J. Mater. Sci.* **1996,** 31, (2), 281-289.

15. van der Putten, D.; Moonen, J. T.; Brom, H. B.; Brokken-Zijp, J. C. M.; Michels, M. A. J. *Phys. Rev. Lett.* **1992,** 69, (3), 494-497.

16. Adriaanse, L. J.; Reedijk, J. A.; Teunissen, P. A. A.; Brom, H. B.; Michels, M. A. J.; Brokken-Zijp, J. C. M. *Phys. Rev. Lett.* **1997,** 78, (9), 1755-1758.

17. van Bommel, M. J.; Groen, W. A.; van Hal, H. A. M.; Keur, W. C.; Bernards, T. N. M. *J. Mater. Sci.* **1999,** 34, (19), 4803-4809.

18. Sumita, M.; Abe, H.; Kayaki, H.; Miyasaka, K. *J. Macromol. Sci., Phys.* **1986,** B25, (1-2), 171-184.

19. Sumita, M.; Sakata, K.; Asai, S.; Miyasaka, K.; Nakagawa, H. *Poly. Bull.* **1991,** 25, (2), 265-271.

20. Levon, K.; Margolina, A.; Patashinsky, A. Z. *Macromolecules* **1993,** 26, (15),

4061-4063.

21. Brokken-Zijp, J. C. M.; van Mechelen, J. B.; Emeis, C. A.; Datema, K. P.; Kramer, A. H.; de Bruijn, D. P.; Meruma, A. J. *US Patent 05319009* **1993**.

22. Brokken-Zijp, J. C. M. *Internal Information from Shell*.

23. Brokken-Zijp, J. C. M.; Yuan, M.; et.al. *"Synthesis and Structure of Novel Aquocyanophthalocyaninato Co(III) Semi-conductor and Its Applications in Conductive Polymer Composites"*. In Preparation.

24. Huijbregts, L. J.; Brom, H. B.; Brokken-Zijp, J. C. M.; Kemerink, M.; Chen, Z.; de Goeje, M. P.; Yuan, M.; Michels, M. A. J. *J. Phys. Chem. B* **2006,** 110, (46), 23115-23122.

25. Huijbregts, L. J.; Brom, H. B.; Brokken-Zijp, J. C. M.; Yuan, M.; Michels, M. A. J. *Phys. Stat. Sol.* **2006,** 3, 259-262.

26. Huijbregts, L. J.; Brom, H. B.; Brokken-Zijp, J. C. M.; Yuan, M.; Michels, M. A. J. *Phys. Stat. Sol.* **2008,** 5, 765-767.

27. Huijbregts, L. J. *Charge Transport and Morphology in Nanofillers and Polymer Nanocomposites*. Ph.D. Thesis, Eindhoven University of Technology, Eindhoven, 2008.

28. Cotton, F. A., *Modern Coordination Chemistry*. Interscience: New York, 1960.

29. Silverstein, R. M.; Webster, F. X., *Spectrometric Identification of Organic Compounds, 6th ed.* John Wiley & Sons: New York, 1997.

30. Voorn, D. J. *Polymer/Platelet Nanocomposite Particles*. Ph.D. Thesis, Eindhoven University of Technology, Eindhoven, 2006.

31. Kittel, C., *Introduction to Solid State Physics, 7th ed.* John Wiley & Sons: New York, 1995.

32. Miller, A.; Abrahams, E. *Phys. Rev. B* **1960,** 120, (3), 745-755.

33. Mott, N. F., *Electronic Processes in Non-Crystalline Materials, 2nd ed.* Clarendon Press: Oxford, 1979.

34. Shklovskii, B. I., *Electronic Properties of Doped Semiconductors*. Springer-Verlag: Berlin, 1984.

35. Bottger, H.; Bryksin, V. V., *Hopping Conduction in Solids*. Akademie-Verlag: Berlin, 1986.

36. Efros, A. L.; Shklovskii, B. I. *J. Phys. C* **1975,** 8, (4), L49-L51.

37. Stauffer, D.; Aharony, A., *Introduction to Percolation Theory, 2nd ed.* Taylor & Francis: London, 1992.

38. Clerc, J. P.; Giraud, G.; Laugier, J. M.; Luck, J. M. *J. Phys. A: Math. Gen.* **1985,** 18, (13), 2565-2582.

39. Mandelbrot, B. B., *The Fractal Geometry of Nature* W. H. Freeman: New York, 1983.

40. Schüth, F.; Sing, K. S. W.; Weitkamp, J.; Ed., *Handbook of Porous Solids*. Wiley-VCH: Weinheim, 2002; Vol. 1.

41. Heaney, M. B. *Phys. Rev. B* **1995,** 52, (17), 12477-12480.

42. Jullien, R.; Kolb, M.; Botet, R. *J. Phys. Lett.* **1984,** 45, (5), L211-L216.

43. Meakin, P. *Phys. Lett. A* **1985,** 107, (6), 269-272.

44. Lachhab, M.; Gonzalez, A. E.; BlaistenBarojas, E. *Phys. Rev. E* **1996,** 54, (5), 5456-5462.

45. Weitz, D. A.; Huang, J. S.; Lin, M. Y.; Sung, J. *Phys. Rev. Lett.* **1984,** 53, (17), 1657-1660.

46. Vermant, J.; Solomon, M. J. *J. Phys.* **2005,** 17, (4), R187-R216.

47. Roldughin, V. I.; Vysotskii, V. V. *Prog. Org. Coat.* **2000,** 39, (2-4), 81-100.

48. Banerjee, P.; Mandal, B. M. *Macromolecules* **1995,** 28, (11), 3940-3943.

49. Slupkowski, T. *Phys. Stat. Sol.* **1984,** 83, (1), 329-333.

50. Michels, M. A. J.; Brokken-Zijp, J. C. M.; van der Putten, D.; Moonen, J. T.; Brom, H. B. *Phys. Rev. Lett.* **1993,** 70, (26), 4161-4161.

5

INFLUENCE OF CURING AGENT AND PROCESSING CONDITIONS ON THE CONDUCTIVITY OF CROSS-LINKED PHTHALCON/EPOXY NANOCOMPOSITES⊛

SYNOPSIS

The influence of chosen cross-linker and processing conditions on the structure-property relations in cross-linked semi-conductive epoxy coatings has been investigated. The conductivity obtained at low filler concentration (φ < 1 vol. %) is realized by forming a continuous fractal particle network through the matrix with the aid of semi-conductive nano-sized phthalocyanine (Phthalcon) particles. In these coatings different fractal particle network structures were found. The type, structure and distribution of these networks strongly depend on the chosen cross-linker and processing conditions. The choice of cross-linker and processing conditions also influence the amount of matrix present between particles in the network and the critical exponent t. Both factors have a large influence on the log σ_v - φ relation, even when the particle distribution and the effective Hamaker constant of the starting formulation from which these coatings are made are same. Our results suggest that for other thermoset polymer composites containing nano-sized (semi)conductive filler particles, very similar effects on the log σ_v - φ relation, particle network structure and distribution are expected.

5.1. Introduction

Conductive polymer composites can be made by incorporating conductive fillers into an insulating polymer matrix. These materials are of major interest due to the possibility of combining electrical properties of the conductive fillers together with the excellent mechanical properties and processability of the polymer matrix.[1-4] To maintain the mechanical properties and processing behavior of the matrix, the filler fraction should be as low as possible; while to obtain a conductive material the filler fraction should be above the percolation threshold φ_c, at which a continuous network of filler particles forms throughout the matrix. However, the commercial applications of conductive polymer composites, at present, are rather limited because a large amount of conductive filler is often required in order to achieve a reasonable DC volume conductivity level σ_v at room temperature. Statistical percolation models predict a φ_c of 16 vol. % for randomly distributed non-overlapping hard spheres.[5-7] This filler fraction is unacceptably high in practice because it deteriorates the properties and processability of the polymer matrix material. Moreover, the cost-price of the composites is often beyond the acceptable range and many of the applications are not commercially attractive anymore.[8]

It has been shown that using (semi)conductive nanofillers with a high aspect ratio, such as carbon nanotubes, can bring φ_c well below 1 vol. %.[9-13] However, severe processing problems prevent the extensive use of these fillers in practice. A low φ_c can also be realized by adding (semi)conductive nanoparticles with a low aspect ratio when the distribution of the particles is optimum and the effective Hamaker constant A_H^{eff} of the starting mixture is large.[1,8,14-16] This approach may be more attractive in practice because the manufacture of these nanocomposites is less problematic.

The increase in σ_v of these polymer nanocomposites is based on the formation of a continuous (semi)conductive nanoparticle network through the polymer matrix.[1-4] The particle network morphology after processing is directly linked to the σ_v because it affects charge transport within the network.[8,14,17-21] This morphology may be a complex arrangement of particle aggregates/networks with different size and shape distributions. These aggregates/networks can exhibit a self-similar structure at different length scales, resulting in fractal particle networks.[8,19,22-24] Furthermore, the properties of filler particles, such as size and intrinsic conductivity, and the amount of insulating polymer matrix between particles in these networks may also strongly influence the σ_v of the polymer nanocomposites.[1-4,8,14-17,20,21] Unfortunately,

knowledge about the influence of starting mixture composition and processing conditions on the nanoparticle network formation, structure, distribution and the amount of insulating matrix between particles in the final particle network is very limited. Moreover, the influence of these factors on σ_v and how to relate the network structure with σ_v are also not well-understood, especially when thermoset polymer matrices are used.

A fractal nanoparticle network is, generally, formed by Brownian movement of well-dispersed particles/aggregates during preparation of the polymer nanocomposite. At the moment the polymer matrix solidifies or reaches its gel point, the viscosity of the system becomes so high that particles/aggregates can hardly move. To obtain a conductive polymer nanocomposite, a continuous fractal particle network must be formed before solidification or gelation. Apart from the initial A_H^{eff} and the distribution of the particles in the starting mixture, we expect that the starting coating composition and the processing conditions may also have large influences on σ_v and particle network formation, structure and distribution, especially for thermoset polymer nanocomposites containing low filler concentration.

Nanocrystals of aquocuanophthalocyaninato Co(III) (Phthalcon 11/12) (Scheme 5.1) can be used as semi-conductive additive in a broad range of thermoplastic and thermoset polymer matrices, resulting in materials with a very low φ_c.[8,14,22,25-28] The use of Phthalcon as nanofiller in (semi)conductive polymer nanocomposites is very attractive. Phthalcon particles can be synthesized with high purity and (almost) monodisperse in size; they are very stable and have a well characterized surface and bulk structure.[20,26] Moreover, these particles generally form fractal particle networks with large correlation lengths which means that these networks can be studied with optical microscopy, whereas to study fractal nanoparticle network structures in polymer composites, in general, TEM is needed.[9,15,29]

In this chapter we report the use of Phthalcon as a nanometer-sized semi-conductive additive in cross-linked epoxy coatings. We focus on the influence of cross-linker and processing conditions on the log σ_v - φ relation of these nanocomposites. We are particularly interested in the relation between σ_v, φ and morphology of Phthalcon particle aggregates/networks before, during and after processing. Special attention is given to the fractal characteristics of Phthalcon particle network and the mechanism

of network formation. The impact of our findings on other (semi)conductive polymer nanocomposites is also addressed.
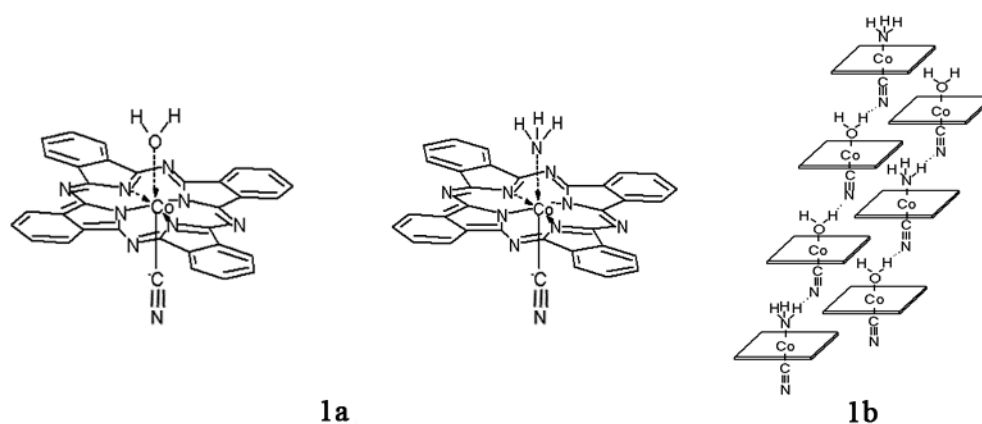
Scheme 5.1. Molecular (a) and crystal (b) structures of Phthalcon 11/12.

5.2. Experimental

5.2.1. Materials

Phthalcon 11/12 (Scheme 5.1) was synthesized in high purity and yield using a two-step reaction as described before.[14,22,25,26,28] The blue Phthalcon powder obtained is highly crystalline, and the primary particle size used here is about 250 nm in length and width and about 50 nm in thickness. In Scheme 5.1 the proposed molecular and crystal structures were confirmed by FT-IR, solid state and liquid ^{13}C-NMR, ^{1}H-NMR, Pyrolysis Combustion Mass Spectrometry analysis (PCME), neutron diffraction, XRD, XPS and crystallographic modeling.[26] The conductivity of compressed powder determined at room temperature is 4 x 10^{-4} S/cm and the intrinsic crystal conductivity is 2 x 10^{-2} S/cm.[20,21] Before use Phthalcon powder was carefully dried at 80 $^{\circ}$C for 48 h under vacuum (~ 0.01 mbar) and ground into fine powder in a mortar.

Epoxy prepolymer (Epikote 828) was purchased from Resolution Nederland BV. The amine cross-linker Jeffamine D230, Jeffamine D400 and Jeffamine D2000 were purchased from Huntsman BV, Belgium. Isophorone-diamine (IPD, $\geq$ 99.0 %, GC) and 4,4-diaminodiphenyl methane (DDM, $\geq$ 97.0 %, GC) were purchased from Fluka. Structures of these compounds are shown in Scheme 5.2. *m*-cresol (spectrophotometric grade) was purchased from Merck. All these chemicals were used as received.

Epikote 828 (m ≈ 0.1)

Jeffamine D230 (n ≈ 2.6)
Jeffamine D400 (n ≈ 5.6)
Jeffamine D2000 (n ≈ 33.2)

IPD

DDM
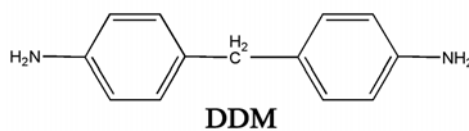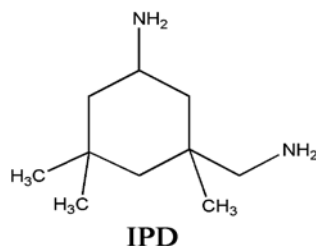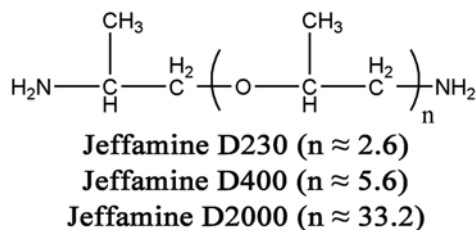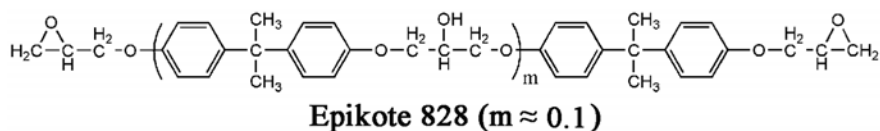
Scheme 5.2. Chemical structures of epoxy coating components.

5.2.2. Coating Preparation

The cross-linked Phthalcon/epoxy composites were prepared using the same method as described before.[14] The Phthalcon powder was first dispersed in *m*-cresol under magnetic (1 h) and ultrasonic stirring (1 h). To this dispersion, cross-linker and Epikote 828 were added by keeping the NH/epoxy molar ratio at 1/1. In order to get a well-dispersed starting formulation, DDM, which is a solid at room temperature, was pre-dissolved in a small amount of *m*-cresol (w/w DDM/*m*-cresol = 7/20). The starting coating formulation was then magnetically stirred for 5 min and ultrasonically degassed for 5 min. Finally, it was cast on a polycarbonate substrate with a 120 μm wet coating thickness using a doctor blade applicator, cured immediately at an elevated temperature (40, 50, 60, 80 or 100 $^{\circ}$C) for 4 h in vacuum (~ 0.01 mbar) and later post-cured at 120 $^{\circ}$C for 8 h under vacuum (~ 0.01 mbar). Under these conditions smooth coatings with layer thicknesses between 40 and 60 μm were obtained.

The concentrations of Phthalcon ranged from 0 to 12 vol. % based on the total volume of cross-linked composites in the starting formulation, by taking into account the densities of Phthalcon and cross-linked epoxy as 1.65 and 1.00 g/cm³, respectively. Generally the Phthalcon particle network was present throughout the whole layer thickness. However, sometimes an insulating bottom layer was found in which Phthalcon particles were not present. In this case the Phthalcon concentrations were corrected for the presence of this layer, and the final concentrations of Phthalcon particles in the cross-linked epoxy could be much higher than 12 vol. %.

5.2.3. Characterization

Optical Microscopy (OM) The morphology of Phthalcon particle networks in the materials after cross-linking was studied by OM. The OM analysis was carried out with a Reichert-Jung Polyvar-Met microscope using transmission bright-field technique. These OM images were later converted to binary images and analyzed using the tiling method to obtain fractal dimensions and correlation lengths of the particle networks.[22] Coatings used in these analyses had a thickness of about 10 μm. Often thin cross-sectional cuts with a thickness of about 2-3 μm were made from coating samples and analyzed with the OM. These cuts were prepared by microtoming at room temperature and were used to assess the Phthalcon particle distribution over the coating thickness.

DC Volume Conductivity σ_v The σ_v of the coatings at room temperature was measured using a standard four-point method with a Keithley 237 high voltage source measuring unit and a Keithley 6517A high voltage electrometer. The measurements were carried out according to standard ASTM D991 and instructions of Keithley "low conductivity level measurements". Silver paste (silver conductive adhesive 416, electron microscopy sciences, USA) was used to ensure good contact between sample surface and measuring electrodes.

From the measured voltage V, current I and (corrected) coating thickness d, the value of σ_v was calculated using the following equation:

$$\sigma_v = \frac{IL}{bdV} \qquad (5.1)$$

where L is the distance between neighboring silver paint traces and b is the trace length. Before each measurement, four silver paint traces were applied on the coating surface with a trace length b of 1 cm and distance L of 1 cm. Coatings used in the

conductivity measurements had a thickness d between 40 and 60 μm, as determined using a digital screw micrometer caliper. The presented σ_v value for each Phthalcon concentration is an average value of at least three coatings measured at three different positions. In coatings made from IPD and DDM cross-linkers Phthalcon particle networks were not present through the whole coating thickness. In these coatings the σ_v values and the Phthalcon concentrations φ were calculated after only taking into account the layer thickness which actually contained Phthalcon particle network as indicated before.

Rheological Measurements Rheological measurements were performed to follow the viscosity changes during cure using an AR1000 rheometer with 20 mm plate-plate geometry. The coating mixture was directly added to the plate, and then the gap between plates was set to be 300 μm. In the beginning of the measurement, the plates were heated from room temperature to curing temperature within 30 sec. All measurements were recorded under N_2 flow.

Surface Energy The surface energies were determined by Wilhelmy plate method using a Krüss digital tensionmeter K10T.[30,31] During the measurement, the plate was moved towards the surface until it reached the meniscus. The surface energy was calculated from the measured force.[30,31] All surface energies given are average values of three measurements on each sample.

5.3. Results and Discussion

5.3.1. Influence of Curing Temperature on log σ_v – φ Relation, Particle Network Structure and Network Formation in Jeffamine Cross-linked Epoxy Coatings
A. Using Jeffamine D230 as Cross-linker
➢ log σ_v – φ Relation
A number of epoxy composites containing different Phthalcon concentrations and cross-linked with Jeffamine D230 at temperatures of 60, 80 and 100 ^{o}C were prepared. The relation between the σ_v of these coatings as a function of Phthalcon concentration φ is shown in Figure 5.1. The curves in Figure 5.1 appear to be similar, especially for coatings cured at 60 and 80 ^{o}C. The value of σ_{max} is around 10^{-7} S/cm. By extrapolating these curves to $\sigma_v = 10^{-16}$ S/cm (the σ_v of pure epoxy matrix[8]), the percolation threshold φ_c was determined and it is similar as well (0.6 vol. %). The presented data in Figure 5.1 correspond with the σ_v and φ_c values reported before for

Phthalcon/Jeffamine D230/Epikote 828 coatings cross-linked at 100 °C (a different Phthalcon batch was used).[14,22,28,32] Hence, taking into account the uncertainty of measurements the log σ_v – φ relations for Jeffamine D230 cross-linked coatings cured between 60-100 °C are (almost) independent of the curing temperature.
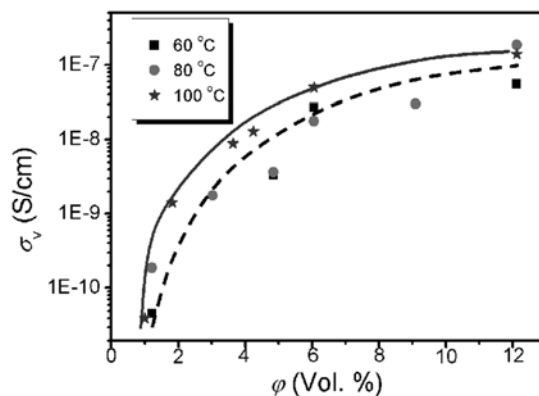
Figure 5.1. log σ_v – φ relations of Phthalcon/epoxy coatings cross-linked with Jeffamine D230. These coatings were cured at 60, 80 or 100 °C for 4 h and post-cured at 120 °C for 8 h.

➢ Phthalcon Particle Network Structures and Distributions

Although the primary Phthalcon particle size is too small to be seen under the OM, the particle network could be easily observed when the Phthalcon concentration is above φ_c because of the fractal nature of the network.[14,22,28] The OM images of these networks in cross-linked Phthalcon/Jeffamine D230/Epikote 828 coatings cured at 60, 80 or 100 °C are shown in Figure 5.2. These OM images suggest that the cross-linked layers made from Jeffamine D230 have a similar fractal particle network structure despite the differences in curing temperature. In order to verify this suggestion, the fractal dimensions d_f of these particle networks were determined using the method of tiling, as described before.[22,28,33,34] Results of fractal structure analyses are summarized in Table 5.1. Table 5.1 reveals that indeed the Phthalcon particle network structures, for coatings cured at different temperatures, have a very similar fractal structure. The d_f value of about 1.75 observed here is close to the theoretical value for diffusion limited cluster aggregation (DLCA),[35-39] and strongly suggests that all fractal particle networks observed in Figure 5.2 are formed by this mechanism.

To assess whether the fractal particle network was homogeneously distributed through the layer, cross-sections were prepared using coatings shown in Figure 5.2. These cross-sections show that the fractal particle network is evenly distributed through the

whole coating thickness (Figure 5.3). A homogeneously distributed fractal Phthalcon particle network in an epoxy coating cross-linked at 100 °C was reported before.[14,32]
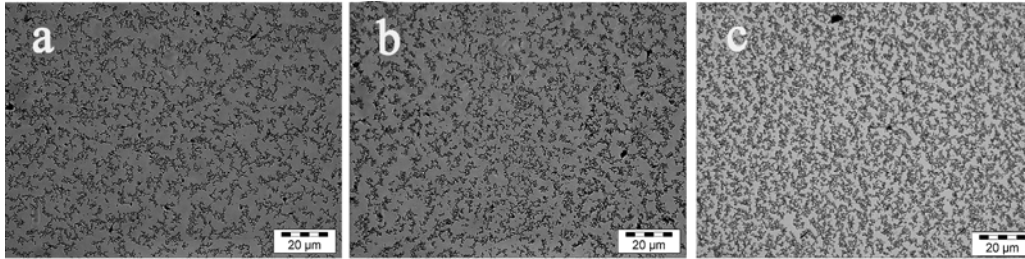
Figure 5.2. OM images of Phthalcon particle networks in Epikote 828/Jeffamine D230 coatings cross-linked at different temperatures. All coatings contained 3 vol. % Phthalcon with respect to the total volume of the coating components in the initial starting formulations. (a) cured at 60 °C; (b) cured at 80 °C; (c) cured at 100 °C.

Table 5.1. Phthalcon particle network structures in Jeffamine D230 cross-linked epoxy coatings cured at various temperatures.[*]

Curing Temperature (°C)	d_f	ξ (μm)
50	1.60	40
60	1.77	20
80	1.75	20
100	1.75	20

[*]Phthalcon concentration was 3 vol. % based on the initial Phthalcon concentration in the starting formulation.
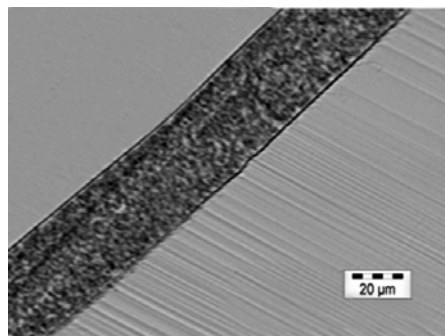
Figure 5.3. OM image of cross-section of Phthalcon/Epikote 828/Jeffamine D230 coating cured at 80 °C. This coating contained 3 vol. % Phthalcon.

➢ Conduction Mechanism

In a previous publication the conduction mechanism of a 12 vol. % Jeffamine D230 cross-linked coating cured at 100 °C was studied in detail. DC and AC conductivity measurements over a broad range of temperatures and frequencies strongly suggest that the conduction mechanism in Phthalcon particle network can be described as variable range hopping by cotunnelling.[20,21,27,40] The similar log $\sigma_v - \varphi$ relations, the similar Phthalcon particle network structures and the similar exponent t values (Equation 5.3, see later discussion) as observed in these coatings suggest that variable range hopping by cotunnelling is also likely to be the conduction mechanism in Phthalcon particle network for coatings cured at 60 °C and 80 °C.
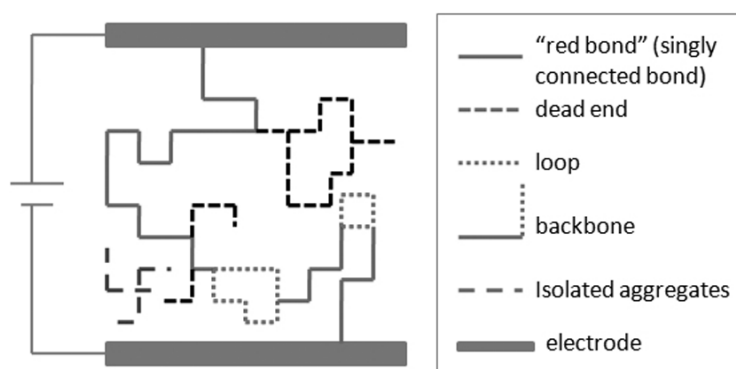
Scheme 5.3. Particle network in a polymer composite.

When voltage is applied, the dead ends and isolated aggregates carry no current, the single connected red bonds carry the total current, and the loops only carry part of the current. The red bonds and loops together form the backbone.

➢ Measured $\sigma_v - \varphi$ Relations vs. Network Structure Models

One way to present the fractal particle network through a polymer matrix is shown in Scheme 5.3. Generally, only part of the network structure carries current. In a fractal particle network the part that carries current is called "backbone", the part which does not carry current is called "dangling chain" or "dead end". Only part of the backbone carries the whole current. These are single connected points which are also called "red bonds". The rest of the backbone only carries part of the total current. This happens in a so-called "loops".[20] Also (a small) part of the fractal particle network may not be connected at all and therefore present as isolated aggregates.

The structure of particle network presented in Scheme 5.3 is complex and difficult to directly correlate with the σ_v. Hence, the particle network structure is often simplified

before a correlation is made. One way to describe fractal particle network is to use stacked fractal aggregates. The average size of these building blocks is the correlation length ξ, which is related to φ and d_f for $\varphi > \varphi_c$ as below:[41,42]

$$\xi = a\varphi^{1/(df-3)} \tag{5.2}$$

In Equation (5.2), a is according to the theory the radius of a primary particle from which the fractal network is built. We assume that for our system a is the radius of a primary Phthalcon particle aggregate, which is on average about 0.7 μm.[22] The calculated ξ value ($\xi \approx 14$ μm) from Equation (5.2) is close to the experimentally determined ξ value ($\xi \approx 20$ μm). Furthermore, we may conclude from Equation (5.2) that with the same Phthalcon concentration φ, the value of ξ is only related to d_f. This is in agreement with our fractal structure analyses on Jeffamine D230 cross-linked coatings cured at different temperatures (Table 5.1). This suggests that this model approach may be applicable to our coating systems. However, the calculation is very sensitive, at least for small changes in particle aggregate size, a value which is determined with great uncertainty.
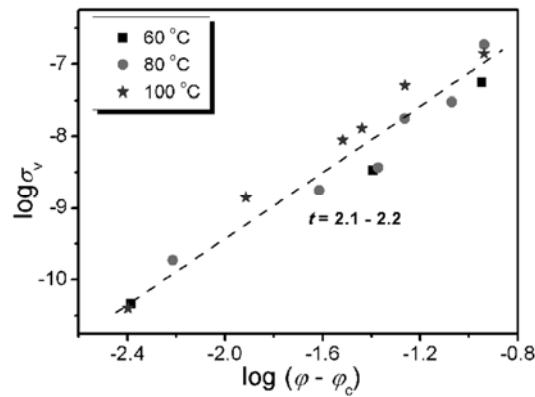
Figure 5.4. log σ_v – log($\varphi - \varphi_c$) relation of Phthalcon/Jeffamine D230/Epikote 828 coatings cross-linked at different temperatures.

To further evaluate Phthalcon particle network structure in coatings cured between 60-100 $^\text{o}$C, the log σ_v values in Figure 5.1 were plotted as a function of log($\varphi - \varphi_c$) based on equation:

$$\sigma_v \approx c(\varphi - \varphi_c)^t \tag{5.3}$$

where c is a constant and t is the critical exponent. The results are shown in Figure 5.4. We found that in these cross-linked epoxy composites, despite the differences in

curing temperature, t is always between 2.1 and 2.2. These t values are in good agreement with the theoretical value of 2.0 predicted for 3D random percolating system, of which the conductivity of all current-carrying bonds in the fractal particle network is equal.

In a recent publication an upper-limit model was described.[21] This model is based on extensive AC and DC conductivity measurements on Phthalcon 11 powder and Phthalcon 11/epoxy coating cross-linked with Jeffamine D230 at 100 ^{o}C, in combination with fractal particle network structure analyses and conductive AFM measurements. This model uses the stacked fractal approach and is called upper-limit model because it is assumed that it could predict the maximum σ_v at each Phthalcon concentration. One important assumption in this model is that the Phthalcon particles in the network really touch each other and that there is no matrix present between these particles. It has been shown that using this model the σ_v of 10^{-7} S/cm obtained at a Phthalcon concentration of 12 vol. % could be explained.[21] However, at a Phthalcon concentration φ below 12 vol. % the model calculations predict a (much) higher σ_v value than we observed in Figure 5.1 (Figure 2.6). This may be explained by the presence of polymer matrix material between particles which limits the charge transport in the network and consequently lowers σ_v. That polymer matrix material is present between Phthalcon in the particle network is also suggested when we compare the log σ_v – φ relation of UV cured Phthalcon/acrylate coatings with Phthalcon/Jeffamine D230/Epikote 828 coatings cured at 100 ^{o}C (Figure 5.5). At low φ the differences in σ_v between UV cured and Jeffamine D230 cured coatings are too large to only attribute them to the differences in loops, dangling chains and isolated aggregates.[43] That a small variation in the amount of polymer matrix present between conducting particles can have a large influence on log σ_v – φ relation has been reported recently in acrylate composites containing ATO nanoparticles.[15] Furthermore, in this upper-limit model a large number of assumptions is made (see chapter 2). Apart from those discussed above, some other assumptions may not be applicable to our cross-linked Jeffamine/Epikote 828 materials. This might also explain the differences observed in σ_v between model calculations and our experimental results.

No σ_v could be measured on coatings cured below 60 ^{o}C using four-point measuring unit. However, homogeneously distributed Phthalcon particle network can still be observed in coating cured at 50 ^{o}C, although the d_f and ξ values are quite different and

the Phthalcon particle network seems to be much coarser (Figure 5.6 & Table 5.1). These observed differences will be discussed in more detail later.
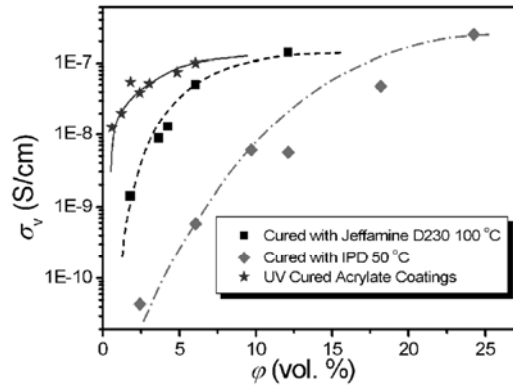
Figure 5.5. log $\sigma_v - \varphi$ relation of UV cured acrylate coatings, Jeffamine D230 and IPD cured epoxy coatings. Jeffamine cross-linked epoxy coatings were cured at 100 ^{o}C; IPD cross-linked epoxy coatings were cured at 50 ^{o}C and the curve has been corrected for the presence of an insulating bottom layer (see later discussion).
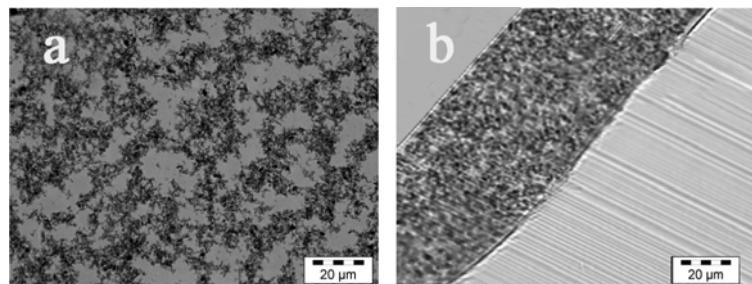
Figure 5.6. (a) OM image of Phthalcon particle network in Jeffamine D230/Epikote 828 coating cured at 50 ^{o}C. (b) cross-section of coating 6(a). Phthalcon concentration was 3 vol. % based on the total volume of the final coating components. Phthalcon particles were evenly distributed through the layer and a continuous particle network was obtained.

➢ Viscosity Changes During Cure

In the starting coating formulations Phthalcon particles are present as primary particles and/or very small particle aggregates.[14] During cross-linking these primary particles/aggregates form a fractal particle network by Brownian movement.[14,22,28] Meanwhile, the prepolymer composition changes from a low molecular weight liquid to a highly cross-linked polymer network. As a result, the mobility of Phthalcon particles/aggregates decreases as the cross-linking reaction proceeds. This indicates

89

that the rate of cross-linking may strongly influence the formation of Phthalcon particle network through the matrix. To understand these influences rheological measurements were performed to study viscosity changes during cross-linking at different curing temperatures.

It is well-known that the addition of a small amount of well-dispersed nanoparticles to a thermoset starting formulation may considerably enhance the viscosity of the system before and during cross-linking. To determine the influence of Phthalcon particles on the viscosity changes over time, Jeffamine D230/Epikote 828 starting formulations were measured in the absence and presence of 3 vol. % Phthalcon. The viscosity changes during cure with/without the presence of *m*-cresol, which was used as a dispersing medium, were also measured. The results are shown in Figure 5.7. These results show that the presence of Phthalcon particles hardly influences the viscosity before and during cure. The presence of *m*-cresol in the starting formulation enhances the viscosity increases over time considerably. This is due to the catalytic effect of *m*-cresol which facilitates the curing reaction between epoxy and amine cross-linker.[44]
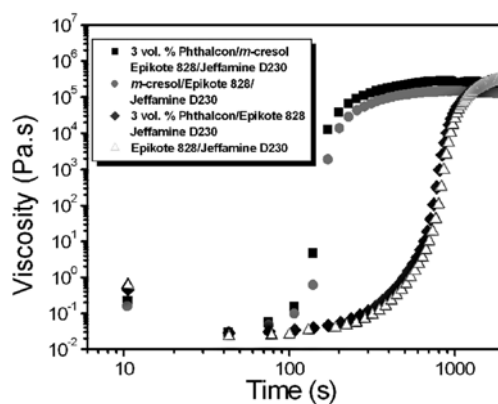
Figure 5.7. Viscosity changes during cure of Jeffamine D230/Epikote 828 with/without 3 vol. % Phthalcon particles and *m*-cresol. The curing temperature was 100 °C.

The observed changes in viscosity during cure of Phthalcon/Jeffamine D230/Epikote 828/*m*-cresol starting formulation at different curing temperatures are shown in Figure 5.8. Taking the moment when the tangent of the loss angle (tan δ) reaches 1 as the gel point, the gel points of these coatings are summarized in Table 5.2. As expected a slower change in viscosity together with retardation in gel point was observed as the curing temperature decreases because of the decrease in cross-linking rate. Moreover, at the initial stage of cross-linking a lowering in viscosity was always observed

(Figure 5.7 & 5.8). This decrease in viscosity becomes larger at higher curing temperature (Figure 5.8). This lowering in viscosity is caused by the external heating and the exotherm nature of cross-linking reaction, whereas the contribution of cross-linking at this initial stage is too small to compensate. This is a well-known behavior for an epoxy starting formulation cured under non-isothermal conditions.[44] We may expect that the viscosity changes over time not only influence the Phthalcon particle network formation, but also stimulate sedimentation during cross-linking, resulting in an insulating layer at the top of the coating.[14] Moreover, the initially formed particle network may rearrange to form a more thermodynamically stable structure[45] or, when the gel time becomes too short, no continuous Phthalcon particle network can be formed through the matrix.[22] In Chapter 4 the effect of primary Phthalcon particle size on particle network formation in Jeffamine D230 cross-linked epoxy coatings cured at 100 $^{\circ}$C was discussed.[28] These results strongly indicate that conductive Phthalcon particle network formation occurs at the early stage of cure, well before the gel time is reached, and that no insulating layers are formed even when the particles are large in size.

The results reported here, such as d_f values of 1.75 and the absence of insulating top layers suggest that ample time is available for the formation of particle network during cure, and that the viscosity changes over time are sufficiently quick to prevent sedimentation or restructuring of Phthalcon particle network when Phthalcon/Epikote 828/Jeffamine D230/*m*-cresol starting formulations were cured between 60 and 100 $^{\circ}$C.
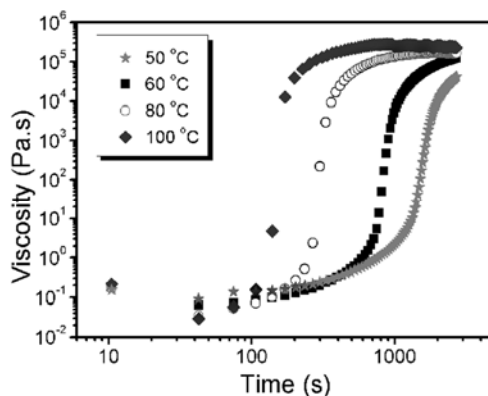
Figure 5.8. Changes in viscosity during curing of Phthalcon/*m*-cresol/Epikote 828/Jeffamine D230. The curing temperature was varied and the concentration of Phthalcon remained 3 vol. % in the starting formulations.

Table 5.2. Gel points of coating components cured at different temperatures.[*]

Cross-linker	Curing Temperature ($^{\mathrm{o}}$C)	Gel Point (s)
Jeffamine D230	60	797
Jeffamine D230	80	288
Jeffamine D230	100	153
Jeffamine D400	100	325
Jeffamine D2000	100	610

[*]All starting formulations contained 3 vol. % Phthalcon.
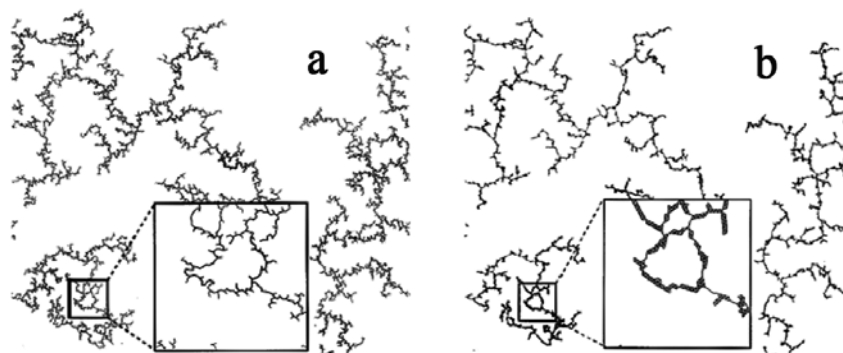
Scheme 5.4. Theoretical simulation on specific gel aggregates. (a) non-relaxed aggregates (d_{f} = 1.42, 2D system); (b) aggregates after relaxation (d_{f} = 1.32, 2D system). A much denser aggregate is obtained as a result of relaxation.[45]

However, this is no longer the case when the same starting formulations were cured at 50 $^{\mathrm{o}}$C. The final particle network becomes coarser and the d_{f} value becomes lower, but the particle network is still fractal. Theoretical model simulations suggest that this phenomena can be explained by the relaxation of particle network initially formed by DLCA (Scheme 5.4).[45] This relaxation may also increase the amount of polymer matrix present between particles in the network and/or change the number of loops, dangling chains or isolated aggregates. This may lower the σ_{v} value of the composites to such a level that it could not be measured with four-point measurements ($\sigma_{\mathrm{v}} < 10^{-12}$ S/cm).

Table 5.3. Surface energies of various coating components.

	Surface Energy (mN/m)	
	20 °C	100 °C[46]
Phthalcon 11/12	> 50	> 50
m-cresol	38.2	29.0
Jeffamine D230	33.1	23.0
DDM	58.0	46.1
IPD	32.0	22.0
Jeffamine D230/Epikote 828 (1/3, w/w)	40.5	31.4
DDM/Epikote 828 (1/6, w/w)	54.3	40.2
IPD/Epikote 828 (1/6, w/w)	40.1	30.0

➢ Particle-Particle and Particle-Matrix Interactions

Besides viscosity, the surface energy of the starting formulation is also subject to marked change during cross-linking. The consequences are that both the particle-matrix and particle-particle interactions change. Neglecting hydrogen bonding, these interactions can be estimated by the differences in surface energies between particles and matrix as stated below:[14]

$$A_H^{eff} \approx 2.1 \times 10^{-21} \left[\gamma_p^{1/2} - \gamma_m^{1/2} \right] \qquad (5.4)$$

where A_H^{eff} is the effective Hamaker constant, and γ_p and γ_m are the surface energies of the particle and the matrix, respectively. When the surface energies of the particle and the matrix are similar, the A_H^{eff} tends towards to zero and the tendency of particles to form a network is reduced to zero. This favours the stabilization of initially well-separated particles in the medium and a particle network formed at a concentration of about 16 vol. % is expected. Likewise, the presence of a large A_H^{eff} leads to a large excess in interfacial energy and particles tend to form particle aggregates/networks at a low filler concentration. That an initial high A_H^{eff} value of semi-conductive polymer nanocomposites can lead to a very low φ_c when the particles are initially well-dispersed has been reported.[8,14,16] The experimentally determined surface energies of the coating components used here are listed in Table 5.3. During cure the surface energies of the coating components are reduced due to the increase in temperature. But at the early stage of cure the surface energy difference between Phthalcon

particles and coating components is still expected to be large. The large A_H^{eff} facilitates the formation of fractal Phthalcon particle aggregates/networks at a very low φ_c.

B. Using Jeffamine D400 and Jeffamine D2000 as Cross-linker

The rate of cross-linking at 100 ^{o}C can be slowed down by enlarging the distance between the two NH$_2$ groups in Jeffamine cross-linker (i.e. using Jeffamine with a higher M_n) (Figure 5.9).[22] However, the influence of this change on surface energy of the cross-linker and the initial A_H^{eff} is minimal. After cure fractal Phthalcon particle networks were always observed in cross-linked Phthalcon/epoxy coatings (Figure 5.10) and the σ_v could be measured over a broad range of φ (Figure 5.11). OM images show that the Phthalcon particle network structure is coarser than for the one observed in Jeffamine D230 cross-linked coatings, the d_f value becomes lower and the rate of cure slows down when the M_n of Jeffamine increases (Table 5.4). These results strongly indicate a relaxation of Phthalcon particle network during cross-linking. The rheology data show that there is more time for particle network to reconstruct because the rate of cross-linking slows down at a higher M_n. A comparison made on viscosity changes over time between a starting formulation containing Jeffamine D230 cured at 60 ^{o}C and a starting formulation containing Jeffamine D2000 cured at 100 ^{o}C shows that in both coating components the viscosity changes over time are similar. However, only Phthalcon particle network cross-linked with Jeffamine D2000 shows relaxation. This is probably caused by the higher mobility of Phthalcon particles, the slightly higher initial decrease in viscosity at the early stage of cross-linking and the slower increase in viscosity over time after the minimum viscosity has been reached for the Jeffamine D2000 containing formulation cured at 100 ^{o}C. The lower extend of relaxation found in coatings cured with Jeffamine D400 confirms this.

Table 5.4. Phthalcon particle network structures in epoxy coatings using Jeffamine with different M_n as cross-linker.[*]

M_n of Jeffamine Cross-linker	d_f	ξ (μm)
230	1.75	25
400	1.61	30
2000	1.55	35

[*] Phthalcon concentration was 3 vol. % based on the initial volume of Phthalcon with respect to the final coating components. All coatings were cured at 100 ^{o}C.
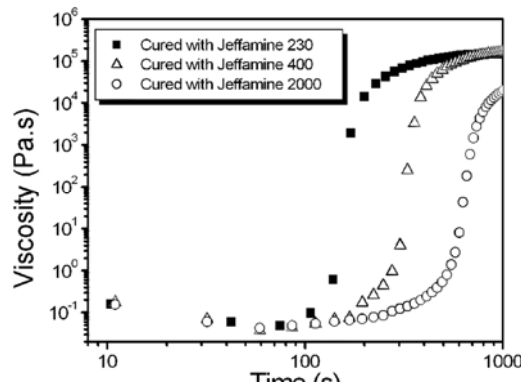
Figure 5.9. Changes in viscosity during cure of Phthalcon/*m*-cresol/Epikote 828/Jeffamine starting formulations. The Jeffamine cross-linker was varied. The curing temperature was 100 $^{\circ}$C and the concentration of Phthalcon was 3 vol. % in the starting formulations.
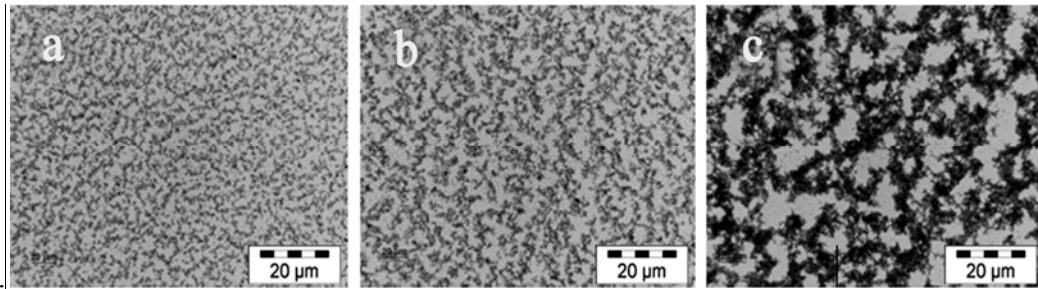
Figure 5.10. OM images of Phthalcon particle networks in epoxy composites cross-linked with Jeffamines. (a) with Jeffamine D230; (b) with Jeffamine D400; (c) with Jeffamine D2000. All coatings contained 3 vol. % Phthalcon in the starting formulations and were cured at 100 $^{\circ}$C.
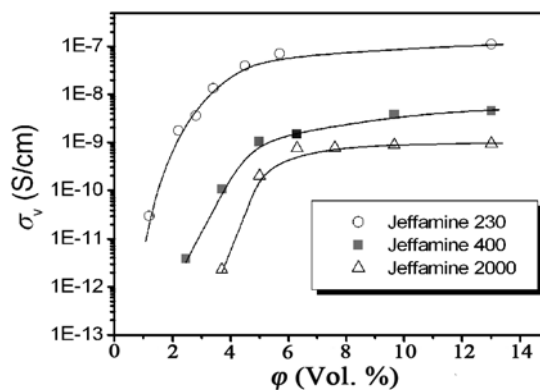
Figure 5.11. log σ_v – φ relation of Jeffamine cross-linked coatings cured at 100 $^{\circ}$C.

C. Summary

Besides the use of Phthalcon/*m*-cresol dispersions, a low φ_c can also be obtained by directly dispersing Phthalcon particles in the curing agent or acrylate monomer.[14,43] When a Phthalcon/Jeffamine D230 dispersion is cured at 100 ^{o}C after addition of Epikote 828, a fractal Phthalcon particle network is also formed. However, the curing rate is so slow in the absence of *m*-cresol (which is also a catalyst for cross-linking) that sedimentation of the particle (network) occurs and an insulating top layer is always obtained.[14] When Phthalcon particles are dispersed in an acrylate monomer and the matrix is UV cured, a fractal Phthalcon particle network is also observed. Fractal structure analysis shows that this UV cured particle network is likely to be formed before cure from the DLCA formed large fractal aggregates in the starting Phthalcon/acrylate monomer dispersion.[43] No insulating top layer is formed due to the rapid UV cure.

It has also been shown before that when a starting Phthalcon/Epikote 828 dispersion is made under low shear conditions, the Phthalcon particles are agglomerated into micrometer-sized structure. This dispersion never leads to cross-linked semi-conductive Phthalcon/epoxy composite and a fractal Phthalcon particle network structure is never observed after cure.[14] Hence, only when a suitable starting Phthalcon dispersion is used, a low φ_c material can be obtained. Furthermore, it has been discussed earlier that to obtain semi-conductive thermoset polymer nanocomposites with a low φ_c, it is important to start with a formulation which has a large A_H^{eff}.

The importance of both factors in obtaining semi-conductive polymer nanocomposites with a very low φ_c is also reported in other systems. New, however, is that to our knowledge only in Phthalcon/epoxy systems several different fractal structures are formed during cure which strongly influence the log σ_v - φ relation. Furthermore, only within a very small processing window an optimum fractal network structure and log σ_v - φ relation can be realized in thermoset matrices containing semi-conductive nanoparticles, and that small changes in starting compositions and/or processing conditions can have such large influences on fractal particle network structures, distributions and log σ_v - φ relations. The results discussed above are summarized in Scheme 5.5 for Phthalcon/thermoset polymer composites. Nevertheless, we think that very similar effects will be observed in other nanofiller/thermoset composites made from their corresponding starting formulations. Scheme 5.5 indicates that an

insulating bottom layer can be formed as well. This will be discussed in more detail below together with the use of other curing agents.

UV Curing
Conductive Fractal Particle Network
Formed by DLCA

High Shear
Fractal Particle Aggregates

Phthalcon Powder
Agglomerates

Thermal Curing
Conductive Fractal Particle Network
Formed by DLCA
With An Insulating Top Layer

Relaxation

Low Shear
Particle Agglomerates

Thermal Curing
Non-Conductive Particle Agglomerates

Conductive Fractal Particle Network   Relaxation

Conductive Fractal Particle Network
With An Insulating Top Layer   Relaxation

Phthalcon Powder
Agglomerates

Well-dispersed
Primary Particles/Aggregates
In Dispersing Medium

Conductive Factal Particle Network
With An Insulating Bottom Layer   Relaxation

Gel Time Too Short To Form
Continuous Paticle Network

Scheme 5.5. Routes to make cross-linked semi-conductive Phthalcon/thermoset composites.

97

5.3.2. Influence of Other Cross-linkers on log $\sigma_v - \varphi$ Relation, Particle Network Structure and Network Formation in Cross-linked Epoxy Coatings

A. Using IPD as Cross-linker

➤ Phthalcon Particle Network Structures and Distributions

Besides Jeffamine cross-linkers, a number of *m*-cresol/Epikote 828 formulations containing different Phthalcon concentrations were cross-linked with IPD at several temperatures. Phthalcon particle network structures in these coatings were observed under the OM and analyzed using the method of tiling (Figure 5.12 & Table 5.5). Cross-sections of these coatings were prepared as well to evaluate the particle network distributions along the layer thickness. The OM images of several cross-sections are shown in Figure 5.13. Below the blue Phthalcon particle network layer a colorless bottom layer was found for all coatings. The origin of this layer is not clear yet. However, a somewhat different evaporation rate of *m*-cresol with respect to coatings cured with Jeffamine cross-linkers could be one of the reasons for the formation of this insulating bottom layer.
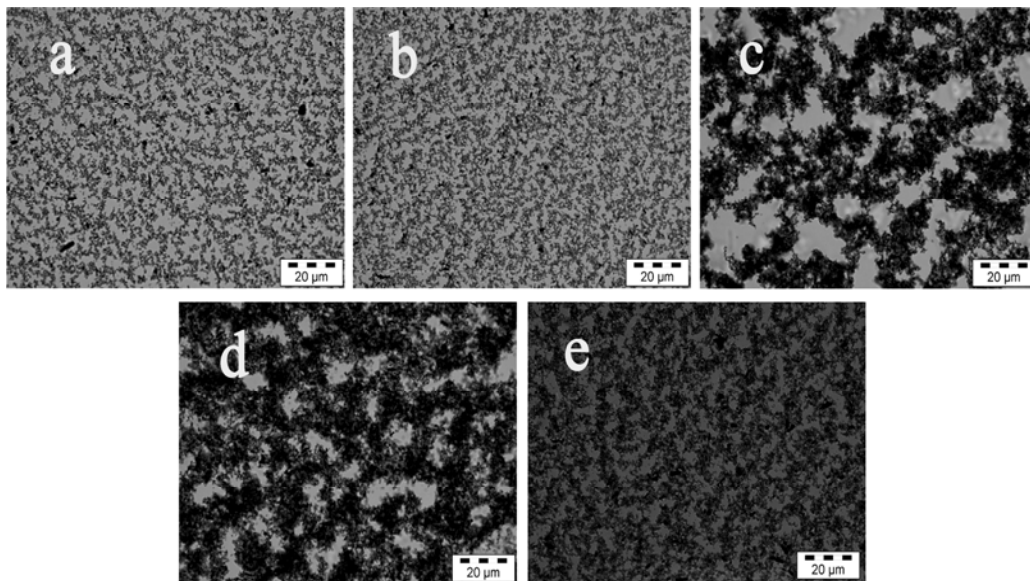
Figure 5.12. OM images of Phthalcon particle networks in Epikote 828/IPD coatings cross-linked at different temperatures. All coatings contained 3 vol. % Phthalcon in the starting formulations (the actual Phthalcon concentrations are shown in Table 5.6). (a) cured at 40 °C; (b) cured at 50 °C; (c) cured at 60 °C; (d) cured at 80 °C; (e) cured at 100 °C.

Table 5.5. Phthalcon particle network structures in epoxy coatings using IPD as cross-linker cured at various temperature.[*]

| Curing Temperature (^{o}C)	d_f	ξ (μm)
40	1.73	25
50	1.72	25
60	1.60	30
80	1.52	40
100	1.65	30

[*] Phthalcon concentration was 3 vol. % based on the initial concentration of Phthalcon with respect to the final coating components.
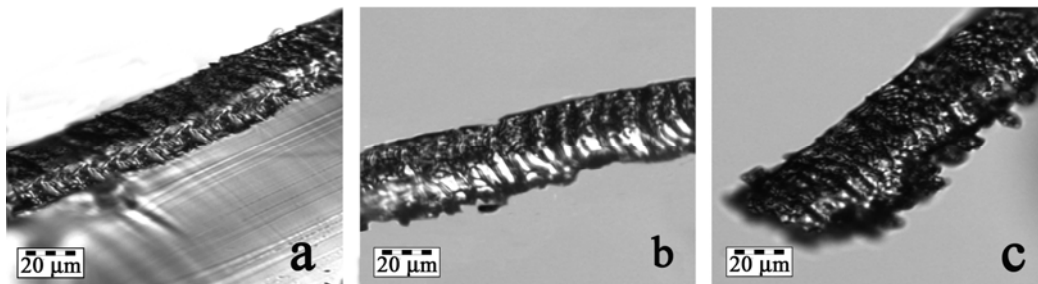
Figure 5.13. OM images of cross-sections of IPD cross-linked epoxy coatings cured at various temperatures. All coatings contained 3 vol. % Phthalcon (the actual concentrations are shown in Table 5.6). (a) cured at 50 ^{o}C; (b) cured at 80 ^{o}C; (c) cured at 100 ^{o}C.

Table 5.6. Phthalcon particle layer thicknesses in cross-linked Epikote 828/IPD coatings cured at different temperatures.[*]

Curing T (^{o}C)	Total Thickness (μm)	Particle Network Thickness (μm)	Actual Phthalcon Concentration (vol. %)
40	40.1	22.3	5.4
50	33.0	16.2	6.1
60	42.6	21.2	5.7
80	42.5	23.9	5.4
100	34.4	16.8	6.1

[*] All calculations were based on 3 vol. % Phthalcon in the starting formulations.
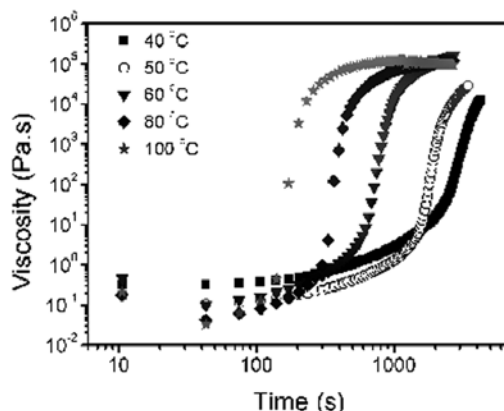
Figure 5.14. Changes in viscosity during cure of Phthalcon/Epikote 828/IPD coatings. The curing temperature was varied and the initial Phthalcon concentration in the starting formulation was 3 vol. %.
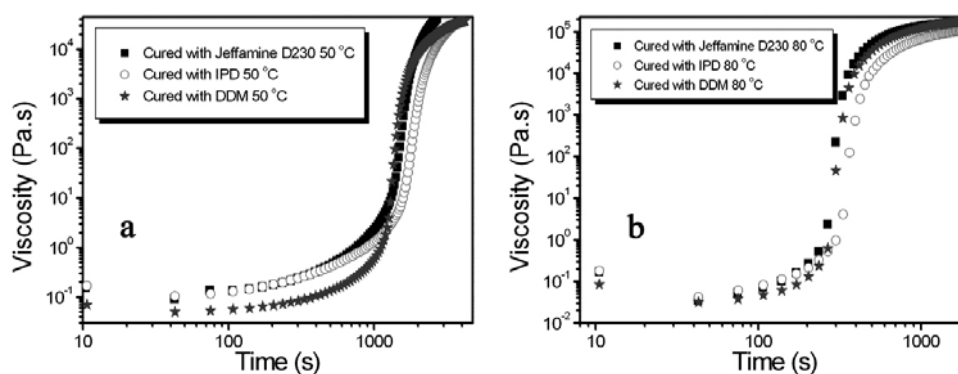
Figure 5.15. Viscosity changes during cure of epoxy coatings made from Jeffamine D230, IPD or DDM cross-linker. (a) coatings cured at 50 $^{\circ}$C; (b) coatings cured at 80 $^{\circ}$C.

➢ Viscosity Changes During Cure

Results from fractal structure analyses and OM images show that different fractal particle networks are present in IPD cured composites. The d_f values found for the coatings cured at 40 or 50 $^{\circ}$C show that these networks are likely to be formed by DLCA, whereas the d_f values and OM images suggest that others particle networks are initially formed by DLCA, but relaxed during cure. This relaxation of nanoparticle networks was studied in more detail with rheological measurements (Figure 5.14). As has been shown before, the Phthalcon particle networks are likely to be formed far before the gel point is reached. Apparently, at 40 and 50 $^{\circ}$C the initial viscosity decrease is too slow and at 100 $^{\circ}$C the viscosity increase is too quick to get severe relaxation of DLCA formed particle network. At a curing temperature of 60 or 80 $^{\circ}$C the viscosity changes over time during cure is such that the relaxation of particle

network may occur. However, when we compare the rheological measurements on the starting formulations containing Jeffamine D230 or IPD this conclusion cannot hold (Figure 5.15). Figure 5.15 shows that at the same curing temperature the viscosity changes during cross-linking are only slightly different when different curing agents are used. Therefore, the observed differences in Figure 5.15 seem too small to explain the differences in relaxation behavior in the particle networks obtained with different curing agents. Furthermore, the surface energies of Jeffamine D230 and IPD are very similar (Table 5.3); hence a similar initial A_H^{eff} is expected. Moreover, a very similar Phthalcon particle dispersion was used. These observations suggest that probably the rate of particle network formation is very similar for the starting formulations containing either cross-linkers at a certain curing temperature. Therefore, the occurrence of relaxation of Phthalcon particle networks at specific curing temperatures for these two different cross-linkers cannot be explained by the viscosity changes and the A_H^{eff} value. This will be discussed in more detail later.

➢ log $\sigma_v - \varphi$ Relation

The relation between σ_v of IPD cured epoxy coatings and Phthalcon concentration φ is shown in Figure 5.16. These data have been corrected for the existence of an insulating bottom layer. These curves show that coatings cured at 50 ^{o}C have the highest conductivity; coatings cured at 100 ^{o}C have the lowest conductivity; while coatings cured at 40, 60 and 80 ^{o}C have a very similar log $\sigma_v - \varphi$ relation and it lies between coatings cured at 50 and 100 ^{o}C. The log $\sigma_v - \varphi$ relation also suggests that for coatings cured at 50 ^{o}C the φ_c and σ_{max} values are close to the one observed in Jeffamine D230 cross-linked coatings cured at 100 ^{o}C (Figure 5.5). In both cases a similar d_f value was observed. However, the σ_{max} value is only reached at a much higher Phthalcon concentration when the material was cured with IPD. The much lower σ_v values observed at the same φ in coatings cross-linked with IPD at 50 ^{o}C are likely to be explained by the presence of more polymer matrix between Phthalcon particles in the network.

When Phthalcon particle network relaxes at 60, 80 or 100 ^{o}C, the σ_v values are lower (Figure 5.16). This may be explained by the increase in the amount of polymer matrix between particles in the network during relaxation. The large difference in log $\sigma_v - \varphi$ relation observed for materials cured at 60, 80 or 100 ^{o}C suggest that this decrease in σ_{max} must be also partially attributed to the changes in loops, dangling chains and/or isolated aggregates in the particle network. When we compare the log $\sigma_v - \varphi$ relation

and the particle network structures in IPD cured coatings (Figure 5.12 & 5.16) with coatings cured with Jeffamine cross-linkers at 100 $^{\circ}$C (Figure 5.10 & 5.11), a similar trend was observed, i.e. a decrease in σ_v at a certain φ when particle network relaxes.
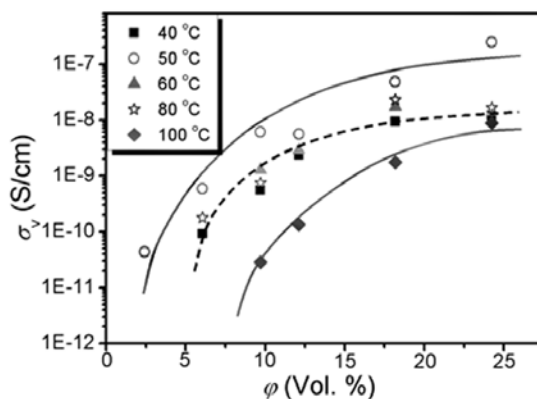
Figure 5.16. log σ_v - φ relation of epoxy coatings using IPD as cross-linker cured at various temperatures. All curves have been corrected for the existence of an insulating bottom layer.

Data in Figure 5.16 were also analyzed using Equation (5.2) to characterize the detailed Phthalcon particle network structures in IPD cured coatings. Surprisingly, the t value ($\varphi_c \approx 1$ vol. %, $t \approx 3$) obtained for coatings cured at 50 $^{\circ}$C is rather different from the one obtained for Jeffamine D230 coatings cured at different temperatures (t = 2.1-2.2) (Figure 5.4). Although it is difficult to determine the exact t values for coatings cured with IPD at other temperatures due to the difficulty in determining φ_c, the data in Figure 5.16 suggest t values ≥ 3 for all these coatings. Such high t values suggest that the charge transport in IPD cured coatings is non-universal.[20]

Non-universal transport behavior ($t \neq 2$) has been reported before, and has been interpreted as a fundamental difference between continuum percolation and lattice percolation.[35,47] Non-universal behavior has been theoretically demonstrated for an anomalous diverging distribution of resistances between conductive elements,[48] for a tunneling-percolation model of conduction between conductive elements in the composites,[49,50] and for a "Swiss-cheese model", where spherical voids are introduced in a continuous conductor.[51] Recently, Balberg, *et al.* showed, by combining experimental electrical measurements and corresponding theoretical analysis, the existence of a tunneling-percolation scenario.[52] The values expected for the critical exponent t, in tunneling-percolation systems in the continuum, are between 2 and the order of 10 for typical ratios of the tunneling decay constant and the size of the

conducting particles.[52] Whether the conduction mechanism in our IPD cross-linked coatings is also tunneling-percolation is still an open question. Nevertheless, this non-universal transport in IPD cured epoxy coatings is related to a particle network structure differents from the one formed by random percolation ($t = 2$). Both Jeffamine and IPD cured coatings are likely to be formed by DLCA, however, even for IPD cured coatings in which the networks do not relax (cured at 40 and 50 $^{\circ}$C) the higher t values suggest that these networks are non-universal. Because the ultimate particle network structures found in IPD cured coatings are different from the ones observed in Jeffamine D230 cured coatings, it may be expected that the relaxation of Phthalcon particle networks occurs at somewhat different curing temperatures, although the initial Phthalcon dispersions, A_H^{eff} and the viscosity changes during cure are very similar. The fact that an insulating bottom layer was found in IPD cured coatings also suggests that the movements of particles in the network during cure are different from those in Jeffamine D230 cross-linked coatings.

B. Using DDM as Cross-linker

Besides Jeffamine and IPD cross-linkers, epoxy composites containing different Phthalcon concentrations and cross-linked with DDM were also prepared at different curing temperatures. The aim of using DDM was to study the effect of a lower initial A_H^{eff} on Phthalcon particle network formation and log σ_v - φ relation of cured coatings (Table 5.3).
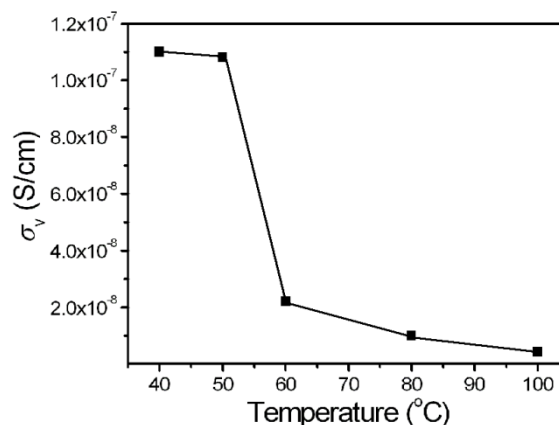
Figure 5.17. Conductivity of epoxy coatings cross-linked with DDM. The initial Phthalcon concentration was 12 vol. % based on the total volume of the coating components, all σ_v shown here have been corrected for the existence of an insulating bottom layer.

DDM is a solid material at room temperature, therefore the starting formulations were made by dissolving DDM first into a small amount of *m*-cresol, and the rest of the processing conditions were kept same. For these DDM cross-linked coatings the σ_v values, the Phthalcon particle network structures and distributions as well as the viscosity changes over time were studied (Figure 5.17, 5.18 & 5.19).
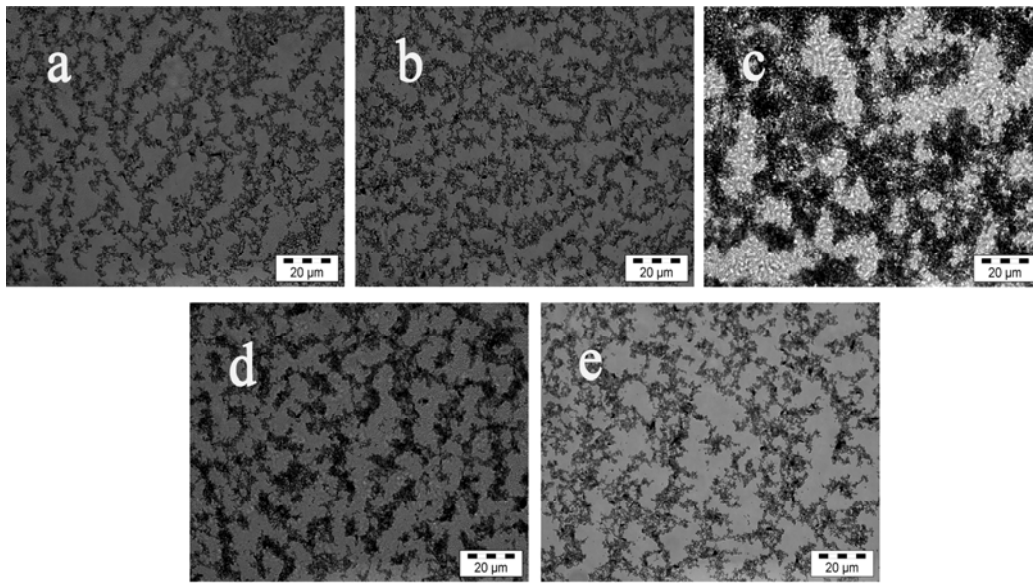
Figure 5.18. OM images of Phthalcon particle networks in Epikote 828/DDM coatings cross-linked at different temperatures. All coatings contained 3 vol. % Phthalcon in the starting formulations. (a) cured at 40 $^{\circ}$C; (b) cured at 50 $^{\circ}$C; (c) cured at 60 $^{\circ}$C; (d) cured at 80 $^{\circ}$C; (e) cured at 100 $^{\circ}$C.
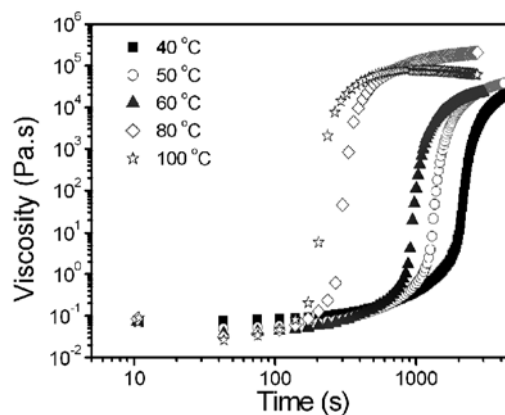
Figure 5.19. Changes in viscosity during cure of Epikote 828/DDM coatings. The curing temperature was varied and the initial Phthalcon concentration in the starting formulation was 3 vol. %.

The fractal dimensions and the OM images of these coatings cured at different temperatures show that some of the Phthalcon particle networks relax (Table 5.7 & Figure 5.18). Probably here initially DLCA formed networks relax as well when the increase in viscosity is sufficiently slow. The cross-sections of cured coatings show that there is always an insulating bottom layer present, and that the thickness of the bottom layer strongly depends on the curing temperature (Table 5.8). Unfortunately, this creates an uncertainty in quantitatively determining the σ_v values, and makes it impossible to obtain quantitative data on the log $\sigma_v - \varphi$ relation for coatings cross-linked at different temperatures. Reliable data were only obtained for coatings which contained 12 vol. % Phthalcon in the initial starting formulations (Figure 5.17). The σ_v of 10^{-7} S/cm for a non-relaxed Phthalcon particle network formed by DLCA at 40 and 50 ^{o}C and σ_v of 2 x 10^{-8} S/cm for a relaxed Phthalcon particle network at 60 ^{o}C are in agreement with the values found for coatings cured with IPD or Jeffamines. For coatings cured at 80 and 100 ^{o}C, no relaxation of the particle network was found. Still the σ_{max} is only 10^{-8} S/cm. This may be explained by either more matrix between particles in the network or by a different network structure (different t values, loops or dangling chains) (Figure 5.2, 5.10, 5.12 & 5.18). These results suggest that at a σ_v value of 10^{-7} S/cm no matrix material is present between particles in the backbone of the network, whereas in a relaxed network matrix material is present between particles. To make these coatings the amount of m-cresol used is larger in the starting formulations for coatings cured with DDM, but rheological measurements indicate that the influence of m-cresol on viscosity changes over time seems to be minimal (Figure 5.20).
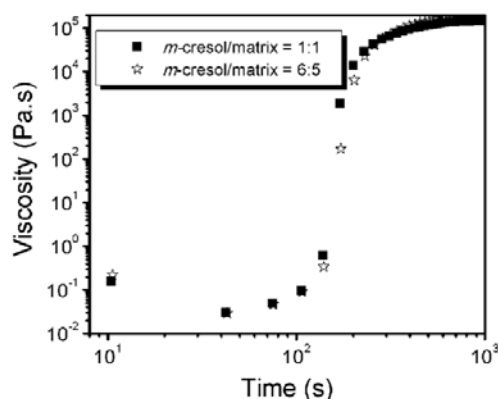
Figure 5.20. Viscosity changes during cure of epoxy coatings. All coatings contained 3 vol. % Phthalcon in the starting formulations and the amount of m-cresol was varied.

Table 5.7. Phthalcon particle network structures in epoxy coatings using DDM as cross-linker cured at various temperatures.[*]

Curing Temperature ($^{\circ}$C)	d_f	ξ (μm)
40	1.69	25
50	1.74	25
60	1.55	35
80	1.72	25
100	1.75	25

[*] Phthalcon concentration was 3 vol. % based on the initial concentration of Phthalcon with respect to the final coating components.

Table 5.8. Phthalcon particle layer thicknesses in cross-linked Epikote 828/DDM coatings cured at different temperatures.[*]

Curing T ($^{\circ}$C)	Total Thickness (μm)	Particle Network Thickness (μm)	Actual Particle Concentration (vol. %)
40	48.9	24.0	6.1
50	51.3	23.5	6.5
60	40.6	17.2	7.1
80	34.9	12.7	8.2
100	53.6	16.7	9.6

[*] All calculations were based on 3 vol. % Phthalcon in the starting formulations.

5.4. Conclusions

By adding a small amount of semi-conductive Phthalcon nanoparticles to epoxy starting formulations, the DC volume conductivity σ_v of the thermally cured composites can be raised considerably due to the formation of fractal Phthalcon particle networks through the matrix. These networks are sometimes formed at a Phthalcon concentration φ just above 0.6 vol. % and the maximum volume conductivity σ_{max} can be as high as 10^{-7} S/cm. However, we found that the log $\sigma_v - \varphi$ relation and the fractal Phthalcon particle network structures and distributions after cross-linking are strongly dependent on the chosen cross-linker and processing conditions. Only within a very small processing window, which is different for each chosen cross-linker, an optimum log $\sigma_v - \varphi$ relation can be obtained.

Not only the distribution of Phthalcon particle network can be different over the coating thickness (insulating top or bottom layer), but also the fractality of the particle network as well as the amount of polymer matrix between particles can vary considerably, strongly depending on the chosen cross-linker and processing conditions.

In our coatings we found that often the differences observed in log $\sigma_v - \varphi$ relations and Phthalcon network structures could not be explained by the differences in A_H^{eff} and the starting Phthalcon dispersions alone, which are generally assumed to be the most important factors. We have shown that the ultimate Phthalcon particle network structure is also strongly dependent on the initial viscosity, viscosity changes over time, the critical exponent t value as well as the evaporation rate of the solvent, if present, during cure. This means that even when the A_H^{eff} and starting Phthalcon dispersion are very similar, the chosen curing agent and curing temperature have major influences on the log σ_v - φ relation. These factors also determine at which temperature the initially formed fractal Phthalcon particle network relaxes.

The results presented here suggest that for other thermoset polymer composites containing a small amount of (semi)conductive nanoparticles similar strong influences of small changes in cross-linker and processing conditions on the fractal particle network structures, network distributions and ultimate log $\sigma_v - \varphi$ relations are expected.

References

1. Skotheim, T. A.; Ed., *Handbook of Conducting Polymers, 2nd ed., Revised and Expanded*. Marcel Dekker: New York, 1997.

2. Nalwa, H. S., *Handbook of Advanced Electronic and Photonic Materials and Devices*. Academic Press: London, 2000.

3. Chandrasekhar, P., *Conducting Polymers, Fundamentals and Applications: A Practical Approach*. Kluwer Academic: Dordrecht, 1999.

4. Gul, V. E., *Structure and Properties of Conducting Polymer Composites*. VSP: Utrecht, 1996.

5. Zallen, R., *The Physics of Amorphous Solids*. Wiley: New York, 1983.

6. Kirkpatrick, S. *Rev. Mod. Phys.* **1973,** 45, (4), 574-588.

7. Sahini, M., *Applications of Percolation Theory*. Taylor & Francis: London, 1994.

8. Brokken-Zijp, J. C. M.; Soloukhin, V. A.; Posthumus, W.; de With, G. *In Proceeding of 2003 Athens Conference on Coatings Science and Technology, Vouliagmeni, Greece*.

9. Zhang, Q. H.; Jin, H. F.; Wang, X. H.; Jing, X. B. *Synth. Met.* **2001,** 123, (3), 481-485.

10. Thongruang, W.; Balik, C. M.; Spontak, R. J. *J. Polym. Sci. B* **2002,** 40, (10), 1013-1025.

11. Lee, S. B.; Katayama, T.; Kajii, H.; Araki, H.; Yoshino, K. *Synth. Met.* **2001,** 121, (1-3), 1591-1592.

12. Chen, Q.; Xi, Y.; Bin, Y.; Matsuo, M. *J. Polym. Sci. B* **2008,** 46, (4), 359-369.

13. Zhang, W.; Dehghani-Sanij, A. A.; Blackburn, R. S. *J. Mater. Sci.* **2007,** 42, (10), 3408-3418.

14. Chen, Z.; Brokken-Zijp, J. C. M.; Michels, M. A. J. *J. Polym. Sci. B* **2006,** 44, (1), 33-47.

15. Kleinjan, W. E.; Brokken-Zijp, J. C. M.; van de Belt, R.; Chen, Z.; de With, G. *J. Mater. Res.* **2008,** 23, (3), 869-880.

16. Soloukhin, V. A.; Brokken-Zijp, J. C. M.; de With, G. *J. Polym. Sci. B* **2007,** 45, (16), 2147-2160.

17. Roldughin, V. I.; Vysotskii, V. V. *Prog. Org. Coat.* **2000,** 39, (2-4), 81-100.

18. Adriaanse, L. J.; Faneyte, I. P.; Martens, H. C. F.; Reedijk, J. A.; Brom, H. B.; Michels, M. A. J.; Brokken-Zijp, J. C. M. *Synth. Met.* **1997,** 84, (1-3), 871-872.

19. Adriaanse, L. J.; Reedijk, J. A.; Teunissen, P. A. A.; Brom, H. B.; Michels, M. A. J.; Brokken-Zijp, J. C. M. *Phys. Rev. Lett.* **1997,** 78, (9), 1755-1758.

20. Huijbregts, L. J. *Charge Transport and Morphology in Nanofillers and Polymer Nanocomposites*. Ph.D. Thesis, Eindhoven University of Technology, Eindhoven, 2008.

21. Huijbregts, L. J.; Brom, H. B.; Brokken-Zijp, J. C. M.; Kemerink, M.; Chen, Z.; de Goeje, M. P.; Yuan, M.; Michels, M. A. J. *J. Phys. Chem. B* **2006,** 110, (46), 23115-23122.

22. Chen, Z.; Brokken-Zijp, J. C. M.; Huinink, H. P.; Loos, J.; de With, G.; Michels, M. A. J. *Macromolecules* **2006,** 39, (18), 6115-6124.

23. van der Putten, D.; Moonen, J. T.; Brom, H. B.; Brokken-Zijp, J. C. M.; Michels, M. A. J. *Phys. Rev. Lett.* **1992,** 69, (3), 494-497.

24. Michels, M. A. J.; Brokken-Zijp, J. C. M.; Groenewoud, W. M.; Knoester, A. *Physica A* **1989,** 157, (1), 529-534.

25. Brokken-Zijp, J. C. M.; van Mechelen, J. B.; Emeis, C. A.; Datema, K. P.; Kramer, A. H.; de Bruijn, D. P.; Meruma, A. J. *US Patent 05319009* **1993**.

26. Brokken-Zijp, J. C. M.; Yuan, M.; et.al. *"Synthesis and Structure of Novel Aquocyanophthalocyaninato Co(III) Semi-conductor and Its Applications in Conductive Polymer Composites"*. In Preparation.

27. Huijbregts, L. J.; Brom, H. B.; Brokken-Zijp, J. C. M.; Yuan, M.; Michels, M. A. J. *Phys. Stat. Sol.* **2006,** 3, 259-262.

28. Yuan, M.; Brokken-Zijp, J. C. M.; Huijbregts, L. J.; de With, G. *J. Polym. Sci. B* **2008,** 46, 1079-1093.

29. Banerjee, P.; Mandal, B. M. *Macromolecules* **1995,** 28, (11), 3940-3943.

30. Pallas, N. R.; Pethica, B. A. *Colloids Surf.* **1983,** 6, (3), 221-227.

31. Dettre, R. H.; Johnson, R. E. *J. Colloid Interface Sci.* **1966,** 21, (4), 367.

32. Yuan, M.; Brokken-Zijp, J. C. M.; de With, G. *"Conductivity of Cross-linked Low Surface Energy Epoxy Coatings"*. Submitted to J. Polym. Sci. B.

33. Mandelbrot, B. B., *The Fractal Geometry of Nature* W. H. Freeman: New York, 1983.

34. Schüth, F.; Sing, K. S. W.; Weitkamp, J.; Ed., *Handbook of Porous Solids*. Wiley-VCH: Weinheim, 2002; Vol. 1.

35. Heaney, M. B. *Phys. Rev. B* **1995,** 52, (17), 12477-12480.

36. Weitz, D. A.; Huang, J. S.; Lin, M. Y.; Sung, J. *Phys. Rev. Lett.* **1984,** 53, (17), 1657-1660.

37. Brady, R. M.; Ball, R. C. *Nature* **1984,** 309, (5965), 225-229.

38. Vermant, J.; Solomon, M. J. *J. Phys.* **2005,** 17, (4), R187-R216.

39. Meakin, P. *Phys. Rev. A* **1983,** 27, (3), 1495-1507.

40. Huijbregts, L. J.; Brom, H. B.; Brokken-Zijp, J. C. M.; Yuan, M.; Michels, M. A. J. *Phys. Stat. Sol.* **2008,** 5, 765-767.

41. Stauffer, D.; Aharony, A., *Introduction to Percolation Theory, 2nd ed.* Taylor & Francis: London, 1992.

42. Shih, W. H.; Shih, W. Y.; Kim, S. I.; Liu, J.; Aksay, I. A. *Phys. Rev. A* **1990,** 42, (8), 4772-4779.

43. Yuan, M.; Brokken-Zijp, J. C. M.; de With, G. *"Conductivity of UV Cured Phthalcon/Acrylate Coatings".* Submitted to Macromolecules.

44. Henry Lee, K. N., *Handbook of Epoxy Resins*. Mcgraw-Hill: Texas, 1981.

45. van Garderen, H. F.; Dokter, W. H.; Beelen, T. P. M.; van Santen, R. A.; Pantos, E.; Michels, M. A. J.; Hilbers, P. A. J. *J. Chem. Phys.* **1995,** 102, 480-496.

46. Brokken-Zijp, J. C. M. *Internal Information from Shell*.

47. Balberg, I. *Philos. Mag. B.* **1987,** 56, 991.

48. Kogut, P. M.; Straley, J. P. *J. Phys. C* **1979,** 12, (11), 2151-2159.

49. Balberg, I. *Phys. Rev. Lett.* **1987,** 59, (12), 1305-1308.

50. Rubin, Z.; Sunshine, S. A.; Heaney, M. B.; Bloom, I.; Balberg, I. *Phys. Rev. B* **1999,** 59, (19), 12196-12199.

51. Feng, S. C.; Halperin, B. I.; Sen, P. N. *Phys. Rev. B* **1987,** 35, (1), 197-214.

52. Grimaldi, C.; Balberg, I. *Phys. Rev. Lett.* **2006,** 96, (6), 066602-4.

6

CONDUCTIVITY OF CROSS-LINKED LOW SURFACE ENERGY EPOXY NANOCOMPOSITES⊛

SYNOPSIS

A new and straightforward method has been described to prepare cross-linked low surface energy semi-conductive epoxy coatings. The low surface energy is obtained by adding a small amount of partially fluorinated bifunctional primary amine Jeffamine D230 cross-linker, and the conductivity is achieved by adding a small amount of semi-conductive nanometer-sized phthalocyanine Co(III) compound Phthalcon 11/12. The use of partially fluorinated cross-linker strongly influences the conductivity, the conductive particle network structure and distribution in the coatings. Compare to coatings that are free of fluorine, variations in fractal dimension, percolation threshold, Phthalcon-containing layer thickness and conductivity level are observed as the amount of fluorinated species varies. These differences can be explained by (local) differences in effective Hamaker constant, viscosity, curing rate, evaporation of the solvent and presence/absence of polymer matrix between particles in the network. Our results suggest that other cross-linked semi-conductive low surface energy epoxy coatings can be realized in a similar manner, but careful optimization of processing conditions is required to obtain the desired conductivity level at low filler concentration.

6.1. Introduction

In the past several approaches have been explored for the modification of polymer surfaces, including chemical reactions, surface grafting, blending and absorption of block-copolymers.[1] In particular, fluorinated surfaces have gained considerable interest because of the advantageous surface properties induced by fluorine atoms, such as excellent hydrophobicity and oleophobicity (due primarily to the low surface energy). Therefore, low surface energy coatings are considered to be easily cleanable. Another attractive property of these coatings is a low coefficient of friction.[2-4] However, often other properties are required for the same coating. One of the requirements is a higher level of volume conductivity. If coatings could be made permanently antistatic, it would further enhance the cleanability and reduce the friction by lowering the charge built up caused by, for instance, rubbing the surface. To see whether a sufficiently high conductivity and a sufficiently low surface energy can be realized in the same coating is the subject of this chapter.

The characteristic of fluorinated molecules in a polymer material is that they can migrate towards the air/coating interface to minimize the interfacial energy.[4-11] Due to surface segregation, self-stratification strategies have been used to create coatings in which desired surface and bulk properties are well balanced and only a very small quantity of fluorinated species is needed to provide a surface with low surface energy, while keeping the bulk properties virtually unchanged.[12-15]

It is well-known that the conductivity of a coating can be raised by the presence of a (semi)conductive nanoparticle network through the polymer matrix, even when the concentration of conductive particles is well below 1 vol. %. The conductivity of these coatings has been extensively studied before.[16-22] In these composites, particle networks are formed by Brownian movement of the particles during processing. The amount of particles needed appears to be dependent on the particle-particle and particle-matrix interactions. The (local) presence of fluorinated species may reduce the surface energy of the matrix tremendously and therefore change (locally) the above mentioned interactions. Moreover, because the surface energy of the nanoparticles is generally much larger than that of the coating components, the presence of nanoparticles may also influence the distribution of fluorinated species in the coating. Therefore, we expect that the surface energy, the conductivity and the morphology of particle network are different from those of fluorine-free coatings.

It has been shown that when partially fluorinated bifunctional primary amine Jeffamine D230 was used as cross-linker, epoxy coatings with low surface energy can be made.[23] It has been also reported that the addition of a small amount of semi-conductive phthalocyanine Co(III) compound Phthalcon 11/12 can increase the conductivity of epoxy coatings cross-linked with non-fluorinated Jeffamine D230.[20,21,24,25] In this chapter, we describe the preparation of cross-linked low surface energy semi-conductive epoxy coatings. The low surface energy is obtained by using partially fluorinated Jeffamine D230 cross-linker and the conductivity is achieved by adding a small amount of semi-conductive nanometer-sized Phthalcon 11/12 particles. We will show that the influence of Phthalcon 11/12 on the surface energy of these coatings is minimal, while the conductivity behaviour of these coatings is completely different from that of fluorine-free coatings. In this chapter, special attention is given to the influence of the amount of fluorine containing species in the starting coating formulation on the surface energy, the coating conductivity, and the morphology of Phthalcon particle network in these cross-linked epoxy coatings. The impact of our findings on other nanofiller/polymer matrix composites is also addressed.

6.2. Experimental

6.2.1. Materials

Phthalcon 11/12 (Scheme 6.1) was synthesized in high purity and yield using a two-step reaction as described before.[24-26] The primary Phthalcon 11/12 particle size used here is about 250 nm in length and width and about 50 nm in thickness. The Phthalcon powder was carefully dried at 80 ^{o}C for 48 h under vacuum (~ 0.01 mbar) and ground into fine powder in a mortar before use. Epoxy prepolymer (Epikote 828) was purchased from Resolution Nederland BV. The amine cross-linker Jeffamine D230 was purchased from Huntsman BV, Belgium. The reagent (2,2,3,3,4,4,5,5,6,6,7,7,8,8,9,9,9-heptadecafluorononyl) oxirane (96 %, EP-F8) was purchased from Aldrich. *m*-cresol (spectrophotometric grade) was purchased from Merck. The chemical formula of EP-F8, Jeffamine D230 and Epikote 828 are given in Scheme 6.2. All chemicals purchased were used as received.
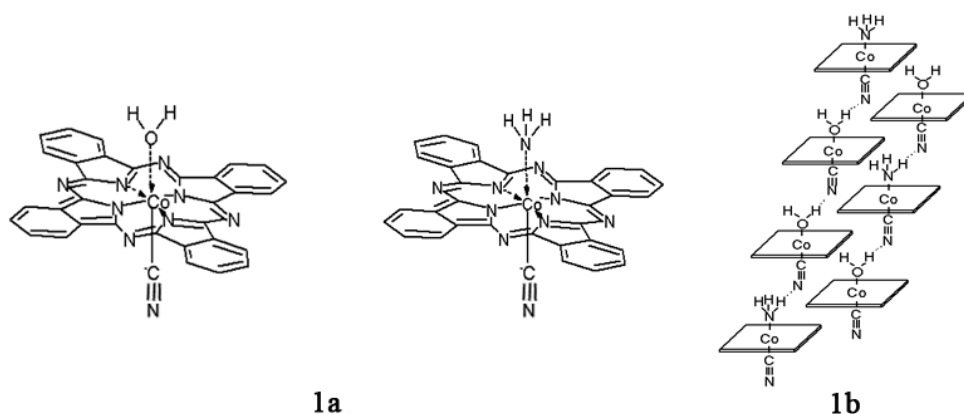
Scheme 6.1. Molecular and crystal structure of Phthalcon 11/12 (1a, 1b), Phthalcon 11/12 contains both NH_3 and H_2O as ligands in the cystal.[25]
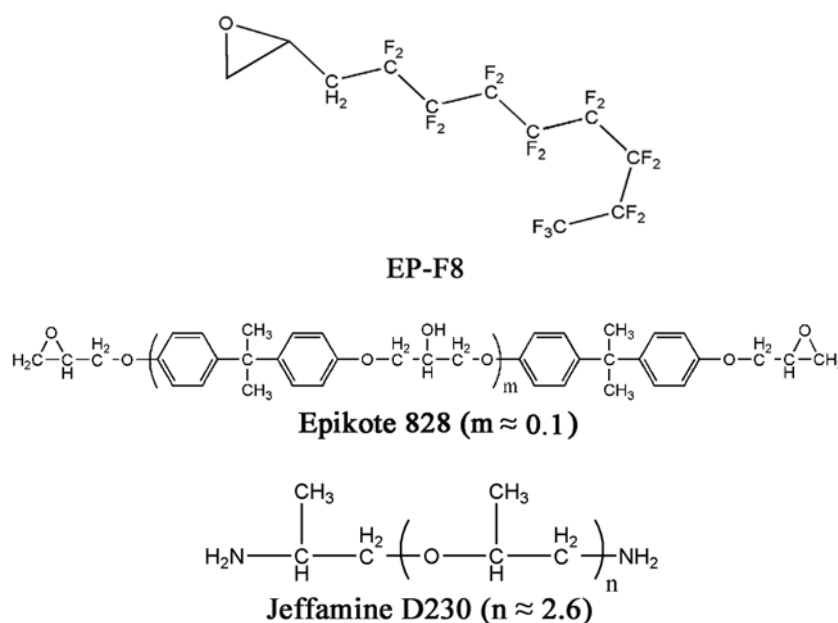
Scheme 6.2. Chemical structures of EP-F8, Epikote 828 and Jeffamine D230.

6.2.2. Sample Preparation

First, several partially fluorinated Jeffamine D230 samples (Jeffamine D230-F) were prepared using the same method as described earlier (Scheme 6.3),[23] e.g.: 17.0 g Jeffamine D230 (a known excess) reacted at 100 $^{\circ}$C with 1.5 g EP-F8 under N_2 flow for 2 h. In this step the fluorinated epoxide was chemically bonded to Jeffamine D230 as confirmed by ^{1}H-NMR.[27] Without changing the processing conditions, the initial ratio between EP-F8 and Jeffamine D230 was varied to adjust the fluorine content in Jeffamine D230-F (Table 6.1). Subsequently, after cooling down to room temperature, a specific amount of Jeffamine D230-F and Epikote 828 was added to a Phthalcon/*m*-

cresol dispersion. This mixture was then magnetically stirred for 5 min and ultrasonically degassed for 5 min. Finally, it was cast on a polycarbonate substrate with a 120 μm wet coating thickness using a doctor blade applicator and cured immediately for 4 h at 100 ^{o}C under vacuum (~ 0.01 mbar) and later post-cured at 120 ^{o}C for 8 h under vacuum (~ 0.01 mbar). Under these conditions smooth coatings with layer thicknesses between 50 and 100 μm were obtained.
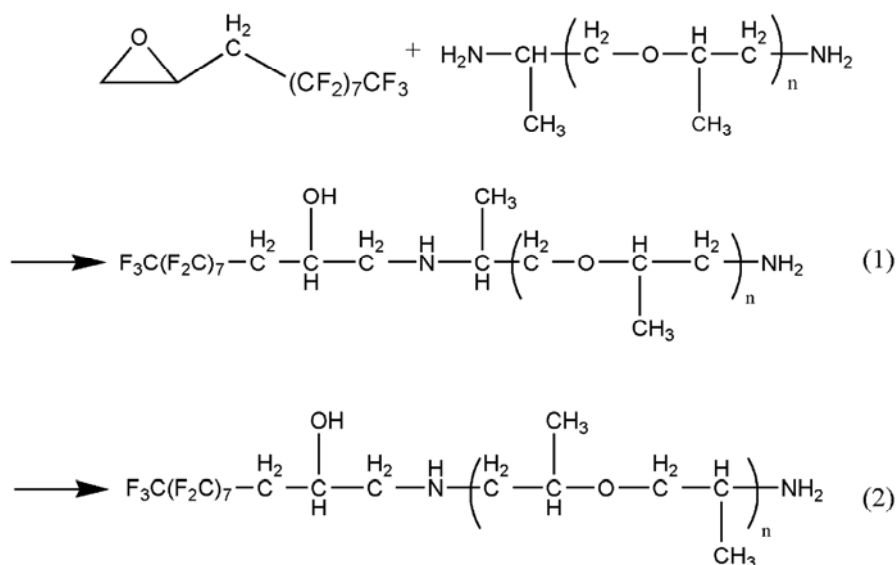
Scheme 6.3. Reaction routes used to prepare Jeffamine D230-F.

Table 6.1. Ratio between EP-F8 and Jeffamine D230.

Jeffamine D230-F (mol %)[#]	EP-F8 (g)	Jeffamine D230 (g)
1.5	0.5	16.5
4.3	1.5	17.0
14.2	5.0	17.0
20.0	7.5	18.5

[#] Based on the initial molar number of Jeffamine D230 present in the mixture before reaction.

The NH/epoxy molar ratio used in the starting formulation for these coatings was always kept 1/1. For comparison epoxy coatings cured with non-fluorinated Jeffamine D230 were also prepared following the same method as described above. The initial volume concentration of Phthalcon 11/12 particles in the final cross-linked epoxy coatings was determined based on the total composition of the composites after cross-

linking, taking into account the densities of Phthalcon particle and cross-linked epoxy as 1.65 and 1.00 g/cm^3, respectively. When an insulating bottom layer was present in which Phthalcon particles were absent, the initially determined particle concentrations were corrected due to the presence of this layer.

6.2.3. Characterization

Contact Angle (CA) CA analyses on cross-linked epoxy coatings were performed in air at room temperature with an OCA30 apparatus from Dataphysics Instruments. The sessile drop method was used to obtain the contact angles. Deionized water and hexadecane (> 99 %, Merck) were used as probe liquids. For each measurement 10 mL probe liquid was applied. The droplet was monitored by a CCD camera and analyzed by drop shape analysis software (DSA Version 1.0, Krüss). The complete profile of the sessile droplet was fitted with an ellipse. All contact angles given are average values measured at three different positions on each coating surface. Surface energies of all coatings were determined using the geometric mean method of Owens-Wendt-Rabel-Kaelble (OWRK)[28] from the advancing angles with deionized water and hexadecane.[29] Because the contact angles given are average values, the calculated surface energies are average values as well. The surface energies γ of the wetting liquids used in these calculations are listed in Table 6.2.[30]

Table 6.2. Surface energies of the wetting liquids.[30]

Wetting Liquid	T (^{o}C)	γ (mN/m)
Deionized Water	25	71.97
Hexadecane	20	27.47

Surface Energy The surface energies of liquid samples were determined at 20 ^{o}C by Wilhelmy plate method using a Krüss digital tensionmeter K10T. During the measurement, the plate was moved towards the surface until it reached the meniscus. The surface energy was calculated from the measured force. All surface energies given are average values of three measurements on each sample.

DC Volume Conductivity The volume conductivity σ_v at room temperature was measured using a standard four-point method, with a Keithley 237 high voltage source measuring unit and a Keithley 6517A high voltage electrometer. The former

unit supplies a constant current through the coating between the two outside electrodes and the latter unit measures the voltage difference between the two inside electrodes. The measurements were carried out on the surface of the coating sample according to standard ASTM D991 and instructions of Keithley "low conductivity level measurements". Silver paint (silver conductive adhesive 416, electron microscopy sciences, USA) was used to ensure good contact of the sample surface with the measuring electrodes. Coatings used in the conductivity measurements had a thickness between 50 and 100 μm, as determined by a digital screw micrometer. In coatings made from Jeffamine D230-F Phthalcon particle network was not present throughout the whole coating. In these coatings the σ_v values and the Phthalcon concentrations were calculated after only taking into account the layer thickness which contained Phthalcon particles.

Optical Microscopy (OM) The morphology of the particle network in the materials after cross-linking was observed with OM (Reichert-Jung Polyvar-Met) using the transmission bright-field technique. These images were later converted into binary images and analyzed using the tiling method to obtain the fractal dimensions and the correlation lengths of the particle networks.[20] The coatings used here had a thickness of about 10 μm.

Often thin cross-sectional cuts about 2-3 μm thick were made from cross-linked coating samples and analyzed with OM to assess Phthalcon particle distribution over the thickness of the coating. These cuts were prepared by microtoming at room temperature.

Rheological Measurements Rheological measurements were performed to follow the viscosity changes during cure using an AR1000 rheometer with 20 mm plate-plate geometry. The coating starting formulation was directly added to the plate, and then the gap between plates was set to be 300 μm. At the beginning of the measurement (t = 0 s), the plates were heated from room temperature to 100 $^{\circ}$C within 30 sec. All measurements were done under N_2 flow.

6.3. Results and Discussion

6.3.1. Surface Energies of Different Coating Components
From the classical Gibbs adsorption law it follows that in multi-component systems

the surface will be preferentially enriched with the component which has the lowest surface energy. In order to get an indication of the concentration of low surface energy species present at the surface, the surface energies of Jeffamine D230-F samples together with Epikote 828, Jeffamine D230 and EP-F8 were determined using Wilhelmy plate method. To check these measurements, the surface energies were also calculated with the aid of Sugden's method using the group contribution method.[31] For Epikote 828, Jeffamine D230 and EP-F8, both the experimentally determined and calculated surface energies are listed in Table 6.3. These values are in good agreement with each other and in line with the reported values.[18,21,23]

Table 6.3. Surface energies of the starting materials at 20 ^{o}C.

	Epikote 828 (mN/m)	Jeffamine D230 (mN/m)	EP-F8 (mN/m)
Wilhelmy Plate	46.0	32.8	16.7
Parachor Estimation	46.6	35.2	15.9
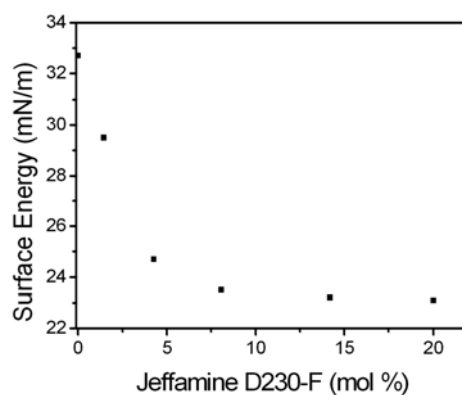
Figure 6.1. The experimentally determined surface energies of several Jeffamine D230-F samples as a function of mol % of fluorinated Jeffamine D230 present in the mixture.

The experimentally determined surface energies of various Jeffamine D230-F species are shown in Figure 6.1. Even when a small amount of fluorinated Jeffamine D230 was present (4.3 mol %), the surface energy decreased from 32.8 to 24.7 mN/m. This value is comparable with the value reported before for a similar Jeffamine D230-F mixture[23] and is also close to the calculated surface energy for Jeffamine D230 in which one of the amino hydrogen atoms is completely replaced by an EP-F8 tail (26.2 mN/m). This strongly indicates that the measured surface energies of all our partially

fluorinated Jeffamine D230-F samples are predominantly governed by the EP-F8-mono-substituted species, which are present at the surface of the liquid.

The surface energies of Jeffamine D230-F samples are always considerably higher than that of EP-F8 (Figure 6.1 & Table 6.3). This confirms that during reaction EP-F8 reacted completely with Jeffamine D230 in all Jeffamine D230-F samples. Furthermore, chemical bonding of all EP-F8 to Jeffamine D230 was indicated by ^{1}H-NMR as well.[27] Hence, we assume in the following discussion that this bonding is quantitative.

The difference in surface energy between Jeffamine D230-F (20.0 mol %) and non-modified Jeffamine D230 is about 9.5 mN/m, and the difference between Jeffamine D230-F (20.0 mol %) and Epikote 828 is as much as 23.0 mN/m. The large difference in surface energy between fluorinated and non-fluorinated components of the starting coating formulation will generate a strong driving force for the fluorinated species to migrate toward the air/coating interface as a result to minimize the surface energy of the liquid mixture, even before cure.

6.3.2. Surface Energies of Cross-linked Epoxy Coatings

The wetting behaviour of cross-linked epoxy coatings made from cross-linking with Jeffamine D230 or Jeffamine D230-F was investigated using contact angle measurements. These contact angle measurements were performed using water and hexadecane as probe liquids. The static water and hexadecane contact angles (θ_{H_2O} and $\theta_{Hexadecane}$, respectively) obtained as a function of Jeffamine D230-F mol % on coatings containing a fixed large amount of Phthalcon particles are shown in Figure 6.2. From these contact angle measurements the surface energies of all cross-linked coatings were determined using the geometric mean method of OWRK (Table 6.4).[29] Compared to contact angles or surface energies of cross-linked epoxy coatings containing the same amount of Phthalcon particles, but are free of fluorine, the water and hexadecane contact angles are significantly higher and their surface energies are considerably lower (Figure 6.2 & Table 6.4). Earlier AFM measurements on epoxy coating made from non-fluorinated Jeffamine D230 show that the coating roughness is small and is not related to the presence of Phthalcon particles.[32] Results in Table 6.4 also show that the presence of Phthalcon 11/12 hardly influences the surface energy over a broad range of Jeffamine D230-F concentrations. Hence, we may conclude that for coatings cross-linked with Jeffamine D230-F the fluorinated species are present at

the air/coating interface and that the influence of Phthalcon on surface energy is minimal.
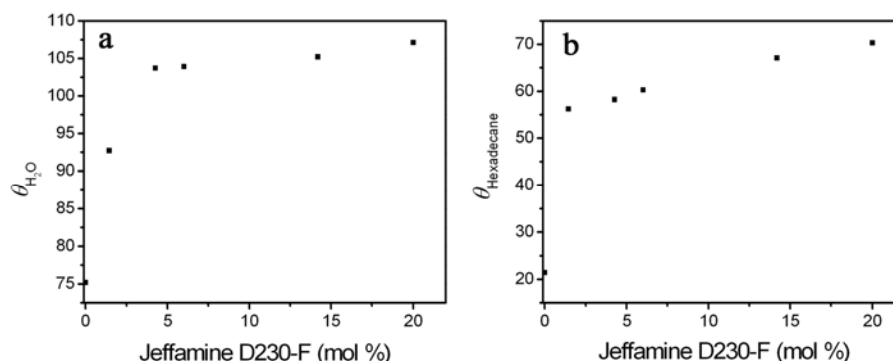
Figure 6.2. Static contact angles (^{o}) of deionized water (a) and hexadecane (b) on 12 vol. % Phthalcon/epoxy coatings as a function of mol % of fluorinated Jeffamine D230 present in the starting formulations. These coatings have a layer thickness of 85 μm and were made using, apart from the cross-linker, the same starting formulations, processing methods and conditions. The concentration of Phthalcon particles given was not corrected for the presence of an insulating bottom layer.

Table 6.4. Surface energies of epoxy coatings cross-linked with Jeffamine D230 with /without the presence of Phthalcon.

Jeffamine D230-F (mol %)	$\gamma^{\#}$ (mN/m)	γ^{*} (mN/m)
0	33.4	33.0
1.5	20.3	21.1
4.3	16.9	15.9
8.0	16.3	16.1
14.2	14.4	13.8
20.0	13.8	13.7

$^{\#}$ Measured on coatings containing 12 vol. % Phthalcon. This concentration was not corrected for the presence of an insulating bottom layer.
* Measured on coatings without Phthalcon.
$^{\square}$ The thicknesses of coatings were about 85 μm.

The plateau value of the contact angles (θ_{H2O} = 105 ^{o}) is reached at 4.3 mol % Jeffamine D230-F. This plateau value is comparable to the value of 108 ^{o} reported

before for a similar system, in which 3.1 mol % Jeffamine D230-F was used.[23] These authors also reported that cross-linked epoxy coatings could not be made when Jeffamine D230-F was higher than 6.2 mol % due to the dewetting problems of the coating formulation.[23] However, this was not observed in our coatings, and coatings containing 20.0 mol % Jeffamine D230-F could still be prepared. These differences are probably caused by a difference in the substrate (metal vs. polycarbonate) on which these coatings were prepared, and/or by slightly different reaction conditions and conversions.

The values of contact angles, using hexadecane as probe liquid, slightly increase further above 4.3 mol % Jeffamine D230-F. Nonpolar probe liquids such as hexadecane are more sensitive to the fluorine concentration. Nevertheless, because this further increase in contact angles is small, it is envisaged that the surface is (almost) filled up with fluorinated species, and that in cross-linked epoxy coating made from a fluorinated Jeffamine D230 concentration higher than 4.3 mol %, the increasing fluorinated species occurs mainly below the surface.

6.3.3. Epoxy Network Formation

During cross-linking of Epikote 828 with Jeffamine D230-F, the system changes from a low molecular weight liquid to a highly cross-linked polymer network. The mobility of fluorinated species, therefore, decreases as the cross-linking reaction proceeds. This may lower the ultimate amount of fluorinated tails present at the surface, resulting from insufficient time for the fluorinated species to migrate through the bulk towards the surface. Furthermore, the use of partially fluorinated cross-linker may affect the initial viscosity and the increase in viscosity during cross-linking. The viscosity behavior may have a strong influence on Phthalcon particle network formation and distribution. Therefore, rheological measurements were performed to study the development of viscosity in different starting formulations during cross-linking.

The observed changes in viscosity are shown in Figure 6.3. It can be seen that due to the changes in molecular weight of the matrix, the viscosity of the system increases strongly in time and that the viscosity changes over time is influenced by the amount of partially fluorinated Jeffamine presents in the formulation as well. When we replaced Jeffamine D230 by Jeffamine D230-F (20.0 mol %), the gel time increased from 152 s to 188 s. This observed retardation of gel time with increasing amount of fluorinated Jeffamine D230 may be explained by the replacement of part of the

primary amine groups by secondary amine groups in the starting formulation. It is well-known that the cross-linking rate of an epoxy group with a secondary amine is much slower than that of a primary amine.[33] Our rheological measurements also show that the presence of Phthalcon particles does not influence the viscosity changes over time.
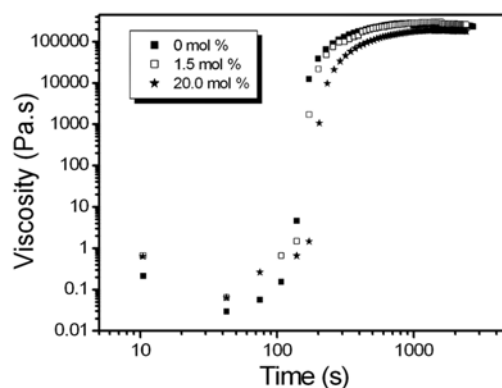
Figure 6.3. Changes in viscosity during cross-linking of Phthalcon/epoxy. The initial decrease in viscosity is mainly due to the temperature increases from room temperature to cross-linking temperature. The amount of fluorinated Jeffamine D230 in the starting formulation was varied. The concentration of Phthalcon in the starting formulation was 2 vol. % based on the total volume of the coating components, and the curing temperature was 100 °C.

6.3.4. Morphology of Phthalcon Particle Network in a Fluorinated Epoxy Matrix

The σ_v of a polymer composite containing semi-conductive particles depends on the morphology of particle network throughout the polymer matrix. It has been shown earlier that the presence of fractal Phthalcon nanoparticle networks in cross-linked epoxy matrices can be observed easily under the OM.[20] Therefore, Phthalcon particle networks in fluorine-free and fluorine-enriched epoxy coatings were also studied using the OM (Figure 6.4). All coatings in Figure 6.4 were prepared, apart from the amount of fluorinated Jeffamine present, using the same processing methods, processing conditions and starting formulations.

Figure 6.4 shows that the higher the amount of fluorinated Jeffamine D230 in the starting formulation, the coarser the particle network. In order to study the structures of these networks in more detail, the fractal dimensions of the particle networks were determined using the method of tiling as described before.[20,34,35] The results from fractal structure analyses are summarized in Table 6.5.
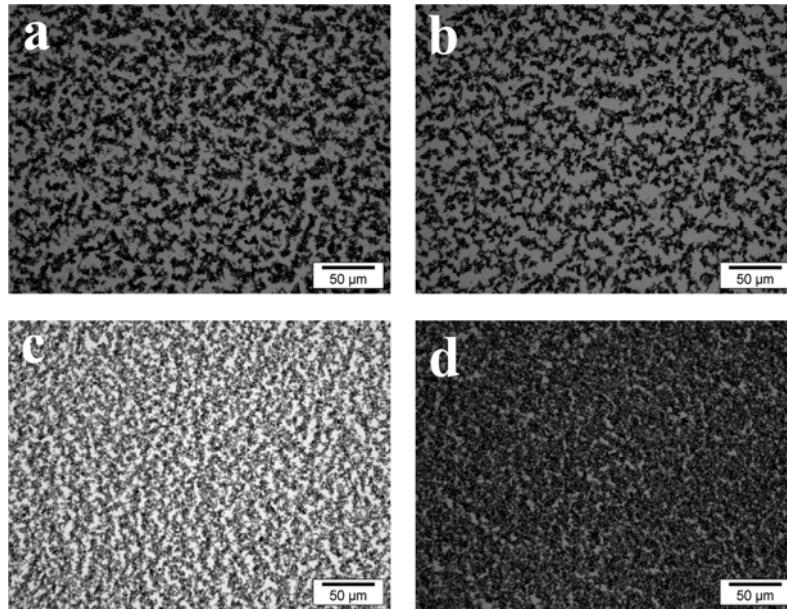
Figure 6.4. Optical microscopic images of cross-linked Phthalcon/epoxy coatings. All coatings contain 3 vol. % Phthalcon based on the total volume of the epoxy components. (a) 1.5 mol % Jeffamine D230-F; (b) 4.3 mol % Jeffamine D230-F; (c) 14.2 mol % Jeffamine D230-F; (d) 20.0 mol % Jeffamine D230-F.

Table 6.5. Phthalcon particle network structures.[*]

Jeffamine D230-F (mol %)	d_f	ξ (μm)
0	1.70	20
1.5	1.72	25
4.3	1.71	25
14.2	1.66	30
20.0	1.58	30

[*] Phthalcon concentration was 3 vol. % based on the initial concentration of Phthalcon with respect to the final coating components.

In general, for a specific system, the particle network may be described as stacked fractal aggregates, and the average size of these building blocks is the correlation length ξ, which is related to particle concentration φ and fractal dimension d_f for $\varphi > \varphi_c$ as shown below:[36,37]

$$\xi = a\varphi^{1/(d_f-3)} \tag{6.1}$$

In Equation (6.1), *a* is the radius of a primary particle from which the fractal network is built. When we assume that for our systems *a* is the radius of a primary Phthalcon particle aggregate which is on average of 0.7 μm,[31] the calculated ξ using Equation (6.1) is very close to the experimental ξ value for coatings made from non-fluorinated Jeffamine D230. When the fluorinated Jeffamine D230 content was higher than 4.3 mol %, an increase in ξ together with a decrease in d_f was observed. However, according to Equation (6.1) a lowering in ξ is expected, not only because of a decrease in d_f, but also due to an increase in the actual Phthalcon particle concentration (see later discussion). Whether this has to be explained by a somewhat larger initial *a* value or by the fact that relaxation (see later discussion) excludes the use of Equation (6.1) is being studied at this moment.
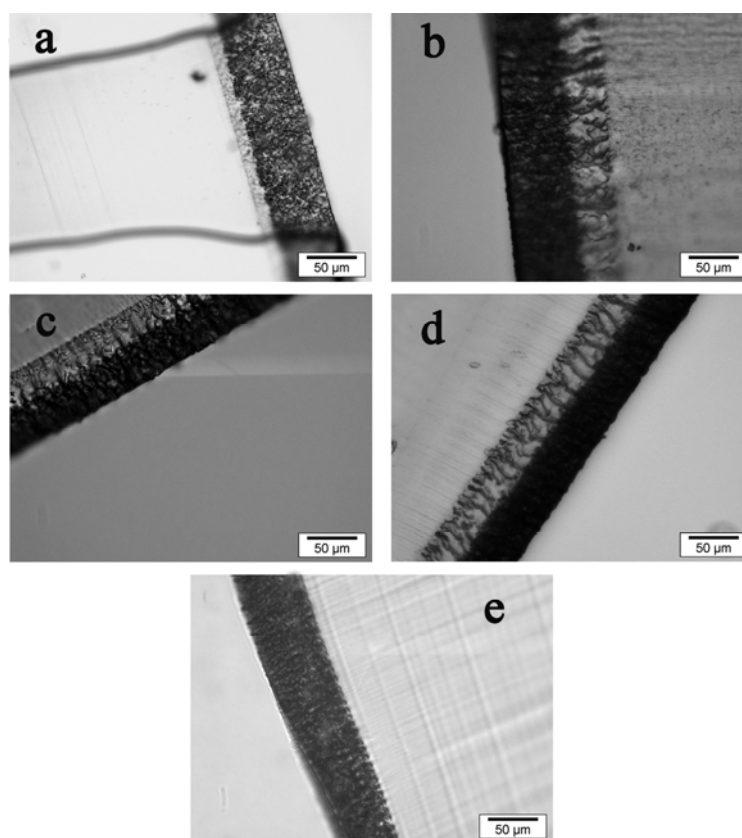
Figure 6.5. OM images of the cross-sections of Phthalcon/epoxy coatings. All coatings contained the same amount of Phthalcon in the starting formulations (3 vol. %;). (a) 1.5 mol % Jeffamine D230-F; (b) 4.3 mol % Jeffamine D230-F; (c) 14.2 mol % Jeffamine D230-F; (d) 20.0 mol % Jeffamine D230-F; (e) 0 mol % Jeffamine D230-F.

Cross-sections of Phthalcon/epoxy coatings, which were used in the conductivity measurements, were also prepared. The OM images of some of these cross-sections are shown in Figure 6.5. Amazingly, we observed an insulating bottom layer in all these coatings in which (almost) no Phthalcon particles are present as can be observed from the lack of blue colour in these layers. These insulating layers become thicker when the amount of fluorinated Jeffamine D230 in the starting formulation is higher. However, in a coating which is free of fluorinated species, Phthalcon particles are homogeneously distributed through the epoxy matrix (Figure 6.5e).[21] As has been discussed in Chapter 5 the formation of a Phthalcon particle network is sensitive in term of certain changes in processing and starting formulation. It is likely that the insulating bottom layer is caused by the (local) differences in particle-particle and particle-matrix interactions, viscosity, curing rate and/or the evaporation rate of *m*-cresol during cure.

6.3.5. log σ_v – φ Relation of Fluorinated Phthalcon/Epoxy Coatings

In general, the concentrations of fillers in polymer composites are calculated based on the amount of filler added with respect to the total volume of the final (cross-linked) composites. This only holds when the filler particles are homogeneously distributed through the matrix, and can only be applied to the non-fluorinated coatings discussed here (Figure 6.5e). Due to the existence of an insulating bottom layer, in our fluorine modified epoxy coatings, for the calculation of actual Phthalcon concentration only the region which contains nanoparticles should be taken into account. In this respect when same amount of Phthalcon is added, the actual Phthalcon concentration in the fluorinated coating is higher than in the non-fluorinated one. Also for the calculation of σ_v, only the actual Phthalcon layer thickness has to be considered (Equation 5.1).

The relation between σ_v and Phthalcon particle concentration φ is shown in Figure 6.6. This figure has been corrected for the existence of an insulating bottom layer (Table 6.6). Coatings made from 1.5 mol % and 4.3 mol % Jeffamine D230-F have a similar log σ_v – φ relation. Particle network analyses indicate that these networks have a very similar d_f value, which is close to the theoretical value for Diffusion Limited Cluster Aggregation (DLCA) (Table 6.5). When the amount of fluorine concentration in Jeffamine D230 further increases, the d_f value decreases, suggesting a relaxation of the DLCA formed network during processing. Furthermore, the influence of the highest fluorinated Jeffamine D230 concentration (20.0 mol %) on log σ_v – φ relation is much larger (Figure 6.6). Data suggest that for these coatings the φ_c is much lower

than the other three systems. The first three systems seem to have an almost equal φ_c.
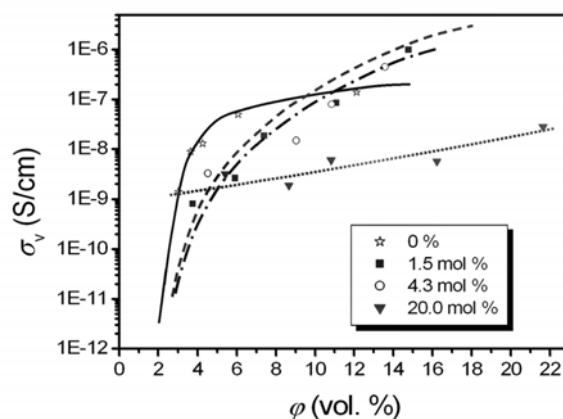
Figure 6.6. The log $\sigma_v - \varphi$ relation of Phthalcon/epoxy coatings containing different amounts of fluorinated Jeffamine D230 (curves are guides for the eye).

Table 6.6. Phthalcon particle layer thickness at various Jeffamine D230-F concentrations.[¤]

Jeffamine D230-F (mol %)	Total Coating Thickness (μm)	Particle Network Thickness (μm)	Actual Phthalcon particle concentration (vol. %)
1.5	72	59	3.7
4.3	101	63	4.8
14.2	73	40	5.5
20.0	81	43	5.7

[¤] All calculations were based on epoxy coatings made from 3 vol. % Phthalcon in the starting formulation. Coatings which were made from 12 vol. % Phthalcon in the starting formulation gave very similar results with respect to the ratio between particle network thickness and total coating thickness.

Hence, the use of a very small amount of fluorinated Jeffamine D230 not only lowers the surface energy of cross-linked coatings, but also has a strong influence on log σ_v - φ relation. Moreover, contrary to what has been observed in the surface energy, the influence of a high fluorinated Jeffamine D230 concentration (20.0 mol %) on log σ_v – φ is severe. Because with a Jeffamine D230-F concentration of 4.3 mol %, the fluorinated species have already covered the coating surface, we expect that at higher Jeffamine D230-F concentration, the amount of fluorinated species present below coating surface increases. Therefore, their influence on Phthalcon particle network

formation in the bulk of the matrix becomes larger as well.

Phthalcon 11/12 primary particles are highly crystalline nanosized flat plates with a low aspect ratio. The surface groups at the bottom and the top of the plate are -OH/ H_2O, $-NH_3/NH_2$ and -CN, whereas the surface groups at the sidewalls are phenyl rings. The phenyl and OH groups in *m*-cresol ensure very strong specific interactions between these particles and the dispersing medium, and the size of Phthalcon agglomerates is easily reduced to submicro-meter level. During processing, by increasing the temperature, the cross-linking reaction starts. The two epoxy groups of Epikote 828 and the amine groups of Jeffamine react with each other to form a three dimensional polymer network. Meanwhile, the solvent *m*-cresol which is also a catalyst for the cross-linking starts to evaporate.[20] Therefore, both the particle-matrix and the particle-particle interactions are subject to change. The consequences are that Phthalcon particles lose their stability and form a particle network through Brownian movement as long as the viscosity of the system is sufficiently low. It has been shown that the concentration at which particle network formation occurs in (pre)polymer nanocomposite depends on the effective Hamaker constant A_H^{eff} of the system.[21] When A_H^{eff} is large, network formation occurs at a lower (nano)filler concentration and material with a large A_H^{eff} is known to have a φ_c well below 1 vol. %.[19,21] When part of the Jeffamine D230 cross-linker is fluorinated and the amount is such that the fluorinated species are also present in the bulk of the coating, the value of A_H^{eff} increases further and an even lower φ_c is expected. The data presented in Figure 6.6 on coatings made from 20.0 mol % Jeffamine D230-F suggest that this is indeed the case.

The rheological measurements show that the rate of cross-linking slows down when fluorinated Jeffamine D230 is present in the starting formulation, depending on the amount of fluorine (Figure 6.3). This means that during cross-linking reaction, the increase in viscosity over time is slower than that of the fluorine-free coatings, and that the initially formed particle network may have more time to relax. That particle network formation can be very quick and probably occurs at the initial state of cross-linking has been discussed in Chapter 4.[25]

At higher filler concentrations, for coatings made from 20.0 mol % Jeffamine D230-F, the σ_v is considerably lower than that of the other three coating systems (Figure 6.6). This lowering is accompanied with a decrease in d_f. That particle network formed by

DLCA can undergo relaxation, resulting in a decrease in d_f value has already been reported.[38] It is likely that relaxation also occurred in our fluorinated Phthalcon/epoxy coatings. Phthalcon particle networks are sensitive to relaxation during cross-linking as has been found when other curing agents were used and this effect has been discussed in previous chapter.

It has been shown for cross-linked Phthalcon/epoxy coatings when the coating thickness becomes comparable or smaller to that of the ξ, the φ_c determined from four-point measurements becomes much higher; and at low φ (close to φ_c) the measured σ_v becomes lower than the actual σ_v value of the bulk.[20] Based on epoxy layer thickness and the ξ of the coatings made from 20.0 mol % Jeffamine D230-F, different σ_v and φ_c values between measured and bulk may be expected. However, it is suggested in Figure 6.6 that even for coating with the lowest Phthalcon concentration, the φ is still far away from the φ_c. Therefore, for all coatings in Figure 6.6 the log σ_v – φ relation describes to a large extend the bulk property of the matrix.

At higher Phthalcon filler concentrations, coatings made from low Jeffamine D230-F concentrations have higher σ_v as compared to coatings made from non-fluorinated Jeffamine D230, whereas coatings made from high fluorinated Jeffamine D230 concentrations have much lower σ_v values. Previous measurements show that for a 12 vol. % Phthalcon/epoxy coating cured with non-fluorinated Jeffamine D230 the Phthalcon particles really touch each other in the particle network.[22] This means that there is no matrix between particles in the network. These measurements also show that most of the conductive channels have a σ_v value between 3 x 10^{-5} - 2 x 10^{-4} S/cm.[22,32] Taking into account these values, the number of conducting contact points at the coating surface, as well as the uncertainty in the orientation of the particles in the network and/or at the surface, for highly filled cross-linked Phthalcon/epoxy coatings the expected σ_v values at room temperature are between 10^{-7} - 10^{-5} S/cm. Hence, the σ_v values of 5 x 10^{-7} - 1 x 10^{-6} S/cm observed in Figure 6.6 for coatings made from 1.5 mol % and 4.3 mol % fluorinated Jeffamine D230 are within this specification. For these coatings the increase in σ_v as compared to that of fluorine-free Jeffamine D230 coatings cannot be explained only by the difference in Phthalcon concentration. It is probably caused by a more favorable orientation or less contact problems of the Phthalcon particles in the network. The much lower σ_v values found for coatings made from 20.0 mol % Jeffamine D230-F are likely to be explained by the presence of polymer matrix between particles in the particle network after the

fractal network has been relaxed.

To our knowledge cross-linked semi-conductive low surface energy epoxy coatings have never been reported. Although in our study only Phthalcon 11/12 was used as semi-conductive filler, we expect that other semi-conductive spherical nanoparticles/polymer starting formulations with a high A_H^{eff} can also been used to make semi-conductive low surface energy coatings. Scouting experiments show that using a fluorinated surface active agent instead of the fluorinated Jeffamine D230 also lowers the surface energy of epoxy coatings. However, the influence on conductivity is much more complex and the interpretation of the results is hindered by reproducibility problems. Therefore, we expect that when other cross-linkers are used, the most likely route for success is to chemically bond them with fluorine and/or use partially fluorinated epoxy prepolymer. Our results presented here also show that to make semi-conductive low surface energy epoxy coatings, careful processing optimization is required to achieve the most attractive conductivity levels at low filler concentration, because the fractal nanoparticle network formation is very sensitive to small changes in viscosity build-up, (local) effective Hamaker constant, temperature and curing rate.

6.4. Conclusions

The route described here offers an interesting and straightforward way to obtain cross-linked semi-conductive low surface energy epoxy coatings by adding a small amount of fluorinated Jeffamine D230 cross-linker and semi-conductive Phthalcon 11/12 nanoparticles. The segregation of fluorinated species at the air/coating interface is confirmed by contact angle measurements and appears to be almost independent of the presence of Phthalcon particles.

The presence of fluorinated species strongly influences the conductivity and the fractal nanoparticle network structure of cross-linked Phthalcon/epoxy coatings. An insulating bottom layer was always observed. The actual Phthalcon particle containing layer decreases as the amount of fluorinated Jeffamine D230 increases. This has been visualized by optical microscopy on coating cross-sections. It is likely that the insulating bottom layer found in these coatings is caused by the (local) differences in particle-particle and particle-matrix interactions, viscosity, curing rate and/or the evaporation of solvent during cross-linking. We also found a decrease in

fractal dimension d_f of the particle network when the amount of fluorinated Jeffamine D230 increases. This is possibly caused by the relaxation of Phthalcon particle network as the cross-linking rate decreases when the amount of fluorinated Jeffamine D230 increases. Likely therefore the fractal Phthalcon particle network has more time to rearrange to form a more stable fractal particle network, which is accompanied with a decrease in percolation threshold φ_c. The lowering in φ_c can be explained by a further increase in the effective Hamaker constant as more fluorinated Jeffamine is present in the starting formulation.

Furthermore, we found a variation in the highest σ_v value when different amount of Jeffamine D230-F was used. When a small amount of fluorinated Jeffamine D230 is present (1.5 mol % and 4.3 mol %), the σ_v value is higher than in the non-fluorinated coatings. This difference can be explained by the differences in contact resistance between particles and/or the orientation of particles in the network. Nevertheless, for coatings made from higher fluorine concentration (20.0 mol %) the σ_v value is much lower. This is probably due to the presence of an insulating polymer matrix layer between particles in the network which is formed during relaxation.

Therefore, through a judicious choice of the fluorinated components, it is not only possible to control the surface energies of the final cured epoxy coatings, but also possible to control the conductivity levels of these materials.

References

1. Chan, C. M., *Polymer Surface Modification and Characterization*. Hanser Gardner: Munich, 1994.

2. Castner, D. G.; Grainger, D. W.; Eds., *Fluorinated Surfaces, Coatings and Films (ACS Symposium Series 787)*. American Chemical Society: 2001.

3. Hougham, G., *Fluoropolymers*. Kluwer Academic: 1999; Vol. 1 & 2.

4. Scheirs, J.; Ed., *Modern Fluoropolymers*. Wiley: New York, 1997.

5. Yoon, S. C.; Ratner, B. D. *Macromolecules* **1986,** 19, (4), 1068-1079.

6. Yoon, S. C.; Ratner, B. D. *Macromolecules* **1988,** 21, (8), 2392-2400.

7. Schmidt, D. L.; Coburn, C. E.; Dekoven, B. M.; Potter, G. E.; Meyers, G. F.; Fischer, D. A. *Nature* **1994,** 368, (6466), 39-41.

8. Thomas, R. R.; Anton, D. R.; Graham, W. F.; Darmon, M. J.; Sauer, B. B.; Stika, K. M.; Swartzfager, D. G. *Macromolecules* **1997,** 30, (10), 2883-2890.

9. Thomas, R. R.; Anton, D. R.; Graham, W. F.; Darmon, M. J.; Stika, K. M. *Macromolecules* **1998,** 31, (14), 4595-4604.

10. Ming, W.; Tian, M.; van de Grampel, R. D.; Melis, F.; Jia, X.; Loos, J.; van der Linde, R. *Macromolecules* **2002,** 35, (18), 6920-6929.

11. van Ravenstein, L.; Ming, W.; van de Grampel, R. D.; van der Linde, R.; de With, G.; Loontjens, T.; Thune, P. C.; Niemantsverdriet, J. W. *Macromolecules* **2004,** 37, (2), 408-413.

12. Funke, W. *J. Oil Colour Chem. As.* **1976,** 59, 398-403.

13. Carr, C.; Wallstom, E. *Prog. Org. Coat.* **1996,** 28, (3), 161-171.

14. Benjamin, S.; Carr, C.; Walbridge, D. J. *Prog. Org. Coat.* **1996,** 28, (3), 197-207.

15. Vink, P.; Bots, T. L. *Prog. Org. Coat.* **1996,** 28, (3), 173-181.

16. Skotheim, T. A.; Ed., *Handbook of Conducting Polymers, 2nd ed., Revised and Expanded*. Marcel Dekker: New York, 1997.

17. Karasek, L.; Sumita, M. *J. Mater. Sci.* **1996,** 31, (2), 281-289.

18. Brokken-Zijp, J. C. M.; Soloukhin, V. A.; Posthumus, W.; de With, G. *In Proceeding of 2003 Athens Conference on Coatings Science and Technology, Vouliagmeni, Greece*.

19. Soloukhin, V. A.; Brokken-Zijp, J. C. M.; de With, G. *J. Polym. Sci. B* **2007,** 45, (16), 2147-2160.

20. Chen, Z.; Brokken-Zijp, J. C. M.; Huinink, H. P.; Loos, J.; de With, G.; Michels, M. A. J. *Macromolecules* **2006,** 39, (18), 6115-6124.

21. Chen, Z.; Brokken-Zijp, J. C. M.; Michels, M. A. J. *J. Polym. Sci. B* **2006,** 44, (1), 33-47.

22. Huijbregts, L. J.; Brom, H. B.; Brokken-Zijp, J. C. M.; Kemerink, M.; Chen, Z.; de Goeje, M. P.; Yuan, M.; Michels, M. A. J. *J. Phys. Chem. B* **2006,** 110, (46), 23115-23122.

23. van de Grampel, R. D.; Ming, W.; van Gennip, W. J. H.; van der Velden, F.; Laven, J.; Niemantsverdriet, J. W.; van der Linde, R. *Polymer* **2005,** 46, (23), 10531-10537.

24. Brokken-Zijp, J. C. M.; van Mechelen, J. B.; Emeis, C. A.; Datema, K. P.; Kramer, A. H.; de Bruijn, D. P.; Meruma, A. J. *US Patent 05319009* **1993**.

25. Yuan, M.; Brokken-Zijp, J. C. M.; Huijbregts, L. J.; de With, G. *J. Polym. Sci. B* **2008,** 46, 1079-1093.

26. Brokken-Zijp, J. C. M.; Yuan, M.; et.al. *"Synthesis and Structure of Novel Aquocyanophthalocyaninato Co(III) Semi-conductor and Its Applications in Conductive Polymer Composites".* In Preparation.

27. Yuan, M.; Brokken-Zijp, J. C. M.; de With, G. *"Conductivity of Cross-linked Low Surface Energy Epoxy Coatings".* Submitted to J. Polym. Sci. B.

28. Owens, D. K.; Wendt, R. C. *J. Appl. Polym. Sci.* **1969,** 13, (8), 1741-1747.

29. Kwok, D. Y.; Neumann, A. W. *Adv. Colloid Interface Sci.* **1999,** 81, (3), 167-249.

30. Dean, J. A.; Ed., *Lange's Handbook of Chemistry, 15th ed.* McGraw-Hill Professional: New York, 1998.

31. Krevelen, D. W. V., *Properties of Polymers - Their Estimation and Correlation with Chemical Structure*. Elsevier: New York, 1989.

32. Huijbregts, L. J. *Charge Transport and Morphology in Nanofillers and Polymer Nanocomposites*. Ph.D. Thesis, Eindhoven University of Technology, Eindhoven, 2008.

33. Henry Lee, K. N., *Handbook of Epoxy Resins*. Mcgraw-Hill: Texas, 1981.

34. Mandelbrot, B. B., *The Fractal Geometry of Nature* W. H. Freeman: New York, 1983.

35. Schüth, F.; Sing, K. S. W.; Weitkamp, J.; Ed., *Handbook of Porous Solids*. Wiley-VCH: Weinheim, 2002; Vol. 1.

36. Stauffer, D.; Aharony, A., *Introduction to Percolation Theory, 2nd ed.* Taylor & Francis: London, 1992.

37. Shih, W. H.; Shih, W. Y.; Kim, S. I.; Liu, J.; Aksay, I. A. *Phys. Rev. A* **1990,** 42, (8), 4772-4779.

38. van Garderen, H. F.; Dokter, W. H.; Beelen, T. P. M.; van Santen, R. A.; Pantos, E.; Michels, M. A. J.; Hilbers, P. A. J. *J. Chem. Phys.* **1995,** 102, 480-496.

7

INFLUENCE OF DISPERSING SOLVENT AND POST-CURE ON THE CONDUCTIVITY OF CROSS-LINKED PHTHALCON/EPOXY NANOCOMPOSITES⊛

SYNOPSIS

The influence of post-cure and dispersing solvents on the conductivity of semi-conductive epoxy coatings has been investigated. It has been shown that the relation between the volume conductivity σ_v and the filler amount φ and the ultimate fractal Phthalcon particle network structure depend on the presence/absence of post-cure treatment and the chosen dispersing solvent.

Our results show that the conductive nanoparticle network structure is very sensitive to the chosen processing conditions. Only within a small processing window, which is very specific for each chosen starting formulation, semi-conductive Phthalcon/thermoset materials can be realized at low filler concentration by forming a continuous fractal Phthalcon particle network throughout the polymer matrix.

⊛ The content of this chapter will be submitted as an article: Yuan, M.; Brokken-Zijp, J. C. M.; de With, G. "*Influence of Dispersing Solvent and Post-cure on the Conductivity of Epoxy Nanocomposites*".

7.1. Introduction

The morphology of conductive particle network after processing plays an important role in the conductivity of a nanocomposite, because it influences the charge transport in the particle network. The morphology may comprise a complex arrangement of particle aggregates/networks with different size and shape distributions. Unfortunately, the factors which account for the morphology and/or to what extent they influence the final conductive particle network structures are complicated. It is generally accepted that the properties of the conductive particles, such as size, aspect ratio and surface groups, the aggregate/agglomerate structure of the conductive filler particles in the polymer matrix before/during/after processing and the interfacial energy between matrix and filler particle determine the morphology of particle network. Therefore, these factors are expected to have large influences on the electrical property of the composites.

Apart from the above mentioned factors, it has been shown in Chapter 5 that the initial viscosity, viscosity changes during cross-linking, the rate of cross-linking, the chosen cross-linker and the evaporation rate of the solvent have large influences on the morphology of particle network in thermoset nanocomposites, even when the effective Hamaker constant A_H^{eff} is very similar. All cross-linked Phthalcon/epoxy materials discussed before were post-cured at 120 ^{o}C under vacuum. Generally, post-cure at elevated temperature is necessary to obtain an extensive cross-linking;[1] it may, therefore, affect the final physical properties of the epoxy coatings and the ultimate morphology of Phthalcon particle networks in the epoxy layers. In order to achieve an optimum electrical conductivity in Phthalcon/epoxy coatings, it is necessary to understand these post-cure effects. Hence, in this chapter the influence of post-cure on the morphology of Phthalcon particle networks and the conductivity of cross-linked epoxy coatings are addressed.

In a very well-dispersed Phthalcon dispersion, during cure of a Phthalcon/*m*-cresol/Epikote 828/amine cross-linker starting formulation the Phthalcon particles lose their colloidal stability due to the cross-linking reaction and the evaporation of dispersing solvent. These stimulate the Phthalcon particle network formation as long as the Brownian movement is large enough and the viscosity of the system is sufficiently low. To obtain a conductive polymer composite a continuous particle network must be formed before gelation. When the viscosity of the coating formulation increases too slowly, the particle network might relax (Chapter 5),

leading to a particle network with a less attractive conductivity level. Therefore, it is important to carefully choose the processing window to obtain an optimum log σ_v - φ relation. It is well-known that the presence of proton donating species can act as catalyst in the cross-linking reaction between amine cross-linker and epoxy prepolymer by facilitating the ring opening process.[1] In this chapter the influence of proton donating catalyst on Phthalcon particle network structure/distribution and σ_v are discussed as well.

As has been shown before that the low percolation threshold φ_c of the cross-linked Phthalcon/epoxy coatings is caused by the fractal nature of Phthalcon particle networks formed through particle-particle and particle-matrix interactions.[2,3] To obtain a fractal structure, the presence of well-dispersed Phthalcon particles in the starting epoxy formulation is essential. In the past, *m*-cresol was chosen as dispersing medium. Phthalcon particles can be well-separated in *m*-cresol, but from the safety point of view, *m*-cresol is toxic in contact with skin and may cause serious burns. Therefore, a much safer and friendlier dispersing solvent will, definitely, make Phthalcon/polymer matrix composites more attractive for practical applications. Based on this, two different solvents with low safety risks were used as dispersing media. The influences of these solvents on Phthalcon particle network structures, as well as the σ_v of final cross-linked Phthalcon/epoxy coatings are investigated.

7.2. Experimental

7.2.1. Materials

Phthalcon 11/12 was synthesized in high purity and yield using a two-step reaction as described before.[4-6] The primary Phthalcon particle size used here is about 250 nm in length and width and about 50 nm in thickness. The Phthalcon powder was always carefully dried at 80 $^\circ$C for 48 h under vacuum (~ 0.01 mbar) and ground into fine powder in a mortar before use.

Epoxy prepolymer (Epikote 828) was purchased from Resolution Nederland BV. The amine cross-linker Jeffamine D230 was purchased from Huntsman BV, Belgium. Isophorone-diamine (IPD, $\geq$ 99.0 %, GC) was purchased from Fluka. *m*-cresol (spectrophotometric grade) was purchased from Merck. The solvents used to replace *m*-cresol are propylene glycol diacetate (PGDA, $\geq$ 99.7 %) and 1-phenoxy-2-propanol (DOWANOL PPh, $\geq$ 93 %). They were both purchased from Aldrich. In some cases

2,4,6-Tris(dimethylaminomethyl)phenol (DMP 30, ≥ 95 %, Aldrich) was used as catalyst instead of *m*-cresol. The chemical structures of these compounds are shown in Scheme 7.1. All materials were used as received.

Propylene glycol diacetate (PGDA)

1-Phenoxy-2-propanol (DOWANOL PPh)

2,4,6-Tris(dimethylaminomethyl)phenol (DMP 30)
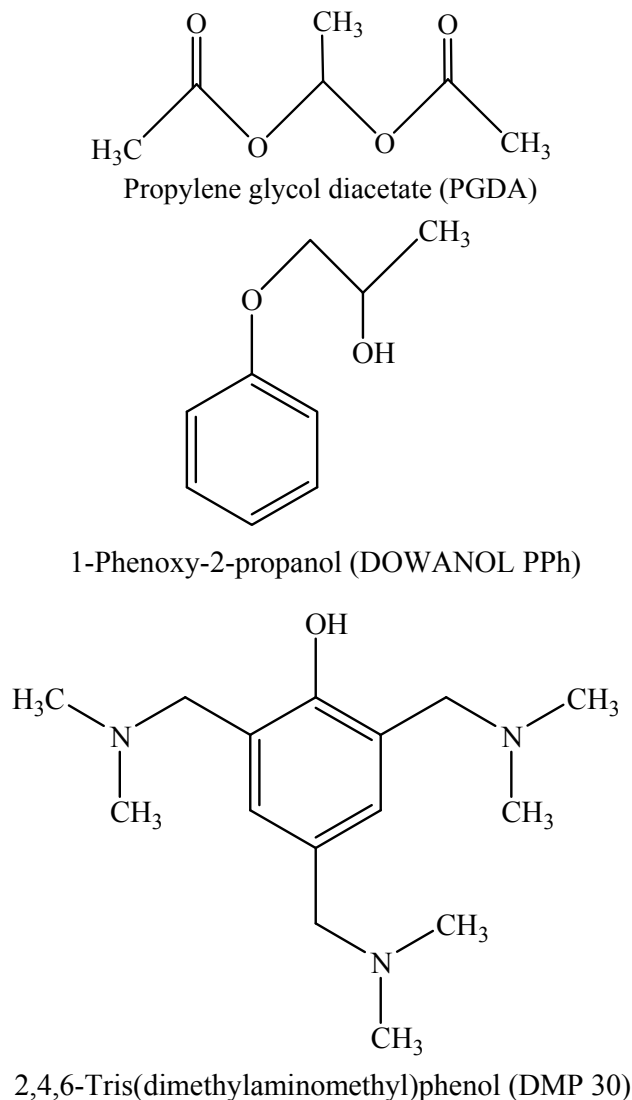
Scheme 7.1. Chemical structures of the compounds used.

7.2.2. Coating Preparation

To study the post-cure effects, the cross-linked Phthalcon/epoxy coatings were prepared starting from a dispersion of Phthalcon particles in *m*-cresol, which was magnetically (1 h) and later on ultrasonically (1 h) mixed. To this dispersion Epikote 828 and Jeffamine D230 (or IPD) were added (the NH/epoxy molar ratio was 1/1). This mixture was magnetically stirred for 5 min, ultrasonically degassed for 5 min, and then casted on a polycarbonate substrate using a doctor blade applicator with an

opening of 120 μm. Next it was cured at 100 ^{o}C under vacuum (~ 0.01 mbar) for 4 h. Sometimes the above prepared coatings were also post-cured at 120 ^{o}C under vacuum (~ 0.01 mbar) for 8 h.

To investigate the influence of *m*-cresol, Phthalcon dispersions containing various amounts of *m*-cresol were prepared using the same method as described before. All coatings studied here were first cured at 100 ^{o}C under vacuum (~ 0.01 mbar) for 4 h and later post-cured at 120 ^{o}C under vacuum (~ 0.01 mbar) for 8 h.

To check the possibility of replacing *m*-cresol by other solvents, propylene glycol diacetate (PGDA) and 1-phenoxy-2-propanol (DOWANOL PPh) were used. The Phthalcon dispersion was also prepared under magnetic (1 h) and ultrasonic (1 h) mixing. To this dispersion, 20 wt. % *m*-cresol or DPM 30 (based on the total amount of the coating components) was added as catalyst to facilitate the cross-linking reaction. This mixture was then magnetically stirred for 5 min, ultrasonically degassed for 5 min and casted on a polycarbonate substrate using a doctor blade applicator with an opening of 120 μm. Next it was cured at 100 ^{o}C under vacuum (~ 0.01 mbar) for 4 h and later post-cured at 120 ^{o}C under vacuum (~ 0.01 mbar) for 8 h.

Under the above described conditions smooth coatings with layer thicknesses between 60 and 80 μm were always obtained. The volume concentration of Phthalcon particles in the final cross-linked epoxy coatings was determined based on the total composition of the composites after cross-linking by taking into account the densities of Phthalcon particle and cross-linked epoxy as 1.65 and 1.00 g/cm^3, respectively.

7.2.3. Characterization

DC Volume Conductivity σ_v The DC volume conductivity σ_v at room temperature was measured using a standard four-point method, with a Keithley 237 high voltage source measuring unit and a Keithley 6517A high voltage electrometer. The former unit supplies a constant current through the coating between the two outside electrodes and the latter unit measures the voltage difference between the two inside electrodes. The measurements were carried out on the surface of the coating sample according to standard ASTM D991 and instructions of Keithley "low conductivity level measurements". Silver paint (silver conductive adhesive 416, electron microscopy sciences, USA) was used to ensure good contact between the sample surface and the measuring electrodes. Coatings used in the conductivity

measurements had a thickness between 60 and 80 μm as determined using a digital screw micrometer caliper. The presented σ_v values are average values of at least three coatings measured at three different positions.

Optical Microscopy (OM) The morphology of the particle network in the materials before and after cross-linking was observed with OM (Reichert-Jung Polyvar-Met) using the transmission bright-field technique. These images were later converted into binary images and analyzed using the tiling method to obtain the fractal dimensions d_f and the correlation lengths ξ of the particle networks.[2] The obtained d_f and ξ values are average values of at least three calculations by varying the size of the tiles. The Phthalcon particle dispersions studied here were prepared by bringing a small amount of dispersion between two glass slides. The post-cured or non-post-cured Phthalcon/epoxy coatings were studied directly under the OM. The thickness of these coatings was about 10 μm to facilitate the observation of the Phthalcon particle networks.

Surface Energy The surface energies of the liquid samples were determined at 20 °C by Wilhelmy plate method using a Krüss Digital Tensionmeter K10T.[7,8] During the measurement, the plate was moved towards the surface until it reached the meniscus. The surface energy was calculated from the measured force. The measured surface energies of the coating components and composites are shown in Table 7.1. The presented values are average values of three measurements on each sample.

Table 7.1. Surface energies of various coating components and compositions.

	Surface Energy (mN/m)	
	20 °C	100 °C[9]
Phthalcon 11/12	> 50	> 50
Jeffamine D230	33.1	23.0
Epikote 828	46.0	36.7
m-cresol	38.2	29.0
PGDA	16.9	
PPh	37.2	
Jeffamine D230/Epikote 828 (1/3, w/w)	40.5	31.4

Rheological Measurements Rheological measurements were performed to follow the viscosity changes during cure using an AR1000 rheometer with 20 mm plate-plate geometry. The coating starting formulation was directly added to the plate, and then the gap between plates was set to be 300 μm. At the beginning of the measurement (t = 0 s), the plates were heated from room temperature to 100 ^{o}C within 30 sec. All measurements were done under N_2 flow.

7.3. Results and Discussion

7.3.1. Influence of Post-cure on the σ_v of Cross-linked Phthalcon/Epoxy Coatings

In previous chapters, the log σ_v - φ relations and Phthalcon particle network structures presented on Phthalcon/epoxy composites were obtained on coatings which were post-cured at 120 ^{o}C. To check the influence of post-cure on the σ_v of epoxy coatings, coatings containing 12 vol. % Phthalcon 11/12 were cross-linked with Jeffamine D230. These coatings were only cured at 100 ^{o}C in vacuum (~ 0.01 mbar) for 4 h without further post-cure. The σ_v obtained from standard four-point measurements show that these coatings reach a σ_v of 4.2 x 10^{-11} S/cm. Compare to a post-cured coating containing the same amount of Phthalcon particles, the σ_v of the non-post-cured coating is a factor of 10^3 lower.[2,3,6,10,11]

The σ_v of a polymer nanocomposite containing semi-conductive particles depends on the morphology of the particle network through the polymer matrix. It has been shown earlier that the presence of a Phthalcon nanoparticle network in a cross-linked epoxy matrix can be easily observed under the OM due to the fractal nature of the particle network.[2] Therefore, the Phthalcon particle networks in epoxy coatings made with/without post-cure were also studied with the OM (Figure 7.1). Both coatings in Figure 7.1 were prepared, apart from the absence/presence of post-cure, using the same processing methods, processing conditions and starting formulations.

Figure 7.1 shows that the Phthalcon particle networks in both coatings have very similar structures, although the particle network after post-cure looks a bit denser. In order to study the structures of these networks in more detail, the fractal dimensions d_f of the particle networks were determined using the method of tiling as described before.[2,12,13] The results are summarized in Table 7.2. The fractal structure analyses reveal that within the uncertainty of measurements the d_f value of post-cured coating is equal to the one obtained from non-post-cured coating; these values are also close

to the theoretical value of $d_f = 1.75$ predicted for a particle network formed by Diffusion Limited Cluster Aggregation (DLCA)[14-17] and suggest that the Phthalcon particle networks in both coatings are formed by this mechanism.
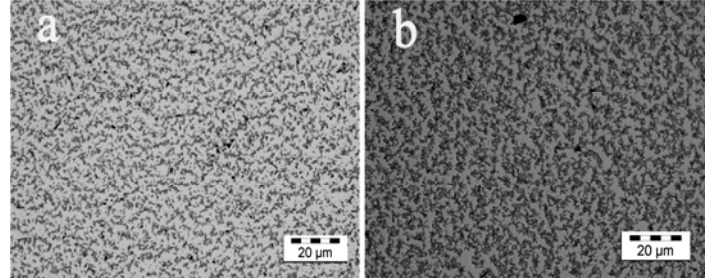
Figure 7.1. OM images of Phthalcon particle networks in Epikote 828/Jeffamine D230 coatings. (a) cured at 100 °C without post-cure; (b) cured at 100 °C and post-cured at 120 °C. Both coatings contained 3 vol. % Phthalcon in the starting formulations.

Table 7.2. Phthalcon particle network structures.[#]

Cross-linker	Curing T (°C)	Post-curing T (°C)	d_f	ξ (μm)	σ_v (S/cm)
Jeffamine D230	100	-	1.79	20	4.2×10^{-11}
Jeffamine D230	100	120	1.75	20	1.0×10^{-7}
IPD	50	-	1.81	20	3.7×10^{-11}
IPD	50	120	1.72	20	1.0×10^{-7}
IPD	60	-	1.70	30	1.8×10^{-11}
IPD	60	120	1.62	40	1.0×10^{-8}
IPD	80	-	1.60	30	1.0×10^{-11}
IPD	80	120	1.51	50	7.0×10^{-9}

[#] All coatings contained 3 vol. % Phthalcon particles in the starting formulations.

In post-cured coatings a critical exponent $t \approx 2$ in Equation (2.1) was observed.[2,3,6,11] This suggests that the Phthalcon particle network is formed by random percolation and that all bonds in the network have the same conductance. Assuming that $t \approx 2$ still holds and that the loops, isolated aggregates, dangling chains and backbone structures do not change in Phthalcon particle networks before post-cure, Equation (7.1) can be used to relate the σ_v of the composite to the fractal particle network structure:[2]

$$\sigma_v \propto \frac{a^{1+x}}{R_f} \xi^{-(2+x)} \tag{7.1}$$

where R_f is the resistance of one particle aggregate plus the resistance between two contacting particle aggregates, a is the radius of a primary particle aggregate, ξ is the correlation length from which the particle network is formed and x is a constant with a value between 0 and 0.4.

Equation (7.1) assumes that the σ_v of a polymer composite is related to the fractal morphology of particle network and R_f. Supposing that x is equal for all coatings with/without post-cure due to the fact that the particle network structures in both coatings are very similar, we may conclude that the σ_v value only relies on R_f, or to be more precise, the value of σ_v only depends on the contact resistance R_c since the resistance of one particle aggregate is constant. Hence, the difference in σ_v between non-post-cured and post-cured coatings may be explained by a difference in the amount of insulating polymer matrix between contacting aggregates.

It has been shown before that Phthalcon particles really touch each other in a post-cured 12 vol. % Phthalcon/Jeffamine D230/Epikote 828 coating.[18,19] Combine this with the conductivity measurements, the actual σ_v values obtained also suggest that before post-cure treatment there is insulating material present between Phthalcon particles in the network.

During cross-linking the initially stabilized Phthalcon/*m*-cresol dispersion starts to lose its colloidal stability due to the increased particle-particle interactions and also due to the evaporation of *m*-cresol. In Chapters 4 and 5 it has been shown that the Phthalcon particle network is formed at the early stage of cross-linking reaction and that the particle network formation is fast.[2,6] It is generally accepted that at the gel point the degree of cross-linking reaction is about 70 %; and that because of the lower degree of cross-linking, non-post-cured epoxy normally shows a lower T_g.[20] Therefore, it is likely that due to the fast particle network formation the remaining *m*-cresol (boiling point 203 $^{\circ}$C), non-cured matrix components and/or partially cured epoxy matrix are trapped in Phthalcon particle network. The presence of such insulating components tremendously increases the contact resistance between Phthalcon particle aggregates and limits the charge transport in the particle network even when the insulating layer is only several Ångstrom thick. As a result, a much lower σ_v value is

obtained.

During post-cure, the temperature further increases; this helps to minimize non-cured or partially cured matrix components and release the remaining solvent. Meanwhile, due to the increased temperature the local motion of Phthalcon particle network increases. These all favour closer contact between Phthalcon particles in the backbone of the network. Therefore, the contact resistance between Phthalcon particle aggregates in the network decreases and the σ_v increases.

To confirm our proposed mechanism, 12 vol. % Phthalcon/epoxy coatings cross-linked with IPD and cured at different temperatures with/without post-cure were prepared. Because it has been shown in Chapter 5 that in IPD cross-linked coatings the Phthalcon particle network structure is very sensitive to the curing temperature and at certain curing temperatures relaxation occurs in these networks, we expect that the influence of post-cure on σ_v and Phthalcon particle network structure will be more severe in these coatings.

The σ_v values measured on these IPD cross-linked coatings are showed in Figure 7.2. These coatings show a similar post-cure effect on the σ_v as those observed in coatings cross-linked with Jeffamine D230. All non-post-cured coatings have a σ_v around 10^{-11} S/cm; after post-cure the σ_v improves, although the extent of increase in σ_v is somewhat different, depending on the chosen curing temperature.
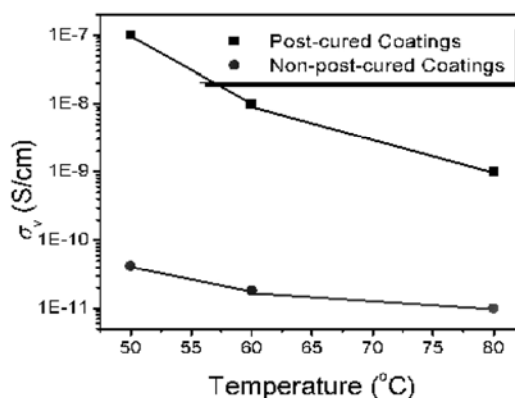
Figure 7.2. The σ_v of coatings cross-linked with IPD with/without post-cure after curing at the temperature indicated. All coatings contained 12 vol. % Phthalcon in the starting formulations. The post-cure was performed in vacuum (~ 0.01 mbar) at 120 °C for 8 h. The lines indicated are a guide to the eye only.
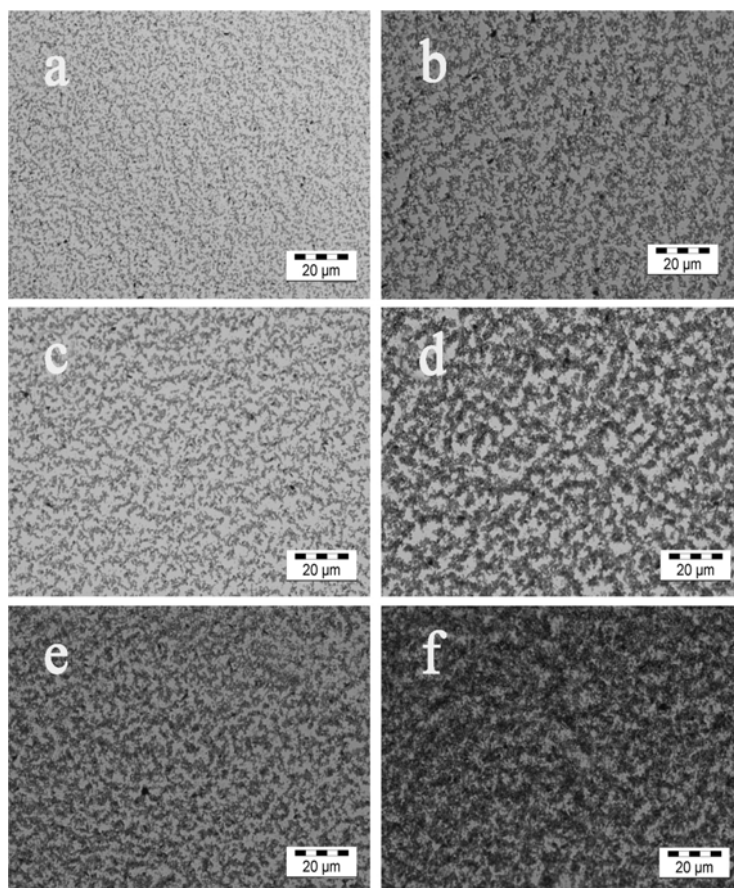
Figure 7.3. OM images of Phthalcon particle networks in Epikote 828/IPD coatings. (a) cured at 50 °C; (b) cured at 50 °C and post-cured at 120 °C; (c) cured at 60 °C; (d) cured at 60 °C and post-cured at 120 °C; (e) cured at 80 °C; (f) cured at 80 °C and post-cured at 120 °C. All coatings contained 3 vol. % Phthalcon.

The OM images of Phthalcon particle networks before and after post-cure in cross-linked Epikote828/IPD coatings are shown in Figure 7.3. Figure 7.3 clearly indicates that although coatings were cured at different temperatures, the Phthalcon particle network structures in non-post-cured coatings are more ramified, while the network structures in post-cured coatings look much denser and coarser. These differences can be explained by the increase in temperature during post-cure which may lead to a local motion of Phthalcon particle network. Results from fractal structure analyses (Table 7.2) suggest that this is indeed the case because a decrease in d_f was always observed in the post-cured coatings with respect to the non-post-cured ones. This decrease in d_f corresponds to a local relaxation of Phthalcon particle network.[21] The d_f values of the non-post-cured coatings obtained at different initial curing temperatures suggest that Phthalcon particle networks partially relax even before post-cure.

However, for coatings cross-linked with Jeffamine D230, within the uncertainty of measurements the d_f values before and after post-cure are equal and correspond to a non-relaxed particle network formed by DLCA. This difference in relaxation behaviour is related to an earlier observation discussed in chapter 5, in which we conclude that IPD cross-linked coatings are more sensitive to relaxation because the initially formed Phthalcon particle network structures ($t \geq 3$) are different from the ones formed in Jeffamine D230 cross-linked coatings ($t \approx 2$). Due to the different Phthalcon particle network structures, Equation (7.1) cannot be applied to explain the variations in σ_v observed in non-post-cured and post-cured IPD cross-linked epoxy coatings. Nevertheless, it is very likely that the increase in σ_v after post-cure is caused, to a large extent, by the presence of less insulating material between particles in the network, which may be non-cured and/or partially cured polymer matrix material. Hence, the charge transport between Phthalcon particle aggregates in the network enhances. The σ_v of IPD cross-linked coating cured at 50 $^\circ$C even reaches a value of 10^{-7} S/cm after post-cure, similar to the one obtained from Jeffamine D230 cross-linked coating cured at 100 $^\circ$C. This suggests that in this coating Phthalcon particles also touch each other and that no matrix is present between particles in the network.[18,19]

The IPD cured coatings nicely confirm the post-cure effects observed in Jeffamine D230 cured coatings, the occurrence of relaxation of the Phthalcon particle network and the dependency of this relaxation on curing temperature (viscosity changes) and chosen cross-linker.

7.3.2. Influence of *m*-cresol on Particle Network Formation and σ_v

In the past, *m*-cresol was always used in our starting formulations to make cross-linked Phthalcon/epoxy coatings. Besides acting as a good dispersing medium, it is well-known that *m*-cresol enhances the cross-linking reaction.[1] This catalytic effect is confirmed by rheological experiments (Figure 7.4). One of the coating formulations used in these experiments contained *m*-cresol and the other one did not. In the latter formulation Phthalcon particles were dispersed directly in Jeffamine D230 and a gel point of 935 s was found. This value is a factor of 6 higher than for the other formulation. The much earlier occurrence of gel point in the presence of *m*-cresol can be explained by its catalytic effect, which is known to act as a proton-donating agent in primary amine/epoxy cross-linking reaction due to its weak acidity (Scheme 7.2).[1]
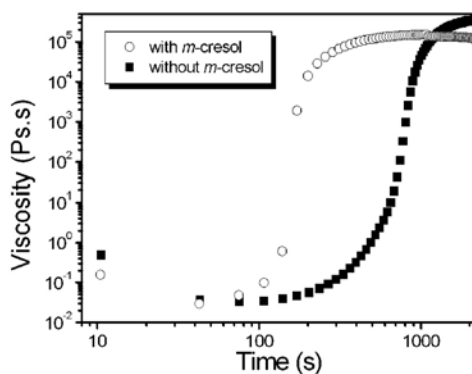
Figure 7.4. viscosity changes during cure of 3 vol. % Phthalcon/Jeffamine D230/Epikote 828 coatings with/without the presence of *m*-cresol. Both formulations were cured at 100 °C.
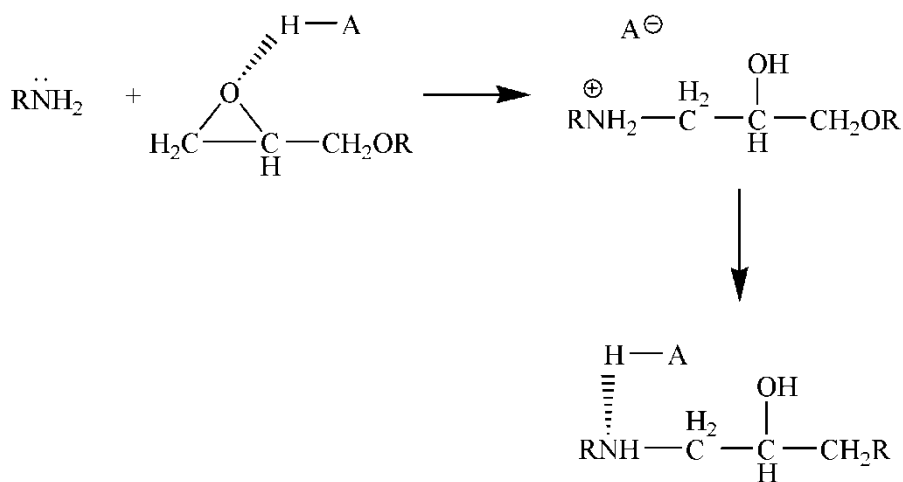

Scheme 7.2. Catalystic effect of proton donating species.[1]

In cross-linked epoxy coatings made in the absence of *m*-cresol, fractal particle networks were also observed. However, the σ_v of these layers could not be measured with standard four-point measurements even when the Phthalcon concentration was as high as 12 vol. %, because a thin insulating top layer was always formed.[3] Apparently, the large fractal Phthalcon particle aggregates/networks present before/during cross-linking and the long gel time stimulate the sedimentation of particle network during cross-linking.[3]

The time at which gelation occurs can also be altered by the amount of *m*-cresol present in the starting formulation. This was studied in more detail for epoxy layers cross-linked with Jeffamine D230 made from Phthalcon dispersions containing various amount of *m*-cresol. Figure 7.5 shows the changes in viscosity during cross-linking of these coating formulations. Taking the moment when the tangent of the loss

145

angle (tan δ) reaches 1 as the gel point, the results show that when the mass ratio between matrix/*m*-cresol is ≤ 5/8, a similar gel point was found (161 s); above this ratio a further increase in gel point was observed (289 s, matrix/*m*-cresol = 1/3). This observed increase in gel point is understandable because the presence of more solvent brings down the total viscosity, and a longer time is required to evaporate the solvent, resulting in a retardation of gel time.
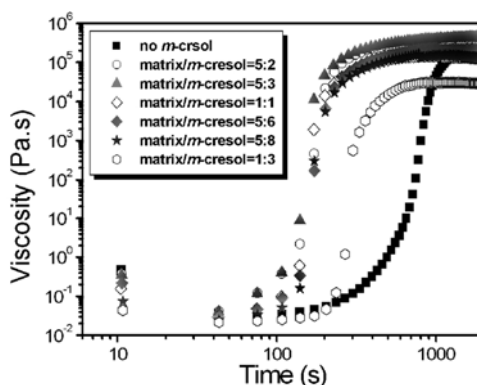

Figure 7.5. Changes in viscosity during cross-linking of 3 vol. % Phthalcon/Epikote 828/Jeffamine D230. The amount of *m*-cresol present in the starting formulation was varied and the curing temperature was 100 °C. The ratios indicated are mass ratio between epoxy matrix and *m*-cresol.

The σ_v values of coatings made from starting formulations containing 12 vol. % Phthalcon and different amount of *m*-cresol were also measured. These coatings, apart from the amount of *m*-cresol present in the starting formulation, were all prepared under the same processing conditions, cured at 100 °C and later post-cured at 120 °C. For coatings made from matrix/*m*-cresol = 1/3 the σ_v reaches a value of 5 x 10^{-9} S/cm; while the σ_v values of coatings made from starting dispersions with a matrix/*m*-cresol mass ratio ≤ 5/8 are very similar, a σ_v value of 1 x 10^{-7} S/cm was always obtained (in a standard coating preparation matrix/*m*-cresol mass ratio = 1/1 was used).

The OM images of these coatings are shown in Figure 7.6. At the matrix/*m*-cresol = 1/3, a denser particle network was observed as compared to the one obtained from a standard starting formulation. These results suggest that during cross-linking relaxation of Phthalcon particle network occurs as was shown earlier for coatings using Jeffamine D230, Jeffamine D400, Jeffamine D2000, IPD or DDM as cross-linkers (Chapter 5). Likely the low initial viscosity and the slow increase in viscosity

over time facilitate the relaxation of initially formed Phthalcon particle network when a matrix/*m*-cresol ratio of 1/3 was chosen. Therefore a denser network was observed accompanied with a decreased d_f and an increased ξ.[2,10,11,21]
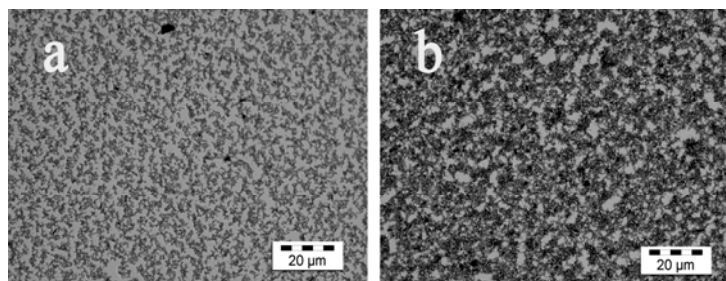
Figure 7.6. OM images of Phthalcon particle networks in cross-linked Jeffamine D230/Epikote 828 coatings cured at 100 °C and post-cured at 120 °C. (a) epoxy/*m*-cresol matrix mass ratio = 1/1; (b) epoxy/*m*-cresol matrix mass ratio = 1/3. Both coatings contained 3 vol. % Phthalcon in the starting formulations.

As shown in equation (7.1), the σ_v value may be related to the particle network structure ξ and the contact resistance R_c between two particle aggregates. During relaxation of particle network a more stable particle network is formed, but this may at the expense of more polymer matrix between particles in the network and/or changes in the backbone of the particle network. Hence, the contact resistance between particles increases and the σ_v decreases. Furthermore, relaxation also lowers the σ_v value.

7.3.3. Influence of Other Dispersing Solvent on Particle Network and σ_v

The formation of a continuous Phthalcon particle network in the cross-linked polymer is, apart from the curing conditions (with/without post-cure), the amount of *m*-cresol present in the starting formulation, the curing temperature, the curing rate and the choice of cross-linker,[11] also influenced by the initial particle dispersion in the composite mixture before cross-linking.[3] The initial particle structure in the dispersing medium influences the final particle network formation, network structure and the aggregation/agglomeration of the particles during cure. The particle-dispersing medium and particle-particle interactions may determine this initial Phthalcon particle structure. Furthermore, to prevent the sedimentation of particle network during cross-linking, in thermally cured epoxy coatings the use of Phthalcon dispersions containing well-dispersed particles/aggregates is essential.[3]

Although the use of *m*-cresol ensures a starting formulation of well-dispersed Phthalcon particles before cure and a continuous particle network formed at a low φ_c after cure, from safety point of view replacing *m*-cresol with much safer and environmentally friendlier dispersing solvents will make Phthalcon/polymer matrix composites more attractive in practice. Therefore, the commercially available solvents propylene glycol diacetate (PGDA) and 1-phenoxy-2-propanol (DOWANOL PPh) with low safety risks were used as dispersing media to prepare cross-linked Phthalcon/epoxy coatings.

Phthalcon/PGDA and Phthalcon/PPh dispersions were prepared using the same dispersing procedure as for Phthalcon/*m*-cresol dispersions. When strongly agglomerated Phthalcon powder was dispersed in *m*-cresol no particle aggregate/agglomerate structures were visible under the OM even at the highest magnifications.[3] When Phthalcon powder was dispersed in PGDA or PPh, a completely different picture was observed which strongly indicates an agglomerate/aggregate structure (Figure 7.7). In Phthalcon/PGDA dispersion much larger Phthalcon aggregates/agglomerates were observed than in PPh dispersion.
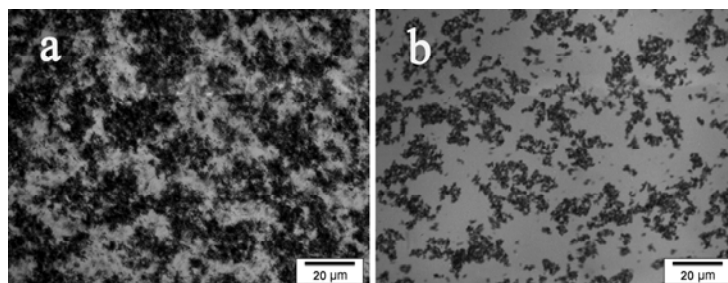
Figure 7.7. OM images of Phthalcon particle aggregates/agglomerates in different dispersing solvents. (a) Phthalcon/PGDA dispersion; (b) Phthalcon/PPh dispersion. Both dispersions contained 3 vol. % Phthalcon.

When the tiling method was used to determine the fractal dimensions d_f of these Phthalcon particle structures in the dispersions, we found that the particle network structure obtained in Phthalcon/PGDA dispersion is less fractal ($d_f = 1.85$), whereas in PPh dispersion Phthalcon particle aggregates are fractal with a d_f value of 1.64 (Table 7.3). Apparently, the chosen dispersing conditions and/or the particle-medium interactions are too weak to break down the large Phthalcon particle agglomerates in PGDA. Because of the less fractal Phthalcon particle structure observed in PGDA

dispersions, we only focuse on Phthalcon/epoxy coatings using PPh as dispersing medium.

Table 7.3. Phthalcon particle network structures.[#][*]

	d_f	$\xi\,(\mu m)$
Phthalcon/PGDA dispersion	1.85	60
Phthalcon/PPh dispersion	1.64	35
Phthalcon/PPh/Jeffamine D230/Epikote 828 dispersion	1.58	30
Phthalcon/PPh/Jeffamine D230/Epikote 828 coating	1.82	50
Phthalcon/PPh/*m*-cresol/Jeffamine D230/Epikote 828 coating	1.60	35
Phthalcon/ *m*-cresol/Jeffamine D400/Epikote 828 coating	1.61	30
Phthalcon/ *m*-cresol/Jeffamine D2000/Epikote 828 coating	1.55	40

[#] All dispersions contained 3 vol. % Phthalcon particles based on the total volume of the dispersing solvent. When presented 20 wt. % *m*-cresol was added with respect to the dispersing medium.

[*] All coatings contained 3 vol. % Phthalcon particles based on the total volume of the epoxy coating components. When presented 20 wt. % *m*-cresol was added with respect to the dispersing medium.
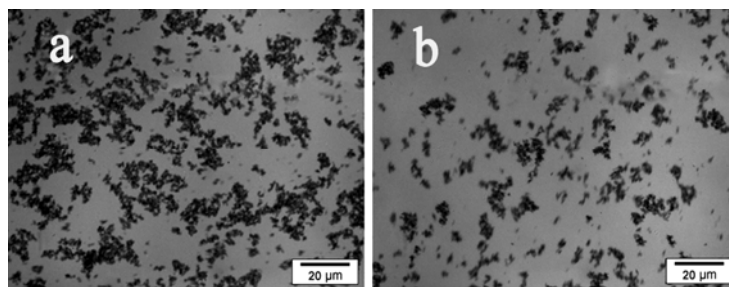
Figure 7.8. OM images of Phthalcon particle aggregates/agglomerates in the starting dispersions. (a) Phthalcon/PPh dispersion; (b) Phthalcon/PPh/Jeffamine D230/Epikote 828 dispersion. Both dispersions contained 3 vol. % Phthalcon.

To make a cross-linked polymer matrix, epoxy prepolymer Epikote 828 and amine cross-linker Jeffamine D230 have to be added to Phthalcon/PPh dispersions. This addition may alter the Phthalcon particle structure because of the changes in particle-dispersing medium and/or the particle-particle interactions as discussed in previous chapters. Figure 7.8 & Table 7.3 show that the addition of coating components

Jeffamine D230 and Epikote 828 slightly lowers the fractal dimension and correlation length of the Phthalcon particle aggregates. The effect of the addition of Jeffamine D230 and Epikote 828 may be explained by a decrease in surface energy difference between Phthalcon particles and matrix components surrounding the particles (Table 7.1). These data suggest a reduction in the effective Hamaker constant A_H^{eff}, and therefore a decrease in particle-particle attraction energy in this medium. However, it is not clear whether the addition of Jeffamine D230 increases the specific interactions between surface groups of Phthalcon (mainly -OH and -CN groups) and medium (mainly -NH$_2$ groups).
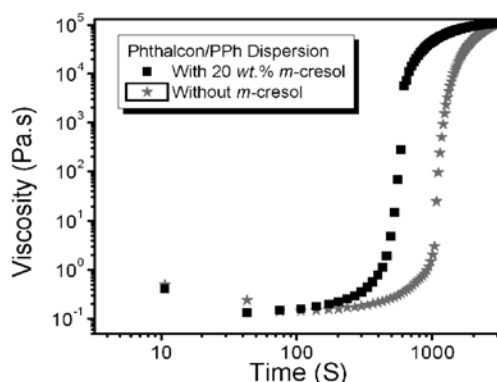
Figure 7.9. Changes in viscosity during cross-linking of Phthalcon/PPh/Jeffamine D230/Epikote 828 coatings with and without the presence of *m*-cresol. The concentration of Phthalcon was 3 vol. % and the curing temperature was 100 ^{o}C.
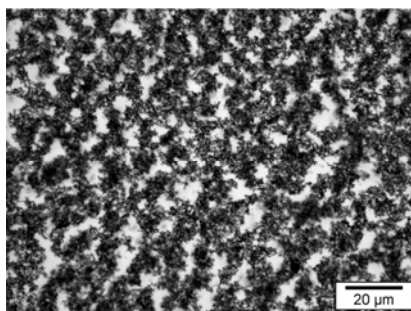
Figure 7.10. OM images of Phthalcon particle network structure in Jeffamine D230/Epikote 828 coating made from Phthalcon/PPh dispersion. The coating contained 3 vol. % Phthalcon, the coating formulation was cured at 100 ^{o}C and later post-cured at 120 ^{o}C.

By increasing the curing temperature to 100 ^{o}C the cross-linking reaction starts, meanwhile the solvent begins to evaporate. Consequently the specific interactions between surface groups of Phthalcon and active groups in the solvent become weaker.

Therefore, particle-particle interactions become dominant and particles tend to aggregate as long as the Brownian movement is sufficiently large and the viscosity of the system is sufficiently low. The viscosity changes over time during cure of Jeffamine D230 cross-linked coatings are shown in Figure 7.9. It clearly indicates a very slow change in viscosity over time in coating formulation made from PPh dispersion (gel time is 1050 s). The OM image of Phthalcon particle network after cure made from PPh starting dispersion is shown in Figure 7.10. The OM image shows a much denser Phthalcon particle network in the cured coating compared to the one observed in PPh/Jeffamine D230/Epikote 828 starting dispersion (Table 7.3). The d_f value obtained in this Phthalcon particle network suggests the particle network structure is less fractal (d_f = 1.82, Table 7.2), even the presence of a continuous particle network can be doubted.

The possible absence of continuous Phthalcon particle networks in coatings made from Phthalcon/PPh/Jeffamine D230/Epikote 828 dispersion is also suggested by the conductivity measurements. No conductivity could be measured from these coatings using the standard four-point measuring unit even at a Phthalcon concentration as high as 12 vol. %, whereas when cross-linked coatings are made from Phthalcon dispersed in *m*-cresol, the σ_v values well above that of the epoxy matrix (σ_v = 10^{-16} S/cm[22]) were found even for coatings containing Phthalcon concentration below 2 vol. %.[2,3,6,10] It has been shown that when (relatively) large Phthalcon particle aggregates/agglomerates are present in the starting dispersion accompanied with a much longer gel time, the resulted Phthalcon particle network is inhomogeneouly distributed through the coating layer (Chapter 5).[3] The particle network is not present in the area close to the coating surface due to sedimentation, therefore the conductivity cannot be determined since our four-point measurements are carried out at the coating surface.[3] It is possible that this sedimentation of Phthalcon particle network stimulated by the long gel point (Figure 7.9) also took place during cure in coatings made from Phthalcon/PPh dispersions.

To prevent sedimentation, the cross-linking of epoxy should take place in a faster manner. Nevertheless, the curing reaction should not be too quick, otherwise Phthalcon particle aggregates/agglomerates might not have sufficient time to form a continuous particle network. 2,4,6-Tris(dimethylaminomethyl)phenol (DMP 30) is known as a catalyst to accelerate the ring opening of epoxy prepolymer. However, even for a 12 vol. % Jeffamine D230 cross-linked Phthalcon/epoxy coating made

from PPh dispersion containing DPM 30 accelerator, no conductivity could be measured. Rheological measurements on viscosity changes over time during cure show that the gel time changes from 1050 s in the absence of catalyst to 736 s in the presence of 20 wt. % DMP 30 (with respect to the total amount of PPh used).

As has been discussed before, *m*-cresol not only acts as a good dispersing medium, but also acts as a proton-donating catalyst which enhances the cross-linking of the epoxy prepolymer. To accelerate the curing reaction, 20 wt. % *m*-cresol (with respect to the total amount of PPh) was added into Phthalcon/PPh dispersions. The rheological measurements on viscosity changes over time during cure show that the gel time changes from 1050 s to 495 s in the presence of *m*-cresol (Figure 7.9).

To see if conductivity could be measured, four-point measurements were carried out and a σ_v value of 5.1 x 10^{-9} S/cm was found for 12 vol. % Phthalcon/PPh/*m*-cresol/epoxy coating. The measured σ_v value suggests the absence of an insulating top layer. However, this σ_v is much lower than what we observed in Jeffamine D230 cross-linked coatings made from Phthalcon/*m*-cresol starting dispersions, because even in the presence of *m*-cresol the gel time of a coating formulation made from a PPh dispersion is still much longer than the one observed in a Phthalcon/*m*-cresol/Jeffamine D230/Epikote 828 starting formulation.

When we compare the viscosity changes over time between Phthalcon/PPh/*m*-cresol/Jeffamine D230/Epikote 828, Phthalcon/*m*-cresol/Jeffamine D400/Epikote 828 and Phthalcon/*m*-cresol/Jeffamine D2000/Epikote 828 starting formulations, the gel point of the starting formulation containing PPh and *m*-cresol lies between the other two starting formulations (Figure 7.11). The fractal structure analysis on the Phthalcon particle network made from this starting formulation (Figure 7.12) reveals a d_f value of 1.60. Within the uncertainty of measurements this d_f value and the σ_v value obtained from a coating containing 12 vol. % Phthalcon are all lie between the ones obtained from Jeffamine D400 and Jeffamine D2000 cross-linked coatings (Table 7.3). Hence, relaxation might happen in a Phthalcon particle network made from PPh dispersion as well. Our results also indicate that it is possible to replace *m*-cresol with much friendlier dispersing solvent, but careful processing optimization, such as dispersing conditions and efficient catalyst, is required to obtain the most attractive electrical property because the nanoparticle structures and distributions in polymer matrix are very sensitive to small changes in starting formulations and processing

methods/conditions.[2,3,10,11]
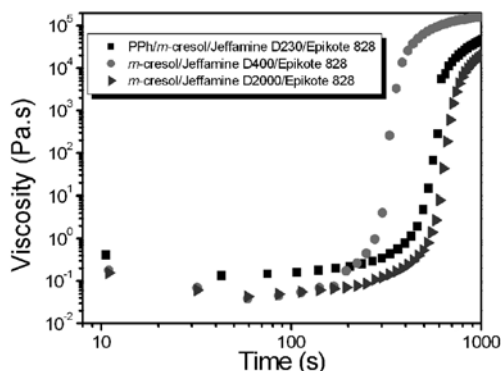
Figure 7.11. Changes in viscosity during cross-linking of 3 vol. % Phthalcon/epoxy. The starting formulations were varied and the curing temperature was 100 °C.
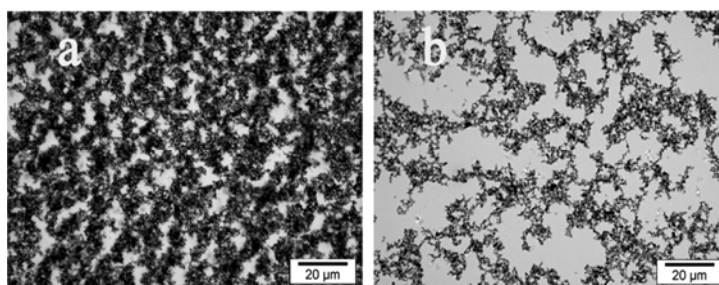
Figure 7.12. The OM images of Phthalcon particle network structures in Jeffamine D230 cross-linked epoxy coatings with/without the addition of *m*-cresol. a) Phthalcon/PPh/epoxy coating; d) Phthalcon/PPh/*m*-cresol/epoxy coating. Both coatings contained 3 vol. % Phthalcon. When *m*-cresol was present, the amount of *m*-cresol was 20 wt. % with respect to the total amount of PPh.

7.4. Conclusions

We have shown in this chapter that post-cure has a large influence on Phthalcon particle network structure and the volume conductivity σ_v of the final coating. During post-cure the cross-linking reaction is optimized, the remaining solvent and insulating layer between particle aggregates is minimized or completely disappeared. Therefore, the σ_v increases, although the extent of improvement in σ_v depends on the cross-linker and the chosen curing temperature. Moreover, further relaxation of Phthalcon particle network may occur during post-cure.

m-cresol is a powerful dispersing medium which breaks down the highly agglomerated Phthalcon powder into well-dispersed submicrometer-sized Phthalcon particles/aggregates; moreover, it also acts as a catalyst which facilitates the ring opening reaction of epoxy prepolymer and prevents the sedimentation of Phthalcon particle network during cure. However, when an excessive amount of *m*-cresol is present in the starting formulation (matrix/*m*-cresol mass ratio $\leq$ 5/8) the gel point is prolonged. This results in a relaxation of initially formed Phthalcon particle network and a decrease in σ_v.

It is also shown that, from safety point of view, it is possible to replace (part of the) *m*-cresol with a much safer and friendlier dispersing solvent, but careful optimization of the starting formulation and processing conditions are needed to realize an optimum log σ_v - φ relation. The presented results confirm that only within a small processing window, which seems to be very specific for each chosen starting formulation, semi-conductive Phthalcon/thermoset materials can be realized at low filler concentration by forming a continuous fractal Phthalcon particle network throughout the matrix. The results also show that the nanoparticle structure and distribution in cured thermoset matrix are likely to be strongly dependent on these factors as well. This means that the ultimate electrical conductivity of these nanocomposites also depends on the processing conditions and starting formulations.

References

1. Henry Lee, K. N., *Handbook of Epoxy Resins*. Mcgraw-Hill: Texas, 1981.

2. Chen, Z.; Brokken-Zijp, J. C. M.; Huinink, H. P.; Loos, J.; de With, G.; Michels, M. A. J. *Macromolecules* **2006,** 39, (18), 6115-6124.

3. Chen, Z.; Brokken-Zijp, J. C. M.; Michels, M. A. J. *J. Polym. Sci. B* **2006,** 44, (1), 33-47.

4. Brokken-Zijp, J. C. M.; Yuan, M.; et al. *"Synthesis and Structure of Novel Aquocyanophthalocyaninato Co(III) Semi-conductor and Its Applications in Conductive Polymer Composites"*. In Preparation.

5. Brokken-Zijp, J. C. M.; van Mechelen, J. B.; Emeis, C. A.; Datema, K. P.; Kramer, A. H.; de Bruijn, D. P.; Meruma, A. J. *US Patent 05319009* **1993**.

6. Yuan, M.; Brokken-Zijp, J. C. M.; Huijbregts, L. J.; de With, G. *J. Polym. Sci. B* **2008,** 46, 1079-1093.

7. Dettre, R. H.; Johnson, R. E. *J. Colloid Interface Sci.* **1966,** 21, (4), 367.

8. Pallas, N. R.; Pethica, B. A. *Colloids Surf.* **1983,** 6, (3), 221-227.

9. Brokken-Zijp, J. C. M. *Internal Information from Shell*.

10. Yuan, M.; Brokken-Zijp, J. C. M.; de With, G. *"Conductivity of Cross-linked Low Surface Energy Epoxy Coatings"*. Submitted to J. Polym. Sci. B.

11. Yuan, M.; Brokken-Zijp, J. C. M.; de With, G. *"Structure-Electrical Property in (Semi)conductive Thermoset Polymer Nanocomposites"*. Submitted to Macromolecules.

12. Mandelbrot, B. B., *The Fractal Geometry of Nature* W. H. Freeman: New York, 1983.

13. Schüth, F.; Sing, K. S. W.; Weitkamp, J.; Ed., *Handbook of Porous Solids*. Wiley-VCH: Weinheim, 2002; Vol. 1.

14. Weitz, D. A.; Huang, J. S.; Lin, M. Y.; Sung, J. *Phys. Rev. Lett.* **1984,** 53, (17), 1657-1660.

15. Brady, R. M.; Ball, R. C. *Nature* **1984,** 309, (5965), 225-229.

16. Vermant, J.; Solomon, M. J. *J. Phys.* **2005,** 17, (4), R187-R216.

17. Meakin, P. *Phys. Rev. A* **1983,** 27, (3), 1495-1507.

18. Huijbregts, L. J. *Charge Transport and Morphology in Nanofillers and Polymer Nanocomposites*. Ph.D. Thesis, Eindhoven University of Technology, Eindhoven, 2008.

19. Huijbregts, L. J.; Brom, H. B.; Brokken-Zijp, J. C. M.; Kemerink, M.; Chen, Z.; de Goeje, M. P.; Yuan, M.; Michels, M. A. J. *J. Phys. Chem. B* **2006,** 110, (46), 23115-23122.

20. Wu, C. S. *J. Mater. Sci.* **1992,** 27, (11), 2952-2959.

21. van Garderen, H. F.; Dokter, W. H.; Beelen, T. P. M.; van Santen, R. A.; Pantos, E.; Michels, M. A. J.; Hilbers, P. A. J. *J. Chem. Phys.* **1995,** 102, 480-496.

22. Brokken-Zijp, J. C. M.; Soloukhin, V. A.; Posthumus, W.; de With, G. *In Proceeding of 2003 Athens Conference on Coatings Science and Technology, Vouliagmeni, Greece.*

8

CONDUCTIVITY OF UV CURED PHTHALCON/ACRYLATE COATINGS⊛

SYNOPSIS

A straightforward method is proposed to prepare UV curable semi-conductive acrylate coatings. The conductivity is achieved by directly dispersing a very small amount of Phthalcon 11/12 particles into acrylate monomer; and then the formulation is UV cured with the aid of photoinitiator. Under the optimum conditions Phthalcon/acrylate coatings are made, which can reach a maximum DC volume conductivity σ_{max} of 10^{-7} S/cm and a percolation threshold φ_c of 0.2 vol. %. Under these conditions, a fractal Phthalcon particle network is formed by diffusion limited cluster aggregation from large fractal particle aggregates present in the starting formulation. It is likely that these Phthalcon particle aggregates are "frozen" in the acrylate matrix as a result of the rapid UV curing of the acrylate monomer. In the cured coatings no matrix seems to be present between particles in the network, and a conductivity level above 10^{-8} S/cm can be realized at a particle concentration below 1 vol. %. Although the presence of nanoparticles may absorb part of the light and slow down the curing rate, UV curing of thermoset materials containing a small amount of semi-conductive nanofiller particles seems to be preferred above thermal curing to prepare permanent antistatic thermoset polymer coatings.

8.1. Introduction

Conductive polymer composites can be made by incorporating conductive fillers into an insulating polymer matrix. These materials are of major interest due to the possibility of combining electrical properties of conductive fillers with the excellent mechanical properties and processability of the polymer matrix. To maintain the mechanical and processing properties of the matrix, the filler fraction should be as low as possible; while to obtain a conductive material, the filler fraction should be above the percolation threshold φ_c at which the filler particles form a continuous particle network through the matrix.[1-4] However, the commercial applications of conductive polymer composites, at present, are limited because a large amount of conductive filler is often required to achieve a reasonable conductivity level σ_v. Statistical percolation models predict a φ_c of 16 vol. % for randomly distributed non-overlapping hard spheres;[5-7] this filler fraction is often unacceptably high in practice because it deteriorates the properties and processability of the polymer matrix material. Moreover, the cost-price of the composites is often beyond an acceptable level so that most of the applications are no longer commercially attractive.[8]

It is widely accepted that the conductivity of a polymer composite is based on the presence of a continuous network of (semi)conductive filler particles.[1-4] The particle network morphology after processing is very important in determining σ_v and φ_c because it affects the charge transport in the network.[1,9-11] The morphology may be a complex arrangement of particle aggregates/networks with different size and shape distributions. If particles can be controlled in a desired manner or can be arranged into a preferred structure, it will tremendously decrease φ_c, improve σ_v and broaden the application possibilities of these materials.

Almost all publications on conductive polymer composites containing (semi)conductive fillers focus on thermoplastic polymer matrices. Knowledge on thermoset polymer composites, especially on UV curable thermoset polymer composites, is limited, although these materials are of major practical interest. Published results on UV curable polymer nanocomposites mainly focus on using inorganic nanoparticles, such as silicium oxide, tin oxide and antimony doped tin oxide (ATO) as (semi-conductive) fillers.[12-18] Due to the hydrophilicity of these inorganic particles, surface modification is often required to improve the compatibility of these fillers with the polymer matrix.[13-18] However, surface modification introduces grafting agent(s) which can act as an insulating layer,

resulting in polymer composites with low conductivity and consequently limit the applications of these materials.

It has been shown that nanocrystals of aquocyanophthalocyaninato Co(III) (Phthalcon 11/12) (Scheme 8.1) can be used as semi-conductive additive in a broad range of thermoplastic and thermoset polymer matrices, resulting in materials with low φ_c.[8,9,19-22] Nevertheless, studies on this promising filler have only concentrated on thermally cured thermoset polymer matrices. If UV cured conductive Phthalcon/polymer composites can be realized through straightforward and easily controlled processing conditions, it will extend the applications of such novel nanofiller.

In this chapter we report the use of nanometer-sized Phthalcon 11/12 as semi-conductive additive in UV curable acrylate composites. The relation between the conductivity of these acrylate coatings and the amount of Phthalcon particles added is discussed. We particularly focus on the morphology of Phthalcon particle networks before and after cure, the fractal characteristics of particle network structures and the mechanism of network formation. Finally, the impact of our findings on other UV cured polymer composites containing nanometer-sized (semi)conductive filler particles is addressed.

8.2. Experimental

8.2.1. Materials

Phthalcon 11/12 (Scheme 8.1) was synthesized in high purity and yield using a two-step reaction as described before.[20-22] The primary Phthalcon 11/12 particle size used here is about 250 nm in length and width and about 50 nm in thickness. Before use the Phthalcon powder was carefully dried at 80 $^{\circ}$C for 48 h under vacuum (~ 0.01 mbar) and ground into fine powder in a mortar.

Acrylate monomer poly(ethylene glycol) diacrylate (PEGDA, $M_n \approx$ 258, 575 & 800) and photoiniator 2-hydroxy-2-methylpropiophenone (97 %) were purchased from Aldrich. The chemical structures of these compounds are shown in Scheme 8.2. All chemicals were used as received.
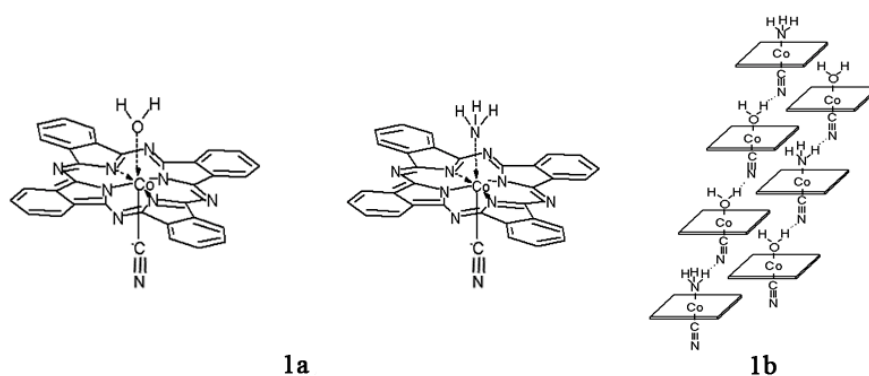
Scheme 8.1. Molecular (1a) and crystal structure (1b) of Phthalcon, Phthalcon 11/12 contains both NH_3 and H_2O as ligands in the cystal.[22]

Poly(ethylene glycol) diacrylate (PEGDA)
(Average M_n = 258, 575, 800)
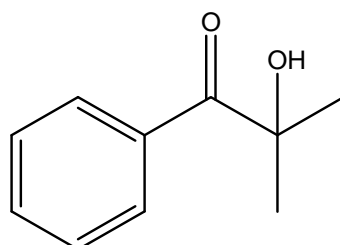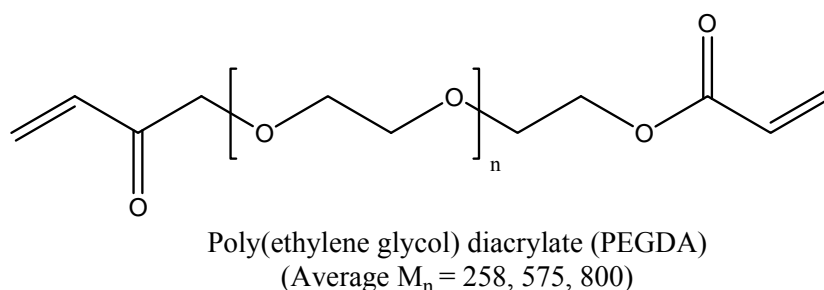
2-hydroxy-2-methylpropiophenone

Scheme 8.2. Chemical structures of PEGDA acrylate monomers and photoinitiator.

8.2.2. Coating Preparation

All acrylate coatings were prepared starting from a dispersion of Phthalcon 11/12 particles in a PEGDA monomer, which was made by magnetical (1 h) and later on ultrasonical (1 h) mixing. To this dispersion 3 wt. % of photoinitiator, 2-hydroxy-2-methylpropiophenone, was added (the amount of photoinitiator added was based on the total amount of PEGDA monomer used). This mixture was then magnetically stirred for 5 min and ultrasonically degassed for 5 min. Finally, it was cast on a polycarbonate substrate with a 10 μm coating thickness using a doctor blade

applicator and cured by exposure to UV light (F lamp, λ = 315-400 nm, 20 mW/cm^2, N$_2$ atmosphere) for 2 min. Under these conditions smooth coatings were obtained.

The concentrations of Phthalcon in the UV cured materials ranged from 0 to 6.1 vol. %, based on the total composition of the composites after cure by taking into account the density of Phthalcon powder and UV cured PEGDA acrylate coating as 1.65 and 1.10 g/cm^3, respectively.

8.2.3. Characterization

Real-time ATR The curing kinetics of PEGDA 575 with/without the presence of Phthalcon particles was studied by real-time ATR (Scheme 8.3).[23] A Spectral Luminator from ORIEL instruments was used as UV light source. Light (λ = 305-325 nm) with an intensity of 14 or 0.043 mW/cm^2 (measured with a photomultiplier) was used to activate the photoinitiator. Before each measurement the starting coating formulation was applied on a diamond ATR crystal which was mounted on a BIORAD Excalibur FTIR unit, and then it was irradiated by UV light through a 6 mm diameter liquid-filled light guide (transmitted light > 300 nm). The sample was covered by quartz plate and kept under N$_2$ flow which suppresses the contact of sample with surrounding air; then light was switched on and the ATR spectra were recorded until the end of curing reaction. The rate of spectra recorded was up to three spectra per second and the thickness of the coating was about 2 μm. The curing reactions of the acrylate monomer were monitored by measuring the peak area centred at 1636 cm^{-1}. The decrease of the peak area reflects the conversion of vinyl groups and is proportional to the degree of cure reached after a certain time. All ATR spectra were recorded under N$_2$ atmosphere and during the measurements the light illumination was kept constant.

UV-Vis Spectroscopy The UV-Vis absorption spectra of 1.95 x 10^{-4} mol/L Phthalcon/ethylene glycol dispersion, 1.04 x 10^{-3} mol/L PEGDA 575/ethanol dispersion and 1.22 x 10^{-4} mol/L photoinitiator/ethanol dispersion were recorded with a Hewlett Packard 8453 spectrophotometer. The dispersion was placed in a 1 cm path length cuvette. The amount of Phthalcon in the path was equivalent to a 2 μm thick coating with a Phthalcon concentration of 3.6 vol. %. The amount of PEGDA and photoinitiator in the path of the measurements was equivalent to a 5.0 mol/L and a 0.6 mol/L dispersion placed in a 2 μm path length, respectively.
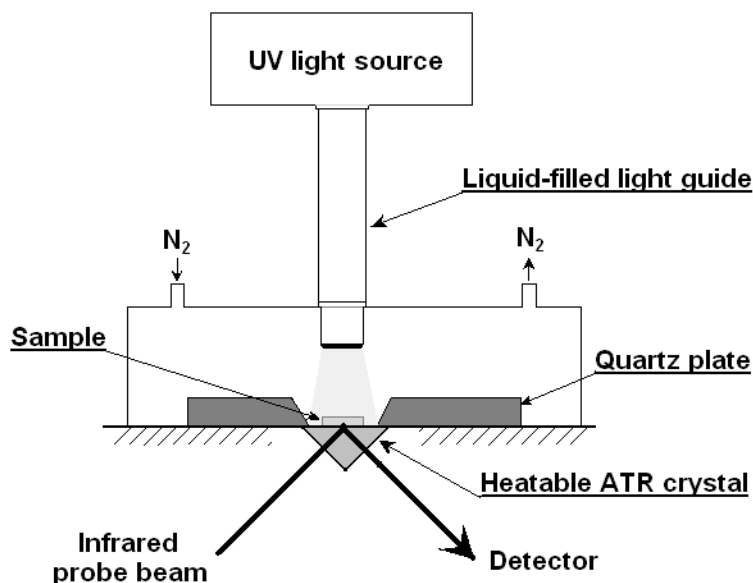
Scheme 8.3. Experimental setup for real-time ATR which was used to monitor UV cure of PEGDA and Phthalcon/PEGDA coatings.

Volume Conductivity Measurements The volume conductivity σ_v of cured Phthalcon/PEGDA coatings at room temperature was measured using a standard four-point method, with a Keithley 237 high voltage source measuring unit and a Keithley 6517A high voltage electrometer. The former unit supplies a constant current through the coating between the two outside electrodes and the latter unit measures the voltage difference between the two inside electrodes. The measurements were carried out on the surface of the coating sample according to standard ASTM D991 and instructions of Keithley "low conductivity level measurements". Silver paint (silver conductive adhesive 416, electron microscopy sciences, USA) was used to ensure good contact between sample surface and measuring electrodes. To calculate σ_v an average coating thickness of about 10 μm was used and the presented σ_v for each Phthalcon concentration is an average value of at least three different coatings measured at three different positions.

Optical Microscopy The morphology of Phthalcon particle network in PEGDA before and after UV cure was studied by optical microscopy (OM). The OM analysis was carried out with a Reichert-Jung Polyvar-Met microscope using the transmission bright-field technique. These OM images were later converted to binary images and analyzed using the tiling method to obtain the fractal dimensions of the particle network.[9] The Phthalcon particle dispersions studied here were prepared by bringing a

small amount of material between two glass slides. The Phthalcon/PEGDA coatings were studied directly without further preparation.

Surface Energy The surface energies of the liquid samples were determined at 20 $^{\circ}$C by Wilhelmy plate method using a Krüss Digital Tensionmeter K10T.[24] During the measurement, the plate was moved towards the surface until it reached the meniscus. The surface energy was calculated from the measured force. All surface energies given are average values of three measurements on each sample.

8.3. Results and Discussion

8.3.1. Curing of PEGDA 575

To get more insight in the curing behavior of acrylate monomers in the presence of Phthalcon 11/12, cure of pure PEGDA 575 in the presence of 3 wt. % photoinitiator (with respect to the total amount of PEGDA 575) was studied first with real-time ATR. During the measurement the sample was irradiated with UV light (305-325 nm) which has an intensity of 14 mW/cm^2 or 0.043 mW/cm^2. This wavelength range was chosen because it corresponds to the absorption of photoinitiator and the available wavelengths transmitted through the liquid-filled light guide. As can be seen from Figure 8.1 and Table 8.1, a large number of peaks disappeared from the ATR spectra during cure. The disappearance of these peaks can be quantitatively explained by the polymerization of PEGDA 575 acrylate monomer.[25] As the carbonyl group within the acrylate monomer is conjugated with the vinyl group, the carbonyl peak at 1700 cm^{-1} shift to a higher wavelength which can be explained by the conversion of the vinyl groups during cure.[25] These quantitative conversions during UV cure of pure PEGDA 575 were reported before.[14]

The curing reactions were monitored by measuring the peak area which is centred at 1636 cm^{-1}. The decrease of the peak area reflects the conversion of vinyl groups and is proportional to the degree of cure reached after a certain time. For PEGDA 575 the signal of vinyl group at 1636 cm^{-1} disappeared within 20 seconds (Figure 8.2). In general, the curing reaction is not retarded as long as the reactive groups are sufficiently mobile. The best indication for the mobility of groups in a polymer is the glass transition temperature T_g. The T_g of a completely cured PEGDA 575 is -30 $^{\circ}$C,[14] thus at room temperature vinyl groups remain mobile. This explains the fast curing rate and the complete disappearance of C=C groups observed in Figure 8.2.
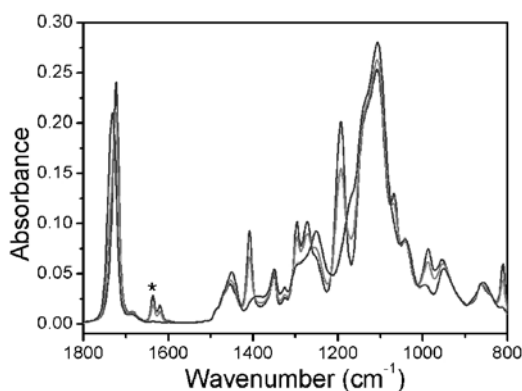
Figure 8.1. Changes in ATR spectra during cure of a 2 μm thick PEGDA 575 coating: the asterisk indicates the peak that was used to monitor the curing rate. All starting formulations contained 3 wt. % photoinitiator. Peaks that disappeared during polymerization are listed in Table 8.1.

Table 8.1. Peaks that disappeared from ATR spectra during polymerization of PEGDA 575.[25#]

Disappearing peaks (cm^{-1})	Vibrations of PEGDA monomer
1636	C=C stretching
1620	C=C stretching
1408	O-CH$_2$ wagging
1298	C-O stretching conjugated with C=C
1273	C-O stretching conjugated with C=C
1192	C-O stretching conjugated with C=C
986	=CH$_2$ wagging
810	=CH$_2$ twist

[#] 3 wt. % Photoinitiator was added based on the total amount of acrylate monomer. The starting formulations did not contain Phthalcon particles.
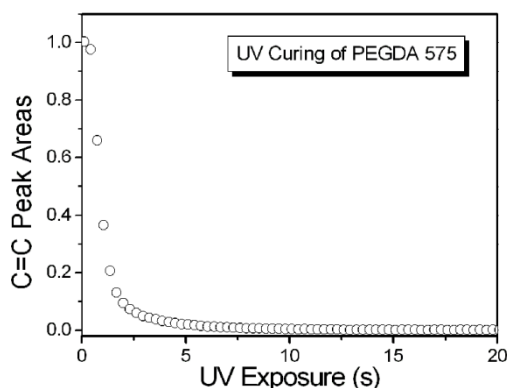
Figure 8.2. The disappearance of C=C group in a 2 μm thick PEGDA 575 in the presence of 3 wt. % photoinitiator. The intensity of UV lamp used was 14 mW/cm^2 and the wavelength used was between 305-325 nm. The measurement was monitored under N$_2$ flow.

8.3.2. Curing of Phthalcon/PEGDA 575

The addition of semi-conductive nanoparticles may influence UV cure in many ways. In general, semi-conductive nanoparticles strongly absorb UV light. Hence, a typical problem that happens during cure is the absorption of UV light by these particles. Consequently, the intensity of UV light in the deeper layers becomes low, possibly resulting in an insufficient cure. Therefore, it is important that sufficient UV light is available through the whole layer thickness. Apart from the absorption of UV light, physical/chemical interactions between filler particles and prepolymer/photoinitiator may also influence the conversion of reactive groups and/or the efficiency of photoinitiator, and hence affect curing rate. Furthermore, the filler particles may act as retarder, inhibitor and/or photoinitiator for radical polymerization.[26] Therefore, side reactions and/or changes in curing rate may occur in the presence of Phthalcon particles. To verify whether the above mentioned effects are present in our system, the influence of Phthalcon particles on UV cure of PEGDA 575 was studied in more detail.

The absorption of a PEGDA 575/ethanol dispersion and a Phthalcon/ethylene glycol dispersion is shown in Figure 8.3. The amount of Phthalcon nanoparticles in the path of the measurement was equivalent to a 2 μm thick coating containing 3.6 vol. % Phthalcon. For this layer light that transmitted through Phthalcon was calculated with equation (8.1):

$$A = -lg\frac{I}{I_o} = -lgT \qquad (8.1)$$

where *A* is absorbance, *T* is transmittance, *I* and I_o represent the intensity of transmitted light and incident light, respectively. At 315 nm 40.0 % of light was transmitted through this Phthalcon layer when the light absorbed by acrylate monomer and photoinitiator was neglected. This assumption is logical because for a 2 μm PEGDA 575 coating formulation the concentrations of PEGDA and photoinitiator are 1.9 mol/L and 0.2 mol/L, respectively. Both concentrations were lower than the equivalent concentrations (5.0 mol/L and 0.6 mol/L, respectively) shown in Figure 8.3. The calculated transmittance indicates that the intensity of UV light is sufficient for a reasonable curing rate even at the bottom of the layer. However, for coating with a much higher Phthalcon concentration the transmitted light is so weak that cure of the bottom layer may be strongly hampered. To prevent this, for all coatings studied here the Phthalcon concentration was not higher than 6.1 vol. %.
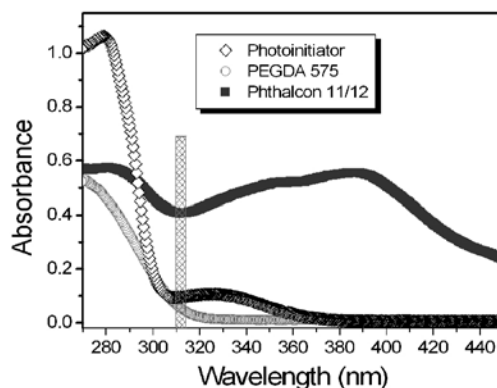
Figure 8.3. Light absorbed by PEGDA 575, photoinitiator and Phthalcon. The amount of Phthalcon in the path of the measurement was equivalent to the amount in a 2 μm thick coating containing 3.6 vol. % Phthalcon; the amount of PEGDA and photoinitiator in the path of the measurements were equivalent to a 5.0 mol/L and a 0.6 mol/L dispersion with a 2 μm path length, respectively. The grey bar indicates the absorbance at around 315 nm.

To study the polymerization rate of PEGDA 575 containing Phthalcon particles, PEGDA 575, Phthalcon and photoinitiator were mixed using the same procedure as described in the experimental part. The results are shown in Figure 8.4, which clearly indicate that with increasing Phthalcon concentration the curing rate of acrylate monomer decreases, but that complete cure was always observed. The decrease in curing rate becomes more remarkable when light with a lower intensity was used (λ = 305-325 nm, 0.043 mW/cm^2, Figure 8.4b): a fully cured pure PEGDA 575 was obtained after 50 seconds, while for PEGDA 575 containing 6.1 vol. % Phthalcon particles 120 seconds of UV exposure was needed. Using Equation (8.1) the light

transmitted through a 2 μm thick PEGDA 575 containing 6.1 vol. % Phthalcon, illuminated by such low incident light, was as low as 8.9 x 10^{-3} mW/cm^2. However, even for this coating a full cure was obtained as can be seen from the disappearance of vinyl groups. Possibly cure of the deeper layer is not only due to the polymerization initialized by the active photoinitiator, but also due to the high mobility of vinyl groups and the diffusion of free radicals from the upper layer.
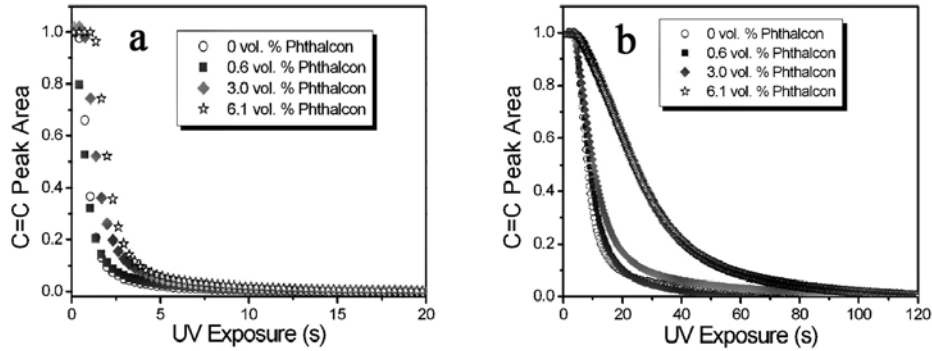
Figure 8.4. Influence of Phthalcon concentration on the curing rate of PEGDA 575 acrylate monomer (3 wt. % photoinitiator, 2 μm coating formulation, λ = 305-325 nm, N$_2$ flow, reaction monitored at 1636 cm^{-1}). (a) UV light intensity was 14 mW/cm^2; (b) the light intensity was 0.043 mW/cm^2.

The acrylate monomer is consumed by chain propagation and the propagation rate R_p is given by:[27]

$$R_p = k_p \times [M]_t \times \sqrt{\phi_i \times I_a / k_t} \tag{8.2}$$

$$I_a = I_0\left(1 - 10^{-\varepsilon_{PI}[PI]d}\right) \tag{8.3}$$

where k_p is the propagation rate constant, $[M]_t$ is the concentration of acrylate monomer at time t, ϕ_i is the number of initiated polymer chains per absorbed photon, I_a is the intensity of absorbed light, I_o is the intensity of incident light, ε_{PI} is the extinction coefficient of photoinitiator, $[PI]$ is the concentration of photointiator, d is the thickness of sample and k_t is the termination rate constant.

When Phthalcon particles are present, light absorbed by Phthalcon particles should also be taken into account. Therefore, I_o in Equation (8.2) should be replaced by I_o':

$$I_o' = I_o \times 10^{-\varepsilon_{Phthalcon}[Phthalcon]d} \tag{8.4}$$

where I_o' is the intensity of total light transmitted through Phthalcon, ε_{PI} is the extinction coefficient of Phthalcon and [*Phthalcon*] is the concentration of Phthalcon particles.

Equation (8.2) becomes:

$$R_p = k_p \times [M]_t$$

$$\times \sqrt{\phi_i \times I_0 \times 10^{-\varepsilon_{Phthalcon}[Phthalcon]d} \times (1 - 10^{-\varepsilon_{PI}[PI]d}) \Big/ k_t} \tag{8.5}$$

Using Equation (8.5) as well as the results on light absorbed by Phthalcon (Figure 8.3), the initial polymerization rate R_p can be calculated. From the first derivative of the disappearance of vinyl groups vs. time $-d[C=C]\big/dt$, the polymerization rate R_p can also be determined from real-time ATR spectra. At the initial curing stage, assuming a monomer conversion of 10 %, the ratios between R_p were calculated from Figure 8.4. Both experimentally (calculated from Figure 8.4 using $-d[C=C]\big/dt$) and theoretically (calculated from Equation 8.5) determined R_p ratios are summarized in Table 8.2. Within the uncertainty of measurements these values are in agreement with each other, and strongly suggest that the observed retardation in curing rate as the amount of Phthalcon increases is caused only by the absorption of UV light by Phthalcon particles. That Phthalcon particle can act as photoinitiator is ruled out because the sample remained uncured when a starting formulation which only contained Phthalcon particles and PEGDA 575 was illuminated under UV light for a long time (10 minutes). Therefore, we assume in the rest of this chapter that Phthalcon particles only act as UV light absorber during UV cure of the acrylate monomer.

We found that smooth coatings were always obtained after cure, even for 10 μm thick layers containing 6.1 vol. % Phthalcon. This suggests a (almost) complete cure of acrylate monomer. However, whether these 10 μm thick coatings were fully cured during illumination or partially cured after switching off the light is unknown. No smooth coatings were obtained from formulations with a Phthalcon concentration

higher than 7.0 vol. %. Therefore, to prevent the hampering of cure at the bottom of coating, the conductivity measurements and the OM analysis were carried out on coatings which had a thickness of about 10 μm and the Phthalcon concentration in the coating formulations was not higher than 6.1 vol. %.

Table 8.2. Experimentally determined and calculated R_p ratios with different Phthalcon particle concentrations.

UV light intensity (mW/cm^2)	$R_p/R_{p'}$	Experimentally Determined R_p	Calculated R_p	
			$R_p{}^*$	$R_p{}^\&$
14	$R_{p(0\,vol.\,\%)}/R_{p(0.6\,vol.\,\%)}$	1.2	1.1	1.0
14	$R_{p(0\,vol.\,\%)}/R_{p(3.0\,vol.\,\%)}$	1.4	1.5	1.3
0.043	$R_{p(0\,vol.\,\%)}/R_{p(0.6\,vol.\,\%)}$	1.1	1.1	1.0
0.043	$R_{p(0\,vol.\,\%)}/R_{p(3.0\,vol.\,\%)}$	1.5	1.5	1.3
	$R_{p(0\,vol.\,\%)}{}^{H}/R_{p(0\,vol.\,\%)}{}^{L\#}$	17.9	18.0	18.0
	$R_{p(0.6\,vol.\,\%)}{}^{H}/R_{p(0.6\,vol.\,\%)}{}^{L}$	16.6	18.0	18.0
	$R_{p(3.0\,vol.\,\%)}{}^{H}/R_{p(3.0\,vol.\,\%)}{}^{L}$	19.7	18.0	18.0

[#] *H*: High light intensity of 14 mW/cm^2; *L*: Low light intensity of 0.043 mW/cm^2.

[*] R_p at the bottom of layer taking into account the total layer thickness of 2 μm.

[&] R_p calculated after taking into account the diffusion depth of the ATR probe beam.

The starting formulations containing 6.1 vol. % Phthalcon was not included in the table due to the uncertainty of layer thickness together with the fact that at high Phthalcon concentration a small variation in layer thickness strongly influences R_p.

8.3.3. Morphology of Phthalcon Particle Network in UV cured PEGDA 575 Coatings

The volume conductivity σ_v of cured Phthalcon/PEGDA 575 coatings containing various Phthalcon concentrations is shown in Figure 8.5. With a small amount of Phthalcon particles (0.6 vol. %), the σ_v reaches a value of 10^{-8} S/cm and the φ_c is as low as 0.2 vol. %. The maximum volume conductivity σ_{max} obtained in these acrylate coatings is 10^{-7} S/cm. As has been shown before the formed continuous fractal Phthalcon particle network through a thermally cured thermoset coating is responsible for the observed volume conductivity σ_v at a low filler concentration.[9,19,22,28] These particle networks can be easily observed under the OM because of the fractal nature of the networks and the large correlation lengths.[9,19,22,28] Likewise, the increase in σ_v in Phthalcon/PEGDA 575 coatings may also result from the presence of Phthalcon

particle networks. Hence, to determine this suggestion, the Phthalcon particle networks in PEGDA coatings were studied with the OM as well (Figure 8.6a). From the OM image, the fractal structure analysis using the same tiling method as described before reveals a d_f value of 1.71 (Figure 8.6b).[9,22] This value is close to the theoretical value reported for a nanoparticle network formed by Diffusion Limited Cluster Aggregation (DLCA),[29-33] and suggests that the particle network in our Phthalcon/PEGDA 575 coatings is also formed by this mechanism. This mechanism of network formation was also found in several thermally cured Phthalcon/epoxy coatings.[9,22,28,34]
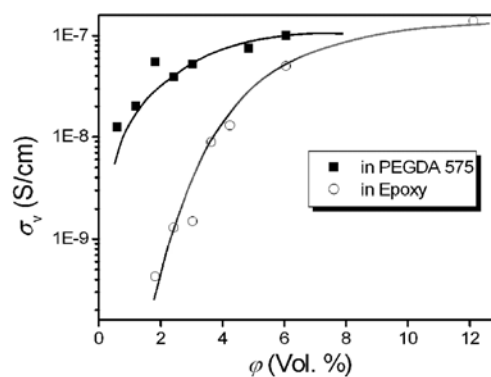

Figure 8.5. log σ_v – φ relation of UV cured Phthalcon/PEGDA 575 coatings (λ = 315-400 nm, 20 mW/cm^2, N$_2$ atmosphere for 2 min) and thermally cured Phthalcon/epoxy coatings cross-linked with Jeffamine D230; these epoxy coatings were made from submicrometer-sized Phthalcon starting dispersions and cured at 100 $^\circ$C.[9,19]
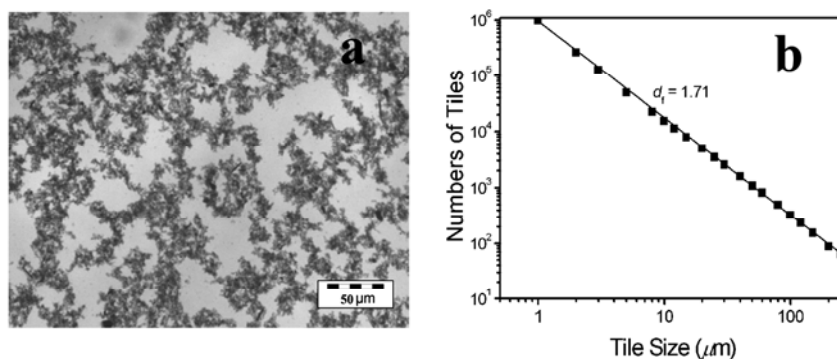
Figure 8.6. (a) OM image of a UV cured PEGDA 575 coating containing 1.5 vol. % Phthalcon; (b) fractal structure analysis of the Phthalcon particle network based on Figure 8.6(a); d_f = 1.71.

Generally, the Phthalcon particle dispersion in the starting formulation has a major influence on the final morphology of Phthalcon particle network; and consequently it influences the log $\sigma_v - \varphi$ relation of Phthalcon/polymer composites.[19] Therefore, the Phthalcon particle distribution in PEGDA 575 dispersion before cure was also studied with the OM. The dispersion was made by directly dispersing Phthalcon powder in PEGDA 575 monomer. The OM image clearly shows a fractal particle aggregate structure (Figure 8.7a). From Figure 8.7a the fractal dimension d_f of Phthalcon aggregates in PEGDA 575 dispersion was calculated and a d_f value of 1.76 was obtained (Figure 8.7b). This d_f value is not only in agreement with the theoretical value predicted for particle aggregates formed by DLCA, but also close to the value calculated from UV cured Phthalcon/PEGDA 575 coating made from this starting dispersion. The similar fractal dimension and particle aggregate/network distribution observed in the starting dispersion and the final cured coating strongly suggest that the Phthalcon particle network in the coating is directly formed from Phthalcon aggregates in the dispersion. Because UV cure of PEGDA 575 monomer is rapid, Phthalcon aggregates/networks may not have sufficient time to reorganize. It is likely that the initial formed fractal particle aggregates/networks in the dispersion are quickly "frozen" in the acrylate matrix during cure.
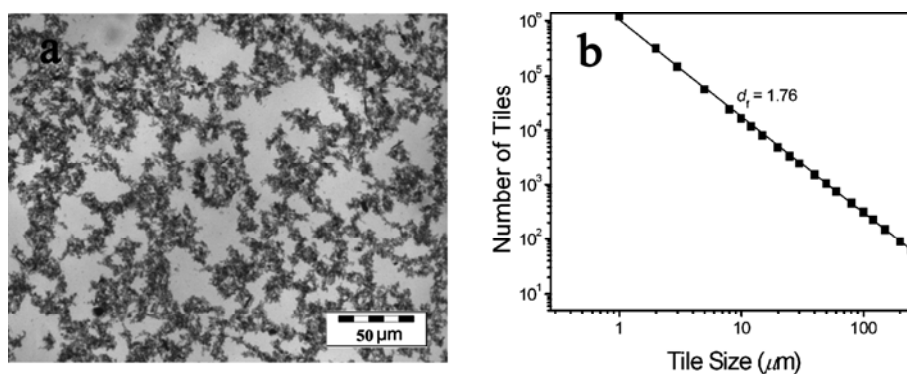
Figure 8.7. (a) OM image of a 1.5 vol. % Phthalcon/PEGDA 575 starting dispersion; (b) fractal structure analysis of Phthalcon particle dispersion in (a); d_f = 1.76.

The Phthalcon aggregate structure found in PEGDA 575 dispersion can be explained by the specific interactions between surface groups of Phthalcon particles and PEGDA, together with the specific interactions between surface groups of Phthalcon particles. The Phthalcon primary particles used here are highly crystalline nano-sized flat plates. Electron diffraction measurements, deuterium NMR experiments on Phthalcon-^{2}H$_2$O, solid-state NMR experiment on Phthalcon-^{13}CN and FT-IR

measurements on labelled and non-labelled Phthalcon show that the surface groups at the bottom and top of the plate are -OH/H_2O, -NH_3/NH_2 and -CN, whereas the surface groups at the sidewalls are phenyl rings.[21] The interactions between surface groups of Phthalcon and PEGDA 575 (mainly hydrogen bonding with carbonyl groups) are relatively strong; hence the particle agglomerates present in the powder can be relatively easy to be broken down.

Besides these specific interactions, other particle-particle and particle-medium interactions should also be taken into account. When hydrogen bonding is negligible, it has been shown that it is possible to use experimentally determined surface energy (Table 8.3) to estimate these interactions via:[19]

$$A_H^{eff} \approx 2.1 \times 10^{-21} \left[\gamma_p^{1/2} - \gamma_m^{1/2} \right]^2 \tag{8.6}$$

A_H^{eff} is the effective Hamaker constant, while γ_p and γ_m are the surface energies of particle and surrounding medium, respectively. When the values of surface energies of the nanoparticle and the dispersing medium are similar, A_H^{eff} tends towards zero and the interfacial energy between dispersed particles and matrix tends to zero. This favours the random distribution of well-separated particles in the medium during mixing. Likewise, a large A_H^{eff} results in a high value of interfacial energy and particles tend to aggregate. Hence, more energy is required to disperse powder of nanoparticles through a dispersing medium. The surface energy of Phthalcon particle is much larger than that of PEGDA 575 (Table 8.3), large fractal Phthalcon aggregates were observed in the starting dispersion formed by DLCA from well-dispersed particles (Figure 8.6a). Apparently, the dispersing force is sufficiently large to break down the Phthalcon particle agglomerates present in the powder. The relatively large viscosity of the starting formulation, the formation of the fractal aggregates and the specific interactions between particles and PEGDA slow down the formation of particle agglomerates in the PEGDA 575 dispersion.

Table 8.3. Surface energies of the starting materials.

T (°C)	PEGDA 258 (mN/m)	PEGDA 575 (mN/m)	PEGDA 800 (mN/m)	*m*-cresol (mN/m)	Phthalcon (mN/m)
20	39.2	40.0	41.5	38.2	> 50

During cure of PEGDA 575 monomer, the particle-medium interactions change because of the consumption of the vinyl groups. However, the fast curing rate ensures an instant increase in viscosity within seconds. Apparently, the large Phthalcon particle aggregates do not have sufficient time to reorganize themselves during cure. The rapid UV cure also ensures that Phthalcon particle aggregates are (almost) "frozen" in their original positions as in the dispersion. The similar fractal particle network structure and fractal dimension observed in Figure 8.6 and Figure 8.7 support these conclusions.

8.3.4. Volume Conductivity of Phthalcon/PEGDA 575 Coatings

The σ_{max} of the cured Phthalcon/PEGDA 575 coatings is 10^{-7} S/cm (Figure 8.5). This value is equal to σ_{max} found in thermally cured cross-linked Phthalcon/epoxy coatings made under optimal conditions.[9,19] It has been shown that under these conditions Phthalcon particles in the network really touch each other at a Phthalcon concentration of 12 vol. %. This means that there is no polymer matrix present between particles in the network.[11] The fractal dimension and Phthalcon particle network structure of UV cured Phthalcon/acrylate coatings are very similar to those found in Phthalcon/epoxy coatings. Hence, for our Phthalcon/acrylate coatings it is also likely that at 6.1 vol. % Phthalcon particle network reaches the optimal structure as well, i.e. particles in the network really touch each other. Figure 8.5 also shows that in PEGDA 575 coatings the σ_v below σ_{max} is considerably higher and the φ_c is considerably lower than what we observed in cross-linked Phthalcon/epoxy coatings. This strongly suggests that for epoxy materials with a σ_v below σ_{max} Phthalcon particles do not touch each other, and that the polymer matrix present between these particles limits the charge transport. When we compare our results on UV cured Phthalcon/PEGDA 575 coatings with model calculations (Figure 2.6) which assume no matrix between Phthalcon particles in the particle network,[11] a strong resemblance between the calculated and experimentally determined log $\sigma_v - \varphi$ relation was observed. This suggests that in Phthalcon/PEGDA 575 coatings Phthalcon particles in the particle network really touch each other over a broad range of concentrations.[11]

It has been shown in (semi)conductive polymer nanocomposites that the A_H^{eff} of the starting formulation determines, to a large extent, φ_c of the composites.[13,19] The larger A_H^{eff}, the lower φ_c. However, the φ_c of Phthalcon/acrylate coatings is much lower than that of Phthalcon/epoxy coatings (Figure 8.5), whereas the d_f value and the mechanism of Phthalcon particle network formation are same.[9,19,22,28] Apparently, the

173

lowering of A_H^{eff} during cure and/or the amount of polymer matrix present between particles in the network increase the φ_c in thermally cured Phthalcon/epoxy coatings.

The cross-linked Phthalcon/epoxy coatings shown in Figure 8.5 were made from a starting dispersion in which Phthalcon particles were very well-dispersed.[19] Semi-conductive cross-linked epoxy coatings can also be made by directly dispersing Phthalcon particles in Jeffamine D230 cross-linker.[19] In these Phthalcon/Jeffamine D230 dispersions large fractal Phthalcon aggregates were also present, although the lower d_f value of 1.44 suggests that these aggregates are formed by a different mechanism. Moreover, the addition of epoxy prepolymer lowers the size as well as the d_f value of the fractal Phthalcon aggregates in the starting formulation.[19] After cure all coatings made from Phthalcon/Jeffamine D230 dispersions have an insulating top layer due to the sedimentation of Phthalcon particle network during much slower thermal cure (Scheme 8.4).[19]
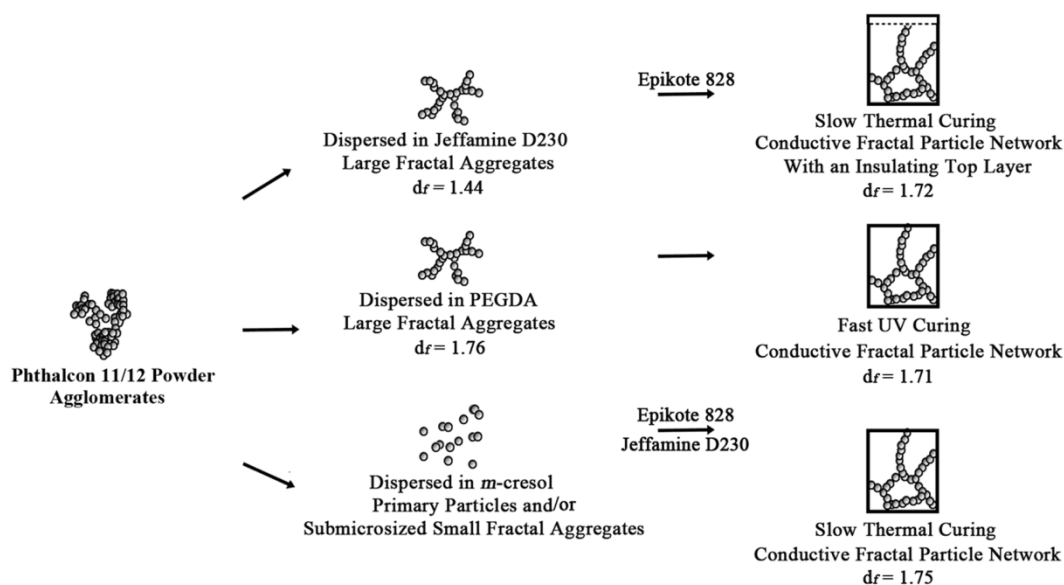

Scheme 8.4. Three different routes to obtain semi-conductive Phthalcon/polymer coatings.

Therefore, to prepare permanent antistatic coatings with the aid of a small amount of Phthalcon particles, the use of UV cure is preferred above thermally cure. Not only because the log $\sigma_v - \varphi$ relation is much more attractive, but also due to the lack of an insulating top layer and the possibility of directly dispersing Phthalcon particles in monomer without the aid of solvent or dispersing agent. These results also indicate that UV cure is, in general, a very attractive route to make semi-conductive coatings using a very small amount of semi-conductive nanoparticles. The attractiveness of UV

cure is also supported by recent results on UV cured ATO/acrylate coatings in which fractal ATO particle network is present through the coating layer ($\varphi_c = 0.3$ vol. %, the diameter of ATO particle is about 7 nm).[35] However, a disadvantage may be the absorption of UV light by the nanofiller particles. As has been shown above when a very small amount of semi-conductive filler particles is added their absorption of UV light is minimal, whereas the conductivity can be increased significantly by forming a fractal particle network through the matrix.

8.3.5. Influence of M_n of PEGDA on Fractal Particle Network Structure and log $\sigma_v - \varphi$ Relation

Besides PEGDA 575, PEGDA with similar molecular structure and surface energy, but different molecular weight M_n, namely, 258 and 800, was also used as polymer matrix for UV cured Phthalcon/acrylate coatings. These coatings were prepared under exactly the same processing conditions as described before. As shown in Figure 8.8, the σ_v of layers made from PEGDA 575 reaches a plateau of around 10^{-7} S/cm, while for those made from PEGDA 800 and PEGDA 258, the values of the plateau are only about 10^{-8} S/cm and 10^{-9} S/cm, although neither the surface energy of the acrylate monomer nor the surface energy of the total component mixture before and during cure is influenced by the M_n of PEGDA (Table 8.3).
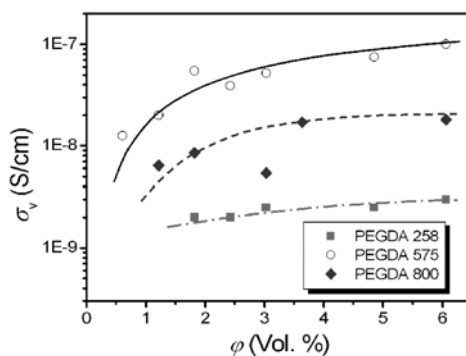

Figure 8.8. log $\sigma_v - \varphi$ relation of cured Phthalcon/PEGDA coatings. The coatings were UV cured at room temperature using different Phthalcon/PEGDA starting dispersions.

From a structure-property point of view, the log $\sigma_v - \varphi$ relation depends on the morphology of particle network inside the polymer matrix. As shown in Figure 8.9, the Phthalcon particle network structures after processing are distinctively different.
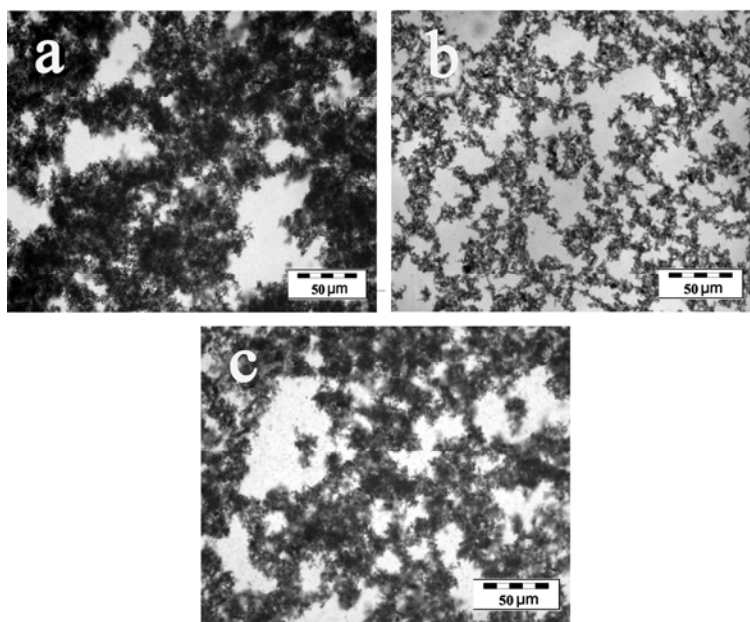
Figure 8.9. Optical microscopic images of Phthalcon particle networks in UV cured PEGDA composites using different Phthalcon/PEGDA dispersions: (a) PEGDA 258, (b) PEGDA 575, and (c) PEGDA 800. All coatings contained 1.5 vol. % Phthalcon. 3 wt. % photoinitiator was used to initialize the UV cure (λ = 315-400 nm).
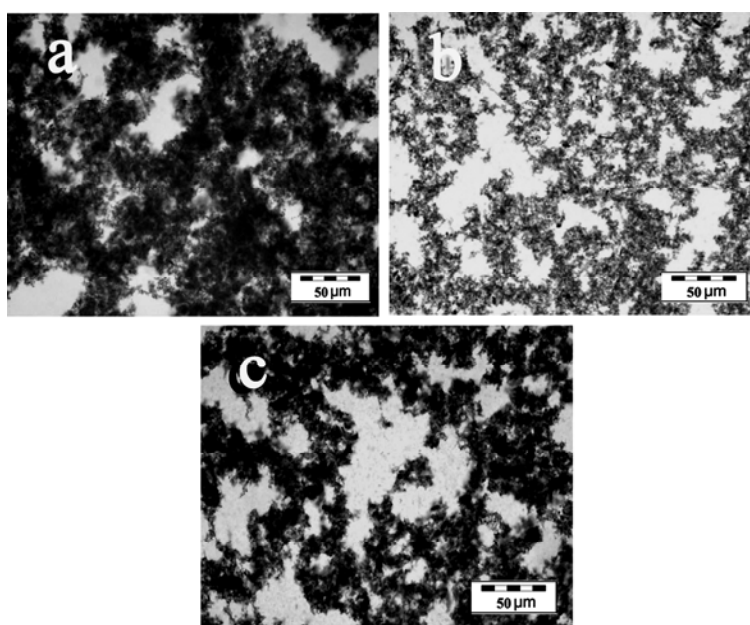
Figure 8.10. OM images of Phthalcon particle aggregates/networks in different PEGDA starting dispersions. (a) PEGDA 258; (b) PEGDA 575; (c) PEGDA 800. All dispersions contained 1.5 vol. % Phthalcon and these dispersions were used to prepare UV cured coatings shown in Figure 8.9.

The layer made from PEGDA 575 has a particle network of ramified fractal structure, while in the layers made from PEGDA 800 and PEGDA 258 the fractal structures are much coarser and denser. The OM images of the corresponding Phthalcon/PEGDA starting dispersions are shown in Figure 8.10. Results from fractal structure analyses based on the OM images of the dispersions as well as the cured coatings are summarized in Table 8.4. These results show that the Phthalcon particle aggregate/network structure in the dispersion is very similar to that in its corresponding cured coating. This strongly indicates that UV cure enables Phthalcon particle distribution to freeze in their (almost) original position as that present in the starting dispersion. Nevertheless, the larger d_f values found in coatings made from PEGDA 258 and PEGA 800 suggest that these structures are much less fractal, and probably still contain micro-sized Phthalcon particle agglomerates. Hence, only a small part of Phthalcon particles are sufficiently dispersed to form a network structure by Brownian movement. Because the viscosity of PEGDA 258 and PEGDA 800 starting formulations is different from the PEGDA 575 starting formulation, the used dispersion preparation is only optimal for Phthalcon/PEGDA 575 dispersions. It is well-known that a non-optimal particle starting dispersion has a negative effect on the $\log \sigma_v - \varphi$ relation of polymer composites containing semi-conductive nanoparticles, it is therefore expected that further optimization of Phthalcon/PEGDA 258 and Phthalcon/PEGDA 800 starting dispersions will improve the $\log \sigma_v - \varphi$ relations of these coatings.

Table 8.4. Fractal dimensions of Phthalcon particle networks in dispersions and final coatings.[#]

	PEGDA 258	PEGDA 575	PEGDA 800
Dispersion	1.92	1.76	1.87
Coating	1.90	1.71	1.83

[#]All dispersions and coatings contained 1.5 vol. % Phthalcon 11/12.

In all cured Phthalcon/PEGDA coatings studied here, the fractal structure analyses show only one linear region (Figure 8.6b and Figure 8.7b). This suggests that the correlation length ξ, which is the average size of the building blocks from which the particle network is formed, at least for Phthalcon/PEGDA 575 coatings is larger than 100 μm. For all acrylate coatings studied here layers with a thickness of about 10 μm were prepared in order to get completely cured coatings. Studies on cross-linked

Phthalcon/epoxy coatings show that the layer thickness has a large influence on the log $\sigma_v - \varphi$ relation, especially when the coating thickness becomes comparable or smaller than ξ.[9] These epoxy coatings were prepared from well-dispersed Phthalcon particle dispersions and Phthalcon particle networks are formed during cure by Brownian movement of the (almost) primary particles by DLCA.[19] Probably the well-dispersed Phthalcon particles are responsible for the much smaller ξ value ($\xi \approx 20 \ \mu$m) obtained in these coatings. This may also explain the influence of layer thickness on the log $\sigma_v - \varphi$ relation because a thin layer might "force" the particle network to be formed from the primary particles along the substrate instead of in a 3D manner, while in Phthalcon/acrylate dispersions large particle aggregates are already present, and they are frozen in the matrix without any changes in structure as a result of rapid UV cure. This suggests that in these coatings there is no layer thickness effect expected on the log $\sigma_v - \varphi$ relation. The agreement between log $\sigma_v - \varphi$ relation and proposed model calculations indeed confirm this suggestion.

Information on UV cured (semi)conductive polymer nanocomposites, especially on the addition of nanoparticles without surface modification, is rather limited. Although in our study only Phthalcon was used as semi-conductive filler, we expect that our findings can also be applied to other polymer nanocomposites. Our results also suggest that careful processing optimization is required in order to achieve the most attractive material properties, because nanoparticle distribution is very sensitive to small changes in the starting particle dispersion, starting formulation and processing methods/conditions, such as viscosity changes over time, curing rate of the polymer matrix and A_H^{eff}.

8.4. Conclusions

It has been shown that semi-conductive UV cured acrylate coatings can be easily made by dispersing a very small amount of nano-sized semi-conductive Phthalcon particles into an acrylate monomer. The curing reaction of the acrylate monomer was followed in detail using real-time ATR. These measurements show that the presence of Phthalcon particles does not affect the curing mechanism of acrylate monomer. The curing rate only slows down due to the absorption of UV light by Phthalcon particles. Still a complete conversion of acrylate monomer was observed even when 6.1 vol. % Phthalcon was added in the starting formulation.

The percolation threshold φ_c of the cured acrylate coatings is as low as 0.2 vol. % and the maximum volume conductivity σ_{max} is as high as 10^{-7} S/cm (with 6.1 vol. % Phthalcon). When an optimal Phthalcon particle starting dispersion was used, the particle network in the cured coating is fractal with a fractal dimension d_f of 1.71. The particle network is formed from large Phthalcon fractal aggregates/networks ($d_f = 1.76$) which were already present in the starting dispersion and the particle network is formed by Diffusion Limited Cluster Aggregation (DLCA).

The log $\sigma_v - \varphi$ relation of cured acrylate composites using PEGDA 575 as starting monomer is much more attractive than that obtained from thermally cured Phthalcon/epoxy coatings. Not only because the φ_c is much lower, but also because the (almost) direct "freezing in" of Phthalcon fractal networks prevents the presence of insulating matrix between particles in the network and prevents particle network sedimentation and reorganization.

The results presented here also suggest that in general for (semi)conductive polymer nanocomposites the log $\sigma_v - \varphi$ relation and the particle distribution through the matrix is very sensitive to the chosen starting particle distribution. Therefore, careful processing optimization is required to achieve the most attractive material properties. Although the presence of semi-conductive particles may absorb part of the light, UV cure still seems to be much more attractive than thermal cure.

References

1. Skotheim, T. A.; Ed., *Handbook of Conducting Polymers, 2nd ed., Revised and Expanded*. Marcel Dekker: New York, 1997.

2. Nalwa, H. S., *Handbook of Advanced Electronic and Photonic Materials and Devices*. Academic Press: London, 2000.

3. Chandrasekhar, P., *Conducting Polymers, Fundamentals and Applications: A Practical Approach*. Kluwer Academic: Dordrecht, 1999.

4. Gul, V. E., *Structure and Properties of Conducting Polymer Composites*. VSP: Utrecht, 1996.

5. Zallen, R., *The Physics of Amorphous Solids*. Wiley: New York, 1983.

6. Kirkpatr.S. *Rev. Mod. Phys.* **1973,** 45, (4), 574-588.

7. Sahini, M., *Applications of Percolation Theory*. Taylor & Francis: London, 1994.

8. Brokken-Zijp, J. C. M.; Soloukhin, V. A.; Posthumus, W.; de With, G. *In Proceeding of 2003 Athens Conference on Coatings Science and Technology, Vouliagmeni, Greece.*

9. Chen, Z.; Brokken-Zijp, J. C. M.; Huinink, H. P.; Loos, J.; de With, G.; Michels, M. A. J. *Macromolecules* **2006,** 39, (18), 6115-6124.

10. Huijbregts, L. J. *Charge Transport and Morphology in Nanofillers and Polymer Nanocomposites*. Ph.D. Thesis, Eindhoven University of Technology, Eindhoven, 2008.

11. Huijbregts, L. J.; Brom, H. B.; Brokken-Zijp, J. C. M.; Kemerink, M.; Chen, Z.; de Goeje, M. P.; Yuan, M.; Michels, M. A. J. *J. Phys. Chem. B* **2006,** 110, (46), 23115-23122.

12. Heiko, S. *Nanocomposites from Flame-made Nanoparticles Radiopaque Ta_2O_2/SiO_2 for Dental Adhensives and Fillings*. Ph.D. Thesis, Swiss Federal Institute of Technology Zurich, Zurich, 2007.

13. Soloukhin, V. A.; Brokken-Zijp, J. C. M.; de With, G. *J. Polym. Sci. B* **2007,** 45, (16), 2147-2160.

14. Posthumus, W. *UV Curable Acrylate Metal Oxide Nanocomposite Coatings*. Ph.D. Thesis, Eindhoven University of Technology, Eindhoven, 2004.

15. Glasel, H. J.; Bauer, F.; Ernst, H.; Findeisen, M.; Hartmann, E.; Langguth, H.; Mehnert, R.; Schubert, R. *Macromol. Chem. Phys.* **2000,** 201, (18), 2765-2770.

16. Cho, J. D.; Ju, H. T.; Hong, J. W. *J. Polym. Sci. A* **2005,** 43, (3), 658-670.

17. Bauer, F.; Mehnert, R. *J. Polym. Res.* **2005,** 12, (6), 483-491.

18. Soloukhin, V. A.; Posthumus, W.; Brokken-Zijp, J. C. M.; Loos, J.; de With, G. *Polymer* **2002,** 43, (23), 6169-6181.

19. Chen, Z.; Brokken-Zijp, J. C. M.; Michels, M. A. J. *J. Polym. Sci. B* **2006,** 44, (1), 33-47.

20. Brokken-Zijp, J. C. M.; van Mechelen, J. B.; Emeis, C. A.; Datema, K. P.; Kramer, A. H.; de Bruijn, D. P.; Meruma, A. J. *US Patent 05319009* **1993**.

21. Brokken-Zijp, J. C. M.; Yuan, M.; et al. *"Synthesis and Structure of Novel Aquocyanophthalocyaninato Co(III) Semi-conductor and Its Applications in Conductive Polymer Composites".* In Preparation.

22. Yuan, M.; Brokken-Zijp, J. C. M.; Huijbregts, L. J.; de With, G. *J. Polym. Sci. B* **2008,** 46, 1079-1093.

23. Scherzer, T.; Decker, U. *Radiation Physics and Chemistry* **1999,** 55, (5-6), 615-619.

24. Pallas, N. R.; Pethica, B. A. *Colloids Surf.* **1983,** 6, (3), 221-227.

25. Lin-Vien, D.; Colthup, N. B.; Fateley, W. G.; Grasselli, J. G., *The Handbook of Infrared and Raman Characteristic Frequencies of Organic Molecules*. Academic Press: New York, 1991.

26. Hoffman, A. J.; Yee, H.; Mills, G.; Hoffmann, M. R. *J. Phys. Chem.* **1992,** 96, (13), 5540-5546.

27. Mehnert, R.; Pincus, A.; Janorsky, I.; Stowe, R.; Berejka, A., *UV & EB Curing Technology & Equipment*. Wiley & Sons: London, 1998; Vol. I.

28. Yuan, M.; Brokken-Zijp, J. C. M.; de With, G. *"Conductivity of Cross-linked Low Surface Energy Epoxy Coatings".* Submitted to J. Polym. Sci. B.

29. Heaney, M. B. *Phys. Rev. B* **1995,** 52, (17), 12477-12480.

30. Weitz, D. A.; Huang, J. S.; Lin, M. Y.; Sung, J. *Phys. Rev. Lett.* **1984,** 53, (17), 1657-1660.

31. Brady, R. M.; Ball, R. C. *Nature* **1984,** 309, (5965), 225-229.

32. Vermant, J.; Solomon, M. J. *J. Phys.* **2005,** 17, (4), R187-R216.

33. Meakin, P. *Phys. Rev. A* **1983,** 27, (3), 1495-1507.

34. Yuan, M.; Brokken-Zijp, J. C. M.; de With, G. *"Structure-Electrical Property in (Semi)conductive Thermoset Polymer Nanocomposites".* Submitted to Macromolecules.

35. Kleinjan, W. E.; Brokken-Zijp, J. C. M.; van de Belt, R.; Chen, Z.; de With, G. *J. Mater. Res.* **2008,** 23, (3), 869-880.

9

CONCLUSIONS AND RECOMMENDATIONS

9.1. Conclusions

Semi-conductive Phthalcon/thermoset nanocomposites have been investigated to:

❖ Get insight in the most important factors which influence the relation between the morphology of Phthalcon particle network and the DC volume conductivity of cured Phthalcon/thermoset composites;

❖ Apply obtained knowledge to find more attractive starting formulations and processing conditions in making low surface energy permanent antistatic cross-linked Phthalcon/epoxy materials; and

❖ Assess the impact of our findings on structure-property relations in other thermoset polymer composites containing nanometer-sized filler particles.

It has been shown that the Phthalcon particle dispersion and the effective Hamaker constant of the starting formulation have a large influence on the relation between DC volume conductivity and Phthalcon filler concentration (log σ_v – φ relation). By studying the Phthalcon particle network structure, network formation and DC volume conductivity of Phthalcon/epoxy nanocomposites prepared under different conditions, the following results are found:

❧ The Influence of primary Phthalcon particle size on the DC volume conductivity σ_v, the maximum volume conductivity σ_{max} and the percolation threshold φ_c is minimal. The very similar fractal particle network structures are likely to be formed by Diffusion Limited Cluster Aggregation (DLCA) at the early stage of cure;

❧ Phthalcon crystals are large enough, hence, no loss in conductivity, due to a reduction of the effective density of states, was observed in Phthalcon/polymer composites;

❧ The choice of dispersing solvent, cross-linking agent, curing temperature, curing method and the presence/absence of catalyst have a tremendous influence on the log σ_v – φ relation and the fractal Phthalcon particle network structure and

distribution in cured epoxy composites; The fractal Phthalcon particle network is likely to be formed initially by DLCA during cure. In some cases the network relaxes during cure, resulting in a fractal particle network with a lower σ_v value; in other cases the particle network locates at the bottom of the layer, the top of the coating or appears homogeneously distributed through the whole layer thickness. Only under very specific processing conditions and starting formulations, the maximum value obtainable for σ_{max} of Phthalcon/epoxy composites can be realized. Under these conditions the Phthalcon particles really touch each other in the network, whereas in general there is always insulating material present between particles in the network which lowers the σ_v of the composites;

ⅎ When partially fluorinated cross-linker is present in the starting formulation, semi-conductive low surface energy coatings are achieved. In addition, the log $\sigma_v - \varphi$ relation and the morphology of Phthalcon particle network change severely due to the presence of fluorinated species; and

ⅎ Besides thermally cured Phthalcon/epoxy coatings, it is also possible to obtain semi-conductive UV cured Phthalcon/acrylate coatings without the aid of a dispersing solvent. Unlike for epoxy coatings, in acrylate coatings the maximum obtainable value for σ_{max} is reached at a lower Phthalcon concentration accompanied with a lower φ_c. Furthermore, due to the rapid UV cure, Phthalcon particle network/aggregates in the dispersion are quickly frozen in the acrylate matrix, and the particle network structure is preserved. Therefore, the log $\sigma_v - \varphi$ relation is more attractive than thermally cured epoxy coatings.

From these results, we conclude that:

℞ The log $\sigma_v - \varphi$ relation and Phthalcon particle network structure and distribution in polymer matrix are strongly influenced by small changes in starting formulations and processing methods/conditions, even when Phthalcon particles are very well-dispersed in the starting formulations and the initial effective Hamaker constant of the formulations is large;

℞ To realize optimum and reproducible structure-conductivity relations in Phthalcon/thermoset composites, a careful optimization process is required; and

℞ It is likely that for other thermoset nanocomposites containing a small amount of conductive filler particles, small changes in processing conditions and starting formulations also have large influences on their structure-property relations.

9.2. Recommendations

The upper-limit model calculations show that when a low φ_c is required, this will always occur at the expense of a low σ_{max}. Our results also show that under the optimum processing conditions and starting formulations, the σ_{max} in Phthalcon/thermoset composites is limited to 10^{-7} S/cm. When a critical filler concentration is desired to remain as low as possible, a drastic increase in σ_v can, therefore, only be obtained by using conductive nanofillers with a (much) higher intrinsic conductivity.

One such filler material could be antimony doped tin oxide (ATO) nanoparticles. However, measurements reveal that the interparticle tunnelling is strongly limited by its small particle size. This is caused by the Coulomb charging energy which reduces the effective density of states for the tunnelling. The loss in conductivity resulted from a reduction in the effective density of states is considered to be negligible for particles with size larger than 100 nm. This is indeed the case for our Phthalcon particles. Hence, for ATO particles a particle size larger than 100 nm is preferred.

To improve the intrinsic conductivity of Phthalcon particles, doping, for instance, replacing Co(III) with other metallic ion or/and substituting existing ligand(s) may be an option. Moreover, further optimization of the Phthalcon particle dispersion in the starting formulations, such as surface modification to improve the compatibility between Phthalcon particles and polymer matrix, may lead to an easier controllable processing, a more attractive formulation and an improved log σ_v - φ relation. If successful, this will broaden the applications of Phthalcon/thermoset composites.

SUMMARY

Tunable Conductivity Level in Nanosized Phthalcon/Polymer

Composites

In recent years, blending of an insulating polymer with conducting filler particle has attracted considerable interest because of the potential applications of these composites in many areas where a certain level of conductivity is required. The increase in conductivity is, generally, caused by the formation of a conductive particle network though the matrix. However, the main problems involved in this field, in general, are the large amount of conducting fillers required in order to increase the conductivity level well above that of the polymer matrix itself; and the inflexibility of the maximum volume conductivity (σ_{max}) obtained. Moreover, the σ_{max} is normally orders of magnitude lower than the intrinsic conductivity of the filler itself. A σ_{max} value closer to the conductivity of the filler, and a much lower filler amount needed would broaden the application possibilities of these composites considerably.

In this thesis, novel nanometer-sized phthalocyanine crystals (known as Phthalcon) with different chemical compositions and particle sizes were synthesized, and used as semi-conductive fillers in different polymer thermoset matrices. We found that even with a small amount of Phthalcon, the conductivity of the polymer matrix can increase tremendously. The influence of Phthalcon particle size, the choice of cross-linker, curing temperature, solvent, catalyst, and the presence of low surface energy fluorine species on the conductivity levels of these polymer composites were studied in detail in epoxy systems. Great attention has been given to the relation between the volume conductivity and the Phthalcon concentration, the particle network morphology in the polymer matrix, the mechanism of the particle network formation and the particle concentration variation throughout the material. Furthermore, we found that besides thermally cured epoxy system, it is also possible to use a relatively simple, easy and fast route to prepare UV-curable Phthalcon/acrylate coatings, which leads to coatings with relatively high conductivity levels. The impact of our finding on other (semi)conductive/polymer nanocomposites is also addressed.

ACKNOWLEDGEMENTS

This thesis would not be accomplished without many helps and supports. Here I would like to express my deepest gratitude to those whose valuable contributions and supports made possible the successful accomplishment of this thesis.

First of all, I would like to thank my promoter Prof. dr. Bert. de With for giving me the opportunity to pursue my PhD in his laboratory. His expertise, understanding and patience added considerably to the research present here. Dear Bert, thank you very much for your continuous support and professional guidance, your never-ending encouragement has been always driving me go further.

I would also like to thank my co-promoter dr. José Brokken-Zijp for sharing with me her profound knowledge in the field of polymer nanocomposites, for her enthusiasm, encouragement, valuable suggestions and also for the nice discussions we had on classic music, contemporary art, etc. Through her I get the best of east and west culture. Dear José, the completion of this thesis would have been difficult without your resourceful ideas and offered help.

I would like to extend my heartiest thanks to Prof. dr. John Kelly, Prof. dr. René. Jassen and Prof. dr. Roeland Nolte for accepting to be members of the core-committee and reading the manuscript of my thesis. I was impressed by their valuable comments. Also thanks to Prof. dr. Richard van de Sanden and Prof. dr. Thijs Michels for their kindness and time to be members of my defense committee.

Furthermore, I would like to convey my deep gratitude to dr. Zhe Chen who brought me into this magnificent coating world. His profound knowledge, valuable comments and sophisticated skills broaden my knowledge and helped me tremendously in the initial stage of my PhD study. I am very grateful to dr. Hans Brom, dr. Laura Huijbregts, dr. Wilfred Kleinjan and Prof. dr. Thijs Michels for their constructive advices on conductivity measurements and fractal structure analyses which improved the quality of this thesis.

I would like to thank many people who offered great helps in the characterization part of this thesis. Thanks to Ir. Otto van Asselen for his professional helps and

189

suggestions on FT-IR, dr. Dong Weifu and dr. Lu Kangbo for coating microtone preparation. Thanks to dr. Jos Laven for his instructions and helps on dynamic light scattering and rheological measurements. Thanks to Baris for contact angle measurements and thanks to Francesca and Przemek for letting me use the "always fully booked" UVA tube. I would also like to express my appreciation to Marco Hendrix for performing XRD measurements, for bearing my endless bothering with optical microscopy and for his smiling radiating positive energy.

I am enormously grateful to dr. Marshall Ming for his valuable suggestions on many scientific issues, and for all the "say your say" discussions on numerous movies. I am very thankful to dr. Alexander (Sasha) Kodentsov, a person nicely combine a great deal of extremes in his extraordinary personality, for his continuous helps (even for the great help which caused my copper-allergy and "disfigured" for almost two weeks), criticisms and encouragement on many occasions.

Working within SMG is a great pleasure and nice experience to me. I would like to thank to my former officemate Anneke for her kind help in using lab facilities and for translating all the Dutch letters I received. Thanks to Huub for his technical support on using vacuum oven. I am grateful to Imanda for all the helps I got starting even before my staying in SMG. Following these acknowledgements, I would like to thank all the former and current SMG colleagues: Francesca, Baris, Przemek, Mark, Beryl, Catarina, Wilfred, Thanos, Adolphe, Laura, Tamara, Danela, Cosi "red team" and many others which would definitely enlarge this list. Thanks for the good working and social environment. Your helps and smiles are, and will always be, cherished in my memory.

Recollect the past six years in the Netherlands, I doubt that I will never be able to convey my appreciation fully for those who provide helps, supports, motivation, encouragement and joy to me. I am exceptionally grateful to my master program coordinator Prof. dr. John Kelly. I still remember how nervous and helpless I was when I first arrived in the Netherlands; I still remember how you and Mary welcomed me with your open arms, and helped me significantly in settling down in Utrecht. Dear John, you are one of the people that truly made a difference in my life. It is my great honor to have you as a member of my core-committee. I am grateful to Ms. Leonie Silkens, a nice lady from international office, Utrecht University. Dear Leonie, it was a great pleasure having you around and knowing that your help was there when it was needed. I would also like to acknowledge dr. Xia Yuhe and my brother's colleagues Mr. Wang Jingyin from Chinese Embassy the Hague, for taking good care of me and transporting a great deal of Chinese delicacies and supplies for me which helped me overcome homesick and survive in the initial stage of my staying in the

CURRICULUM VITAE

Ming Yuan was born on the 5th of April 1979 in Tianjin, China. In 1997, she started her undergraduate study at the Department of Chemistry, Nankai University, Tianjin, China. After obtaining her B.Sc. degree in Chemistry in June 2001, she pursued her graduate study at Research Institute of Element-Organic Chemistry, Nankai University, Tianjin, China. In September 2002 she attended Utrecht University (the Netherlands) to conduct her master study in Chemistry of Condensed Matter, under the supervision of Prof. dr. John Kelly, in the research of Influence of Capping Molecules on the Optical Properties of CdSe and CdTe Quantum Dots. In February 2004 she performed an internship in Philips Research Laboratory, Eindhoven, the Netherlands, on the topic of Characterization of Semi-conductive Nanowire Devices. She received her M.Sc. degree in Chemistry and Physics with honours in July 2004. In the same year she joined, as a PhD student, the Laboratory of Materials and Interface Chemistry within the Department of Chemical Engineering and Chemistry at Eindhoven University of Technology, the Netherlands, under the supervision of Prof. dr. Bert de With and dr. José Brokken-Zijp. This research was focused on Tunable Conductive Levels in Nanosized Phthalcon/Polymer Composites. The results of her research have resulted in this thesis.

LIST OF PUBLICATIONS

Yuan, M.; Brokken-Zijp, J. C. M., Huijbregts, L. J.; Brom, H. B.; de With, G. *Influence of Filler Size on the Conductivity of Polymer Nanocomposites*, **J. Poly. Sci. B**. *2008*, 46, 1079.

Yuan, M.; Brokken-Zijp, J. C. M.; de With, G. *Conductivity of Cross-linked Low Surface Energy Epoxy Coatings*, Submitted to **J. Poly. Sci. B**.

Yuan, M.; Brokken-Zijp, J. C. M.; de With, G. *Structure-Electrical Property in Semi-conductive Thermoset Polymer Nanocomposites,* Submitted to **Macromolecules**.

Yuan, M.; Brokken-Zijp, J. C. M.; de With, G. *UV Curable Semi-conductive Phthalcon/Polymer Nanocomposites*, Submitted to **Macromolecules**.

Brokken-Zijp, J. C. M.; Yuan, M.; de With, G. et al. *Synthesis and Structure of Novel Aquocyanophthalocyaninato Cobalt(III) Semi-conductor and Its Applications in Conductive Polymer Composites*, In Preparation.

Huijbregts, L. J.; Brom, H. B.; Brokken-Zijp, J. C. M.; Yuan, M.; Michels, M. A. J. *Hopping Parameters in Densely Packed Submicro Crystallites*, **Phys. Stat. Sol.** *2008*, 5, 765.

Huijbregts, L. J.; Brom, H. B.; Brokken-Zijp, J. C. M.; Kemerink, M.; Chen, Z.; de Goeje, M.; Yuan, M.; Michels, M. A. J. *The Optimal Structure-Conductivity Relation in an Epoxy-Phthalocyanine Nanocomposite*, **J. Phys. Chem. B.** *2006*, 110, 23115.

Huijbregts, L. J.; Brom, H. B.; Brokken-Zijp, J. C. M.; Michels, M. A.; de Goeje, M.; Yuan, M.; *The Intrinsic Conductivity of Nanosized Semiconducting Crystals from Dielectric Powder Data*, **Phys. Stat. Sol.** *2006*, 3(2), 259.